Hematopoiesis in the developing zebrafish embryo

Sasja Franke

COLOFON

The work described in this thesis was performed at the Hubrecht Institute for Developmental Biology and Stem Cell Research (Royal Netherlands Academy of Arts and Sciences, KNAW), which is part of the research school Cancer Stem Cells & Developmental Biology (CS&D), which is part of the Utrecht Graduate School of Life Sciences (Utrecht University).

Printed by: Gildeprint - Enschede
Layout by: Sasja Franke
Cover design by: Nicole Lambers

Coverdesign: Artist impression of a 5 day old zebrafish embryo stained for B-Globin

Title pages: designed by Nicole Lambers

ISBN: 978-94-6419-275-9

Hematopoiesis in the developing zebrafish embryo

Hematopoiese in het ontwikkelende zebravis embryo
(met een samenvatting in het Nederlands)

Proefschrift

ter verkrijging van de graad van doctor aan de Universiteit Utrecht op gezag van de rector magnificus, prof.dr. H.R.B.M. Kummeling, ingevolge het besluit van het college voor promoties in het openbaar te verdedigen op dinsdag 7 september 2021 des middags te 14.15 uur

door

Sasja Franke

Geboren op 8 maart 1991

te Oldenzaal

Promotoren:

Prof. dr. J.P.W.M. Bakkers

Prof. dr. J. den Hertog

TABLE OF CONTENTS

Chapter 1

Introduction

Hematopoiesis

Blood is essential for life and without it the body would stop functioning. It provides the body of oxygen, nutrients, removes waste products, transports messengers, such as hormones and has immunological functions. Hematopoiesis is the formation of all of the cellular components of blood and blood plasma, which occur in the hematopoietic organs, spleen, bone marrow and liver in humans. When the hematopoietic system does not function properly, several severe conditions can occur, such as leukemia, multiple myeloma, lymphoma, anaemia, and sickle cell disease, to name a few.

Hematopoiesis has been studied in several model organisms, mainly chicken, zebrafish and mouse. Since mice and humans share a very similar embryonic development and organogenesis, mice are widely used as model organism. As the mouse genome is completely sequenced and annotated [1,2] and genetic modifications, such as knock-outs and knock-ins are mainstream methods in molecular genetics laboratories, and have become even easier due to CRISPR/Cas9 [3], mice have extensively been used to model genetic mutations leading to human diseases. One of the disadvantages of using mice is that, as in humans, embryonic development occurs *in utero*, making it difficult to observe and manipulate this process. Development in mice also takes relatively long, as gestation takes around 20 days. Per litter, 7-12 pups are developing and haematopoiesis starts around one week after fertilization.

Zebrafish are also increasingly being used as model system to study hematopoiesis. Zebrafish lack several disadvantages of the mouse model and are therefore an attractive alternative. Zebrafish embryos develop *ex utero*, and one pair of zebrafish produces several hundreds of embryos per week. Moreover, zebrafish embryos are translucent and develop a functional blood circulatory system within 24 hpf. Nowadays, the zebrafish genome is fully sequenced and annotated and it was shown that 71.4% of all human genes have at least one zebrafish ortholog and that is true for 82% of all human disease causing genes [4]. Zebrafish have a highly conserved physiology and possess fully recognizable organ systems, such as heart, liver, kidneys and the hematopoietic system. These systems fulfill very similar functions compared to their human counterparts.

Hematopoiesis during embryonic development

Stem cells define a specific type of cells that maintain self-renewal capacity and may differentiate into multiple cell types at the same time. Hematopoietic stem cells (HSCs) are responsible for the production and replenishment of all blood cell types during the entire lifespan of an organism. HSCs are defined as cells that have the ability to reconstitute multi-lineage hematopoiesis in lethally irradiated recipient mice upon transplantation. In zebrafish, it is yet unclear what the exact markers are to identify true HSCs, therefore the term hematopoietic stem/progenitor cells (HSPCs) is used to identify the cells that produce all blood lineages. McCulloch and Till [5] identified HSCs for the first time in mice in 1960. By 1988, HSCs were isolated for the first time [6] and later on HSCs were purified to an increasing purity [7,8]. Between species the developmental processes, genes and molecular

signalling pathways are highly conserved [9–12], whereas the sites of hematopoiesis are less conserved. Hematopoiesis during development occurs in two waves: the primitive wave, in which primitive erythrocytes and macrophages are produced. Subsequently, the definitive wave occurs, in which HSCs are formed that will differentiate into all blood lineages and will continue to replenish themselves for the rest of the life of the organism.

Primitive wave

The primitive wave starts when vascular and hematopoietic cells differentiate from mesodermal progenitors and form the blood islands in the extra-embryonic yolk sac, where the first primitive erythroblasts are produced at embryonic day (E) E2 (chicken) and E7.25 of mouse development [13,14]. At the same time in mouse development progenitors of macrophages and platelets are formed, which play a role in the development of blood and lymphatic vasculatures [15,16]. The equivalent of the extra-embryonic yolk sac is found in zebrafish at two sites: the anterior lateral mesoderm (ALM) and the posterior lateral mesoderm (PLM) that later forms the intermediate cell mass (ICM) and is located intra-embryonically. Primitive myelopoiesis occurs in the ALM, whereas primitive erythropoiesis occurs in the ICM [17,18]. The primitive wave transiently produces cells that do not last to adulthood, except for the macrophages that are formed in this period. These macrophages later on produce microglia in the brain in both adult mice and zebrafish [19–21].

In zebrafish, both the ALM and PLM express hematopoietic markers, such as *scl, lmo2* and *gata2* as well as vascular transcription factors such as *fli1* and *flk1*, indicating formation of HSCs and angioblasts [18]. It is suggested that bipotent hemangioblasts exist, which can give rise to both endothelial and hematopoietic cells [22,23]. Primitive erythropoiesis forms proerythroblasts that later mature into erythrocytes. In mice, only the embryonic erythrocytes are nucleated, whereas in zebrafish all erythrocytes are nucleated, both during embryonic development and in adulthood. In the ALM, cells express similar transcription factors as in the PLM, except *gata1*, since no erythroblasts are formed here. Two distinct populations of primitive myeloid progenitors can be found in the ALM, a granulocyte population and a population that represents monocytes and macrophages [24]. In the ICM, the myeloid specific factor *pu.1* (*spi1b)* is expressed with *gata1* and the balance between these two factors regulates the formation of erythroid and myeloid cells. Loss of *gata1* results in a transformation of erythroid progenitors into myeloid progenitors [25] and loss of *pu.1* induced the formation of erythrocytes in the ALM [26]. This also holds true in mice. When GATA1 was overexpressed, myeloid progenitors were transformed into erythroid progenitors and when PU.1 was overexpressed, erythroid progenitors turned into myeloid progenitors [27,28]. This suggests that *gata1* and *pu.1* regulate the balance between myeloid and erythroid progenitors during primitive hematopoiesis either by promoting their respective fates or by suppressing the opposite population [25–28].

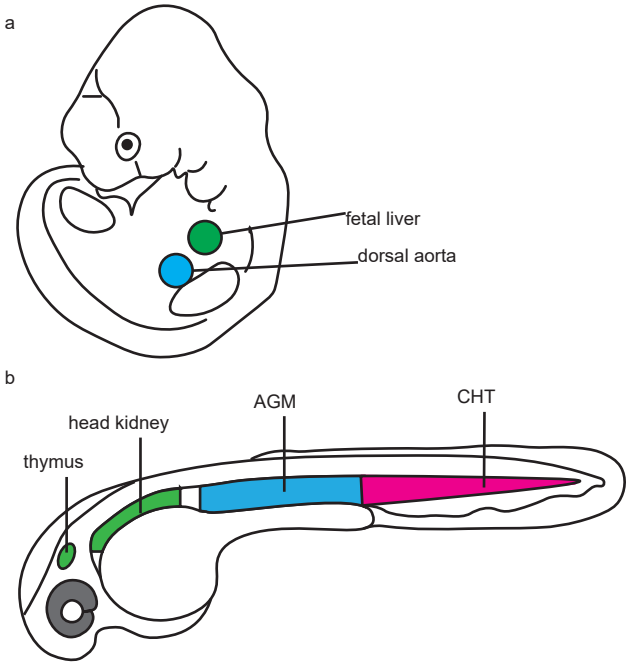

Figure 1. Sites of the definitive wave of hematopoiesis in mice and zebrafish. (a) in mice definitive hematopoiesis starts with HSCs emerging in the dorsal aorta at E10.5, after which they migrate to the fetal liver to mature and proliferate. Finally, HSCs will migrate to the adult hematopoietic organ, the bone marrow. (b) in zebrafish definitive hematopoiesis starts in the AGM at 36 hpf with the emerging of HSPCs, which then migrate to the CHT (the equivalent of the mammalian fetal liver). After several days of maturing and proliferating in the CHTs HSPCs will then migrate to the adult hematopoietic organs, the head kidney and the thymus. AGM, aorta-gonad-mesonephros. CHT, caudal hematopoietic tissue. Like colors represent organs with similar function during definitive hematopoiesis.

Definitive wave

In both mammals and zebrafish, the first HSCs arise in the ventral wall of the dorsal aorta (VDA) in the aorta-gonad-mesonephros (AGM) [29–33], through an endothelial-hematopoietic-transition (EHT) [34,35] (figure 1). In the mouse embryo, intra-aortic hematopoietic clusters (IAHCs) have been found in the large arteries, such as the aorta, vitelline and umbilical arteries starting at E10.5 [35], but also in the vasculature of the placenta starting at E11-E11.5 [36,37]. These IAHCs express various hematopoietic markers (c-kit, CD41, CD45) that are also expressed by embryonic HSCs [38], as well as endothelial markers (VE-cadherin, CD31, CD34) [35,38]. It was shown that IAHCs have a hematopoietic identity [39] and that both IAHCs and HSCs have an endothelial origin [40,41]. Later on, *ex vivo* culturing and overnight time lapse imaging showed that endothelial CD31+ cells underwent cell shape remodelling and started budding into the lumen of the aorta. Moreover, these cells then also started

expressing the HSC markers CD41 and c-kit [38] (figure 2a). In zebrafish, EHT can be followed *in vivo* using an endothelial transgenic *kdrl:eGFP* reporter line. Here, endothelial cells undergo a specific set of remodelling between 33 and 54 hours post fertilization (hpf)

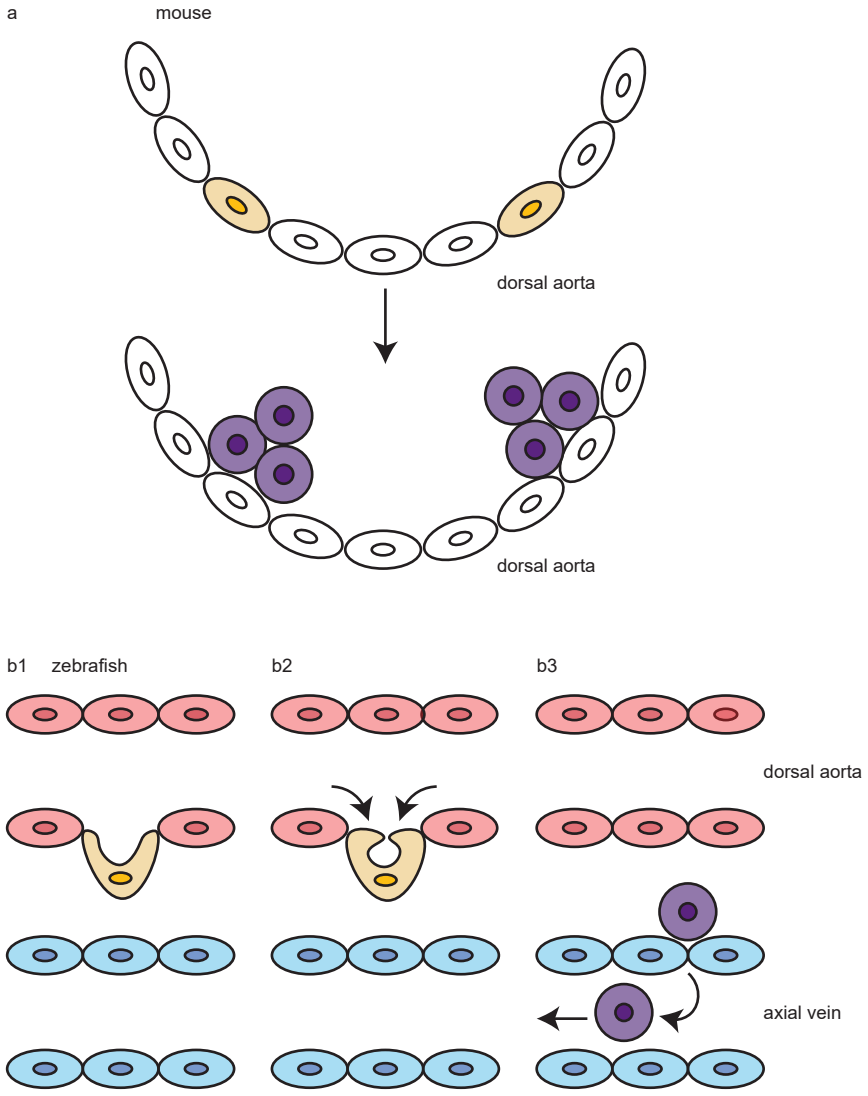

Figure 2. In both mice and zebrafish hemogenic endothelial cells transdifferentiate into HSPCs. (a) in mice hemogenic endothelial cells (yellow) from the dorsal aorta start a process in which they aqcuire a round shape and form clusters (IAHCs) (purple) that express HSC markers (c-kit, CD41, CD45). (b) in zebrafish hemogenic endothelial cells in the floor of the VDA (yellow) undergo a series of remodeling steps to become HSPCs. (b1) First, an endothelial cell in the VDA bends towards the subaortic space, (b2) then rounds up and (b3) lastly buds off from the VDA into the subaortic space, and is now a HSPCs (purple) and then migrates into the axial vein and joins circulation.

before they become HSPCs and enter circulation [34]. First, cells in the floor of the VDA start to bend towards the subaortic space, then cells round up and bud off from the VDA to enter the sub-aortic mesenchyme, where they either divide or directly enter the circulation via the axial vein [34] (figure 2 b). The start of HSPCs emergence in the zebrafish coincides with the expression of several HSC markers, such as *cd41*, *runx1*, *lmo2*, *scl* and *c-myb* [42–44]. It is estimated that in zebrafish around 3 HSPCs per hour enter the circulation [44], with some of them being true HSCs [45,46]. The peak of HSPCs emergence is at 48 hpf and around that time, 30 different HSC clones have emerged that contribute to definitive hematopoiesis [47], which seems to be in line with the numbers found during mouse development. There it is estimated that 2 HSCs and at least 12 transplantable pre-HSCs [48] are present in the aorta that contribute to the 66 HSCs found at E12 in the fetal liver [49]. After HSPCs enter circulation they migrate to the caudal hematopoietic tissue (CHT) in zebrafish [33,50] and the fetal liver in mice, where they expand and further mature [51–53]. Next, HSPCs migrate to the thymus and whole kidney marrow in zebrafish and bone marrow in mice, which are the adult hematopoietic organs [12,43,44].

Several transcription factors and signalling pathways have been shown to be essential for HSCs emergence in both mice and zebrafish. *Runx1* is a key regulator of definitive hematopoiesis and is an HSC marker. In mutant *Runx1* mice definitive hematopoiesis is severely affected, with HSCs not being able to generate in the embryonic aorta [39]. More specifically, *Runx1* is essential during EHT. When *Runx1* is conditionally knocked-out in endothelial cells, no IAHCs or HSCs are formed in mice [41]. In zebrafish *runx1* knockdown embryos EHT events are initiated, but much less than in normal embryos and the events are abortive. Right before the cell buds off from the VDA to become a HSPC, the cell bursts into pieces. As a consequence, the CHT and thymus are not seeded [34]. *Gata2* is also essential during EHT and for HSC formation in the AGM as *Gata2* knockout mice are embryonically lethal and die of severe anaemia [54]. Both *Scl* (*Tal1)* and *Lmo2* are individually essential for development of both primitive and definitive hematopoiesis [55]. Embryos lacking either *Scl* or *Lmo2* are not forming any blood cells and it is thought that these factors specify a blood rather than a vascular fate in the hemogenic endothelium. BMP signalling restricts haemato-vascular development of the lateral mesoderm, possibly acting through a pathway involving *Lmo2* and possibly *Gata2* [56]. Whereas these studies elucidated pathways to understand the complex signals needed for HSC production, we are still far away from understanding the whole complexity of HSC formation.

Phosphatases

Cellular signalling is regulated by many different factors, one being the phosphorylation and de-phosphorylation of proteins. Proteins are phosphorylated on tyrosine residues by protein tyrosine kinases (PTKs) and dephosphorylated by protein tyrosine phosphatases (PTPs). PTPs are important regulators of cellular processes, such as proliferation, differentiation, stem cell fate and development [57]. Mutations in PTPs often results in disrupted cell signalling and disease. To date, 125 PTPs have been identified in the human genome and they can mainly be divided in three classes: the classical PTPs, dual-specificity

PTPs and the low molecular weight PTPs [58,59] (reviewed in [60]).

Here, I will highlight two PTPs, *Pten* and *Ptpn11*, that have a central role in cell signaling and are involved in multiple processes, including stem cell fate determination and hematopoiesis.

PTEN

Phosphatase and Tensin homolog (PTEN) belongs to the PTP family and more specifically to the dual-specificity PTPs [61]. PTEN is involved in the PI3K-AKT pathway. Upon receptor activation by a ligand and subsequent PI3K activation, Akt signaling is activated, which causes an intracellular response. PTEN antagonizes catalytic PI3K activity by dephosphorylating phosphatidylinositol 3,4,5-triphosphate (PIP3) to phosphatidylinositol 4,5-biphosphate (PIP2), and thereby balancing Akt signaling (figure 3). Loss of PTEN causes hyperactivation of the PI3K signalling pathway and results in increased tumour susceptibility and increased proliferation, survival and self-renewal of stem cells [62,63]. Mice that lack *Pten* are embryonically lethal, indicating an important role for *Pten* during development [64–66].

Zebrafish have two *pten* genes, *ptena* and *ptenb*, that are redundant in function and highly homologous to human PTEN. Zebrafish lacking both *ptena* and *ptenb* are embryonically lethal around 5-7 dpf and furthermore are characterized by an enlarged head en heart oedema [67]. These *pten* mutant embryos also show disrupted angiogenesis, as they have upregulated levels of Vegfaa and show hyper-vascularization [68]. However, it is the lipid

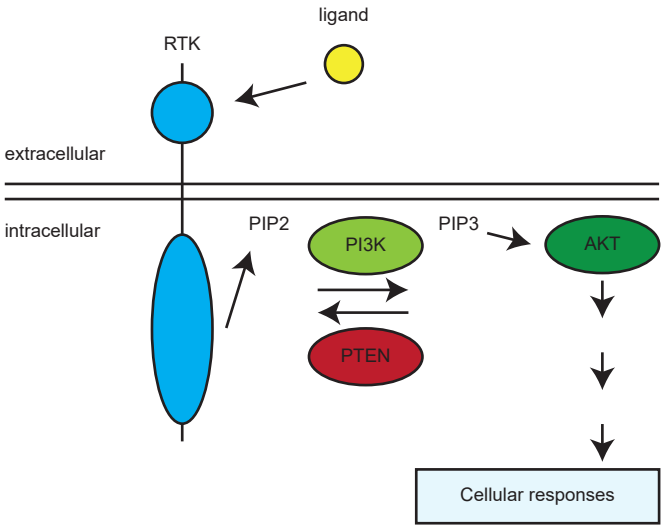

Figure 3. PTEN antagonizes PI3/Akt signaling. Simplified scheme of PTEN signaling. Ligand binding to its receptor activates the receptor and subsequently PI3K activation, resulting in increased levels of phosphatidylinositol (3,4,5) triphosphate (PIP3) and activation of downstream signaling via Akt. PTEN dephosphorylates PIP3 and loss of PTEN results in hyperactivation of the signaling pathway. Adapted from Stumpf *et al.* (2015)[88].

phosphatase activity of Pten and the spatial expression that is essential for regulation of angiogenesis, instead of the protein phosphatase activity. Pten-mutants with an increased plasma membrane localization in mammalian and zebrafish cells rescue the phenotype of hyper-vascularization in *pten* mutant embryos [69,70].

When PTEN is overexpressed in mice, a reduction in endothelial cell proliferation, vascular density and abnormal angiogenesis is observed [71]. This suggests that a fine balance between low and high PTEN activity is needed for proper angiogenesis. Loss of function mutations in PTEN are often identified in many different types of cancer [72–74] and additionally missense mutations have been identified in rare human autosomal dominant cancer syndromes, such as Cowden syndrome [75].

PTPN11

PTPN11 is a gene that encodes for cytoplasmic SHP2 and is a ubiquitously expressed PTP with two Src homology 2 (SH2) domains [76–78]. SHP2 positively regulates extracellular regulated kinase (ERK)/MAPK signalling, downstream of most receptor tyrosine kinases (RTKs). Other signaling pathways are regulated by SHP2 as well, including the Jak-STAT pathway and the PI3K-AKT pathway [77,78]. Various mutations, both activating and inactivating SHP2 function, are associated with human disease [79]. Mutations that either increase or decrease the catalytic activity of SHP2 are associated with Noonan syndrome (NS) and Noonan syndrome with multiple lentigines (NS-ML, formerly known as LEOPARD syndrome). These patients have characteristic cranio-facial abnormalities, heart defects, short stature and an increased risk of developing juvenile myelomonocytic leukemia (JMML). NS is caused by mutations that activate SHP2 catalytic activity (*e.g.* D61G), whereas NS-ML is caused by mutations in SHP2 that reduce the catalytic activity (*e.g.* A461T). Recently, several NS-ML mutations in SHP2 have been found to have reduced catalytic activity but show the structural properties that are typically observed in activating mutations, possibly explaining why NS and NS-ML patients show similar symptoms[80,81]. The SHP2 mutant proteins of NS and NS-ML patients appear to have an increased tendency to adopt an open conformation and have a longer interaction with scaffolding adaptors, prolonging substrate turnover, and in this way compensate for the reduced catalytic activity [80,81]. It is evident that the RAS/MAPK pathway has a role in NS and NS-ML, but it is yet unclear what the exact mechanism is that causes mutant SHP2 to induce these syndromes.

SHP2 is also involved in hematopoiesis. In mice it has been observed that SHP2 promotes embryonic stem cells to differentiate into hemogenic endothelium [82]. Later on, SHP2 is essential for the maintenance of the HSC pool and differentiation into all blood lineages. Loss of *Ptpn11* in HSCs in mice resulsd in loss of almost all HSCs and progenitors of hematopoietic lineages, with lethal consequences within 6-8 weeks after birth [83]. Overexpression of SHP2 or gain-of-function mutations lead to abnormal differentiation and proliferation in HSCs [30,84–86]. Zebrafish have two *ptpn11* genes, *ptpn11a* and *ptpn11b*, encoding Shp2a and Shp2b, respectively [57]. Both Shp2a and Shp2b are highly homologous to human SHP2 and harbor catalytic activity, but they differ in expression levels during

early embryonic development. *Ptpn11a* is constantly expressed up until 5 dpf and *ptpn11b* expression increases over time [87]. *Ptpn11a*$^{-/-}$ mutant embryos are embryonically lethal from 5-6 dpf onwards, whereas *ptpn11b*$^{-/-}$ mutant embryos are developing normally and are viable and fertile [87]. Whereas Shp2a and Shp2b have similar biochemical activities, the *in vivo* function is distinct, which appears to be due to the difference in expression pattern.

Outline Thesis

The general aim of this thesis is to study hematopoiesis in developing zebrafish, with an emphasis on the role of two phosphatases, *pten* and *ptpn11*. The zebrafish is used as a model organism, exploiting its genetic manipulability, transparency and ease of analysis. In **chapter 2**, we study the role of *pten* during hematopoiesis in zebrafish using live imaging techniques and single cell RNA sequencing. In **chapter 3** we introduce a novel zebrafish genetic mutant, created by CRISPR/Cas9 knock-in of a common NS-patient associated mutation, Shp2-D61G. We demonstrate that the phenotype developed by the Shp2-D61G zebrafish mutant is very similar to the phenotype observed in human NS-patients with this mutation. In **chapter 4** *ptpn11b* is found to have a role during the onset of the definitive wave. *Ptpn11b* mutants show abortive events during EHT, but hematopoiesis seems unaffected after this stage. In **chapter 5** we provide evidence that kdrl marks the shift from embryonic to adult HSPCs, in that kdrl/cd41^{low} cells represent embryonic HSPCs and cd41^{low} cells without kdrl adult HSPCs. **Chapter 6** aims to put the results of this thesis in perspective, in the form of a summarizing discussion.

References

1. Consortium, M. G. S. *et al.* Initial sequencing and comparative analysis of the mouse genome. *Nature* **420**, 520–562 (2002).
2. Guigó, R. *et al.* Comparison of mouse and human genomes followed by experimental verification yields an estimated 1,019 additional genes. *Proc. Natl. Acad. Sci. U. S. A.* **100**, 1140–1145 (2003).
3. Cong, L. *et al.* Multiplex Genome Engineering Using CRISPR/Cas Systems. *Science (80-.).* **339**, 819–823 (2013).
4. Howe, K. *et al.* The zebrafish reference genome sequence and its relationship to the human genome. *Nature* **496**, 498–503 (2013).
5. McCulloch, E. A. & Till, J. E. The Radiation Sensitivity of Normal Mouse Bone Marrow Cells, Determined by Quantitative Marrow Transplantation into Irradiated Mice. *Radiat. Res.* **13**, 115 (1960).
6. Spangrude, G. J., Heimfeld, S. & Weissman, I. L. Purification and characterization of mouse hematopoietic stem cells. *Science (80-.).* **241**, 58–62 (1988).
7. Osawa, M., Hanada, K. -i., Hamada, H. & Nakauchi, H. Long-Term Lymphohematopoietic Reconstitution by a Single CD34-Low/Negative Hematopoietic Stem Cell. *Science (80-.).* **273**, 242–245 (1996).
8. Kiel, M. J. *et al.* SLAM Family Receptors Distinguish Hematopoietic Stem and Progenitor Cells and Reveal Endothelial Niches for Stem Cells. *Cell* **121**, 1109–1121 (2005).
9. Chen, A. T. & Zon, L. I. Zebrafish blood stem cells. *J. Cell. Biochem.* **108**, 35–42 (2009).
10. Huang, H.-T. H.-T. & Zon, L. I. Regulation of Stem Cells in the Zebra Fish Hematopoietic System. *Cold Spring Harb. Symp. Quant. Biol.* **73**, 111–8 (2008).
11. Paik, E. J. & Zon, L. I. Hematopoietic development in the zebrafish. *Int. J. Dev. Biol.* **54**, 1127–1137 (2010).
12. Traver, D. *et al.* Transplantation and in vivo imaging of multilineage engraftment in zebrafish bloodless mutants. *Nat. Immunol.* **4**, 1238–1246 (2003).
13. FERKOWICZ, M. & YODER, M. Blood island formation: longstanding observations and modern interpretations. *Exp. Hematol.* **33**, 1041–1047 (2005).
14. Jaffredo, T. & Yvernogeau, L. How the avian model has pioneered the field of hematopoietic development. *Exp. Hematol.* **42**, 661–668 (2014).
15. Xu, M. J. *et al.* Evidence for the presence of murine primitive megakarycytopoiesis in the early yolk sac. *Blood* **97**, 2016–2022 (2001).
16. Bertozzi, C. C. *et al.* Platelets regulate lymphatic vascular development through CLEC-2-SLP-76 signaling. *Blood* **116**, 661–670 (2010).
17. Detrich, H. W. *et al.* Intraembryonic hematopoietic cell migration during vertebrate development. *Proc. Natl. Acad. Sci.* **92**, 10713–10717 (1995).
18. Davidson, A. J. *et al.* cdx4 mutants fail to specify blood progenitors and can be rescued by multiple hox genes. *Nature* **425**, 300–306 (2003).
19. Ginhoux, F. *et al.* Primitive Macrophages. *Science (80-.).* **701**, 841–845 (2010).
20. Ginhoux, F., Lim, S., Hoeffel, G., Low, D. & Huber, T. Origin and differentiation of microglia. *Front. Cell. Neurosci.* **7**, 1–14 (2013).
21. Herbomel, P., Thisse, B. & Thisse, C. Zebrafish early macrophages colonize cephalic mesenchyme and developing brain, retina, and epidermis through a M-CSF receptor-dependent invasive process. *Dev. Biol.* **238**, 274–288 (2001).
22. Dooley, K. A., Davidson, A. J. & Zon, L. I. Zebrafish scl functions independently in hematopoietic and endothelial development. *Dev. Biol.* **277**, 522–536 (2005).
23. Vogeli, K. M., Jin, S. W., Martin, G. R. & Stainier, D. Y. R. A common progenitor for haematopoietic and endothelial lineages in the zebrafish gastrula. *Nature* **443**, 337–339 (2006).
24. Bennett, C. M. *et al.* Myelopoiesis in the zebrafish, Danio rerio. *Blood* **98**, 643–651 (2001).
25. Galloway, J. L., Wingert, R. A., Thisse, C., Thisse, B. & Zon, L. I. Loss of Gata1 but not Gata2 converts erythropoiesis to myelopoiesis in zebrafish embryos. *Dev. Cell* **8**, 109–116 (2005).
26. Berman, J. N., Kanki, J. P. & Look, A. T. Zebrafish as a model for myelopoiesis during embryogenesis. *Exp. Hematol.* **33**, 997–1006 (2005).
27. Iwasaki, H. *et al.* GATA-1 converts lymphoid and myelomonocytic progenitors into the megakaryocyte/erythrocyte lineages. *Immunity* **19**, 451–462 (2003).
28. Yamada, T. *et al.* Lineage switch induced by overexpression of Ets family transcription factor PU.1 in murine erythroleukemia cells. *Blood* **97**, 2300–2307 (2001).
29. De Bruijn, M. F. T. R., Speck, N. A., Peeters, M. C. E. & Dzierzak, E. Definitive hematopoietic stem cells first develop within the major arterial regions of the mouse embryo. *EMBO J.* **19**, 2465–2474 (2000).
30. Li, Z. *et al.* Mouse embryonic head as a site for hematopoietic stem cell development. *Cell Stem Cell* **11**, 663–675 (2012).
31. Medvinsky, A. & Dzierzak, E. Definitive hematopoiesis is autonomously initiated by the AGM region. *Cell* **86**,

897–906 (1996).
32. Müller, A. M., Medvinsky, A., Strouboulis, J., Grosveld, F. & Dzierzakt, E. Development of hematopoietic stem cell activity in the mouse embryo. *Immunity* **1**, 291–301 (1994).
33. Murayama, E. *et al.* Tracing Hematopoietic Precursor Migration to Successive Hematopoietic Organs during Zebrafish Development. *Immunity* **25**, 963–975 (2006).
34. Kissa, K. & Herbomel, P. Blood stem cells emerge from aortic endothelium by a novel type of cell transition. *Nature* **464**, 112–115 (2010).
35. Yokomizo, T. & Dzierzak, E. Three-dimensional cartography of hematopoietic clusters in the vasculature of whole mouse embryos. *Development* **137**, 3651–3661 (2010).
36. Rhodes, K. E. *et al.* The Emergence of Hematopoietic Stem Cells Is Initiated in the Placental Vasculature in the Absence of Circulation. *Cell Stem Cell* **2**, 252–263 (2008).
37. Azevedo Portilho, N., Tavares Guedes, P., Croy, B. A. & Pelajo-Machado, M. Localization of transient immature hematopoietic cells to two distinct, potential niches in the developing mouse placenta. *Placenta* **47**, 1–11 (2016).
38. Boisset, J. C. *et al.* In vivo imaging of haematopoietic cells emerging from the mouse aortic endothelium. *Nature* **464**, 116–120 (2010).
39. North, T. *et al.* Cbfa2 is required for the formation of intra-aortic hematopoietic clusters. *Development* **126**, 2563–2575 (1999).
40. Zovein, A. C. *et al.* Fate Tracing Reveals the Endothelial Origin of Hematopoietic Stem Cells. *Cell Stem Cell* **3**, 625–636 (2008).
41. Chen, M. J., Yokomizo, T., Zeigler, B. M., Dzierzak, E. & Speck, N. A. Runx1 is required for the endothelial to haematopoietic cell transition but not thereafter. *Nature* **457**, 887–891 (2009).
42. Thompson, M. A. *et al.* The cloche and spadetail genes differentially affect hematopoiesis and vasculogenesis. *Dev. Biol.* **197**, 248–269 (1998).
43. Bertrand, J. Y., Kim, A. D., Teng, S. & Traver, D. CD41+ cmyb+ precursors colonize the zebrafish pronephros by a novel migration route to initiate adult hematopoiesis. *Development* **135**, 1853–1862 (2008).
44. Kissa, K. *et al.* Live imaging of emerging hematopoietic stem cells and early thymus colonization. *Blood* **111**, 1147–56 (2008).
45. Bertrand, J. Y. *et al.* Haematopoietic stem cells derive directly from aortic endothelium during development. *Nature* **464**, 108–111 (2010).
46. Ma, D., Zhang, J., Lin, H. F., Italiano, J. & Handin, R. I. The identification and characterization of zebrafish hematopoietic stem cells. *Blood* **118**, 289–297 (2011).
47. Henninger, J. *et al.* Clonal fate mapping quantifies the number of haematopoietic stem cells that arise during development. *Nat. Cell Biol.* 1–9 (2016) doi:1038/ncb34
48. Boisset, J.-C. *et al.* Progressive maturation toward hematopoietic stem cells in the mouse embryo aorta. *Blood* **125**, 465–469 (2015).
49. Kumaravelu, P. *et al.* Erratum: Quantitative developmental anatomy of definitive haematopoietic stem cells/ long-term repopulating units (HSC/RUs): Role of the aorta-gonad-mesonephros (AGM) region and the yolk sac in colonisation of the mouse embryonic liver (Development) vol. *Development* **130**, 425 (2003).
50. Tamplin, O. J. *et al.* Hematopoietic stem cell arrival triggers dynamic remodeling of the perivascular niche. *Cell* **160**, 241–252 (2015).
51. Ivanovs, A. *et al.* Highly potent human hematopoietic stem cells first emerge in the intraembryonic aorta-gonad-mesonephros region. *J. Exp. Med.* **208**, 2417–2427 (2011).
52. Batsivari, A. *et al.* Understanding Hematopoietic Stem Cell Development through Functional Correlation of Their Proliferative Status with the Intra-aortic Cluster Architecture. *Stem Cell Reports* **8**, 1–14 (2017).
53. Laurenti, E. & Göttgens, B. From haematopoietic stem cells to complex differentiation landscapes. *Nature* **553**, 418–426 (2018).
54. Tsai, F. Y. *et al.* An early haematopoietic defect in mice lacking the transcription factor GATA- *Nature* **371**, 221–226 (1994).
55. Kim, S. I. & Bresnick, E. H. Transcriptional control of erythropoiesis: Emerging mechanisms and principles. *Oncogene* **26**, 6777–6794 (2007).
56. Burns, C. E., Traver, D., Mayhall, E., Shepard, J. L. & Zon, L. I. Hematopoietic stem cell fate is established by the Notch – Runx pathway. *Genes Dev.* **19**, 2331–2342 (2005).
57. van Eekelen, M., Overvoorde, J., van Rooijen, C. & den Hertog, J. Identification and expression of the family of classical protein-tyrosine phosphatases in zebrafish. *PLoS One* **5**, 1–16 (2010).
58. Alonso, A. & Pulido, R. The extended human PTPome: A growing tyrosine phosphatase family. *FEBS J.* **283**, 1404–1429 (2016).
59. Tonks, N. K. Protein tyrosine phosphatases - From housekeeping enzymes to master regulators of signal transduction. *FEBS J.* **280**, 346–378 (2013).
60. Hale, A. J., ter Steege, E. & den Hertog, J. Recent advances in understanding the role of protein-tyrosine phosphatases in development and disease. *Dev. Biol.* **428**, 283–292 (2017).
61. Song, M. S., Salmena, L. & Pandolfi, P. P. The functions and regulation of the PTEN tumour suppressor. *Nat. Rev. Mol. Cell Biol.* **13**, 283–296 (2012).
62. Alva, J. A., Lee, G. E., Escobar, E. E. & Pyle, A. D. Phosphatase and tensin homolog regulates the pluripotent

state and lineage fate choice in human embryonic stem cells. *Stem Cells* **29**, 1952–1962 (2011).
63. Alimonti, A. *et al.* Subtle variations in Pten dose determine cancer susceptibility. *Nat. Genet.* **42**, 454–458 (2010).
64. Di Cristofano, A., Pesce, B., Cordon-Cardo, C. & Pandolfi, P. P. Pten is essential for embryonic development and tumour suppression. *Nat. Genet.* **19**, 348–355 (1998).
65. Suzuki, A. *et al.* High cancer susceptibility and embryonic lethality associated with mutation of the PTEN tumor suppressor gene in mice. *Curr. Biol.* **8**, 1169–1178 (1998).
66. Stambolic, V. *et al.* Negative regulation of PKB/Akt-dependent cell survival by the tumor suppressor PTEN. *Cell* **95**, 29–39 (1998).
67. Faucherre, a, Taylor, G. S., Overvoorde, J., Dixon, J. E. & Hertog, J. Den. Zebrafish pten genes have overlapping and non-redundant functions in tumorigenesis and embryonic development. *Oncogene* **27**, 1079–1086 (2008).
68. Choorapoikayil, S., Weijts, B., Kers, R., de Bruin, A. & den Hertog, J. Loss of Pten promotes angiogenesis and enhanced vegfaa expression in zebrafish. *Dis. Model. Mech.* **6**, 1159–66 (2013).
69. Stumpf, M., Blokzijl-Franke, S. & den Hertog, J. Fine-Tuning of Pten Localization and Phosphatase Activity Is Essential for Zebrafish Angiogenesis. *PLoS One* **11**, e0154771 (2016).
70. Stumpf, M. & Den Hertog, J. Differential requirement for pten lipid and protein phosphatase activity during zebrafish embryonic development. *PLoS One* **11**, 1–16 (2016).
71. Serra, H. *et al.* PTEN mediates Notch-dependent stalk cell arrest in angiogenesis. *Nat. Commun.* **6**, 7935 (2015).
72. Li, J. *et al.* PTEN, a putative protein tyrosine phosphatase gene mutated in human brain, breast, and prostate cancer. *Science (80-.).* **275**, 1943–1947 (1997).
73. Li, D. M. & Sun, H. TEP1, encoded by a candidate tumor suppressor locus, is a novel protein tyrosine phosphatase regulated by transforming growth factor β. *Cancer Res.* **57**, 2124–2129 (1997).
74. Ali, I. U., Schriml, L. M. & Dean, M. Mutational spectra of PTEN/MMAC1 gene: A tumor suppressor with lipid phosphatase activity. *J. Natl. Cancer Inst.* **91**, 1922–1932 (1999).
75. Blumenthal, G. M. & Dennis, P. A. PTEN hamartoma tumor syndromes. *Eur. J. Hum. Genet.* **16**, 1289–1300 (2008).
76. Dance, M., Montagner, A., Salles, J. P., Yart, A. & Raynal, P. The molecular functions of Shp2 in the Ras/Mitogen-activated protein kinase (ERK1/2) pathway. *Cell. Signal.* **20**, 453–459 (2008).
77. Feng, G. S. Shp-2 tyrosine phosphatase: Signaling one cell or many. *Exp. Cell Res.* **253**, 47–54 (1999).
78. Neel, B. G., Gu, H. & Pao, L. The 'Shp'ing news: SH2 domain-containing tyrosine phosphatases in cell signaling. *Trends Biochem. Sci.* **28**, 284–293 (2003).
79. Tajan, M., de Rocca Serra, A., Valet, P., Edouard, T. & Yart, A. SHP2 sails from physiology to pathology. *Eur. J. Med. Genet.* **58**, 509–525 (2015).
80. Yu, Z. H. *et al.* Structural and mechanistic insights into LEOPARD syndrome-associated SHP2 mutations. *J. Biol. Chem.* **288**, 10472–10482 (2013).
81. Yu, Z. H. *et al.* Molecular basis of gain-of-function LEOPARD syndrome-associated SHP2 mutations. *Biochemistry* **53**, 4136–4151 (2014).
82. Chan, R. J., Johnson, S. A., Li, Y., Yoder, M. C. & Feng, G. A definitive role of Shp-2 tyrosine phosphatase in mediating embryonic stem cell differentiation and hematopoiesis. *Blood* **102**, 2074–2080 (2003).
83. Chan, G. *et al.* Essential role for Ptpn11 in survival of hematopoietic stem and progenitor cells. *Blood* **117**, 4253–4261 (2011).
84. Chan, G. *et al.* Leukemogenic Ptpn11 causes fatal myeloproliferative disorder via cell-autonomous effects on multiple stages of hematopoiesis. *Blood* **113**, 4414–4424 (2009).
85. Dong, L. *et al.* Leukaemogenic effects of Ptpn11 activating mutations in the stem cell microenvironment. *Nature* **539**, 304–308 (2016).
86. Xu, D. *et al.* A germline gain-of-function mutation in Ptpn11 (Shp-2) phosphatase induces myeloproliferative disease by aberrant activation of hematopoietic stem cells. *Blood* **116**, 3611–3621 (2010).
87. Bonetti, M. *et al.* Distinct and overlapping functions of ptpn11 genes in zebrafish development. *PLoS One* **9**, (2014).
88. Stumpf, M., Choorapoikayil, S. & den Hertog, J. Pten function in zebrafish: Anything but a fish story. *Methods* **77–78**, 191–196 (2015).

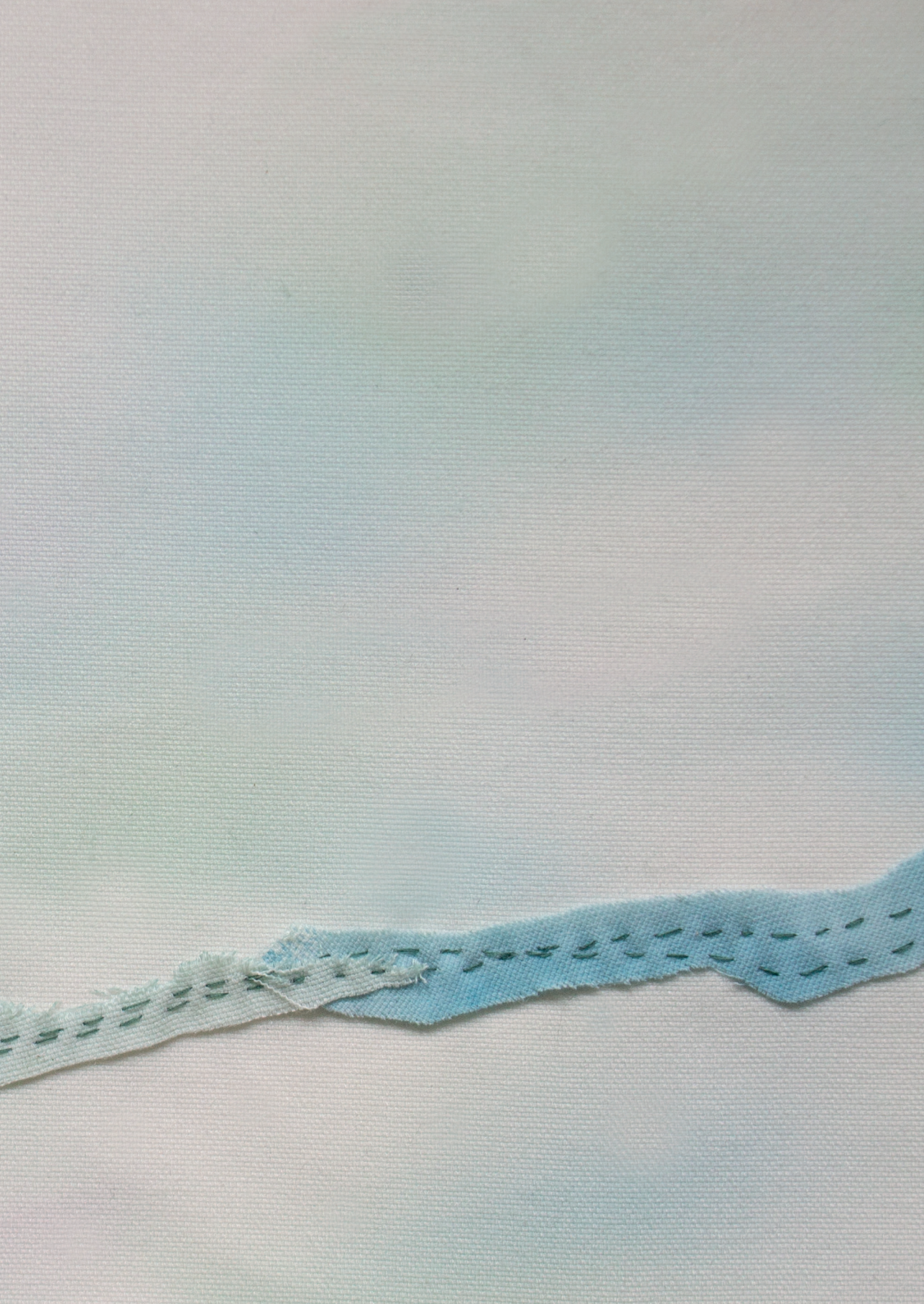

Chapter 2

Phosphatidylinositol-3 Kinase Signaling Controls Survival and Stemness of Hematopoietic Stem and Progenitor Cells

Blokzijl-Franke S, Ponsioen B, Schulte-Merker S, Herbomel P, Kissa K, Choorapoikayil S and den Hertog J

Adapted from Oncogene 40(15):2741-2755 (2021)

Abstract

Hematopoietic Stem and Progenitor Cells (HSPCs) are multipotent cells giving rise to all blood lineages during life. HSPCs emerge from the ventral wall of the dorsal aorta (VDA) during a specific timespan in embryonic development through endothelial hematopoietic transition (EHT). We investigated the ontogeny of HSPCs in mutant zebrafish embryos lacking functional pten, an important tumor suppressor with a central role in cell signaling. Through in vivo live imaging, we discovered that in pten mutant embryos a proportion of the HSPCs died upon emergence from the VDA, an effect rescued by inhibition of phosphatidylinositol-3 kinase (PI3K). Surprisingly, inhibition of PI3K in wild type embryos also induced HSPC death. Surviving HSPCs colonized the caudal hematopoietic tissue (CHT) normally and committed to all blood lineages. Single cell RNA sequencing indicated that inhibition of PI3K enhanced survival of multi-potent progenitors, whereas the number of HSPCs with more stem-like properties was reduced. At the end of the definitive wave, loss of Pten caused a shift to more restricted progenitors at the expense of HSPCs. We conclude that PI3K signaling tightly controls HSPCs survival and both up- and downregulation of PI3K signaling reduces stemness of HSPCs.

Introduction

Stem cells define a particular type of cells that maintain self-renewal capacity and may differentiate into multiple cell types at the same time. HSPCs are multipotent cells giving rise to all blood lineages during life[1–3]. In all vertebrates, an initial primitive wave of hematopoiesis occurs in the embryo, giving rise to primitive erythrocytes and myeloid cells. A definitive wave follows in which HSPCs are generated that will found multi-lineage hematopoiesis in developmentally successive hematopoietic organs up to adulthood. Our understanding of the emergence of HSPCs during the definitive wave is derived primarily from pioneer live *in vivo* imaging[4–6]. HSPCs emerge in a process whereby cells in the ventral wall of the dorsal aorta (VDA) undergo an endothelial to hematopoietic transition (EHT)[6] and then transiently colonize the fetal liver in mammals[7], or the caudal hematopoietic tissue (CHT) in zebrafish[8]. There, HSPCs expand and differentiate into all blood lineages and supply the developing embryos with mature blood cells. Subsequently, HSPCs migrate again to colonize the thymus and the bone marrow in mammals [7] or whole kidney marrow in fish[8] to produce blood cells in the adult.

HSPCs are tightly regulated in terms of dormancy, self-renewal, proliferation and differentiation. Disrupting this balance can have pathological consequences such as bone marrow failure or hematologic malignancy. The tumor suppressor, PTEN, has an important role in hematologic malignancies, particularly T-lineage acute lymphoblastic leukemia (T-ALL). Deleterious mutations in *PTEN* appear in 5-10% of T-ALL cases and about 17% of patients lack PTEN expression in the hematopoietic lineage[9,10]. PTEN counteracts phosphatidylinositol-3 kinase (PI3K) and hence acts upstream in the PI3K-Akt (also known as Protein kinase B, PKB) pathway[11]. Loss of PTEN function results in hyperactivation of the PI3K-Akt signaling pathway. Clonal evolution of leukemia-propagating cells in zebrafish highlights the role of Akt signaling in the process[12]. Conditional deletion of Pten in mice in hematopoietic stem cells (HSCs) in adult bone marrow promotes HSC proliferation, resulting in depletion of long-term HSCs, indicating that Pten is essential for the maintenance of HSCs[13,14].

The zebrafish genome encodes two *pten* genes with redundant function designated *ptena* and *ptenb*[15]. Single mutants display no morphological phenotype and are viable and fertile, but mutants that retain only a single wild type copy of *pten* develop hemangiosarcomas during adulthood[16]. *Ptena*$^{-/-}$*ptenb*$^{-/-}$ mutants lack functional Ptena and Ptenb, are embryonic lethal at 5-6 days post fertilization (dpf) and display hyperplasia and dysplasia[15]. We reported that double mutant zebrafish larvae lacking functional Pten display increased numbers of HSPCs in the CHT at 4-5 dpf. Whereas these HSPCs commit to different blood lineages, they fail to differentiate into mature blood cells. Inhibition of PI3K using LY294002, which compensates for the loss of Pten, restores differentiation of HSPCs into mature blood cells. Hence loss of Pten enhances HSPCs proliferation and arrests differentiation[17].

The past decades have led to an increase in our knowledge of hematopoiesis, but we are still far from a complete understanding of how HSPCs are established. Likewise, the role of Pten in steady-state hematopoiesis has been studied, but its potential role in the ontogeny

of HSPCs is not fully understood. We have addressed these questions in zebrafish larvae. We imaged the emergence of HSPCs from the VDA *in vivo* in *ptena*$^{-/-}$*ptenb*$^{-/-}$ embryos and in PI3K-inhibitor treated wild type embryos, which showed surprisingly similar defects. Furthermore, we performed single cell RNA sequencing (scRNA-seq) during the onset and at the end of the definitive wave. Our results indicate that elevated and reduced PI3K signaling had opposite effects on HSPCs at the end of the definitive wave.

Results

The onset of the definitive wave of hematopoiesis is independent of Pten

The onset of the definitive wave starts at 32 hours post fertilization (hpf) with the specification of endothelial cells that will become HSPCs in the floor of the dorsal aorta (DA) in the AGM region (Figure 1a), a conserved process between mammals and zebrafish[4–6]. *Runx1* expression from 32 hpf onwards and *c-myb* expression from 35 hpf onwards mark the hemogenic endothelium of the VDA and its HSPC progeny[8,18]. We found

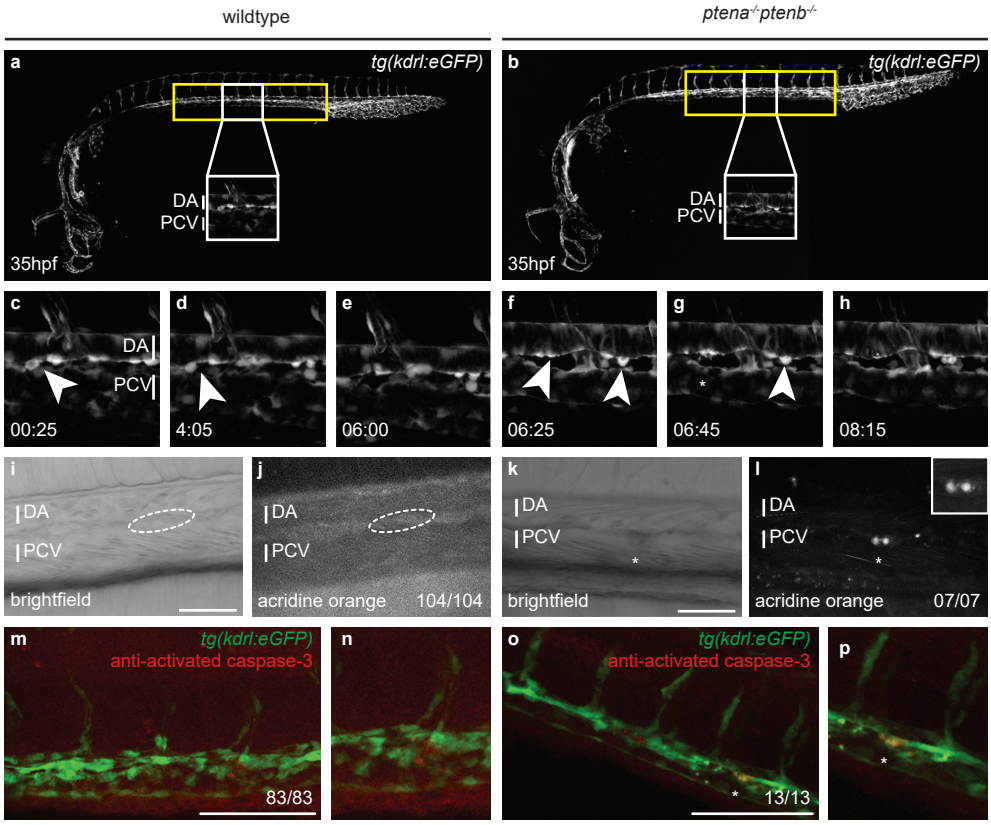

that *ptena*$^{-/-}$*ptenb*$^{-/-}$ mutant embryos expressed *runx1* and *c-myb* along the VDA during the period that HSPCs emerge (between 30 and 44 hpf) just like their siblings (Figure S1), indicating that loss of Pten does not affect the number of hemogenic endothelial cells.

Loss of Pten results in apoptosis of HSPCs during EHT in ptena-/-ptenb-/- mutant embryos.

In zebrafish, endothelial cells from the VDA transform into HSPCs in a process called EHT[6]. Subsequently, HSPCs join the blood flow in the underlying posterior cardinal vein (PCV) to transiently seed the CHT[4,6,8]. We monitored EHT events in the AGM by time-lapse confocal imaging of an area spanning two adjacent intersegmental vessels in the tg*(kdrl:eGFP)* transgenic background from 35 to 48 hpf (Figure 1a,b). The vasculature of *ptena*$^{-/-}$ *ptenb*$^{-/-}$ mutants and siblings was indistinguishable at this stage[19]. The floor of the aorta in *ptena*$^{-/-}$*ptenb*$^{-/-}$ mutant embryos displayed the characteristic contraction then bending of cells towards the subaortic space[6], indicating that the initiation of EHT was normal in *ptena*$^{-/-}$*ptenb*$^{-/-}$ mutant embryos. However, half of the EHT events in *ptena*$^{-/-}$*ptenb*$^{-/-}$ mutant embryos were abortive, in that 13 out of 24 HSPCs (54% in 9 embryos) failed to detach and disintegrated (Figure 1c-h, Movie S1). In contrast, siblings or wild type embryos did not display abortive EHT (n=75 in total). Live imaging using acridine orange[20] revealed apoptotic cells in the DA of *ptena*$^{-/-}$*ptenb*$^{-/-}$ mutant embryos, but not siblings (Figure 1i-l). Activated-caspase-3 immunostaining[21] confirmed apoptosis of *kdrl:eGFP*-positive cells at the VDA in *ptena*$^{-/-}$*ptenb*$^{-/-}$ mutant embryos (Figure 1m-p). Hence, about half of the HSPCs in *ptena*$^{-/-}$*ptenb*$^{-/-}$ mutant embryos failed to complete EHT and instead underwent apoptosis.

The number of HSPCs that colonize the CHT is reduced in ptena-/-ptenb-/- mutant embryos

Following EHT, HSPCs transiently colonize the CHT[8]. We generated a tg*(kdrl:Dendra2)* transgenic line. The Dendra2 protein along the entire VDA was photoconverted green-to-red between 26 and 28 hpf, *i.e.* before the onset of EHT events (Figure 2a). Photoconverted HSPCs in *ptena*$^{-/-}$*ptenb*$^{-/-}$ mutant embryos colonized the CHT between 50 and 60 hpf, albeit less HSPCs were detected than in the CHT of siblings (Figure 2 b,c). We quantified the number of HSPCs that colonized the CHT at 48 hpf, *i.e.* by the peak of HSPC emergence

Figure 1. A population of HSPCs fails to complete EHT and undergoes apoptosis in *ptena*$^{-/-}$*ptenb*$^{-/-}$ mutant embryos. (a, b) Brightfield image of a wild type or *ptena*$^{-/-}$*ptenb*$^{-/-}$ mutant zebrafish embryo at 35 hpf. The area from which HSPCs originate is indicated with a yellow box. A close up is indicated with a white box. (c-h) Four-dimensional imaging of *tg(kdrl:eGFP)* wild type or *ptena*$^{-/-}$*ptenb*$^{-/-}$ mutant embryos between 35 hpf and 48 hpf. Still frames from Movie S1. Arrowheads: HSPCs undergoing EHT; asterisk: disintegrating HSPCs. Confocal image z-stacks (2µm step size, with 40x objective and 2x zoom; anterior to the left; maximum projections of a representative embryo; time in hh: mm. (I-l) Acridine orange staining. Arrows and circles: HSPCs in VDA of 40-45 hpf embryos. Asterisks: apoptotic HSPCs. Scale bar: 50µm. Representative embryos are shown and the number of embryos that showed this pattern/total number of embryos is indicated. DA: dorsal aorta; PCV: posterior cardinal vein. (m-p) confocal images of apoptotic endothelial cells in the VDA of fixated wild type or *ptena*$^{-/-}$*ptenb*$^{-/-}$ mutant zebrafish embryos. In green: *tg(kdrl:eGFP)*; in red: anti-activated caspase-3 immunohistochemistry staining. Apoptotic cells are indicated with an asterisk. Representative embryos are shown and the number of embryos displaying this particular pattern/total number of embryos is indicated in the bottom right. Anterior to the left; 2µm step size; maximum projections; scale bar: 100µm.

from the VDA, using tg*(cd41:eGFP)* embryos, which express low GFP (GFP^{low}) in HSPCs[22,23]. Consistent with the initial apoptosis of half of the EHT derived HSPCs, 51% less GFP^{low} HSPCs were detected in the CHT of *ptena*$^{-/-}$*ptenb*$^{-/-}$ mutant embryos at 48 hpf compared to siblings (Figure 2d-f, Figure S2). When injected with *ptenb*-mRNA at the one-cell stage,

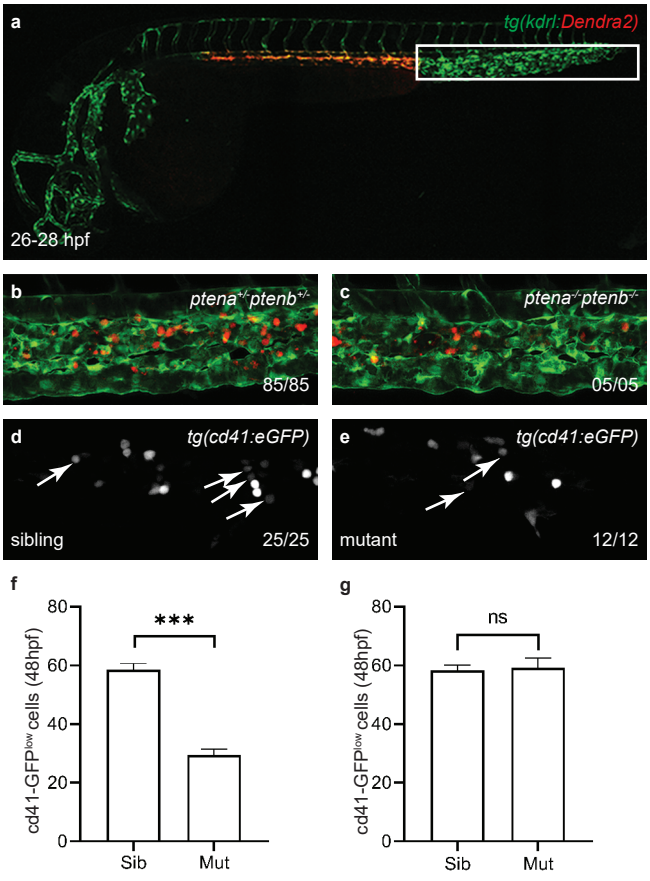

Figure 2. Less HSPCs colonize the CHT in *ptena*$^{-/-}$*ptenb*$^{-/-}$ mutant embryos than in wild type. (a) The VDA of *tg(kdrl:Dendra2)* was photoconverted green-to-red at 26-28 hpf. By 50-60 hpf red HSPCs derived from the photoconverted VDA had colonized the CHT in (b) sibling and (c) *ptena*$^{-/-}$*ptenb*$^{-/-}$ larvae. (d) The number of GFP^{low} HSPCs at 48 hpf in the CHT of *tg(cd41:eGFP)* siblings (sib)(n=25) (e) and *ptena*$^{-/-}$*ptenb*$^{-/-}$ mutants (mut) (n=12) (f) is expressed as average number of cells in siblings (n=41) or *ptena*$^{-/-}$*ptenb*$^{-/-}$. mutants (n=18). (g) is expressed as average number of cells in siblings (n=33) or *ptena*$^{-/-}$*ptenb*$^{-/-}$ mutants after injection with synthetic *ptenb* mRNA (n=15). Error bars indicate standard error or the mean (SEM). Shapiro Wilk Test for normal distribution and Welch's two-tailed t-test were used for statistical analysis; ***p<0.001. Representative embryos are shown and the number of embryos that showed this pattern/total number of embryos is indicated.

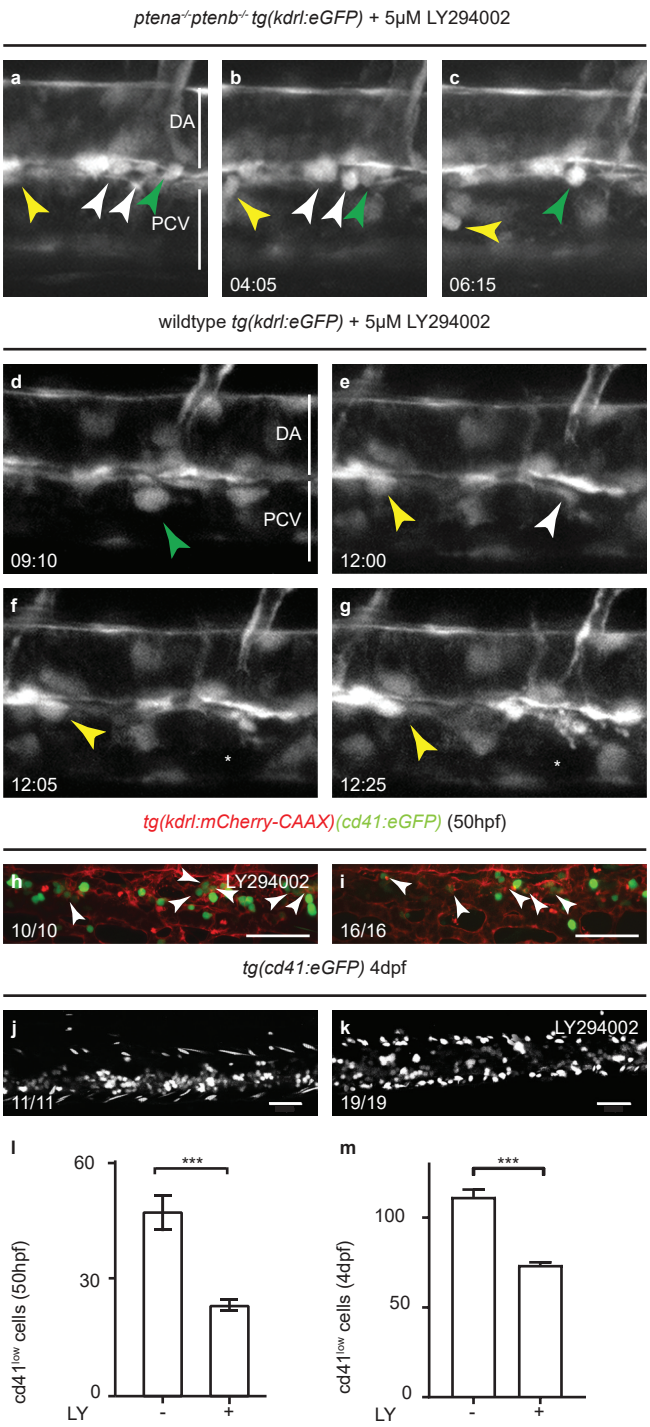

Figure 3. Inhibition of PI3K rescued EHT in *ptena*$^{-/-}$ *ptenb*$^{-/-}$ mutant embryos, but induced abortive EHT in wild type embryos. (a-g) Four-dimensional imaging of *tg(kdrl:eGFP)* transgenic embryos. (a-c) *ptena*$^{-/-}$*ptenb*$^{-/-}$ mutant embryos and (d-g) wild type embryos. Imaging was done from 35 hpf onwards following treatment with 5 μM LY294002 from 32 hpf. Still frames from movie S3 (a-c) and movie S4 (d-g). arrowheads: HSPCs. Asterisks: disintegrating HSPCs. Different colors of arrowheads distinguish separate EHT events. Images were taken with 40x objective and 1x zoom. Time in hh:mm; DA: dorsal aorta; PCV: posterior cardinal vein. (h, i) CHTs of *tg(kdrl:mCherry-CAAX/ cd41:eGFP)* control (n=10) and LY294002 treated (5 μM, 32-50 hpf) (n=16) embryos were imaged at 50 hpf. The vasculature is highlighted in red (mCherry) and some GFP^{low} HSPCs are indicated by arrows. (j-k) CHTs of tg(cd41:eGFP) control(n=11) and LY294002-treated (5μM, 30-60 hpf) (n=19) embryos were imaged at 4 dpf. Anterior to the left; 2 μm step size. Representative embryos are shown and the number of embryos that showed this pattern/ total number of embryos is indicated. (l-m) the number of GFP^{low} HSPCs was determined at 50 hpf (l) and 4 dpf (m) and is expressed as average number of cells; error bars indicate standard error of the mean (SEM). Shapiro Wilk Test for normal distribution and Welch's two-tailed t-test were used for statistical analysis; *** p<0.001.

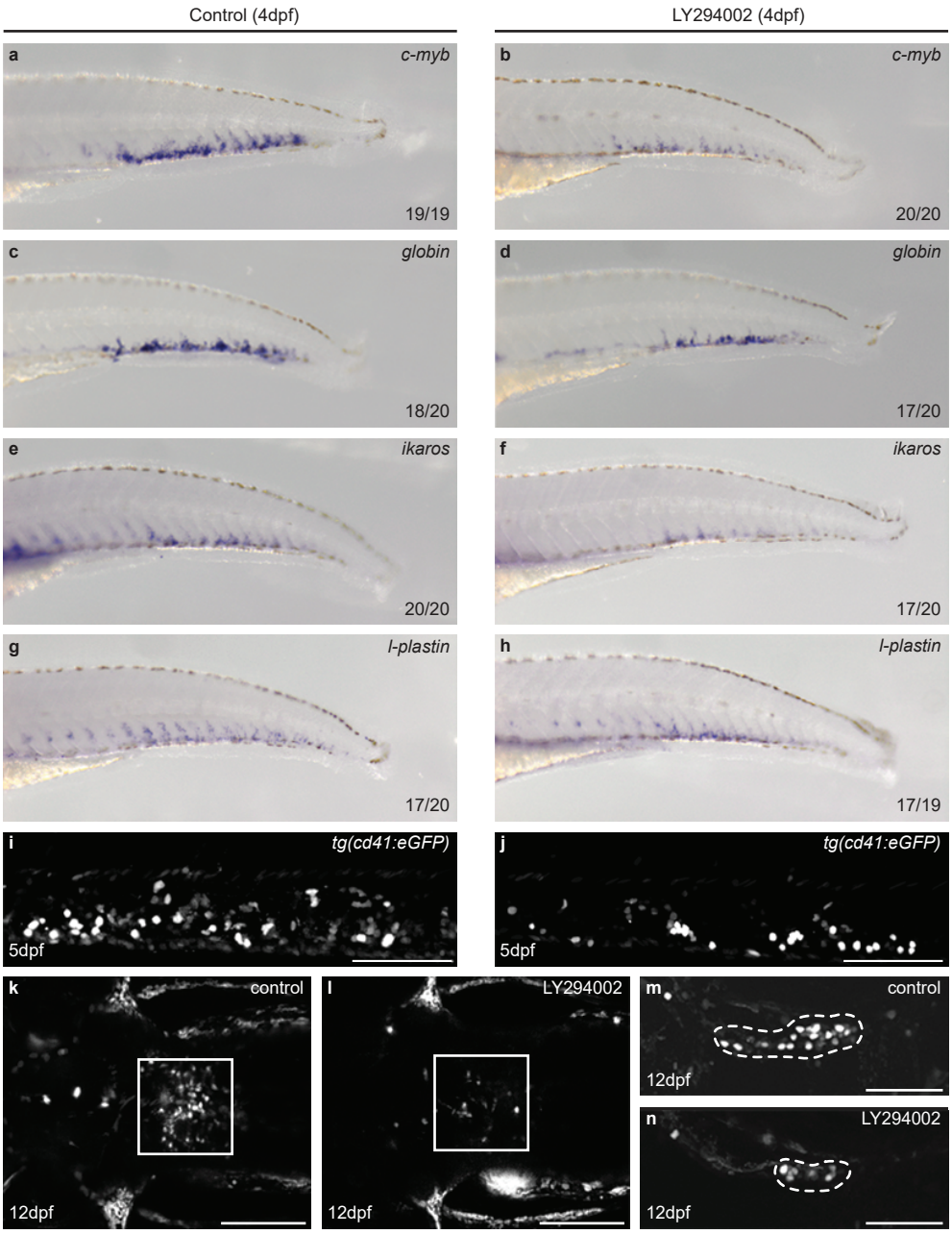

Figure 4. HSPCs of LY294002-treated embryos engage in all blood lineages, but show impaired colonization of definitive hematopoietic organs. (a-h) Control and LY294002-treated (from 32-60 hpf) embryos were fixed at 4 dpf. Markers for definitive blood lineages were assessed by *in situ* hybridization in the CHT: *c-myb* (HSPCs; a,b), *globin* (erythrocyte lineage; c,d), *ikaros* (lymphocyte lineage; e,f), *l-plastin* (leukocytes; g,h). Representative embryos are shown, with anterior to the left. The number of embryos that showed a particular pattern/total number of embryos is indicated in the bottom right corner of each panel. (i-j) GFP^{high} thrombocytes were imaged

ptena$^{-/-}$*ptenb*$^{-/-}$ mutant embryos did no longer show a significant loss of HSPCs compared to their siblings (Figure 2g), indicating that the observed defects indeed were caused by loss of functional Pten.

PI3K inhibition rescues EHT events in ptena$^{-/-}$*ptenb*$^{-/-}$ *mutant embryos but is detrimental for HSPCs in wild type embryos.*

To address whether apoptosis of half of the EHT-derived HSPCs was due to enhanced PI3K signaling, embryos were treated with the PI3K inhibitor LY294002 from the onset of EHT (32 hpf) onwards. Inhibition of PI3K prevented apoptosis of HSPCs in *ptena*$^{-/-}$*ptenb*$^{-/-}$ mutant embryos, in that none of the HSPCs that we imaged disintegrated (table 1) (Fisher's exact test, p=0.0013) (Figure 3a-c). Surprisingly, in wild type and sibling embryos that were treated with LY294002 in parallel with the *ptena*$^{-/-}$*ptenb*$^{-/-}$ mutant embryos, disintegrating HSPCs in the VDA were observed (n=6) (Figure 3d-g, Movie S2) (Fisher's exact test, p=0.021).

			HSPCs			
		embryos (n)	apoptosis	escapers	% apoptosis	%escapers
Wildtype	control	13	0	24	0	100
	LY294002	6	6	9	40	60
ptena$^{-/-}$ *ptenb*$^{-/-}$	control	9	13	11	54	46
	LY294002	5	0	21	0	100

Table 1. Number of apoptotic cells during EHT. The number of cells undergoing apoptosis during EHT was determined in control and LY294002 (5µM from 32 hpf onwards) treated wild type and *ptena*$^{-/-}$*ptenb*$^{-/-}$ embryos (35-48 hpf) by confocal time lapse imaging. The number of embryos that was imaged is given as well as the number of apoptotic HSPCs or surviving HSPCs. The percentages of emerging or apoptotic HSPCs, relative to the total number of HSPCs are also indicated.

Consistent with abortive EHT events upon LY294002 treatment, significantly less GFP^{low} HSPCs in *tg(cd41:eGFP)* transgenic embryos colonized the CHT of LY294002-treated wild type embryos at 50 hpf (Figure 3h-i,l), comparable to the reduction observed in *ptena-/-ptenb-/-* mutant embryos (Figure 2d). This reduction of HSPCs persisted through 4 dpf in LY294002-treated embryos (Figure 3j-k,m). These data suggest that normal, *i.e.* not too high and not too low PI3K activity levels are essential for emergence of HSPCs.

at 5dpf in *tg(cd41:eGFP)* embryos. Scale bar: 100µm. (k-n) High-resolution imaging at 12 dpf of kidney (l, m, dorsal view) (control, n=6; LY294002-treated, n=8; 4 µm step size) and thymus (n, o, lateral view) (control, n=6; LY294002-treated, n=7; 2 µm step size). Anterior to the left; maximum projections of representative larvae. Scale bar: 100 µm.

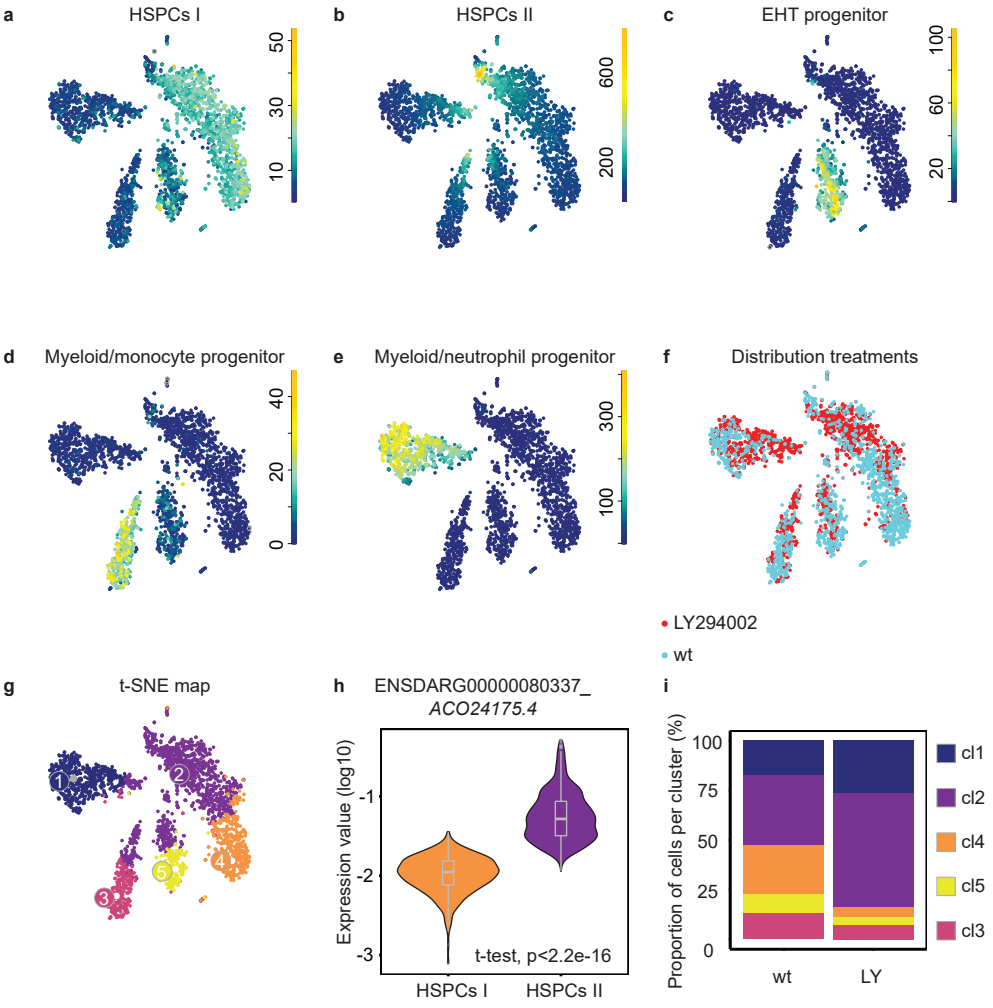

Figure 5. scRNA-seq reveals two types of HSPCs, one of which is lost upon inhibition of the PI3K-pathway. Tissue from control and LY294002-treated embryos (~2,000 each) was dissected, the AGM regions pooled, dissociated and FACS sorted, after which the SORT-seq protocol was performed. (a-e) t-SNE maps highlighting the expression of marker genes for each of the different cell types found. Transcript counts are given in a linear scale. (a) HSPCs I, (b) HSPCs II, (c) EHT progenitor, (d) Myeloid/monocyte progenitors, (e) Myeloid/neutrophil progenitors. (f) t-SNE map highlighting the distribution of cells from LY294002-treated embryos and their controls (g). Visualization of k-medoid clustering and cell-to-cell distances using t-SNEs. Each dot represents a single cell. Colors and numbers indicate cluster and correspond to colors in (i). The distribution of in total 2,512 cells over the five clusters are shown as percentage of total for control and LY294002-treated embryos. Fisher's Exact test with multiple testing correction (Fdr) were used for statistical analysis. *** p<0.001. cl1: Myeloid/neutrophil progenitor, cl2: HSPC II, cl3: myeloid/monocyte progenitor, cl4: HSPC I, cl5: EHT progenitor.(h) normalized expression level of ENSDARG00000080337_*ACO24175.4* for HSPC I and HSPC II cluster using violin plots. Normalized expression is plotted on a log10 scale.

PI3K inhibition in wild type embryos results in HSPCs that engage in all blood lineages

In situ hybridization was performed using a panel of blood progenitor markers. LY294002-treatment reduced expression of the HSPC marker *c-myb* at 4 dpf (Figure 4 a,b). The lineage markers *globin* (erythroid lineage), *ikaros* (lymphoid lineage) and *l-plastin* (pan-leukocytic, including myeloid lineage) were expressed, but reduced in LY294002-treated larvae compared to controls (Figure 4c-h). LY294002-treated HSPCs also committed to the thrombocytic lineage as demonstrated by GFP^{high} cells in tg*(cd41:eGFP)* embryos at 5 dpf[23] (Figure 4i,j). The number of GFP^{low} cells in the definitive hematopoietic organs, thymus and kidney of 8 and 12 dpf *tg(cd41:eGFP)* larvae was reduced in response to LY294002 (Figure 4k-n). These results show that reduced PI3K signaling did not block specification of particular blood lineages, but that the reduction in HSPC numbers affected founding of the definitive hematopoietic organs by HSPCs.

Singe cell RNA sequencing reveals two types of HSPCs, one of which is preferentially lost upon inhibition of the PI3K-pathway.

To investigate transcriptomic changes in HSPCs between LY294002-treated embryos and their controls during EHT, we performed scRNA-seq. Transgenic tg*(kdrl:mCherry-CAAX/ cd41:eGFP)* embryos were treated with LY294002 and AGM regions were isolated by dissection at 36 hpf. The AGM regions of approximately 2000 control embryos were pooled and likewise, 2000 LY294002-treated embryos. The cells were dissociated and sorted for $mCherry^{+}$/ $eGFP^{low}$ using FACS, after which the SORT-Seq protocol was performed[24] (Figure S3). Isolation of 3,219 cells in total, *i.e*. less than one $kdrl^{+}/cd41^{low}$ ($mCherry^{+}/GFP^{low}$) HSPC per embryo, was in line with earlier reports (3 HSPCs per embryo per hour[6,25]). After FACS filtering, 2512 cells remained. RaceID3[26] was used for differential gene expression analysis and clustering of the cells (Figure 5). The resulting t-SNE map highlighted particular cell types, in line with recent scRNA-seq studies of hematopoietic organs of zebrafish[27–34], which expressed validated hematopoietic lineage markers (Table S1). Cells in cluster 2 and 4 expressed HSPC-related genes, such as *gata2b, gfi1aa, meis1b, myb* and *pmp22b,* consistent with expression in mammalian HSCs and zebrafish HSPCs[27,29–33] (Figure 5a,b). RaceID3 subdivided the main HSPC cluster into two, HSPCs I and HSPCs II. Expression of *ENSDARG00000080337_ACO24175.4* and *tmed1b* was higher in the HSPCs II cluster (cl2) than the HSPCs I cluster (cl4) (Figure 5h, S3) and the expression of several other genes was also significantly different between these clusters (Figure S4). Cells in cluster 5 expressed endothelial transcripts, that are known to be involved in the EHT-process (*cdh5*[35,36]*, adgrg1*[28,37]*)*, indicating an EHT-progenitor lineage (Figure 5c, S3). Signature genes *mpx, lyz, marco,* and *mfap4* were expressed in cluster 1 and 3[38], indicating a myeloid/neutrophil- and myeloid/monocyte- progenitor lineage, respectively (Figure 5d,e, S3). All markers that were used to identify clusters are listed in Table S1 and the distribution of expression of selected markers is depicted in Figure S5.

Cells from LY294002-treated embryos had an uneven distribution over all clusters. In HSPCs II and myeloid/neutrophil progenitors, cells from LY294002-treated embryos were overrepresented compared to control embryos (Fisher's Exact test, $p<0.001$). In HSPCs I, EHT- and myeloid/monocyte progenitors, cells from LY294002-treated embryos were underrepresented (Fisher's Exact test, $p<0.001$) (Figure 5f,i). These data indicate that

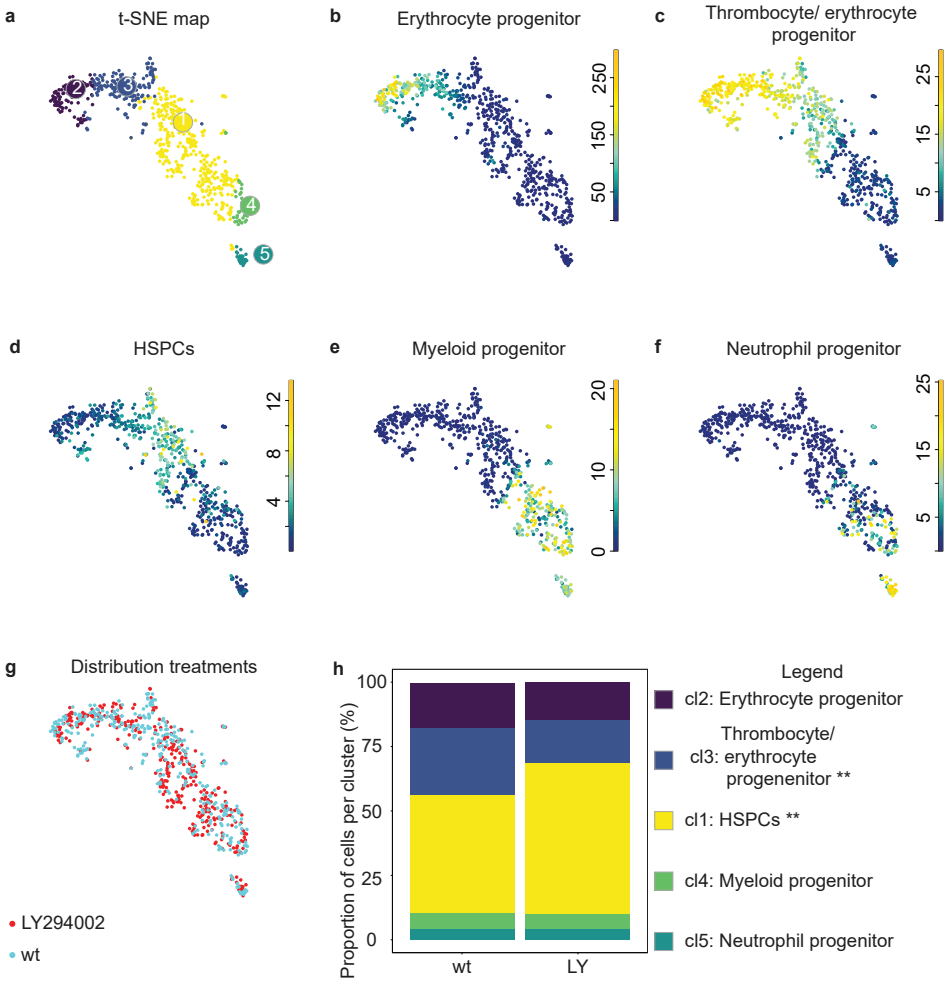

Figure 6. ScRNA-seq seq reveals a shift towards HSPCs in LY294002-treated 5dpf old embryos. CHTs of control and LY294002-treated embryos (5 dpf, ~100 embryos each) were dissected, pooled, dissociated, FACS-sorted and submitted to SORT-seq. (a) Visualization of k-medoid clustering and cell-to-cell distances using t-SNEs. Each dot represents a single cell. Colors and numbers indicate cluster and correspond to colors in (h). In total 684 cells are shown. (b-f) t-SNEs maps highlighting the expression of marker genes for each of the different cell types found. Transcript counts are given in a linear scale. (b) Erythrocyte progenitors, (c), Thrombocyte/erythrocyte progenitors, (d) HSPCs, (e) Myeloid progenitors, (f) Neutrophil progenitors. (g) t-SNE map highlighting the distribution of LY294002-treated embryos and their controls (h). The percentage of cells from LY294002-treated embryos and their controls in the different clusters. Fisher's Exact test with multiple testing correction (Fdr) were used for statistical analysis. ** p<0.01, *** p<0.001.

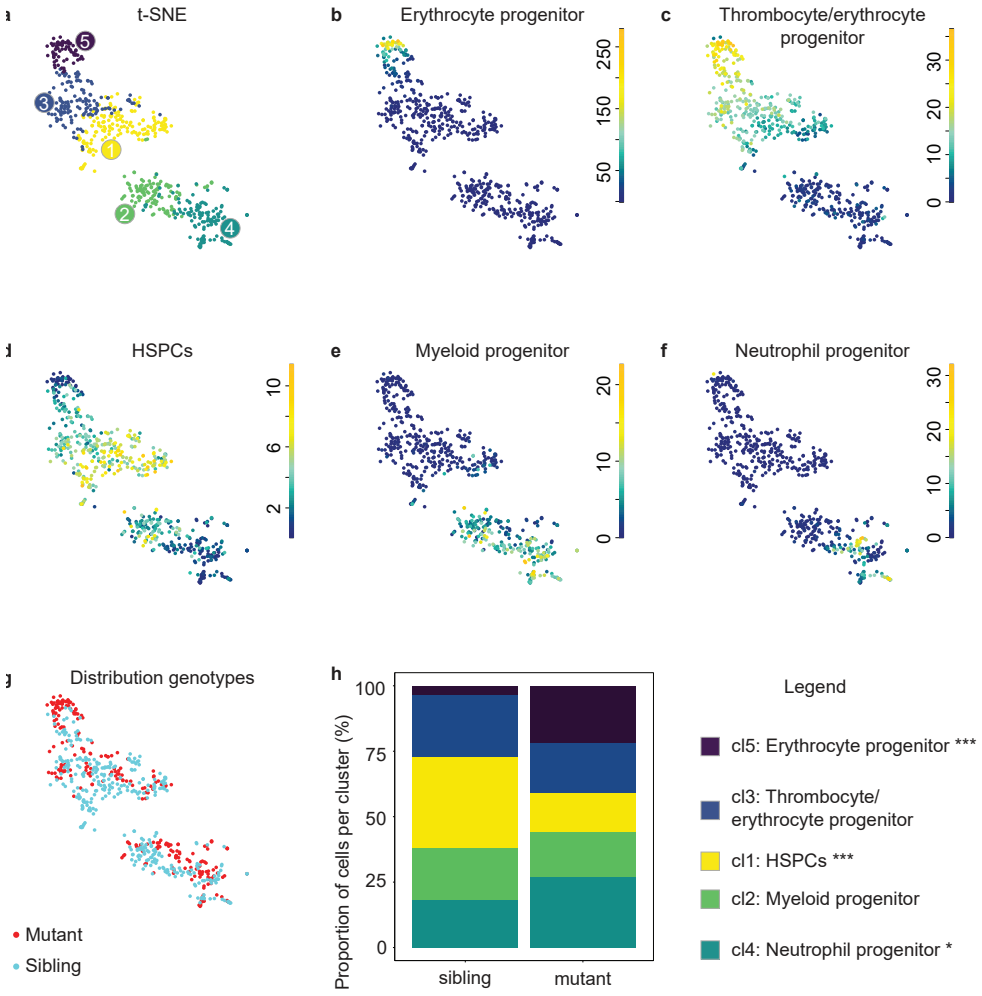

Figure 7. ScRNA-seq seq reveals a shift towards more differentiated cell types in 5 dpf old *ptena*$^{-/-}$*ptenb*$^{-/-}$ mutant embryos. CHTs of control and *ptena*$^{-/-}$*ptenb*$^{-/-}$ mutant embryos (5 dpf, ~100 embryos each) were dissected, pooled, dissociated, FACS-sorted and submitted to SORT-seq. (a) Visualization of k-medoid clustering and cell-to-cells distances using t-SNEs. Each dot represents a single cell. Colors and numbers indicate cluster and correspond to colors in (h). In total 614 cells are shown. (b-f) t-SNEs maps highlighting the expression of marker genes for each of the different cell types found. Transcript counts are given in a linear scale. (b) Erythrocyte progenitors, (c), Thrombocyte/erythrocyte progenitor, (d) HSPCs, (e) Myeloid progenitors, (f) Neutrophil progenitors. (g) t-SNE map highlighting the distribution of *ptena*$^{-/-}$*ptenb*$^{-/-}$ mutant embryos and their siblings. (h). The percentages of cells from *ptena*$^{-/-}$*ptenb*$^{-/-}$ mutant embryos and their siblings in the different clusters. Fisher's Exact test with multiple testing correction (Fdr) were used for statistical analysis. * p<0.05, *** p<0.001.

LY294002-treatment led predominantly to loss of cells from HSPCs I cluster, which is consistent with the imaging data where half of the HSPCs fail to complete EHT (Figure 3d-g). The loss of HSPCs I in response to PI3K inhibition is accompanied by an increase in HSPCs II and myeloid/neutrophil progenitors.

More HSPCs upon inhibition of PI3K and less HSPCs in pten mutants

The CHTs of approximately 100 control and 100 LY294002-treated embryos were processed for scRNA-seq. Of the 928 cd41^{low} cells that were analyzed, 684 remained after filtering. RaceID3 separated the cells in distinct clusters (Figure 6a). Cells in cluster 2 expressed erythrocyte progenitor-related genes (*hbbe2, alas2* and *cahz*) (Figure 6b). Cluster 3 is characterized by cells expressing genes related to thrombocyte/erythrocyte progenitors (*gata1a, klf1*[27,38,39]) (Figure 6c). Cells in cluster 1 express genes indicative of HSPCs, including *c-myb* (Figure 6d). Cluster 4 represents early myeloid progenitors, as *runx3, pu.1 (*also known as *spi1b)* and *cebpb*[38] are highly expressed (figure 6e). Cluster 5 is characterized by neutrophil progenitor-related gene expression (*mpx)* (figure 6f). Analysis of the distribution of hematopoietic cells, using a Fisher's exact test indicated that the thrombocyte/erythrocyte progenitor cells were underrepresented in the LY294002-treated embryos ($p<0.01$) and HSPCs were significantly overrepresented ($p<0.001$) (Figure 6g,h). These results indicate a significant shift towards HSPCs at the expense of the thrombocyte/erythrocyte progenitor cluster in response to LY294002 treatment.

Likewise, we assessed transcriptomic differences by scRNA-seq in HSPCs from the CHT between *ptena*$^{-/-}$*ptenb*$^{-/-}$ mutant embryos and their siblings at 5 dpf. Approximately 100 *ptena*$^{-/-}$*ptenb*$^{-/-}$ mutant embryos and siblings were selected based on phenotype[15], which yielded 614 cd41^{low} cells after filtering. RaceID3 indicated that clusters emerged representing the same hematopoietic lineages as described for the wild type and LY294002- treated data (cf. Figure 6 and 7). Analysis of the distribution of hematopoietic cells from *pten* mutants and their siblings over the five clusters indicated that the erythrocyte- and neutrophil progenitor cells were overrepresented in the pten mutant ($p<0.001$ and $p<0.05$) and that HSPCs were significantly underrepresented ($p<0.001$)(Figure 7g-h, S6). These results indicate a significant shift in *ptena*$^{-/-}$*ptenb*$^{-/-}$ mutant embryos towards erythrocyte progenitor and neutrophil progenitors at the expense of HSPCs.

Discussion

We used zebrafish mutant embryos lacking functional Pten to investigate how loss of Pten affects the ontogeny of hematopoiesis. Characterization of zebrafish *ptena*$^{-/-}$*ptenb*$^{-/-}$ mutant embryos led to the unexpected finding that half of the HSPCs undergo apoptosis upon emergence from the VDA during EHT at the onset of the definitive wave (Figure 1). Loss of function of Pten is usually linked to enhanced cell survival, such as for instance in *Pten* knock-out mice[40]. We reported that ɣ-irradiation reduces apoptosis in *ptena*$^{-/-}$*ptenb*$^{-/-}$ mutant embryos[15]. Apoptosis of zebrafish HSPCs has been reported before, in that *grechetto* mutants display decreasing numbers of HSPCs due to apoptosis[35].

Runx1 knockdown also induced abortive EHT events due to apotosis[6]. *Runx1* expression was not affected in the VDA of *ptena*$^{-/-}$*ptenb*$^{-/-}$ mutants (Figure S1), suggesting that the mechanism underlying EHT defects in *ptena*$^{-/-}$*ptenb*$^{-/-}$ mutant embryos and Runx1 morphants are distinct. Apoptosis of HSPCs in *pten* mutants is due to enhanced PI3K-mediated signaling, because treatment with a PI3K inhibitor rescued apoptosis of HSPCs. Surprisingly, treatment of wild type embryos with the PI3K inhibitor induced death of half of the HSPCs upon emergence from the VDA as well (Figure 3). These results suggest that upon emergence from the VDA, HSPCs require a moderate level of PI3K signaling, as hyperactivation of PI3K signaling in Pten mutants as well as inhibition of PI3K signaling induced apoptosis of emerging HSPCs.

After emerging from the VDA, the surviving HSPCs enter circulation and seed the CHT, as demonstrated by photoconversion of endothelial cells prior to EHT in *ptena*$^{-/-}$*ptenb*$^{-/-}$ mutant embryos and siblings (Figure 2). Half of the HSPCs of *ptena*$^{-/-}$*ptenb*$^{-/-}$ mutant embryos and LY294002-treated embryos colonized the CHT, compared to wild type embryos (Figure 2,3, Table 1). In LY294002-treated embryos the decrease in HSPCs remained, whereas in *ptena*$^{-/-}$*ptenb*$^{-/-}$ mutant embryos the surviving HSPCs hyperproliferate leading to an increase in HSPCs at later stages[17]. Surviving HSPCs from *ptena*$^{-/-}$*ptenb*$^{-/-}$ mutants engage in all blood lineages[17]. However, definitive differentiation of major blood lineages is arrested in the *ptena*$^{-/-}$*ptenb*$^{-/-}$ mutants, consistent with the inverse correlation of proliferation and differentiation of stem cells[41]. The surviving HSPCs of LY294002-treated embryos also engaged in all blood lineages (Figure 4), demonstrating pluripotency of the HSPCs.

Using scRNA-seq at the onset of the definitive wave (36hpf) of hematopoiesis two HSPC clusters were identified, that both expressed HSPC markers. In control embryos equal numbers of cells populated the HSPCs I and HSPCs II clusters. Predominantly the cells from the HSPCs I cluster were lost upon PI3K-inhibition (Figure 5). Our imaging data indicated that half of the HSPCs disintegrated upon treatment with LY294002 (Figure 3). It is tempting to speculate that the surviving half of the HSPCs all belong to the HSPCs II cluster. Whereas both HSPCs clusters expressed HSPC markers, several genes are significantly differentially expressed (Figure S4), albeit subtle. Expression of ENSDARG00000080337_*ACO24175.4* and to a lesser extent *tmed1b* distinguished the HSPCs II cluster from the HSPCs I cluster. *In situ* hybridization using an ENSDARG00000080337_*ACO24175.4*-specific probe indicated high expression throughout the embryo, which did not allow validation of the difference in expression in HSPCs I and HSPCs II cells (Figure S3). Little is known about ENSDARG00000080337_*ACO24175.4*, except that it is a mitochondrial ribosomal gene (mt rDNA). Interestingly, HSCs have significantly lower rates of protein synthesis than other hematopoietic cells[42]. The protein product of ENSDARG00000080337_*ACO24175.4* may have a role in protein synthesis. Hence, the difference in expression levels may indicate that the HSPCs II cells that survive PI3K-inhibition are less stem cell-like and more progenitor-like, poised to differentiate.

In response to LY294002-treatment the number of cd41^{low} HSPCs was reduced in the CHT at 4 dpf and in the definitive hematopoietic organs at 8 and 12 dpf (Figure 3,4). scRNA-seq of putative HSPCs (cd41^{low}, kdrl^{+} cells) at the end of the definitive wave (5dpf) indicated initiation of differentiation in different blood lineages (Figure 6), consistent with *in situ*

hybridization (Figure 4). Yet, inhibition of PI3K arrested differentiation, i.e. increased HSPC fate, predominantly at the expense of thrombocyte/erythrocyte progenitor fate (Figure 6). Overall, it is evident that there is a significant reduction in hematopoietic cell number (Figure 4, 6), which may be caused by preferential loss of HSPCs with more stem cell-like properties (Figure 5).

ScRNA-seq at the end of the definitive wave showed a significant increase in erythrocyte- and neutrophil- progenitors in *ptena*$^{-/-}$*ptenb*$^{-/-}$ mutant embryos (Figure 7, S6), consistent with earlier *in vivo* data[17]. However, we reported an overall increase in HSPCs, due to hyperproliferation, whereas here, we observed a decrease in HSPCs in the scRNA-seq data. An explanation for this apparent discrepancy is that the hyperproliferating HPSCs we observed earlier[17] actually have initiated differentiation already and are scored as erythrocyte and neutrophil progenitors by scRNA-seq.

Conditional knock-out of *Pten* in HSCs in mouse adult bone marrow, drives HSCs into the cell cycle, resulting in transient expansion of the spleen and eventually in depletion of HSCs in the bone marrow. These conditional PTEN-deficient mice die of a myeloproliferative disorder that resembles acute myeloid/lymphoid leukemia, indicating that PTEN is required for maintenance of HSCs[13,14]. It is noteworthy that there are differences between the conditional mouse models and the zebrafish model we used. In the mouse, Pten is deleted in adult bone marrow cells, well after HSCs have formed, whereas in zebrafish, Pten is systemically deleted and therefore effective prior to the emergence of HSPCs. Studies in mice showed that regardless of cell state, HSCs and multi-potent progenitors had a lower protein synthesis rate than more restricted hematopoietic progenitors. Loss of PTEN in HSCs caused depletion of HSCs, due to a higher rate of protein synthesis[42], which is consistent with our observation that loss of Pten in zebrafish caused HSPCs to hyperproliferate and become less stem-cell like.

Long-term HSCs are quiescent, whereas short-term HSCs proliferate more[2]. It would be tempting to speculate that the HSPCs that undergo apoptosis upon loss of Pten or upon PI3K-inhibition are involved in long-term colonization of definitive hematopoietic organs. The surviving HSPCs in *pten* mutants at the onset of the definitive wave would then represent multi-potent progenitors that only have limited potential for self-renewal. Investigating the regulatory network underlying the surviving and disintegrating HSPCs will further expand our understanding of short- and long-lived HSPCs and will eventually contribute to the development of efficient stem cell based therapies[43,44].

Methods

Ethics statement

All animal experiments described in this manuscript were approved by the local animal experiments committee (Hubrecht Institute: Koninklijke Nederlandse Akademie van Wetenschappen-Dierexperimenten commissie protocol HI180701 and University Montpellier: Direction Sanitaire et Vétérinaire de l'Hérault and Comité d'Ethique pour l'Expérimentation Animale under reference CEEA-LR-13007) and performed according to local guidelines and policies in compliance with national and European law.

Zebrafish husbandry

Ptena$^{-/-}$*ptenb*$^{-/-}$*, ptena*$^{-/-}$*, ptenb*$^{-/-}$[15] *, Tg(kdrl:eGFP)*[45] *, Tg(kdrl:mCherry-CAAX)*[46]*,* and *Tg(cd41:eGFP)*[23] were maintained according to FELASA guidelines, crossed, raised and staged as described[47–49]. *Pten* mutant fish (embryos) were genotyped by sequencing[15]. The *tg(kdrl:Dendra2)* line was derived by Tol2-mediated transgenesis[50] of a construct containing the ~7.0kb *kdrl*-promoter (a kind gift from D. Stainier), driving the expression of Dendra2[51]. From 24hpf onwards, all embryos were grown in PTU-containing medium to block pigmentation.

LY294002 treatment

Embryos were treated with 5 µM LY294002 (Calbiochem, San Diego, CA, USA) or DMSO control in the dark. For early treatment, embryos were incubated with LY294002 from 32 hpf onwards and mounted after 4 hours for time-lapse confocal imaging. For late treatment and to investigate thymus and kidney colonization, embryos were treated with 5 µM LY294002 from 32 to 60 hpf and imaged.

Constructs, mRNA synthesis and microinjections

The Ptenb-mCherry fusion construct in the vector pCS2+ was obtained as described in [15,52] and linearized with NotI. To synthesize 5' capped sense mRNA, the mMessage mMachine SP6 kit (Ambion) was used. mRNA injections were performed at the one-cell stage using a total of 300 pg of mRNA.

Confocal, fluorescence, brightfield microscopy and time-lapse imaging

Fluorescence images of transgenic embryos were acquired using TCS-SPE and time-lapse imaging using TCS-SP2 as described[53] and processed with ImageJ[54]. For all live imaging embryos were anesthetized with tricaine[49], mounted on a glass cover dish with 0.7% low melting agarose and covered with standard E3 medium. Whole mount bright field images were taken with a Leica DC 300F stereomicroscope.

In situ hybridization

Whole mount *in situ* hybridization was performed according to standard protocols[55] and images were taken using a Zeiss Axioplan microscope connected to a Leica DFC480 camera.

Acridine orange staining and whole mount immunohistochemistry

Embryos were incubated with 5 µg/ml acridine orange[20] for 20 minutes between 35 and 40 hpf and subsequently washed with standard E3 medium. Embryos were then imaged as described above. Immunohistochemical labeling performed using fixed (40 hpf) embryos to detect apoptosis using an activated caspase-3-specific antibody (BD Pharmingen)[21]. After confocal images were collected embryos were genotyped.

Photoconversion

Fluorescent tracing of VDA-derived HSPCs colonizing the CHT was done using the *tg(kdrl:Dendra2)* line as described before[56,57] with a Leica SP5 confocal microscope with a 20x dry objective. At 28 hpf an area of approximately 40x750 nm around the VDA, parallel to the yolk sac extension was photoconverted. The 405nm UV laser intensity and exposure time were optimized for strong Dendra2-conversion without cell damage. After photoconversion embryos were transferred to E3 medium and at 50-60 hpf their CHT areas were imaged on a Leica SPE Live confocal microscope using a 20x dry objective. To exclude bleed-through of Dendra-green, red channel detection was set stringently (630-680nm).

Quantification of GFP^{low} progenitor cells using tg(cd41:eGFP)

GFP^{low} and GFP^{high} expressing cells were quantified in the CHT at 48 hpf ,50 hpf or 4 dpf using confocal imaging and Volocity and Imaris software. *Ptena$^{+/-}$ptenb$^{-/-}$* mutants on *tg(cd41:eGFP)* background were crossed and offspring was mounted at 48 hpf. Wild type *tg(cd41:eGFP)* embryos were treated with 5 µM LY294002 as described above and mounted and imaged at 50 hpf or 4 dpf. All GFP^{low} expressing cells were counted in the entire CHT.

Flow cytometry

The aorta-gonad-mesonephros (AGM) of approximately 4000 36 hpf and 400 CHTs of 5 dpf old *tg(kdrl:mCherry/cd41:eGFP)* embryos were dissected and collected in Leibovitz-medium. After washing with phosphate-buffered saline the AGMs were deyolked using calcium-free Ringer's solution (116mM NaCl, 2.9mM KCl and 5mM HEPES) and then AGMs and CHTs were dissociated in TrypLE Express (Gibco) for 45 minutes at 32°C. The resulting cell suspension was washed in phosphate-buffered saline and passed through a 40-µm filter after resuspension in phosphate-buffered saline supplemented with 2mM ethylenediaminetetraacetic acid, 2% fetal calf serum and 0.5µg/ml 4',6-diamidino-2-phenylindole (DAPI), to exclude dead cells. Cells with kdrl- and cd41^{low}-positive signal were subjected to fluorescence-activated cell sorting (FACS) using a BD FACSAriaII and BD FACSFusion.

ScRNA-seq with SORT-seq

ScRNA-seq was performed by Single Cell Discoveries BV (Utrecht, the Netherlands), according to an adapted version of the SORT-seq protocol[24,58], with adapted primers described in[59].

Data analysis

During sequencing, Read1 used for identification of the Ilumina library barcode, cell barcode and UMI. Read2 was used to map to the reference transcriptome of Zv9 *Danio rerio*. Data was demultiplexed as described[60]. Single cell transcriptomics analysis was done using the RaceID3 algorithm, following an adapted version of the RaceID manual (https://cran.r-project.org/web/packages/RaceID/vignettes/RaceID.html). Cells that had less than 1500 UMIs and genes that were detected in less than 5 UMIs in 5 cells were discarded. The number of initial clusters was set at 5. Differential gene expression analysis was done as described in[24] with an adapted version of the DESseq2 algorithm[61].

Data sharing statement

For original data, please contact j.denhertog@hubrecht.eu.

scRNA data are available at GEO under accession number GSE166900

Acknowledgements

The authors would like to thank Mark Reijnen and animal caretakers for excellent management of the fish facility. Microscopy was done in the Hubrecht Imaging Centre. The authors would like to thank Stefan van der Elst and Reinier van der Linden for FACS-sorting. The authors would like to thank Jeroen Paardekooper Overman for statistical analysis, Laila Ritsma, Sylvain de Rossi and Miriam Stumpf for technical support and Bas Castelijns for help with scRNA data analysis. This work was supported in part by an EU (FP7) grant, ZF-CANCER (HEALTH-F2-2008-201439).

Conflict of interest disclosure

There is no conflicting interest to disclose

Authorship

S.B.F, S.C. and J.d.H. designed experiments with input from K.K. and P.H.; S.B.F and S.C.

performed the experiments; B.P. and S.S.M. generated the Tg(kdrl:Dendra) line and helped perform the photoconversion experiments; K.K. and J.d.H. supervised the work; S.B.F, S.C., P.H., K.K. and J.d.H. wrote the manuscript.

Correspondence and requests for materials should be addressed to: Jeroen den Hertog, Hubrecht Institute, Uppsalalaan 8, 3584 CT Utrecht, the Netherlands, e-mail: j.denhertog@hubrecht.eu.

Supplementary table 2 can be found in its entirety at https://www.nature.com/articles/s41388-021-01733-5. Upregulated genes per clusters for the different datasets.

References

1. Kondo, M. *et al.* Biology of Hematopoietic stem cells and progenitors: implication for clinical application. *Annu. Rev. Immunol.* **21**, 759–806 (2003).
2. Orkin, S. H. & Zon, L. I. Hematopoiesis: An Evolving Paradigm for Stem Cell Biology. *Cell* **132**, 631–644 (2008).
3. Stachura, D. L. & Traver, D. Cellular Dissection of Zebrafish Hematopoiesis. in *Methods in Cell Biology* vol. 101 75–110 (Elsevier Ltd, 2011).
4. Bertrand, J. Y. *et al.* Haematopoietic stem cells derive directly from aortic endothelium during development. *Nature* **464**, 108–111 (2010).
5. Boisset, J. C. *et al.* In vivo imaging of haematopoietic cells emerging from the mouse aortic endothelium. *Nature* **464**, 116–120 (2010).
6. Kissa, K. & Herbomel, P. Blood stem cells emerge from aortic endothelium by a novel type of cell transition. *Nature* **464**, 112–115 (2010).
7. Godin, I. & Cumano, A. The hare and the tortoise: An embryonic haematopoietic race. *Nat. Rev. Immunol.* **2**, 593–604 (2002).
8. Murayama, E. *et al.* Tracing Hematopoietic Precursor Migration to Successive Hematopoietic Organs during Zebrafish Development. *Immunity* **25**, 963–975 (2006).
9. Palomero, T. *et al.* Mutational loss of PTEN induces resistance to NOTCH1 inhibition in T-cell leukemia. *Nat. Med.* **13**, 1203–1210 (2007).
10. Van Vlierberghe, P., Ferrando, A., Vlierberghe, P. Van & Ferrando, A. The molecular es basis of T cell acute lymphoblastic leukemia. *J. Clin. Invest.* **122**, 3398–3406 (2012).
11. Song, M. S., Salmena, L. & Pandolfi, P. P. The functions and regulation of the PTEN tumour suppressor. *Nat. Rev. Mol. Cell Biol.* **13**, 283–296 (2012).
12. Blackburn, J. S. *et al.* Clonal evolution enhances leukemia-propagating cell frequency in T cell acute lymphoblastic leukemia through Akt/mTORC1 pathway activation. *Cancer Cell* **25**, 366–378 (2014).
13. Yilmaz, Ö. H. *et al.* Pten dependence distinguishes haematopoietic stem cells from leukaemia-initiating cells. *Nature* **441**, 475–482 (2006).
14. Zhang, J. *et al.* PTEN maintains haematopoietic stem cells and acts in lineage choice and leukaemia prevention. *Nature* **441**, 518–522 (2006).
15. Faucherre, a, Taylor, G. S., Overvoorde, J., Dixon, J. E. & Hertog, J. Den. Zebrafish pten genes have overlapping and non-redundant functions in tumorigenesis and embryonic development. *Oncogene* **27**, 1079–1086 (2008).
16. Choorapoikayil, S., Kuiper, R. V., De Bruin, A. & Den Hertog, J. Haploinsufficiency of the genes encoding the tumor suppressor Pten predisposes zebrafish to hemangiosarcoma. *DMM Dis. Model. Mech.* **5**, 241–247 (2012).
17. Choorapoikayil, S., Kers, R., Herbomel, P., Kissa, K. & Den Hertog, J. Pivotal role of Pten in the balance between proliferation and differentiation of hematopoietic stem cells in zebrafish. *Blood* **123**, 184–190 (2014).
18. Gering, M. & Patient, R. Hedgehog signaling is required for adult blood stem cell formation in zebrafish embryos. *Dev. Cell* **8**, 389–400 (2005).
19. Choorapoikayil, S., Weijts, B., Kers, R., de Bruin, A. & den Hertog, J. Loss of Pten promotes angiogenesis and enhanced vegfaa expression in zebrafish. *Dis. Model. Mech.* **6**, 1159–66 (2013).
20. Darzynkiewicz, Z. *et al.* Features of apoptotic cells measured by flow cytometry. *Cytometry* **13**, 795–808 (1992).
21. Bolli, N. *et al.* Cpsf1 is required for definitive HSC survival in zebrafish. *Blood* **117**, 3996–4007 (2011).
22. Bertrand, J. Y. *et al.* Characterization of purified intraembryonic hematopoietic stem cells as a tool to define their site of origin. *Proc. Natl. Acad. Sci. U. S. A.* **102**, 134–139 (2005).
23. Lin, H. F. *et al.* Analysis of thrombocyte development in CD41-GFP transgenic zebrafish. *Blood* **106**, 3803–3810 (2005).
24. Muraro, M. J. *et al.* A Single-Cell Transcriptome Atlas of the Human Pancreas. *Cell Syst.* **3**, 385–394 (2016).
25. Kissa, K. *et al.* Live imaging of emerging hematopoietic stem cells and early thymus colonization. *Blood* **111**, 1147–56 (2008).
26. Herman, J. S., Sagar & Grün, D. FateID infers cell fate bias in multipotent progenitors from single-cell RNA-seq data. *Nat. Methods* **15**, 379–386 (2018).
27. Athanasiadis, E. I. *et al.* Single-cell RNA-sequencing uncovers transcriptional states and fate decisions in haematopoiesis. *Nat. Commun.* **8**, (2017).
28. Baron, C. S. *et al.* Single-cell transcriptomics reveal the dynamic of haematopoietic stem cell production in the aorta. *Nat. Commun.* **9**, (2018).
29. Baron, C. S. *et al.* Cell Type Purification by Single-Cell Transcriptome-Trained Sorting. *Cell* **179**, 527-542.e19 (2019).
30. Buenrostro, J. D. *et al.* Integrated Single-Cell Analysis Maps the Continuous Regulatory Landscape of Human Hematopoietic Differentiation. *Cell* **173**, 1535-1548.e16 (2018).

31. Kowalczyk, M. S. *et al.* Single-cell RNA-seq reveals changes in cell cycle and differentiation programs upon aging of hematopoietic stem cells. *Genome Res.* **25**, 1860–1872 (2015).
32. Lai, S. *et al.* Comparative transcriptomic analysis of hematopoietic system between human and mouse by Microwell-seq. *Cell Discov.* **4**, (2018).
33. Nestorowa, S. *et al.* A Single Cell Resolution Map of Mouse Haematopoietic Stem and Progenitor Cell Differentiation Running title: Single Cell Map of HSPC Differentiation. *Blood* **128**, 20–32 (2016).
34. Xue, Y. *et al.* A 3D Atlas of Hematopoietic Stem and Progenitor Cell Expansion by Multi-dimensional RNA-Seq Analysis. *Cell Rep.* **27**, 1567-1578.e5 (2019).
35. Chen, M. J., Yokomizo, T., Zeigler, B. M., Dzierzak, E. & Speck, N. A. Runx1 is required for the endothelial to haematopoietic cell transition but not thereafter. *Nature* **457**, 887–891 (2009).
36. Zovein, A. C. *et al.* Fate Tracing Reveals the Endothelial Origin of Hematopoietic Stem Cells. *Cell Stem Cell* **3**, 625–636 (2008).
37. Kartalaei, P. S. *et al.* Whole-transcriptome analysis of endothelial to hematopoietic stem cell transition reveals a requirement for Gpr56 in HSC generation. *J. Exp. Med.* **212**, 93–106 (2015).
38. Davidson, A. J. & Zon, L. I. The 'definitive' (and 'primitive') guide to zebrafish hematopoiesis. *Oncogene* **23**, 7233–7246 (2004).
39. Svoboda, O. *et al.* Dissection of vertebrate hematopoiesis using zebrafish thrombopoietin. *Blood* **124**, 220–228 (2014).
40. Sun, H. *et al.* PTEN modulates cell cycle progression and cell survival by regulating phosphatidylinositol 3,4,5,-trisphosphate and Akt/protein kinase B signaling pathway. *Proc. Natl. Acad. Sci. U. S. A.* **96**, 6199–6204 (1999).
41. Reya, T., Morrison, S. J., Clarke, M. F. & Weissman, I. L. Stem cells, cancer, and cancer stem cells. *Nature* **414**, 105–111 (2001).
42. Signer, R. A. J., Magee, J. A., Salic, A. & Morrison, S. J. Haematopoietic stem cells require a highly regulated protein synthesis rate. *Nature* **509**, 49–54 (2014).
43. Challen, G. A., Boles, N., Lin, K. K. Y. & Goodell, M. A. Mouse hematopoietic stem cell identification and analysis. *Cytom. Part A* **75**, 14–24 (2009).
44. Lin, H. T., Otsu, M. & Nakauchi, H. Stem cell therapy: An exercise in patience and prudence. *Philos. Trans. R. Soc. B Biol. Sci.* **368**, 4–6 (2013).
45. Jin, S.-W., Beis, D., Mitchell, T., Chen, J.-N. & Stainier, D. Y. R. Cellular and molecular analyses of vascular tube and lumen formation in zebrafish. *Development* **132**, 5199–209 (2005).
46. Hogan, B. M. *et al.* ccbe1 is required for embryonic lymphangiogenesis and venous sprouting. *Nat. Genet.* **41**, 396–398 (2009).
47. Aleström, P. *et al.* Zebrafish: Housing and husbandry recommendations. *Lab. Anim.* **0**, 1–12 (2019).
48. Kimmel, C. B., Ballard, W. W., Kimmel, S. R., Ullmann, B. & Schilling, T. F. Stages of embryonic development of the zebrafish. *Dev Dyn* **203**, 253–310 (1995).
49. Westerfield, M. The zebrafish book. A guide for the laboratory use of zebrafish (Danio rerio). 4th ed. *Univ. Oregon Press. Eugene* (2000).
50. Urasaki, A., Morvan, G. & Kawakami, K. Functional dissection of the Tol2 transposable element identified the minimal cis-sequence and a highly repetitive sequence in the subterminal region essential for transposition. *Genetics* **174**, 639–649 (2006).
51. Gurskaya, N. G. *et al.* Engineering of a monomeric green-to-red photoactivatable fluorescent protein induced by blue light. *Nat. Biotechnol.* **24**, 461–465 (2006).
52. Stumpf, M., Blokzijl-Franke, S. & den Hertog, J. Fine-Tuning of Pten Localization and Phosphatase Activity Is Essential for Zebrafish Angiogenesis. *PLoS One* **11**, e0154771 (2016).
53. Renaud, O., Herbomel, P. & Kissa, K. Studying cell behavior in whole zebrafish embryos by confocal live imaging: application to hematopoietic stem cells. *Nat. Protoc.* **6**, 1897–1904 (2011).
54. Schneider, C. A., Rasband, W. S. & Eliceiri, K. W. NIH Image to ImageJ: 25 years of image analysis. *Nat. Methods* **9**, 671–675 (2012).
55. Thisse, C. & Thisse, B. High-resolution in situ hybridization to whole-mount zebrafish embryos. *Nat. Protoc.* **3**, 59–69 (2008).
56. Dixon, G., Elks, P. M., Loynes, C. A., Whyte, M. K. B. & Renshaw, S. A. A Method for the In Vivo Measurement of Zebrafish Tissue Neutrophil Lifespan . *ISRN Hematol.* **2012**, 1–6 (2012).
57. Tian, Y. *et al.* The first wave of T lymphopoiesis in zebrafish arises from aorta endothelium independent of hematopoietic stem cells. *J. Exp. Med.* **214**, 3347–3360 (2017).
58. Hashimshony, T. *et al.* CEL-Seq2: sensitive highly-multiplexed single-cell RNA-Seq. *Genome Biol.* **17**, 77 (2016).
59. Van Den Brink, S. C. *et al.* Single-cell sequencing reveals dissociation-induced gene expression in tissue subpopulations. *Nat. Methods* **14**, 935–936 (2017).
60. Grün, D., Kester, L. & van Oudenaarden, A. Validation of noise models for single-cell transcriptomics. *Nat. Methods* **11**, 637–640 (2014).
61. Love, M. I., Huber, W. & Anders, S. Moderated estimation of fold change and dispersion for RNA-seq data with DESeq2. *Genome Biol.* **15**, 1–21 (2014).

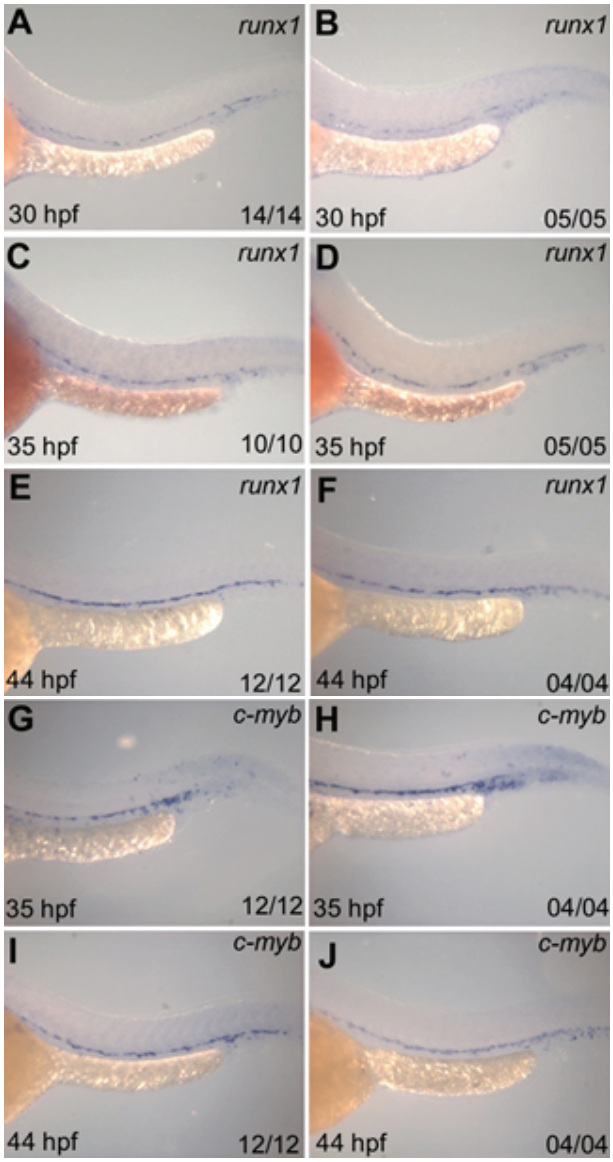

Figure S1. Hemogenic endothelium markers are present in *ptena*$^{-/-}$*ptenb*$^{-/-}$ mutants during onset of definitive hematopoiesis. Related to figure 1. *Ptena*$^{+/-}$*ptenb*$^{-/-}$ fish were incrossed and embryos were fixed at different time points as indicated (30, 35 and 44 hpf). *In situ* hybridization using HSPC markers *runx1* (a-f) and *c-myb* (g-j) was done, pictures were taken and subsequently the genotypes of these embryos was established by sequencing. No differences were observed between *ptena*$^{-/-}$*ptenb*$^{-/-}$ mutant embryos and siblings. Representative embryos are depicted with anterior to the left; the number of embryos that showed a particular pattern/total number of embryos is indicated in the bottom right corner of each panel.

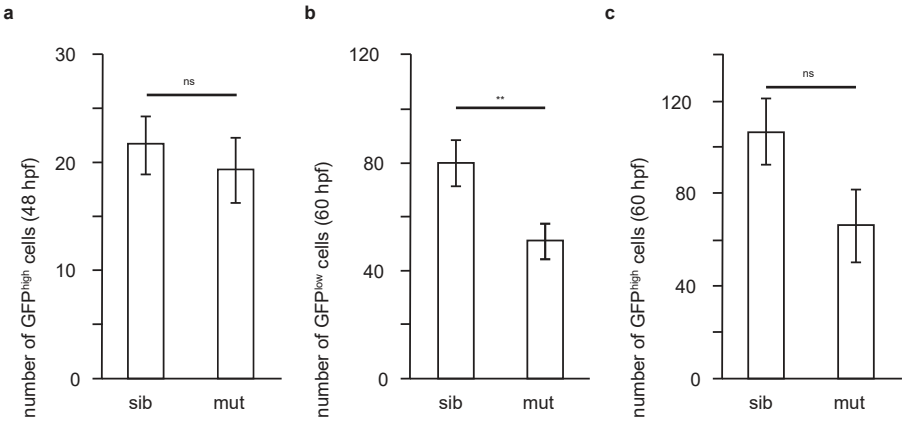

Figure S2. Reduced number of GFP^{low}, but not GFP^{high} cells in the CHT of *tg(cd41:eGFP)*. *Ptena*$^{-/-}$*ptenb*$^{-/-}$ mutant embryos, compared to siblings. Related to figure 2. (a) the number of GFP^{high} thrombocytes at 48 hpf in the CHT of *tg(cd41:eGFP)* siblings (sib) and *ptena*$^{-/-}$*ptenb*$^{-/-}$ mutants (mut), expressed as average number of cells. (b,c) the number of GFP^{low} HSPCs (b) and GFP^{high} thrombocytes (c) in the CHT of 60 hpf in the CHT of *tg(cd41:eGFP)* siblings (sib) and *ptena*$^{-/-}$*ptenb*$^{-/-}$ mutants (mut), expressed as average number of cells. Note that the diference in GFP^{low} HSPCs is smaller due to enhanced proliferation and the apparent difference in GFP^{high} cells is almost significant, due to an arrest in differentiation. Error bars indicate standard error of the mean (SEM). Shapiro Wilk test for normal distribution and two-tailed t-test were used for statistical analysis; p-values are: (a) 0.57 (not significant, ns), (b) 0.013 (**), (c) 0.066 (not significant, ns).

Figure S3. Single cell RNA seq of control and PI3K inhibitor treated embryos at the onset of definitive hematopoiesis. Related to Figure 5. (a) Workflow of scRNA seq. Tissue from control and LY294002-treated embryos (~2,000 each) was dissected, the AGM regions pooled, dissociated and FACS sorted, after which the SORT-seq protocol was performed. (b) Normalized expression of ENSDARG00000080337_ACO24175.4 and tmed1b over all clusters. Normalized expression is plotted on log10 scale using violin plots and boxplots. cl1: Myeloid/neutrophil progenitor, cl2: HSPC II, cl4: HSPC I, cl5: EHT progenitor, cl3: myeloid/monocyteprogenitor. (c) Normalized expression of signature genes for cluster identities using violin plots. Normalized expression value is plotted on a log10 scale. (d) whole mount ISH of 36 hpf wild type embryos using a probe specific for ENSDARG00000080337_ACO24175.4. Forwardprimer: 5'TTAAAGCCCCGAATCCAGGT 3', reverse primer with T7 promoter: GAGTAATACGACTCACTATAGGTTTTGGTAAACAGGCGAGGC. At this stage, this gene is expressed throughout the embryo at a very high level, which does not allow to distinguish between individual blood cells.

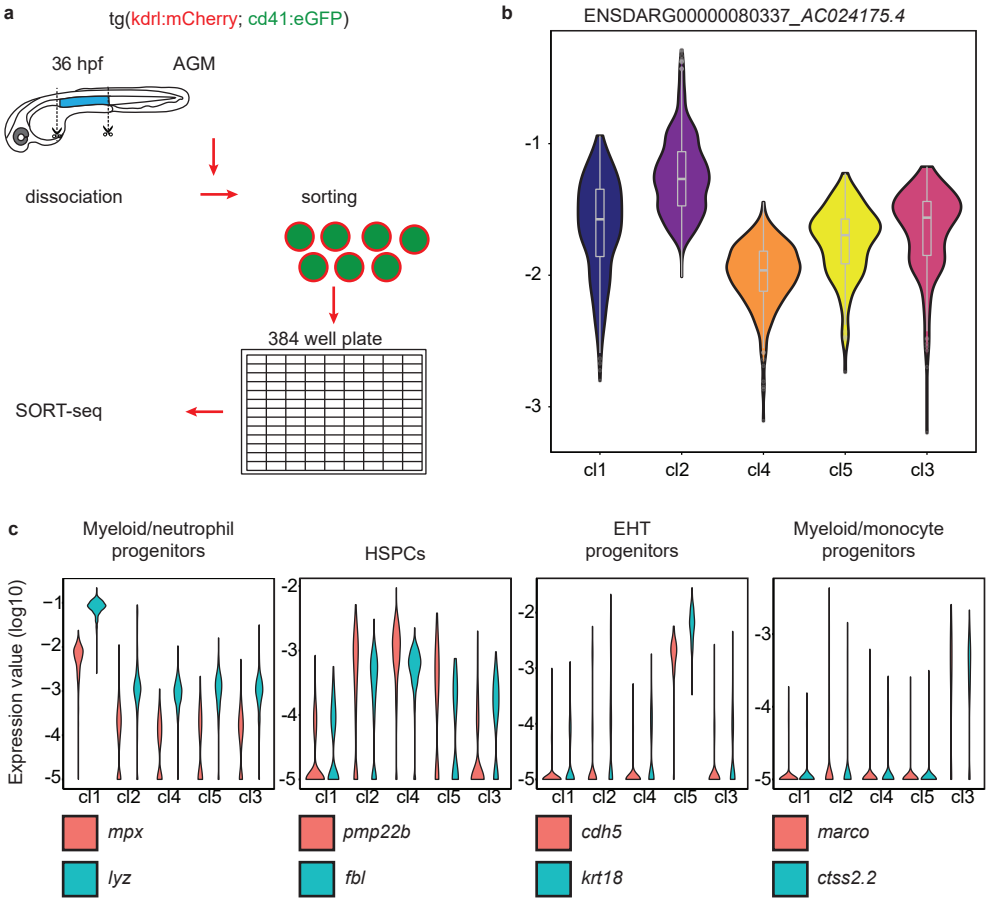
a
tg(kdrl:mCherry; cd41:eGFP)
36 hpf
AGM
dissociation
sorting
384 well plate
SORT-seq
b
ENSDARG00000080337_AC024175.4
-1
-2
-3
cl1
cl2
cl4
cl5
cl3
c
Myeloid/neutrophil progenitors
HSPCs
EHT progenitors
Myeloid/monocyte progenitors
Expression value (log10)
mpx
lyz
pmp22b
fbl
cdh5
krt18
marco
ctss2.2
d
ACO24175.4
1mm

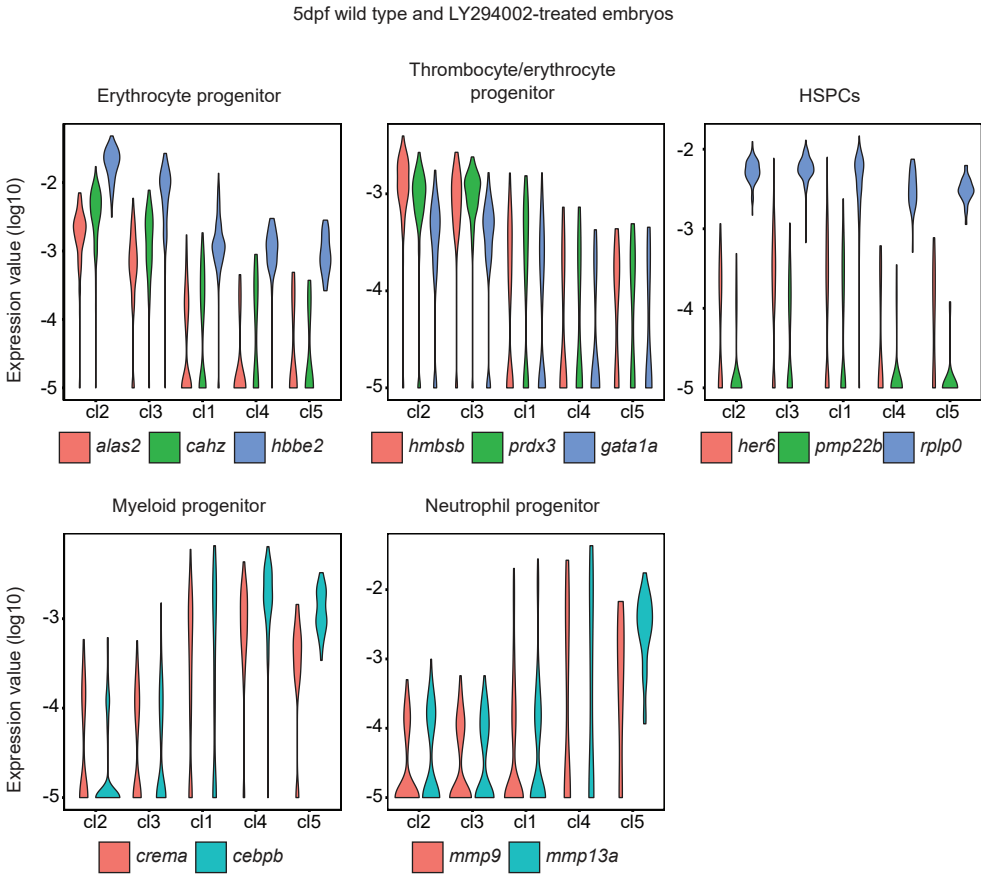

Figure S4. Cluster identities at 5 dpf for wild type and LY294002-treated embryos. Related to Figure 6. Normalized expression of signature genes for cluster identities using violin plots. Normalized expression value is plotted on a log10 scale.

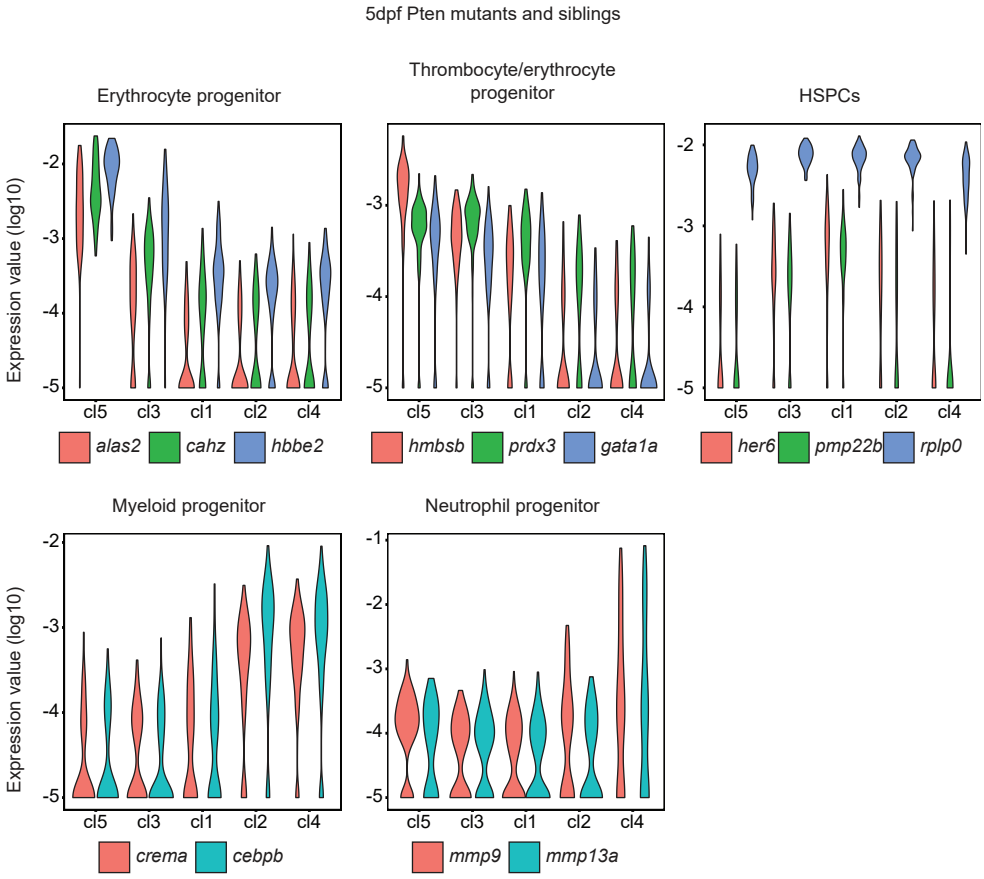

Figure S5. Cluster identities at 5 dpf for *ptena*$^{-/-}$*ptenb*$^{-/-}$ mutant embryos and their siblings. Related to Figure 7. Normalized expression of signature genes for cluster identities using violin plots. Normalized expression value is plotted on a log10 scale.

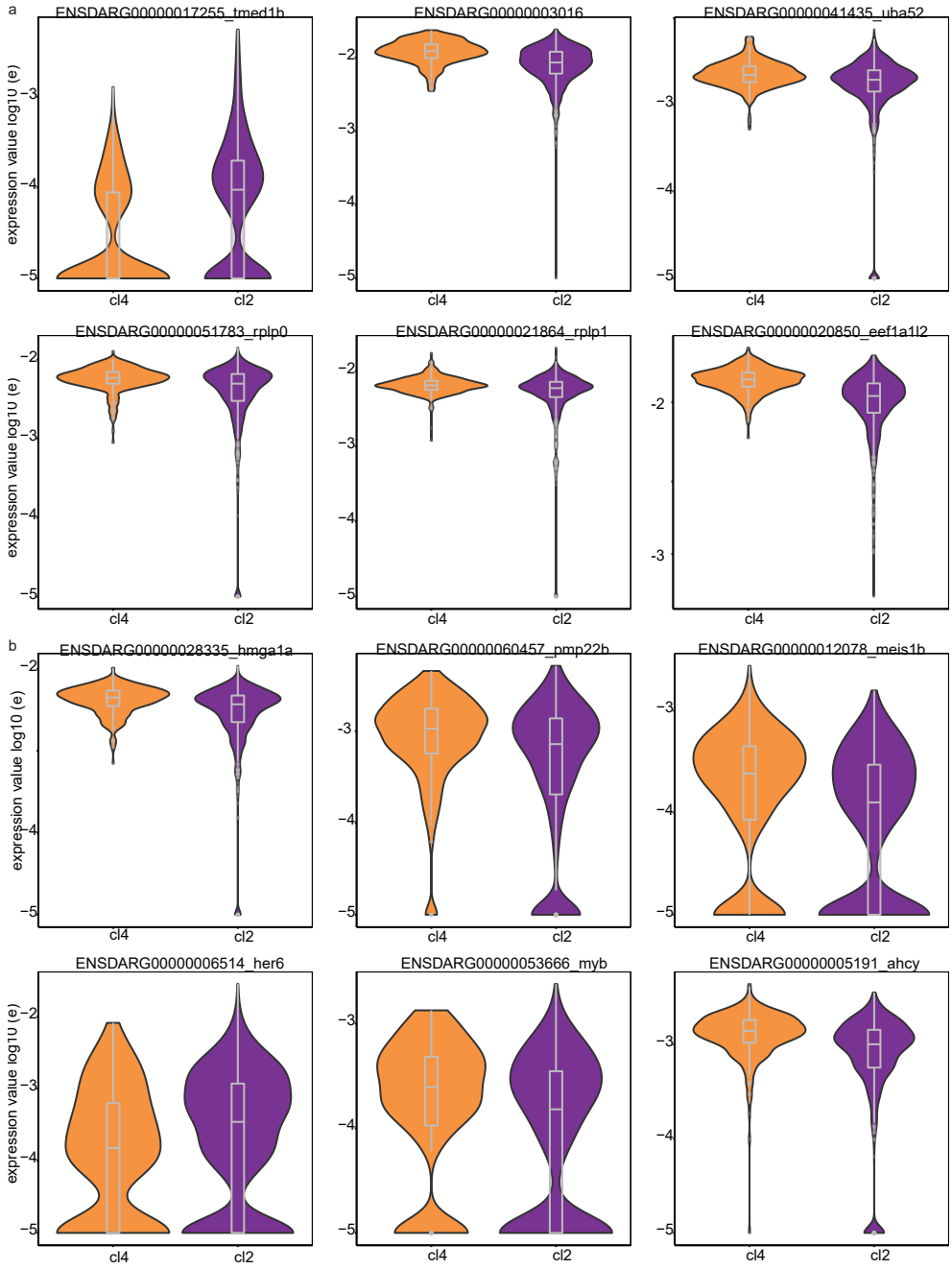

Figures S6. Cluster identities at 36 hpf for LY294002-treated embryos and their controls for only HSPCs clusters. Related to figure 5. Normalized expression of signature genes for HSPCs II (a) and HSPCs I (b) using violin plots. Normalized expresssion value is plotted on a log10 scale. All genes are significantly different expressed between clusters (t-test, p<0.001). Cluster 4 is HSPCs I, cluster 2 is HSPCs II.

table S1. Marker genes for scRNA-seq

Cluster/Cell type	**Gene**	**ENSDARG**
Thrombocyte/erythrocyte progenitors	*hmbsb*	ENSDARG00000055991
	prdx3	ENSDARG00000032102
	urod	ENSDARG00000006818
	uros	ENSDARG00000027491
	tubb1	ENSDARG00000053066
	klf1	ENSDARG00000017400
	gata1a	ENSDARG00000013477
	epb41b	ENSDARG00000029019
Erythrocyte progenitors	*alas2*	ENSDARG00000038643
	cahz	ENSDARG00000011166
	hbbe2	ENSDARG00000045143
	hbae3	ENSDARG00000079305
	rhag	ENSDARG00000019253
	epor	ENSDARG00000090834
HSPCs	*myb*	ENSDARG00000053666
	her6	ENSDARG00000006514
	ahcy	ENSDARG00000005191
	pmp22b	ENSDARG00000060457
	ncl	ENSDARG00000002710
	adh5	ENSDARG00000080010
	hmga1a	ENSDARG00000028335
	fbl	ENSDARG00000053912
	mycb	ENSDARG00000007241
	dkc1	ENSDARG00000016484
	pes	ENSDARG00000018902
	meis1b	ENSDARG00000012078
	tal1 (scl)(Davidson & Zon 2004)	ENSDARG00000019930
	gata2b	ENSDARG00000009094
	gfi1aa	ENSDARG00000020746
	adgrg1	ENSDARG00000027222

Cluster/Cell type	Gene	ENSDARG
Myeloid progenitor	*crema*	ENSDARG00000023217
	itm2bb	ENSDARG00000041505
	runx3	ENSDARG00000052826
	cebpb	ENSDARG00000042725
	cxcr4b	ENSDARG00000041959
	zfp36l1a	ENSDARG00000016154
	coro1a	ENSDARG00000054610
	nr4a3	ENSDARG00000055854
	pu.1 (spi1b)	ENSDARG00000000767
Neutrophil progenitor	*cpa5*	ENSDARG00000021339
	lect2l	ENSDARG00000033227
	npsn	ENSDARG00000010423
	sms	ENSDARG00000008155
	abcb9	ENSDARG00000056200
	ch25hl2	ENSDARG00000038728
	mpx	ENSDARG00000019521
	lyz	ENSDARG00000057789
	srgn	ENSDARG00000077069
	mmp9	ENSDARG00000042816
Monocyte progenitor	*marco*	ENSDARG00000059294
	ctss2.2	ENSDARG00000013771
	mfap4	ENSDARG00000090783
	marckls1a	ENSDARG00000039034
	ctsba	ENSDARG00000055120
	cxcr3.3	ENSDARG00000070669
	timp2b	ENSDARG00000075261
	lgmn	ENSDARG00000039150
	ndrg1a	ENSDARG00000032849
EHT markers	*edn2*	ENSDARG00000017255
	efna1b	ENSDARG00000018787
	cdh5	ENSDARG00000075549
	krt18	ENSDARG00000018404
	krt8	ENSDARG00000058358
	dab2	ENSDARG00000031761

Cluster/Cell type	Gene	ENSDARG
EHT markers	*serpinh1b*	ENSDARG00000019949
	anxa2a	ENSDARG00000003216
	ctsla	ENSDARG00000007836
	hapln1b	ENSDARG00000068516
	clic2	ENSDARG00000010625
	cd81a	ENSDARG00000036080
	tie1	ENSDARG00000004105
HSPCs II 36hpf	*AC024175.4*	ENSDARG00000080337
	tmed1b	ENSDARG00000017255

table S2, 36 hpf data

1	2	3	4	5
ENSDARG00000057789 lyz	ENSDARG00000091038	ENSDARG00000088745 MFAP4	ENSDARG00000094975 FP015823.2	ENSDARG00000018404 krt18
ENSDARG00000010423 npsn	ENSDARG00000052402 dnmt3ba	ENSDARG00000074322 si:ch211-194m7.3	ENSDARG00000043126 blf	ENSDARG00000023713 aqp1a.1
ENSDARG00000019521 mpx	ENSDARG00000036791 dnmt3bb.1	ENSDARG00000090783 mfap4	ENSDARG00000008333 znfl2a	ENSDARG00000058358 krt8
ENSDARG00000021339 cpa5	ENSDARG00000015123 dnase1l4.1	ENSDARG00000056874 lygl1	ENSDARG00000060457 pmp22b	ENSDARG00000075549 cdh5
ENSDARG00000075664 si:ch1073-429i10.1	ENSDARG00000080337 AC024175.4	ENSDARG00000086947 si:ch211-147m6.1	ENSDARG00000015123 dnase1l4.1	ENSDARG00000060675
ENSDARG00000012395 mmp13a	ENSDARG00000035773	ENSDARG00000043436 si:dkey-5n18.1	ENSDARG00000014329 npm1a	ENSDARG00000021443 zfp36l1b
ENSDARG00000077069 srgn	ENSDARG00000094975 FP015823.2	ENSDARG00000069844 irg1	ENSDARG00000023299 snu13b	ENSDARG00000044975 krt94
ENSDARG00000008155 sms	ENSDARG00000044129 FP015823.1	ENSDARG00000055120 ctsba	ENSDARG00000005513 naca	ENSDARG00000055678 akap12b
ENSDARG00000033227 lect2l	ENSDARG00000090106 slc17a7b	ENSDARG00000090890 cmklr1	ENSDARG00000035761	ENSDARG00000039576 fstl1b
ENSDARG00000036966 hsd3b7	ENSDARG00000076532 si:ch211-222l21.1	ENSDARG00000054942 lgals2a	ENSDARG00000044129 FP015823.1	ENSDARG00000094719 CR318588.3
ENSDARG00000042816 mmp9	ENSDARG00000060457 pmp22b	ENSDARG00000058941	ENSDARG00000004169 stmn1a	ENSDARG00000010625 clic2
ENSDARG00000038728 ch25hl2	ENSDARG00000012820 nop56	ENSDARG00000031776 zgc:92066	ENSDARG00000053912 fbl	ENSDARG00000018787 efna1b
ENSDARG00000056200 abcb9	ENSDARG00000062138 ranbp10	ENSDARG00000058731 slc2a6	ENSDARG00000012078 meis1b	ENSDARG00000068516 hapln1b
ENSDARG00000035326 nccrp1	ENSDARG00000043126 blf	ENSDARG00000055226 slc7a7	ENSDARG00000004757 ybx1	ENSDARG00000004105 tie1

1	2	3	4	5
ENSDARG00000091236 cst14b.2	ENSDARG00000016484 dkc1	ENSDARG00000028618 KRT18	ENSDARG00000052402 dnmt3ba	ENSDARG00000061165 slc6a4a
ENSDARG00000018263 pdia2	ENSDARG00000071052 si:dkey-150i13.2	ENSDARG00000090352 CR855311.1	ENSDARG00000035993 sumo3b	ENSDARG00000070171
ENSDARG00000043457 gapdh	ENSDARG00000087616 maptb	ENSDARG00000024540 tspan36	ENSDARG00000041895 cad	ENSDARG00000074201 flna
ENSDARG00000012972 cfl1l	ENSDARG00000070956	ENSDARG00000019861 fgl2a	ENSDARG00000056186 eif5a2	ENSDARG00000070155 tuba8l3
ENSDARG00000056600 papss2b	ENSDARG00000070404 fam212ab	ENSDARG00000036427 slc3a2a	ENSDARG00000062199 GSE1	ENSDARG00000026751
ENSDARG00000006029 lta4h	ENSDARG00000071657 si:dkey-19a16.4	ENSDARG00000057853 atp6v0ca	ENSDARG00000087438 si:dkey-257i7.5	ENSDARG00000004621 gpm6ab
ENSDARG00000055064 prdx5	ENSDARG00000028323	ENSDARG00000040178 havcr1	ENSDARG00000054155 pcna	ENSDARG00000019949 serpinh1b
ENSDARG00000034187 calm1b	ENSDARG00000004169 stmn1a	ENSDARG00000025903 lgals9l1	ENSDARG00000039578 pa2g4a	ENSDARG00000023963 tpm4a
ENSDARG00000024116 vamp8	ENSDARG00000079012 CBFA2T3	ENSDARG00000057698 ctsd	ENSDARG00000076532 si:ch211-222l21.1	ENSDARG00000030125 sox7
ENSDARG00000070398	ENSDARG00000095268 si:dkey-261h17.1	ENSDARG00000025237	ENSDARG00000005191 ahcy	ENSDARG00000056920 tmem88a
ENSDARG00000035018 thy1	ENSDARG00000058337	ENSDARG00000005419	ENSDARG00000053666 myb	ENSDARG00000031761 dab2
ENSDARG00000053381 plpp1a	ENSDARG00000070434 rhov	ENSDARG00000013968 psap	ENSDARG00000043960 rpf2	ENSDARG00000087956 she
ENSDARG00000033735 ncf1	ENSDARG00000091150 mki67	ENSDARG00000030694 atp6v1e1b	ENSDARG00000002710 ncl	ENSDARG00000015815
ENSDARG00000059388 bdh1	ENSDARG00000056929 kdm6bb	ENSDARG00000059679	ENSDARG00000079949 supt16h	ENSDARG00000070425 dll4
ENSDARG00000033285 gsto2	ENSDARG00000062077 acsbg1	ENSDARG00000013443 atp6v1ba	ENSDARG00000070404 fam212ab	ENSDARG00000036080 cd81a

1	2	3	4	5
ENSDARG00000039884	ENSDARG00000014329 npm1a	ENSDARG00000018806	ENSDARG00000044220	ENSDARG00000042874 phlda2
ENSDARG00000013561 pgm1	ENSDARG00000056438 her9	ENSDARG00000059294 marco	ENSDARG00000039682 si:ch211-121a2.2	ENSDARG00000040432 klf2b
ENSDARG00000002021 pygb	ENSDARG00000002710 ncl	ENSDARG00000070622	ENSDARG00000092033 si:dkey-239h2.3	ENSDARG00000015805 cgnl1
ENSDARG00000067545 adam19b	ENSDARG00000041895 cad	ENSDARG00000067566 sftpbb	ENSDARG00000055868 rsl1d1	ENSDARG00000043376
ENSDARG00000063295 myh9a	ENSDARG00000053912 fbl	ENSDARG00000079932 zgc:152830	ENSDARG00000058337	ENSDARG00000013976 anxa13
ENSDARG00000019236 gsr	ENSDARG00000073681	ENSDARG00000013771 ctss2.2	ENSDARG00000030789 ddx18	ENSDARG00000043531 jun
ENSDARG00000035459 spns3	ENSDARG00000043304 nop2	ENSDARG00000008423	ENSDARG00000087616 maptb	ENSDARG00000008359
ENSDARG00000022165 mgst1.2	ENSDARG00000088325	ENSDARG00000004954 grna	ENSDARG00000070657 pa2g4b	ENSDARG00000009123 sele
ENSDARG00000010556 CABZ01030094.1	ENSDARG00000029252 ssb	ENSDARG00000091078	ENSDARG00000018961 gtpbp4	ENSDARG00000014059 cldn5b
ENSDARG00000058734 prdx1	ENSDARG00000077264 wdr43	ENSDARG00000087353	ENSDARG00000039887 c1qbp	ENSDARG00000019815 fn1a
ENSDARG00000035136 sepw1	ENSDARG00000059634 thumpd3	ENSDARG00000094451 cfp	ENSDARG00000045776 cnbpa	ENSDARG00000069912 hmga2
ENSDARG00000053542 kctd12.2	ENSDARG00000056226 creb3l3a	ENSDARG00000070378 ccl35.2	ENSDARG00000003920 setb	ENSDARG00000000002 ccdc80
ENSDARG00000025375 idh1	ENSDARG00000052290 rab33ba	ENSDARG00000076003	ENSDARG00000092164	ENSDARG00000033307 igf2b
ENSDARG00000007682 ppdpfa	ENSDARG00000069422 nhp2	ENSDARG00000076789 cx32.2	ENSDARG00000009094 gata2b	ENSDARG00000092035 si:ch211-156j16.1
ENSDARG00000054755 alox5ap	ENSDARG00000053624 csf1rb	ENSDARG00000076318 atp6v1ab	ENSDARG00000069977 myg1	ENSDARG00000060189

1	2	3	4	5
ENSDARG00000043102 lxn	ENSDARG00000008976 mdn1	ENSDARG00000027529 hmox1a	ENSDARG00000040245 kpnb3	ENSDARG00000007836 ctsla
ENSDARG00000036940 ctss1	ENSDARG00000020984 slc16a10	ENSDARG00000005463 slc30a1a	ENSDARG00000010246 prmt1	ENSDARG00000055009 col4a1
ENSDARG00000068784 VSIR	ENSDARG00000070538 hey1	ENSDARG00000055504 si:ch211-212k18.7	ENSDARG00000069422 nhp2	ENSDARG00000037895 ramp2
ENSDARG00000059110	ENSDARG00000062199 GSE1	ENSDARG00000043081 ctsz	ENSDARG00000063626 ddx21	ENSDARG00000014588 adcy2b
ENSDARG00000036382 ponzr6	ENSDARG00000053136 b2m	ENSDARG00000068382 pglyrp5	ENSDARG00000019230 rpl7a	ENSDARG00000071196 sdprb
ENSDARG00000015343 pgd	ENSDARG00000003680 runx1t1	ENSDARG00000033587 CABZ01088134.1	ENSDARG00000077264 wdr43	ENSDARG00000091479
ENSDARG00000044125 txn	ENSDARG00000058606 sik1	ENSDARG00000031681 atp6v0b	ENSDARG00000024561 nolc1	ENSDARG00000003216 anxa2a
ENSDARG00000012016 hpgd	ENSDARG00000076847 tnrc6c1	ENSDARG00000054543 samsn1a	ENSDARG00000026491	ENSDARG00000056795 serpine1
ENSDARG00000052766 EVI5L	ENSDARG00000080009 bahcc1b	ENSDARG00000055290 mpeg1.1	ENSDARG00000091038	ENSDARG00000005150 tbx20
ENSDARG00000004979 elovl5	ENSDARG00000087438 si:dkey-257i7.5	ENSDARG00000077648 FNIP2	ENSDARG00000041754	ENSDARG00000019371 flt1
ENSDARG00000019062 arpc5b	ENSDARG00000005834 gatad2b	ENSDARG00000009511 tnfa	ENSDARG00000004433 btk	ENSDARG00000036028 arrdc3b
ENSDARG00000058348 scinlb	ENSDARG00000024561 nolc1	ENSDARG00000003931 cndp2	ENSDARG00000029252 ssb	ENSDARG00000068709 fam174b
ENSDARG00000086337 si:dkey-102g19.3	ENSDARG00000095019 lmo2	ENSDARG00000035715 marcksl1b	ENSDARG00000053990 hmgb2b	ENSDARG00000005368 mcamb
ENSDARG00000009208 prkcda	ENSDARG00000082180	ENSDARG00000076914 lacc1	ENSDARG00000030700 ctps1a	ENSDARG00000070391 tspan4b
ENSDARG00000062543	ENSDARG00000095670 BX855614.2	ENSDARG00000013598 tnfb	ENSDARG00000058606 sik1	ENSDARG00000068401 yap1

1	2	3	4	5
ENSDARG00000055562	ENSDARG00000035120 GLDC	ENSDARG00000059906 sdc4	ENSDARG00000057026 ran	ENSDARG00000037879 lfng
ENSDARG00000023188 lcp1	ENSDARG00000077721 knop1	ENSDARG00000039150 lgmn	ENSDARG00000007216 abce1	ENSDARG00000052690 arrdc3a
ENSDARG00000093248 si:dkey-238m4.4	ENSDARG00000060070 adcy7	ENSDARG00000026049 mxf	ENSDARG00000035151 si:dkey-261j4.3	ENSDARG00000026329 arhgap29a
ENSDARG00000067976 ar	ENSDARG00000056167 hspe1	ENSDARG00000074656 ctss2.1	ENSDARG00000076721 zgc:171686	ENSDARG00000079900 shroom4
ENSDARG00000093124 scpp8	ENSDARG00000017568	ENSDARG00000053227	ENSDARG00000011125 snrpb	ENSDARG00000002013 grb10a
ENSDARG00000054610 coro1a	ENSDARG00000017255 tmed1b	ENSDARG00000061120 slc43a2b	ENSDARG00000045565 noc4l	ENSDARG00000011571 calcrlb
ENSDARG00000026829 cotl1	ENSDARG00000029058 rbbp4	ENSDARG00000057035 stoml3b	ENSDARG00000053395 cdkn2aipnl	ENSDARG00000070578 edn2
ENSDARG00000012987 gpia	ENSDARG00000079472 F2RL2	ENSDARG00000005481 nfkbiaa	ENSDARG00000021252 cct6a	ENSDARG00000067719 wwtr1
ENSDARG00000036776 aldh8a1	ENSDARG00000094181 shroom1	ENSDARG00000021287 zgc:91909	ENSDARG00000018902 pes	ENSDARG00000087303 cebpd
ENSDARG00000058302 sh3bgrl	ENSDARG00000096403 CT027638.1	ENSDARG00000077308 gpr84	ENSDARG00000015862 rpl5b	ENSDARG00000059933 plpp3
ENSDARG00000019260 dhrs9	ENSDARG00000090493	ENSDARG00000070542 mafbb	ENSDARG00000059070 gars	ENSDARG00000011876 ednraa
ENSDARG00000027852	ENSDARG00000076526 gar1	ENSDARG00000090873 ccl34a.4	ENSDARG00000035132 rgs3b	ENSDARG00000031228 podxl
ENSDARG00000057882 arpc3	ENSDARG00000052480 pdcd11	ENSDARG00000027464	ENSDARG00000016173 cct3	ENSDARG00000076484 stab1
ENSDARG00000055108 gde1	ENSDARG00000096287 BX510989.2	ENSDARG00000069461 rnaseka	ENSDARG00000076526 gar1	ENSDARG00000053868 etv2
ENSDARG00000041505 itm2bb	ENSDARG00000035415 ptger4b	ENSDARG00000019556 clcn7	ENSDARG00000022410 rrp12	ENSDARG00000032765 net1

1	2	3	4	5
ENSDARG00000052656 si:ch211-193e13.5	ENSDARG00000042558	ENSDARG00000027750 dpp7	ENSDARG00000005840 got2b	ENSDARG00000009978 icn
ENSDARG00000053858 crip1	ENSDARG00000076657 plagl2	ENSDARG00000016745 slc35f6	ENSDARG00000028323	ENSDARG00000035858 cnn2
ENSDARG00000093887	ENSDARG00000088717 ecrg4b	ENSDARG00000022315 atp6v1g1	ENSDARG00000014017 rrm1	ENSDARG00000055751 fosb
ENSDARG00000011239 ppp1r14aa	ENSDARG00000090600 si:ch211-213a13.1	ENSDARG00000089383 il1fma	ENSDARG00000036675 hnrnpa1b	ENSDARG00000006514 her6
ENSDARG00000043587 srd5a2a	ENSDARG00000060041 lig1	ENSDARG00000069025 si:ch211-283g2.2	ENSDARG00000024109 naa40	ENSDARG00000042690 s1pr1
ENSDARG00000086869	ENSDARG00000018902 pes	ENSDARG00000088439 gm2a	ENSDARG00000028335 hmga1a	ENSDARG00000034718 tfpia
ENSDARG00000088091 pfn1	ENSDARG00000077473 mych	ENSDARG00000004405 snx10a	ENSDARG00000014499 nutf2l	ENSDARG00000074829 rasip1
ENSDARG00000045224 glipr1a	ENSDARG00000079808 si:ch73-208g10.1	ENSDARG00000062352 sema4ab	ENSDARG00000036791 dnmt3bb.1	ENSDARG00000025254 s100a10b
ENSDARG00000000767 spi1b	ENSDARG00000045132 vdac1	ENSDARG00000037153 atp6ap1b	ENSDARG00000092693 tpt1	ENSDARG00000037429 tll1
ENSDARG00000018283 cyba	ENSDARG00000059486 cplx4b	ENSDARG00000076221 zgc:198419	ENSDARG00000008680	ENSDARG00000025428 socs3a
ENSDARG00000007769 sult5a1	ENSDARG00000056621 ctcf	ENSDARG00000043403 paox1	ENSDARG00000031495 seta	ENSDARG00000074849 rac1a
ENSDARG00000053836 si:ch211-284o19.8	ENSDARG00000019529 parp1	ENSDARG00000031731 si:ch73-27e22.6	ENSDARG00000069619 atf7ip	ENSDARG00000070653
ENSDARG00000054588 cox6a2	ENSDARG00000030789 ddx18	ENSDARG00000034534 atp6v1aa	ENSDARG00000004342	ENSDARG00000038025 cbx7a
ENSDARG00000078734 myo1f	ENSDARG00000003920 setb	ENSDARG00000008735 atp6ap2	ENSDARG00000034785 dachb	ENSDARG00000015495 klf3
ENSDARG00000070315	ENSDARG00000093507	ENSDARG00000059883 trpv1	ENSDARG00000016889 eif3g	ENSDARG00000053561 ms4a17a.11

1	2	3	4	5
ENSDARG00000031153	ENSDARG00000015566 dnmt3ab	ENSDARG00000071586 tgfbi	ENSDARG00000089426	ENSDARG00000044251 rasgef1bb
ENSDARG00000005230 ssr2	ENSDARG00000010246 prmt1	ENSDARG00000005039	ENSDARG00000019930 tal1	ENSDARG00000080020 il13ra1
ENSDARG00000039007 eno3	ENSDARG00000004433 btk	ENSDARG00000075831 slc7a8a	ENSDARG00000020901 gabrp	ENSDARG00000087796
ENSDARG00000029695 pgp	ENSDARG00000023299 snu13b	ENSDARG00000067797 spi1a	ENSDARG00000082894	ENSDARG00000026039
ENSDARG00000057708 PHTF1	ENSDARG00000004926	ENSDARG00000093549 sepp1a	ENSDARG00000012820 nop56	ENSDARG00000045524 lamb1b
ENSDARG00000078193 si:ch211-67e16.3	ENSDARG00000044402 nop16	ENSDARG00000042793 tpp1	ENSDARG00000056167 hspe1	ENSDARG00000014947
ENSDARG00000057430	ENSDARG00000035750	ENSDARG00000011175 atp6v1d	ENSDARG00000045399 cct5	ENSDARG00000008030 myl9b
ENSDARG00000006019 tktb	ENSDARG00000092033 si:dkey-239h2.3	ENSDARG00000045980 cst14b.1	ENSDARG00000023330 anp32b	ENSDARG00000020235 sept9a
ENSDARG00000076229 mkl1b	ENSDARG00000087387 znf1038	ENSDARG00000074782 CABZ01056055.1	ENSDARG00000052480 pdcd11	ENSDARG00000015759 tspan7
ENSDARG00000013705 ccm2	ENSDARG00000055389 si:dkey-67c22.2	ENSDARG00000052712 suclg1	ENSDARG00000033945	ENSDARG00000013853 lmo4a
ENSDARG00000090730 zgc:158446	ENSDARG00000087238 si:ch211-161h7.4	ENSDARG00000089307 pmaip1	ENSDARG00000058419 gcn1	ENSDARG00000061579 myo1cb

table S2, 5 dpf wild type vs LY294002 treated

1	2	3	4	5
ENSDARG00000091038	ENSDARG00000087390 hbbe1.3	ENSDARG00000032102 prdx3	ENSDARG00000005419	ENSDARG00000057789 lyz
ENSDARG00000060457 pmp22b	ENSDARG00000089124 hbae1.3	ENSDARG00000008840 hmbsa	ENSDARG00000074322 si:ch211-194m7.3	ENSDARG00000075664 si:ch1073-429i10.1
ENSDARG00000080337 AC024175.4	ENSDARG00000079305 hbae3	ENSDARG00000029019 epb41b	ENSDARG00000091078	ENSDARG00000021339 cpa5
ENSDARG00000082753 AC024175.17	ENSDARG00000077504 si:ch211-103n10.5	ENSDARG00000057206 nmt1b	ENSDARG00000079736	ENSDARG00000010423 npsn
ENSDARG00000080009 bahcc1b	ENSDARG00000089475 hbae1	ENSDARG00000013110 dmtn	ENSDARG00000043436 si:dkey-5n18.1	ENSDARG00000077069 srgn
ENSDARG00000019130 plk2b	ENSDARG00000011166 cahz	ENSDARG00000055991 hmbsb	ENSDARG00000087353	ENSDARG00000019521 mpx
ENSDARG00000084962	ENSDARG00000045143 hbbe2	ENSDARG00000012881 slc4a1a	ENSDARG00000032849 ndrg1a	ENSDARG00000008155 sms
ENSDARG00000012820 nop56	ENSDARG00000038643 alas2	ENSDARG00000092164	ENSDARG00000026829 cotl1	ENSDARG00000033227 lect2l
ENSDARG00000035773	ENSDARG00000089963 hbbe1.1	ENSDARG00000014947	ENSDARG00000058731 slc2a6	ENSDARG00000056200 abcb9
ENSDARG00000082180	ENSDARG00000088330 AL935210.1	ENSDARG00000076858 C8orf4	ENSDARG00000035715 marcksl1b	ENSDARG00000038728 ch25hl2
ENSDARG00000096145	ENSDARG00000045142 hbae5	ENSDARG00000075180 tmem14ca	ENSDARG00000037870 actb2	ENSDARG00000056600 papss2b
ENSDARG00000028323	ENSDARG00000090689 hbbe1.2	ENSDARG00000041607 eif4ebp3l	ENSDARG00000027063 arpc1b	ENSDARG00000035326 nccrp1
ENSDARG00000095268 si:dkey-261h17.1	ENSDARG00000045144 hbz	ENSDARG00000030490 sptb	ENSDARG00000069844 irg1	ENSDARG00000006029 lta4h
ENSDARG00000005834 gatad2b	ENSDARG00000055991 hmbsb	ENSDARG00000019253 rhag	ENSDARG00000088439 gm2a	ENSDARG00000043457 gapdh

1	2	3	4	5
ENSDARG00000070212	ENSDARG00000096667 si:dkey-25o16.2	ENSDARG00000070843 arid3a	ENSDARG00000054610 coro1a	ENSDARG00000036966 hsd3b7
ENSDARG00000055868 rsl1d1	ENSDARG00000042310	ENSDARG00000006818 urod	ENSDARG00000077777 tmsb4x	ENSDARG00000035018 thy1
ENSDARG00000080010 adh5	ENSDARG00000012881 slc4a1a	ENSDARG00000054155 pcna	ENSDARG00000020929 fam49ba	ENSDARG00000036940 ctss1
ENSDARG00000043317 kita	ENSDARG00000023713 aqp1a.1	ENSDARG00000068822 purba	ENSDARG00000018283 cyba	ENSDARG00000025147 cd63
ENSDARG00000042940 nab1a	ENSDARG00000026655 tspo	ENSDARG00000017400 klf1	ENSDARG00000044129 FP015823.1	ENSDARG00000059388 bdh1
ENSDARG00000006514 her6	ENSDARG00000053066 tubb1	ENSDARG00000038097 pigq	ENSDARG00000090783 mfap4	ENSDARG00000070398
ENSDARG00000058337	ENSDARG00000034852 nt5c2l1	ENSDARG00000042310	ENSDARG00000054543 samsn1a	ENSDARG00000036074 cebpa
ENSDARG00000008976 mdn1	ENSDARG00000006260 tuba8l4	ENSDARG00000026655 tspo	ENSDARG00000068784 VSIR	ENSDARG00000058593 sri
ENSDARG00000018961 gtpbp4	ENSDARG00000006818 urod	ENSDARG00000019930 tal1	ENSDARG00000058941	ENSDARG00000053381 plpp1a
ENSDARG00000036791 dnmt3bb.1	ENSDARG00000018461 zgc:56095	ENSDARG00000043665 glrx5	ENSDARG00000090890 cmklr1	ENSDARG00000063295 myh9a
ENSDARG00000004588 sox4a	ENSDARG00000020890 tmod4	ENSDARG00000004392 hdr	ENSDARG00000086947 si:ch211-147m6.1	ENSDARG00000053542 kctd12.2
ENSDARG00000016484 dkc1	ENSDARG00000008840 hmbsa	ENSDARG00000068820 h2afva	ENSDARG00000059906 sdc4	ENSDARG00000009208 prkcda
ENSDARG00000054290 acin1a	ENSDARG00000025350 prdx2	ENSDARG00000052815	ENSDARG00000036637 arl11	ENSDARG00000058348 scinlb
ENSDARG00000027777 tnfaip3	ENSDARG00000057206 nmt1b	ENSDARG00000054929 zgc:110540	ENSDARG00000028618 KRT18	ENSDARG00000055064 prdx5
ENSDARG00000087504	ENSDARG00000044212 CR735126.1	ENSDARG00000035750	ENSDARG00000036427 slc3a2a	ENSDARG00000058734 prdx1

1	2	3	4	5
ENSDARG00000008109	ENSDARG00000058471 plk1	ENSDARG00000003462 fech	ENSDARG00000019062 arpc5b	ENSDARG00000035136 sepw1
ENSDARG00000063626 ddx21	ENSDARG00000008678 snx3	ENSDARG00000044968 vcla	ENSDARG00000009978 icn	ENSDARG00000015343 pgd
ENSDARG00000032868 pde4ba	ENSDARG00000015551 fth1a	ENSDARG00000078085	ENSDARG00000054942 lgals2a	ENSDARG00000010556 CABZ01030094.1
ENSDARG00000079553 cd83	ENSDARG00000071697 zgc:66433	ENSDARG00000020621 ap1b1	ENSDARG00000033735 ncf1	ENSDARG00000013561 pgm1
ENSDARG00000041895 cad	ENSDARG00000030490 sptb	ENSDARG00000096667 si:dkey-25o16.2	ENSDARG00000055504 si:ch211-212k18.7	ENSDARG00000054755 alox5ap
ENSDARG00000040503 sb:cb81	ENSDARG00000002790 ap2m1a	ENSDARG00000025350 prdx2	ENSDARG00000088091 pfn1	ENSDARG00000024116 vamp8
ENSDARG00000031756 mef2aa	ENSDARG00000029019 epb41b	ENSDARG00000042533 gstm.1	ENSDARG00000086869	ENSDARG00000031153
ENSDARG00000026723 syncripl	ENSDARG00000010792 cdc25b	ENSDARG00000070657 pa2g4b	ENSDARG00000013598 tnfb	ENSDARG00000057882 arpc3
ENSDARG00000076532 si:ch211-222l21.1	ENSDARG00000008333 znfl2a	ENSDARG00000042894 tyms	ENSDARG00000036893 f13a1b	ENSDARG00000077777 tmsb4x
ENSDARG00000002710 ncl	ENSDARG00000027491 uros	ENSDARG00000027491 uros	ENSDARG00000023188 lcp1	ENSDARG00000039884
ENSDARG00000077264 wdr43	ENSDARG00000017400 klf1	ENSDARG00000025200	ENSDARG00000022139 ocstamp	ENSDARG00000054610 coro1a
ENSDARG00000088673	ENSDARG00000052815	ENSDARG00000092546 pdap1a	ENSDARG00000017653 rgs13	ENSDARG00000012395 mmp13a
ENSDARG00000023290 fabp3	ENSDARG00000054929 zgc:110540	ENSDARG00000070670 crip2	ENSDARG00000056615 cybb	ENSDARG00000023188 lcp1
ENSDARG00000041959 cxcr4b	ENSDARG00000038066 kpna2	ENSDARG00000002790 ap2m1a	ENSDARG00000042370 ptafr	ENSDARG00000070315
ENSDARG00000037919 rbbp6	ENSDARG00000075180 tmem14ca	ENSDARG00000053066 tubb1	ENSDARG00000043257 ckbb	ENSDARG00000053858 crip1

1	2	3	4	5
ENSDARG00000005191 ahcy	ENSDARG00000023330 anp32b	ENSDARG00000058725 rfesd	ENSDARG00000036785 si:ch211-226m16.2	ENSDARG00000052438 actr2a
ENSDARG00000035990 cited4a	ENSDARG00000025200	ENSDARG00000013477 gata1a	ENSDARG00000033614 rasgef1ba	ENSDARG00000004034 arhgdig
ENSDARG00000032327 usp36	ENSDARG00000087554 cdk1	ENSDARG00000071670 tma7	ENSDARG00000039034 marcksl1a	ENSDARG00000034187 calm1b
ENSDARG00000014587 slc38a5b	ENSDARG00000010948 kif11	ENSDARG00000015551 fth1a	ENSDARG00000025147 cd63	ENSDARG00000043102 lxn
ENSDARG00000032849 ndrg1a	ENSDARG00000014013 lbr	ENSDARG00000077620 cdca7a	ENSDARG00000075748 NCKAP1L	ENSDARG00000002021 pygb
ENSDARG00000053666 myb	ENSDARG00000035519 hist1h1l	ENSDARG00000088330 AL935210.1	ENSDARG00000056874 lygl1	ENSDARG00000042876 abracl
ENSDARG00000058419 gcn1	ENSDARG00000063345	ENSDARG00000011166 cahz	ENSDARG00000014348 stk17b	ENSDARG00000013670 hyou1
ENSDARG00000030053 eef1db	ENSDARG00000053467 gtpbp1	ENSDARG00000038643 alas2	ENSDARG00000060926 rnf19b	ENSDARG00000088091 pfn1
ENSDARG00000029150 hsp90ab1	ENSDARG00000088554	ENSDARG00000043713 asf1bb	ENSDARG00000095556 CR318588.4	ENSDARG00000053956 sptbn2
ENSDARG00000043126 blf	ENSDARG00000035423	ENSDARG00000074581 add2	ENSDARG00000041505 itm2bb	ENSDARG00000035622 xbp1
ENSDARG00000014329 npm1a	ENSDARG00000045618 clta	ENSDARG00000023330 anp32b	ENSDARG00000075989 arpc2	ENSDARG00000038010 rac2
ENSDARG00000005481 nfkbiaa	ENSDARG00000042894 tyms	ENSDARG00000009315 clgn	ENSDARG00000013681 si:dkey-42i9.6	ENSDARG00000053836 si:ch211-284o19.8
ENSDARG00000056438 her9	ENSDARG00000086112 si:ch211-266i6.3	ENSDARG00000038792 klf17	ENSDARG00000059679	ENSDARG00000019236 gsr
ENSDARG00000015164 mknk2b	ENSDARG00000038792 klf17	ENSDARG00000040041 mcm4	ENSDARG00000051888 ist1	ENSDARG00000012972 cfl1l
ENSDARG00000058606 sik1	ENSDARG00000051923 ccnb1	ENSDARG00000021702 pdcd4a	ENSDARG00000057882 arpc3	ENSDARG00000093887

1	2	3	4	5
ENSDARG00000013489	ENSDARG00000041623 mt2	ENSDARG00000006260 tuba8l4	ENSDARG00000042876 abracl	ENSDARG00000036967 smox
ENSDARG00000044129 FP015823.1	ENSDARG00000001558 kifc1	ENSDARG00000014017 rrm1	ENSDARG00000055120 ctsba	ENSDARG00000025375 idh1
ENSDARG00000035751 ipo7	ENSDARG00000022934	ENSDARG00000025635	ENSDARG00000074262 nck1a	ENSDARG00000044619 birc2
ENSDARG00000028335 hmga1a	ENSDARG00000054447 slc29a1b	ENSDARG00000024295 slc11a2	ENSDARG00000038458	ENSDARG00000058858
ENSDARG00000062543	ENSDARG00000071863 itgb1a	ENSDARG00000002659 mapre1b	ENSDARG00000044670	ENSDARG00000027063 arpc1b
ENSDARG00000054272 caprin1b	ENSDARG00000017864	ENSDARG00000093572 lamc3	ENSDARG00000005463 slc30a1a	ENSDARG00000037746 actb1
ENSDARG00000023217 crema	ENSDARG00000024295 slc11a2	ENSDARG00000039578 pa2g4a	ENSDARG00000012395 mmp13a	ENSDARG00000033738 zgc:153867
ENSDARG00000017568	ENSDARG00000018146 gpx1a	ENSDARG00000018461 zgc:56095	ENSDARG00000010423 npsn	ENSDARG00000058225 arpc4l
ENSDARG00000040184 syncrip	ENSDARG00000002194 rhd	ENSDARG00000052304 uqcrc1	ENSDARG00000031681 atp6v0b	ENSDARG00000026829 cotl1
ENSDARG00000003599 rpl3	ENSDARG00000031775 ube2s	ENSDARG00000044550 hif1al2	ENSDARG00000035676 ptp4a2b	ENSDARG00000033735 ncf1
ENSDARG00000040439 rsl24d1	ENSDARG00000032102 prdx3	ENSDARG00000003693 hars	ENSDARG00000058348 scinlb	ENSDARG00000055562
ENSDARG00000052856 khdrbs1a	ENSDARG00000020442 snx5	ENSDARG00000023713 aqp1a.1	ENSDARG00000077308 gpr84	ENSDARG00000067545 adam19b
ENSDARG00000013351 cirbpb	ENSDARG00000077383 anxa11a	ENSDARG00000015911	ENSDARG00000016886 dnajb9b	ENSDARG00000024314 herpud1
ENSDARG00000096403 CT027638.1	ENSDARG00000020504 h3f3b.1	ENSDARG00000020454 psmd8	ENSDARG00000043802 ms4a17a.9	ENSDARG00000037870 actb2
ENSDARG00000042725 cebpb	ENSDARG00000013110 dmtn	ENSDARG00000057912 eif1axb	ENSDARG00000040528 lgals3bpb	ENSDARG00000012987 gpia

1	2	3	4	5
ENSDARG00000030602 rps19	ENSDARG00000055498 si:ch1073-184j22.1	ENSDARG00000068724	ENSDARG00000070378 ccl35.2	ENSDARG00000075989 arpc2
ENSDARG00000056119 eef1g	ENSDARG00000043137 cdca8	ENSDARG00000012684 atp2b1a	ENSDARG00000088745 MFAP4	ENSDARG00000076229 mkl1b
ENSDARG00000056186 eif5a2	ENSDARG00000005454 tacc3	ENSDARG00000020890 tmod4	ENSDARG00000010191	ENSDARG00000077991
ENSDARG00000011201 rplp2l	ENSDARG00000058226 ak3	ENSDARG00000062338 zeb2a	ENSDARG00000038822 mrc1b	ENSDARG00000039007 eno3
ENSDARG00000083950 snoU83B	ENSDARG00000020192	ENSDARG00000053646 adrb3a	ENSDARG00000022303 higd1a	ENSDARG00000016939 itgb2
ENSDARG00000015862 rpl5b	ENSDARG00000009315 clgn	ENSDARG00000044212 CR735126.1	ENSDARG00000039914 gapdhs	ENSDARG00000018259 atp1a3a
ENSDARG00000030585	ENSDARG00000003462 fech	ENSDARG00000043493 cltca	ENSDARG00000037746 actb1	ENSDARG00000043257 ckbb
ENSDARG00000011405 rps9	ENSDARG00000004926	ENSDARG00000074076	ENSDARG00000070426 chac1	ENSDARG00000014348 stk17b
ENSDARG00000035692 rps3a	ENSDARG00000038097 pigq	ENSDARG00000089963 hbbe1.1	ENSDARG00000089706 ANPEP	ENSDARG00000014433
ENSDARG00000037350 rpl9	ENSDARG00000057432	ENSDARG00000020008 vcp	ENSDARG00000004034 arhgdig	ENSDARG00000033437 rps6ka1
ENSDARG00000036161 hnrnpa0l	ENSDARG00000078654 tpx2	ENSDARG00000071697 zgc:66433	ENSDARG00000018174 gnai2a	ENSDARG00000078734 myo1f
ENSDARG00000068992 hspa8	ENSDARG00000043250 ppm1ab	ENSDARG00000073850 hdac7b	ENSDARG00000075592 tnfaip8l2a	ENSDARG00000078888 iqgap1
ENSDARG00000020153	ENSDARG00000021439 ncoa4	ENSDARG00000019507 mcm5	ENSDARG00000093549 sepp1a	ENSDARG00000057430
ENSDARG00000036174	ENSDARG00000071442	ENSDARG00000057414 phb	ENSDARG00000096508 BX322618.1	ENSDARG00000089776
ENSDARG00000015490	ENSDARG00000071410 cks2	ENSDARG00000011404 fen1	ENSDARG00000086246	ENSDARG00000045836 mapk11

1	2	3	4	5
ENSDARG00000053291 pnrc2	ENSDARG00000068820 h2afva	ENSDARG00000091150 mki67	ENSDARG00000025493	ENSDARG00000039914 gapdhs
ENSDARG00000036629 rps14	ENSDARG00000052638 fam210b	ENSDARG00000035423	ENSDARG00000058606 sik1	ENSDARG00000057867 lasp1
ENSDARG00000039641	ENSDARG00000044550 hif1al2	ENSDARG00000003920 setb	ENSDARG00000068628 rab8b	ENSDARG00000044125 txn
ENSDARG00000019230 rpl7a	ENSDARG00000091209 ucp3	ENSDARG00000005540 xpo7	ENSDARG00000015278 plxnc1	ENSDARG00000059110
ENSDARG00000029533 rpl18	ENSDARG00000020621 ap1b1	ENSDARG00000045399 cct5	ENSDARG00000043608 eif4ebp1	ENSDARG00000026369 dbi
ENSDARG00000010516 rpl21	ENSDARG00000035770 ube2c	ENSDARG00000010194 eif4bb	ENSDARG00000004979 elovl5	ENSDARG00000054063 arpc4
ENSDARG00000034897 rps10	ENSDARG00000037188 rpa2	ENSDARG00000020101 psmc2	ENSDARG00000035652 sat1a.1	ENSDARG00000039142 arpc5a
ENSDARG00000006413 rpl38	ENSDARG00000063385 cenpe	ENSDARG00000043126 blf	ENSDARG00000031153	ENSDARG00000086869
ENSDARG00000046119	ENSDARG00000040163 prim1	ENSDARG00000052816 shmt1	ENSDARG00000054063 arpc4	ENSDARG00000056090 capza1b
ENSDARG00000013012	ENSDARG00000002403 nusap1	ENSDARG00000043631 bcas2	ENSDARG00000016465	ENSDARG00000007682 ppdpfa
ENSDARG00000041811 rps25	ENSDARG00000019231 spna2	ENSDARG00000037038 psmc6	ENSDARG00000086826 sult6b1	ENSDARG00000075592 tnfaip8l2a

table S2, 5dpf pten mutants vs siblings

1	2	3	4	5
ENSDARG00000043126 blf	ENSDARG00000091038	ENSDARG00000019253 rhag	ENSDARG00000079736	ENSDARG00000079305 hbae3
ENSDARG00000006514 her6	ENSDARG00000044129 FP015823.1	ENSDARG00000041607 eif4ebp3l	ENSDARG00000095351 CU914776.2	ENSDARG00000087390 hbbe1.3
ENSDARG00000060457 pmp22b	ENSDARG00000019130 plk2b	ENSDARG00000032102 prdx3	ENSDARG00000036637 arl11	ENSDARG00000089124 hbae1.3
ENSDARG00000043317 kita	ENSDARG00000095268 si:dkey-261h17.1	ENSDARG00000073850 hdac7b	ENSDARG00000027063 arpc1b	ENSDARG00000038643 alas2
ENSDARG00000040503 sb:cb81	ENSDARG00000091419 nrarpa	ENSDARG00000038559 h1f0	ENSDARG00000042816 mmp9	ENSDARG00000077504 si:ch211-103n10.5
ENSDARG00000007241 mycb	ENSDARG00000042725 cebpb	ENSDARG00000070843 arid3a	ENSDARG00000091993 CR792453.2	ENSDARG00000011166 cahz
ENSDARG00000070670 crip2	ENSDARG00000054632 fli1a	ENSDARG00000021702 pdcd4a	ENSDARG00000077777 tmsb4x	ENSDARG00000045143 hbbe2
ENSDARG00000019930 tal1	ENSDARG00000090444 ponzr1	ENSDARG00000025350 prdx2	ENSDARG00000012395 mmp13a	ENSDARG00000088330 AL935210.1
ENSDARG00000092164	ENSDARG00000032868 pde4ba	ENSDARG00000090834 epor	ENSDARG00000037870 actb2	ENSDARG00000055498 si:ch1073-184j22.1
ENSDARG00000086927 pik3c2b	ENSDARG00000073681	ENSDARG00000003281 pik3ip1	ENSDARG00000014348 stk17b	ENSDARG00000044212 CR735126.1
ENSDARG00000041895 cad	ENSDARG00000079808 si:ch73-208g10.1	ENSDARG00000076858 C8orf4	ENSDARG00000026829 cotl1	ENSDARG00000089475 hbae1
ENSDARG00000053666 myb	ENSDARG00000042940 nab1a	ENSDARG00000035810 rgcc	ENSDARG00000010423 npsn	ENSDARG00000055991 hmbsb
ENSDARG00000035810 rgcc	ENSDARG00000087504	ENSDARG00000022165 mgst1.2	ENSDARG00000019521 mpx	ENSDARG00000088554

1	2	3	4	5
ENSDARG00000031817 trim2a	ENSDARG00000031683 fosab	ENSDARG00000019507 mcm5	ENSDARG00000023188 lcp1	ENSDARG00000023713 aqp1a.1
ENSDARG00000005191 ahcy	ENSDARG00000058606 sik1	ENSDARG00000005897 dera	ENSDARG00000089706 ANPEP	ENSDARG00000020890 tmod4
ENSDARG00000095749	ENSDARG00000087616 maptb	ENSDARG00000031756 mef2aa	ENSDARG00000054610 coro1a	ENSDARG00000012881 slc4a1a
ENSDARG00000034785 dachb	ENSDARG00000035773	ENSDARG00000040041 mcm4	ENSDARG00000019062 arpc5b	ENSDARG00000045144 hbz
ENSDARG00000035573 AK6	ENSDARG00000079553 cd83	ENSDARG00000018461 zgc:56095	ENSDARG00000067566 sftpbb	ENSDARG00000053467 gtpbp1
ENSDARG00000031756 mef2aa	ENSDARG00000035622 xbp1	ENSDARG00000078691 gigyf1	ENSDARG00000043257 ckbb	ENSDARG00000096667 si:dkey-25o16.2
ENSDARG00000070404 fam212ab	ENSDARG00000052402 dnmt3ba	ENSDARG00000030756 dnmt1	ENSDARG00000079387 si:ch211-102c2.4	ENSDARG00000029019 epb41b
ENSDARG00000080009 bahcc1b	ENSDARG00000004034 arhgdig	ENSDARG00000016477 eif4a2	ENSDARG00000036628 cd74b	ENSDARG00000026655 tspo
ENSDARG00000008333 znfl2a	ENSDARG00000093817	ENSDARG00000016651 znf106a	ENSDARG00000058348 scinlb	ENSDARG00000053066 tubb1
ENSDARG00000060012 f2r	ENSDARG00000028335 hmga1a	ENSDARG00000019930 tal1	ENSDARG00000094708 sftpba	ENSDARG00000090689 hbbe1.2
ENSDARG00000053912 fbl	ENSDARG00000070315	ENSDARG00000024295 slc11a2	ENSDARG00000006029 lta4h	ENSDARG00000021439 ncoa4
ENSDARG00000014587 slc38a5b	ENSDARG00000095556 CR318588.4	ENSDARG00000018146 gpx1a	ENSDARG00000090730 zgc:158446	ENSDARG00000042751 riok3
ENSDARG00000090834 epor	ENSDARG00000094975 FP015823.2	ENSDARG00000070670 crip2	ENSDARG00000071437 ptprc	ENSDARG00000089963 hbbe1.1
ENSDARG00000026489 khsrp	ENSDARG00000088371	ENSDARG00000079012 CBFA2T3	ENSDARG00000044395	ENSDARG00000025200
ENSDARG00000002710 ncl	ENSDARG00000039007 eno3	ENSDARG00000004392 hdr	ENSDARG00000016774 plekho2	ENSDARG00000013110 dmtn

1	2	3	4	5
ENSDARG00000037897	ENSDARG00000074378 junba	ENSDARG00000057683 mcm6	ENSDARG00000090473 si:ch211-269k10.5	ENSDARG00000009867
ENSDARG00000019253 rhag	ENSDARG00000076532 si:ch211-222l21.1	ENSDARG00000062338 zeb2a	ENSDARG00000021339 cpa5	ENSDARG00000034852 nt5c2l1
ENSDARG00000012820 nop56	ENSDARG00000000796 nr4a1	ENSDARG00000008333 znfl2a	ENSDARG00000038458	ENSDARG00000006818 urod
ENSDARG00000004392 hdr	ENSDARG00000041041 cxcr3.2	ENSDARG00000063345	ENSDARG00000041505 itm2bb	ENSDARG00000068096 atf5a
ENSDARG00000073850 hdac7b	ENSDARG00000017653 rgs13	ENSDARG00000070866 tmem11	ENSDARG00000053484 syne2b	ENSDARG00000057206 nmt1b
ENSDARG00000079605 prmt5	ENSDARG00000076120 foxp4	ENSDARG00000017400 klf1	ENSDARG00000088091 pfn1	ENSDARG00000019231 spna2
ENSDARG00000077264 wdr43	ENSDARG00000035990 cited4a	ENSDARG00000014969 ankhb	ENSDARG00000070306	ENSDARG00000003462 fech
ENSDARG00000012244 ube2e3	ENSDARG00000078473 nucks1a	ENSDARG00000063626 ddx21	ENSDARG00000086337 si:dkey-102g19.3	ENSDARG00000092945 si:ch211-250g4.3
ENSDARG00000023290 fabp3	ENSDARG00000021113 ptmaa	ENSDARG00000015551 fth1a	ENSDARG00000057882 arpc3	ENSDARG00000042310
ENSDARG00000028323	ENSDARG00000010556 CABZ01030094.1	ENSDARG00000058538 alcamb	ENSDARG00000009782 myh11a	ENSDARG00000058476 stc1l
ENSDARG00000075666 tsc22d3	ENSDARG00000041959 cxcr4b	ENSDARG00000000103 myh10	ENSDARG00000009087 cd74a	ENSDARG00000010792 cdc25b
ENSDARG00000014591 ilf2	ENSDARG00000074301 cth	ENSDARG00000013110 dmtn	ENSDARG00000075748 NCKAP1L	ENSDARG00000008840 hmbsa
ENSDARG00000023299 snu13b	ENSDARG00000001873 phgdh	ENSDARG00000042310	ENSDARG00000023578 lpp	ENSDARG00000030490 sptb
ENSDARG00000033440 metap1	ENSDARG00000052826 runx3	ENSDARG00000057206 nmt1b	ENSDARG00000088439 gm2a	ENSDARG00000035256 eef2l2
ENSDARG00000014329 npm1a	ENSDARG00000040076 pycard	ENSDARG00000013477 gata1a	ENSDARG00000035136 sepw1	ENSDARG00000089309

1	2	3	4	5
ENSDARG00000005834 gatad2b	ENSDARG00000067850 jund	ENSDARG00000068822 purba	ENSDARG00000016939 itgb2	ENSDARG00000054447 slc29a1b
ENSDARG00000077473 mych	ENSDARG00000004702 irf2bp2a	ENSDARG00000042533 gstm.1	ENSDARG00000000767 spi1b	ENSDARG00000052942 aspg
ENSDARG00000039887 c1qbp	ENSDARG00000089933 rasal3	ENSDARG00000030490 sptb	ENSDARG00000037746 actb1	ENSDARG00000027491 uros
ENSDARG00000076532 si:ch211-222l21.1	ENSDARG00000055713 fmnl1a	ENSDARG00000035761	ENSDARG00000005419	ENSDARG00000024295 slc11a2
ENSDARG00000035043 pfdn5	ENSDARG00000079193	ENSDARG00000074581 add2	ENSDARG00000020929 fam49ba	ENSDARG00000061591 abcb10
ENSDARG00000017568	ENSDARG00000094408 MFAP4	ENSDARG00000045019 aamp	ENSDARG00000068784 VSIR	ENSDARG00000025338 hagh
ENSDARG00000010246 prmt1	ENSDARG00000023217 crema	ENSDARG00000053666 myb	ENSDARG00000010785 thbs1b	ENSDARG00000022934
ENSDARG00000095019 lmo2	ENSDARG00000036791 dnmt3bb.1	ENSDARG00000035750	ENSDARG00000017653 rgs13	ENSDARG00000093572 lamc3
ENSDARG00000008109	ENSDARG00000056346 acap1	ENSDARG00000052815	ENSDARG00000063295 myh9a	ENSDARG00000010948 kif11
ENSDARG00000053485 aldh6a1	ENSDARG00000045695 myca	ENSDARG00000037393 slc43a1a	ENSDARG00000053279 apln	ENSDARG00000015551 fth1a
ENSDARG00000045776 cnbpa	ENSDARG00000058593 sri	ENSDARG00000029019 epb41b	ENSDARG00000055759 efhd2	ENSDARG00000052815
ENSDARG00000069422 nhp2	ENSDARG00000002131 celf2	ENSDARG00000027491 uros	ENSDARG00000094965 nfil3-5	ENSDARG00000032951 nrbp2a
ENSDARG00000040128	ENSDARG00000019307 dusp5	ENSDARG00000015911	ENSDARG00000068233 CD53	ENSDARG00000009315 clgn
ENSDARG00000055868 rsl1d1	ENSDARG00000056111 lmod1a	ENSDARG00000008840 hmbsa	ENSDARG00000076772	ENSDARG00000020984 slc16a10
ENSDARG00000039578 pa2g4a	ENSDARG00000039034 marcksl1a	ENSDARG00000075180 tmem14ca	ENSDARG00000007682 ppdpfa	ENSDARG00000052638 fam210b

1	2	3	4	5
ENSDARG00000010244 rpl22l1	ENSDARG00000043608 eif4ebp1	ENSDARG00000079848 gmps	ENSDARG00000039884	ENSDARG00000010437 fam46c
ENSDARG00000070475 khdrbs1b	ENSDARG00000076562	ENSDARG00000076116	ENSDARG00000055186 ccr9a	ENSDARG00000002790 ap2m1a
ENSDARG00000071670 tma7	ENSDARG00000005423 pgam1a	ENSDARG00000039578 pa2g4a	ENSDARG00000075989 arpc2	ENSDARG00000020192
ENSDARG00000018961 gtpbp4	ENSDARG00000022684 fkbp1aa	ENSDARG00000052638 fam210b	ENSDARG00000053542 kctd12.2	ENSDARG00000059682 slc43a3a
ENSDARG00000092807 RPL41	ENSDARG00000040623 fosl2	ENSDARG00000020621 ap1b1	ENSDARG00000023217 crema	ENSDARG00000025350 prdx2
ENSDARG00000014123	ENSDARG00000053858 crip1	ENSDARG00000027515	ENSDARG00000062721 dennd4a	ENSDARG00000035519 histh1l
ENSDARG00000036044 rps20	ENSDARG00000020759 ef1	ENSDARG00000096667 si:dkey-25o16.2	ENSDARG00000013916	ENSDARG00000071863 itgb1a
ENSDARG00000006413 rpl38	ENSDARG00000036482 hexim1	ENSDARG00000006200 eif4g1a	ENSDARG00000093124 scpp8	ENSDARG00000058471 plk1
ENSDARG00000058337	ENSDARG00000088325	ENSDARG00000054320 ap2a1	ENSDARG00000018283 cyba	ENSDARG00000017400 klf1
ENSDARG00000056167 hspe1	ENSDARG00000056438 her9	ENSDARG00000077264 wdr43	ENSDARG00000059110	ENSDARG00000058725 rfesd
ENSDARG00000011125 snrpb	ENSDARG00000039269 arg2	ENSDARG00000006818 urod	ENSDARG00000058225 arpc4l	ENSDARG00000043604
ENSDARG00000042389	ENSDARG00000001169 hsd17b8	ENSDARG00000018961 gtpbp4	ENSDARG00000006640 eomesa	ENSDARG00000005540 xpo7
ENSDARG00000039347 rps24	ENSDARG00000086768	ENSDARG00000012881 slc4a1a	ENSDARG00000077069 srgn	ENSDARG00000043250 ppm1ab
ENSDARG00000041232 rps29	ENSDARG00000062049 hmha1b	ENSDARG00000005926 ak2	ENSDARG00000042725 cebpb	ENSDARG00000005454 tacc3
ENSDARG00000056008 atp5g1	ENSDARG00000069846 zgc:162944	ENSDARG00000054155 pcna	ENSDARG00000016154 zfp36l1a	ENSDARG00000001558 kifc1

1	2	3	4	5
ENSDARG00000008243 cct8	ENSDARG00000044562 cycsb	ENSDARG00000026655 tspo	ENSDARG00000046004	ENSDARG00000051923 ccnb1
ENSDARG00000054818 rpl32	ENSDARG00000013351 cirbpb	ENSDARG00000002790 ap2m1a	ENSDARG00000031153	ENSDARG00000071697 zgc:66433
ENSDARG00000006316 rpl23a	ENSDARG00000058858	ENSDARG00000088449 wu:fb55g09	ENSDARG00000038010 rac2	ENSDARG00000006260 tuba8l4
ENSDARG00000029500 rpl34	ENSDARG00000010965 psma8	ENSDARG00000053485 aldh6a1	ENSDARG00000056615 cybb	ENSDARG00000094977 si:ch211-156j22.4
ENSDARG00000077717 rpl29	ENSDARG00000042502	ENSDARG00000095019 lmo2	ENSDARG00000054063 arpc4	ENSDARG00000031164 tuba8l2
ENSDARG00000036316 rpl39	ENSDARG00000055186 ccr9a	ENSDARG00000076815 eif3s10	ENSDARG00000058647 hck	ENSDARG00000068724
ENSDARG00000070437 rpl22	ENSDARG00000052856 khdrbs1a	ENSDARG00000010194 eif4bb	ENSDARG00000004378 yrk	ENSDARG00000035770 ube2c
ENSDARG00000088030 rpl35a	ENSDARG00000036161 hnrnpa0l	ENSDARG00000028323	ENSDARG00000041524	ENSDARG00000055350 sun1
ENSDARG00000036875 rps12	ENSDARG00000020893 slc25a22	ENSDARG00000013623 vdac2	ENSDARG00000044694 si:ch211-147j13.3	ENSDARG00000077954
ENSDARG00000035860 rps28	ENSDARG00000022129 rbm4.3	ENSDARG00000009447 atp5g3b	ENSDARG00000054543 samsn1a	ENSDARG00000063345
ENSDARG00000058105 rpl36a	ENSDARG00000003429 hnrpdl	ENSDARG00000043976 etf1b	ENSDARG00000036382 ponzr6	ENSDARG00000070656 si:ch211-69g19.2
ENSDARG00000053365 rpl31	ENSDARG00000087636 hmgn6	ENSDARG00000040439 rsl24d1	ENSDARG00000055854 nr4a3	ENSDARG00000096554 si:dkey-25o16.4
ENSDARG00000011665 aldoaa	ENSDARG00000011665 aldoaa	ENSDARG00000019230 rpl7a	ENSDARG00000040623 fosl2	ENSDARG00000063385 cenpe
ENSDARG00000001788 atp5o	ENSDARG00000053990 hmgb2b	ENSDARG00000055996 rps8a	ENSDARG00000033437 rps6ka1	ENSDARG00000090044
ENSDARG00000035871 rpl30	ENSDARG00000004735 hnrnpub	ENSDARG00000045143 hbbe2	ENSDARG00000015657 zgc:77112	ENSDARG00000008678 snx3

1	2	3	4	5
ENSDARG00000058451 rpl6	ENSDARG00000035652 sat1a.1	ENSDARG00000011405 rps9	ENSDARG00000028618 KRT18	ENSDARG00000018461 zgc:56095
ENSDARG00000034291 rpl37	ENSDARG00000013938 psmb3	ENSDARG00000019181 rpsa	ENSDARG00000055276 rel	ENSDARG00000009901 slc38a5a
ENSDARG00000044521 eef1b2	ENSDARG00000036162 hnrnpa0b	ENSDARG00000058337	ENSDARG00000004034 arhgdig	ENSDARG00000045999 saa
ENSDARG00000057556 rpl17	ENSDARG00000042049	ENSDARG00000055991 hmbsb	ENSDARG00000021113 ptmaa	ENSDARG00000070230 aldh1l2
ENSDARG00000013012	ENSDARG00000007960 hnrnpaba	ENSDARG00000059654 eif3ba	ENSDARG00000007628	ENSDARG00000002403 nusap1
ENSDARG00000035756	ENSDARG00000058128 msna	ENSDARG00000083950 snoU83B	ENSDARG00000036967 smox	ENSDARG00000006251 ell2
ENSDARG00000040439 rsl24d1	ENSDARG00000056160 hspd1	ENSDARG00000010244 rpl22l1	ENSDARG00000075853 sh3kbp1	ENSDARG00000014013 lbr
ENSDARG00000011405 rps9	ENSDARG00000089426	ENSDARG00000055868 rsl1d1	ENSDARG00000033928 ndfip2	ENSDARG00000074581 add2
ENSDARG00000042566 rps7	ENSDARG00000057167 eif4g2b	ENSDARG00000035692 rps3a	ENSDARG00000000796 nr4a1	ENSDARG00000015254 fzr1a
ENSDARG00000043453 rps5	ENSDARG00000096403 CT027638.1	ENSDARG00000015862 rpl5b	ENSDARG00000088325	ENSDARG00000002194 rhd
ENSDARG00000005791 rpl28	ENSDARG00000062326 hmgn7	ENSDARG00000044565 ola1	ENSDARG00000002021 pygb	ENSDARG00000013477 gata1a

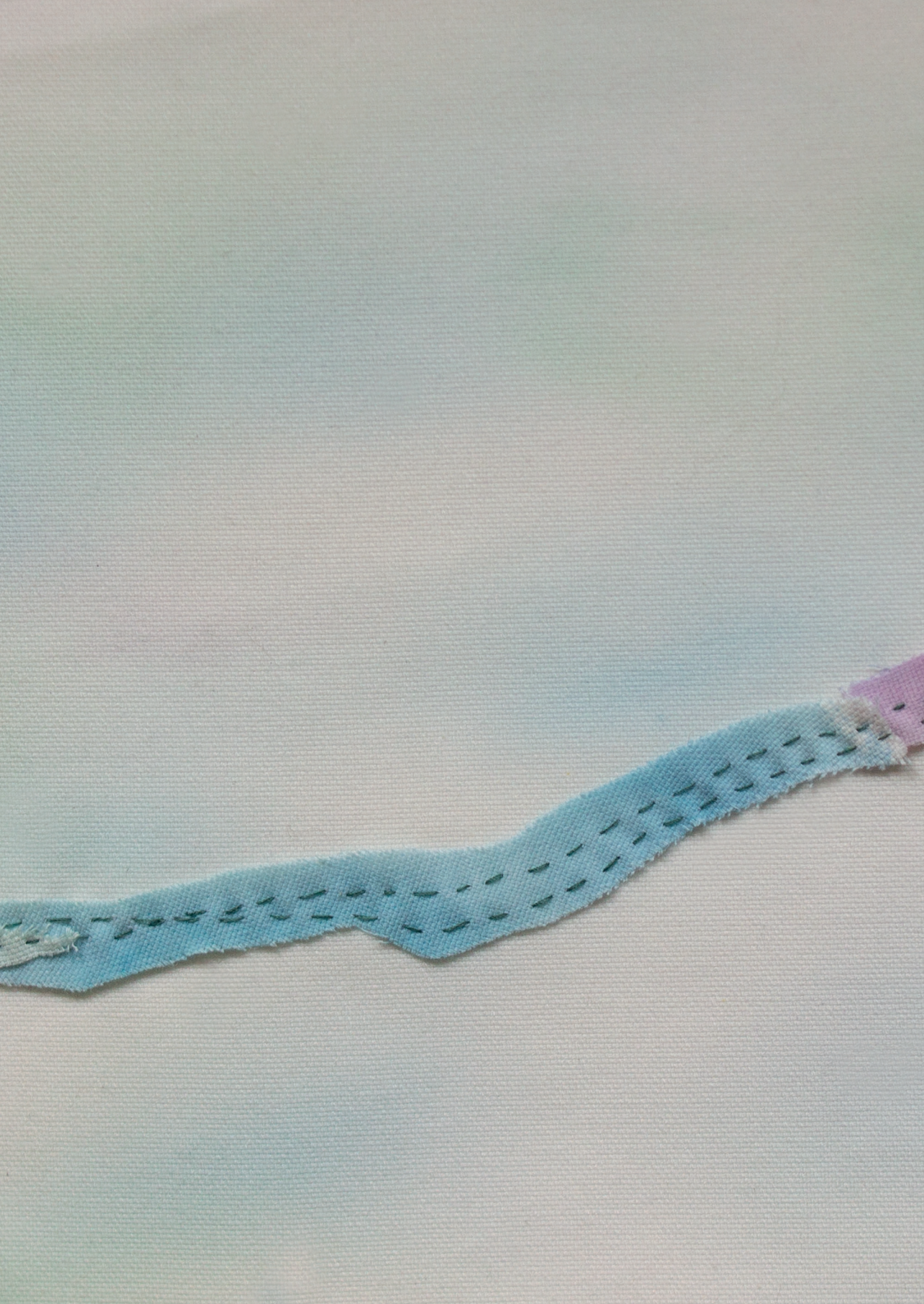

Chapter 3

Inflammatory Response Potentiates Juvenile Myelomonocytic Leukemia in Shp2 Mutant Noonan Syndrome

Solman M, Blokzijl-Franke S, Yan C, Yang Q, Kamel SM, Bakkers J, Langenau D and den Hertog J

Manuscript under review

Abstract

The RASopathy Noonan syndrome (NS) is a frequent, yet poorly understood genetic disorder which affects the development systemically. Among other features, NS children are predisposed to develop juvenile myelomonocytic leukemia (JMML). Here we present a novel zebrafish genetic mutant, generated by a CRISPR/Cas9 knock-in of a common NS-patient associated mutation Shp2-D61G. Shp2D61G zebrafish recapitulate major NS traits, including a JMML-like phenotype originating from defective hematopoietic stem and progenitor cells (HSPCs). Single cell RNA sequencing of mutant HSPCs revealed expansion of monocyte/macrophage progenitor cells associated with developmentally regulated cytokine production and elevated inflammation. Importantly, an anti-inflammatory agent rescued the JMML-like phenotype. Our results reveal a role for developmentally-induced inflammation in genesis of NS/JMML blood phenotypes and suggest anti-inflammatory drugs as potential new therapies.

Introduction

RAS signaling plays a central role in fundamental cellular processes, such as proliferation, cellular growth and differentiation, and is frequently altered during oncogenesis [1]. Additionally, germline mutations in components of the RAS pathway are associated with a group of developmental disorders, termed RASopathies [2,3]. The most common RASopathy is Noonan syndrome (NS), affecting 1:1,500 individuals [4]. NS has a systemic impact on development, causing short stature, congenital heart defects (predominantly pulmonary valve stenosis) and specific craniofacial characteristics, such as hypertelorism, low set ears and webbed neck. NS is a dominant autosomal disorder and 50% of NS patients carry heterozygous mutations in the protein-tyrosine phosphatase SHP2 (PTPN11), which is a positive regulator of RAS signaling [5–7]. Most of the mutations are affecting residues found at the N-SH2/PTP interface, disrupting the autoinhibitory allosteric regulatory mechanism and consequently increasing the basal activity of SHP2 [8,9]. Importantly, D61 is one of the most commonly mutated residues found in Noonan syndrome patients [7,10].

A portion of NS children develop a hematological defect resembling transient juvenile myelomonocytic leukemia (JMML)-like myeloproliferative disease (MPD) (NS/JMML-like MPD), which can progress into the aggressive and often fatal JMML form (NS/JMML) [11,12]. NS/JMML-like MPD and NS/JMML phenotypes are most commonly present in patients carrying a mutation in SHP2 [12,13]. JMML is characterized by excessive proliferation of the monocyte and macrophage lineage and hypersensitivity of myeloid progenitors to granulocyte-macrophage colony stimulating factor (GM-CSF) [14,15]. Other blood lineages also seem to be affected, since patients, in addition to monocytosis, often present with thrombocytopenia, anemia and increased fetal hemoglobin (HbF) levels [16]. NS/JMML-like MPD and NS/JMML are considered to be polyclonal diseases arising from multipotent hematopoietic stem cells (HSCs). However, little is known about the mechanisms that remodel the hematopoietic stem and progenitor cells (HSPCs) compartment during early pathogenesis.

Zebrafish (Danio rerio), having a conserved RAS signaling network, rapid development, transparent embryos, and a capacity for in vivo drug screens, serves as a robust tool to study the effect of mutations found in RASopathies on various developmental lineages [17,18]. Ectopic expression of NS-associated mutants affects zebrafish embryonic development profoundly, inducing shorter body axis length, craniofacial defects, defective gastrulation and impaired heart looping [19–23]. Due to the challenges in gene knock-in editing technologies in zebrafish [24], studying the effects of RASopathies-associated activating mutations still relies on ubiquitous overexpression of mutant proteins.

Here we describe a novel genetic zebrafish model of NS, which carries the patient associated Shp2D61G mutation at the endogenous locus, and reconstitutes major NS-associated traits. Interestingly, embryos of the Shp2D61G zebrafish developed hematological defects originating in defective HSPCs and resembling NS/JMML. In the search for novel mechanisms and potential treatment strategies for JMML-like hematological malignancies in NS, transcriptomes of the HSPCs derived from the Shp2D61G zebrafish mutant were studied on a single cell level. We identified a profound

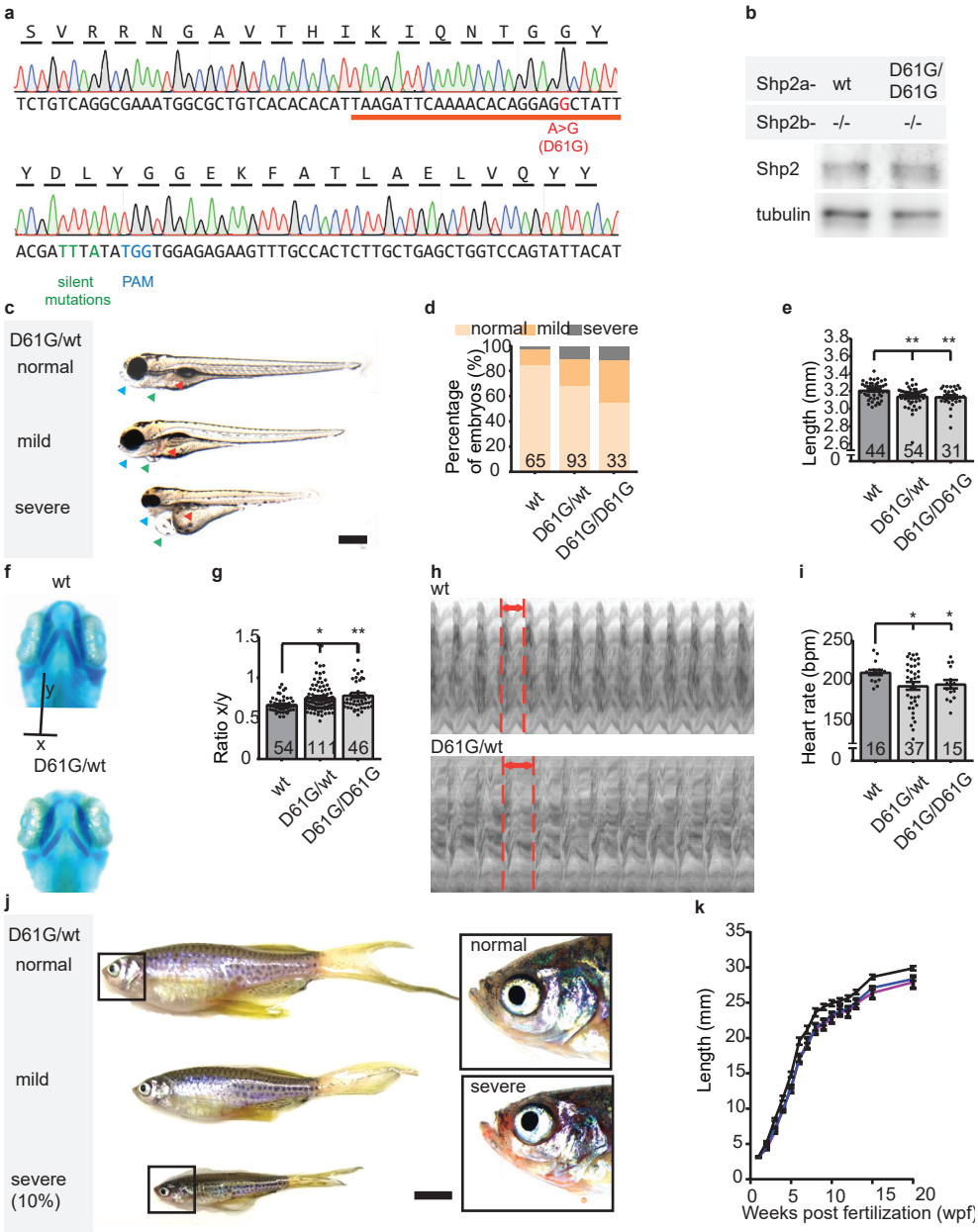

Figure 1. Shp2^{D61G} zebrafish display NS-like traits. (a) Sequencing trace derived from Shp2$^{D61G/D61G}$ zebrafish. Oligonucleotide sequence used to generate the model is underlined. Nucleotide substitutions for D61G mutation (red), silent mutations close to the PAM site (green) and the PAM site (blue) are indicated. (b) Immunoblot of Shp2 levels from 5 pooled Shp2a^{wt}Shp2b$^{-/-}$ or Shp2a$^{D61G/D61G}$Shp2b$^{-/-}$ embryos using antibodies for Shp2 and tubulin (loading control). (c) Representative images of typical Shp2^{D61G} zebrafish embryonic phenotypes at 5dpf. Blue arrows: jaw, green arrows: heart, red arrows: swim bladder. (d) Quantification of phenotypes of Shp2^{wt}, Shp2$^{D61G/wt}$ and Shp2$^{D61G/D61G}$ embryos scored as in (c) normal, mild and severe. (e) Body axis length of Shp2^{wt}, Shp2$^{D61G/wt}$ and Shp2$^{D61G/D61G}$ embryos at 5dpf. (f) Representative images of Alcian blue stained head-cartilage of 4dpf Shp2^{wt} and

role of Shp2 evoked inflammatory program in the monocyte/macrophage primed population of HSPCs in NS/JMML pathogenesis.

Results

Novel Shp2D61G mutant generated by CRISPR/Cas9 mediated knock-in

The zebrafish genome contains two *ptpn11* genes (*ptpn11a* and *ptpn11b*), encoding Shp2a and Shp2b. Shp2a is indispensable during zebrafish development, whereas loss of Shp2b function does not affect development [19]. We established a zebrafish genetic model of NS by knock-in of a patient-associated mutation in codon 61 (Asp to Gly) of the zebrafish ptpn11a gene using CRISPR/Cas9-mediated homology directed repair approach (figure S1 a) [25]. Sequencing confirmed that the oligonucleotide used for the homology repair was incorporated correctly into the genome (figure 1 a) and the introduced mutations did not have a detectable effect on Shp2a protein expression (figure 1 b). Prior to phenotypical analyses, the mutant lines were outcrossed twice to ensure that potential background mutations due to the CRISPR/Cas9 approach were removed. Henceforth, the mutant zebrafish line will be referred to as Shp2^{D61G} mutant and when necessary Shp2$^{D61G/wt}$ and Shp2$^{D61G/D61G}$ mutant to further specify hetero- and homozygosity, respectively.

Shp2D61G mutant zebrafish display typical Noonan syndrome traits

The effect of the Shp2-D61G mutation was obvious during early development in 32% and 45% of 5 days post fertilization (dpf) old Shp2$^{D61G/wt}$ and Shp2$^{D61G/D61G}$ embryos, respectively (figure 1 d). The observed phenotypical defects were mostly mild, but in some cases severe defects were found, including severely stunted growth, edemas of the heart and jaw, and absence of the swim bladder (figure 1 c). Since the mutant embryos were mostly mildly affected, just as the NS patients, we performed more meticulous characterization of the typical NS traits. Body axis length was significantly reduced in Shp2^{D61G} mutant embryos at 5dpf (figure 1 e). Furthermore, imaging of Alcian blue stained cartilage revealed NS-reminiscent craniofacial defects in the 4dpf Shp2^{D61G} mutant embryos, characterized by broadening of the head (figure 1 f), leading to increased ratio of the width of the ceratohyal and the distance to Meckel's cartilage (figure 1 g). We also assessed the function and general morphology of the mutant embryonic hearts. A decrease in heart rate (figure 1 I), ejection fraction and cardiac output (figure S1 c,d) was detected from the ventricular kymographs obtained from high speed video recordings of the Shp2^{D61G} mutant

Shp2$^{D61G/wt}$ embryos. (x) width of ceratohyal, (y) distance to Meckel's cartilage. (g) Quantified craniofacial defects (x/y ratio). (h) Representative ventricular kymographs derived from high-speed video recordings of beating hearts of 5dpf Shp2^{wt} and Shp2$^{D61G/wt}$ embryos. Red dotted lines indicate one heart period. (i) Heart rates derived from the ventricular kymographs. (j) Representative images of typical Shp2^{D61G} zebrafish adult phenotypes at 24wpf. Scale bar is 0.5cm. Insets, zoom-in of boxed regions. (k) Body axis lengths of 10 Shp2^{wt}, 25 Shp2$^{D61G/wt}$ and 10 Shp2$^{D61G/D61G}$ zebrafish measured weekly between 5dpf and 20wpf of age. (d,e,g,i) Measurements originate from three distinct experiments. Number on bars: number of embryos. (e,g,i,k) Error bars: standard error of the mean (SEM), *p < 0.05; **p < 0.01, ANOVA complemented by Tukey HSD.

hearts at 5dpf (figure 1 h)[26]. Effects on cardiac function varied from embryo to embryo, which is reminiscent of variable heart defects in human patients. Whole-mount *in situ* hybridization (WISH) with cardiomyocyte (*myl7*), ventricular (*vhmc*) and atrial (*ahmc*) markers identified no obvious morphological heart defects, such as change in the heart size or its looping, as well as the heart chamber specification at 3dpf (figure S1 b).

Since most of the embryos with obvious phenotypical defects did not develop a swim bladder, they did not survive to adulthood. The rest of both $Shp2^{D61G/wt}$ and $Shp2^{D61G/D61G}$ mutant zebrafish grew up normally and displayed rather mild obvious defects in adult stages, such as shorter body axis (figure 1 j), with markedly reduced length observed from the embryonic stage of 5dpf until the fully developed adults (figure 1 k). In 10% of $Shp2^{D61G}$ mutants the phenotypes were more severe, with markedly reduced body axis length compared to their siblings, they were skinny and with overall redness, especially in the head and gill region (figure 1 j). Taken together, the NS $Shp2^{D61G}$ mutant zebrafish we established phenocopied several of the typical NS traits, such as stunted growth, craniofacial defects, and heart defects.

Shp2D61G zebrafish embryos develop NS/JMML-like phenotype

NS/JMML-like MPD and NS/JMML phenotype are mostly linked to mutations in SHP2 [12,13]. Thus, we explored hematopoietic abnormalities in the $Shp2^{D61G}$ zebrafish. We were not able to observe any effect of the $Shp2^{D61G}$ mutation on primitive hematopoiesis in embryos at 2dpf using WISH for markers of erythroid progenitors (*gata-1*), myeloid progenitors (*pu.1*) and white blood cells (WBCs) (*l-plastin*) (figure S2). On the other hand, a significant effect of the Shp2-D61G mutation on definitive hematopoiesis at 5dpf was observed (figure 2). An increase of *l-plastin* positive cells, marking all WBCs, was detected in both caudal hematopoietic tissue (CHT) and head kidney region of the $Shp2^{D61G}$ mutants (figure 2 a,b). These cells appear not to be lymphocytes, since the size of the ikaros-positive thymus, was not affected (figure 2 c,d). By contrast, the myeloid lineage was markedly expanded, evident from the increase in the number of mpx-GFP positive neutrophils (figure 2 e,f), and mpeg-mCherry positive macrophages (figure 2 e,g), in the *tg(mpx:GFP/ mpeg:mCherry)* double transgenic mutant embryos. One of the clinical hallmarks of JMML is the hypersensitivity of myeloid progenitors to GM-CSF. In zebrafish, effects of

Figure 2. Myeloid bias and increased sensitivity to Gcsfa, Gcsfb is observed in the $Shp2^{D61G/wt}$ zebrafish. (a) WISH of 5dpf $Shp2^{wt}$ and $Shp2^{D61G/wt}$ embryos using *l-plastin* specific probe. Head kidney (arrow) and CHT (box) are indicated and zoom-in in insert. Scale bars,150µm. (b) Quantification of $^{l\text{-}plastin}$ expression in $Shp2^{wt}$, $Shp2^{D61G/wt}$ and $Shp2^{D61G/D61G}$ embryos scored as low, mid and high. (c) WISH of 5dpf $Shp2^{wt}$ and $Shp2^{D61G/wt}$ embryos using *ikaros* specific probe. Thymus is indicated (arrow). (d) Size of ikaros-positive thymus. (e) Representative images of $Shp2^{wt}$ and $Shp2^{D61G}$ zebrafish embryos in *Tg(mpx:GFP/ mpeg:mCherry)* background at 5dpf. Mpx:GFP marks neutrophils and mpeg:mCherry macrophages. Scale bars,150µm. (f, g) Number of mpx:GFP and mpeg:mCherry positive cells. (h) Representative images of colonies developed from WKM cells prepared from $Shp2^{wt}$, $Shp2^{D61G/wt}$ and $Shp2^{D61G/D61G}$ adult zebrafish, grown in methylcellulose with zebrafish cytokines Gcsfa and Gcsfb for 2 days. Scale bar, 20µm. (i) Quantification of number of colonies from (h). (j) Number of cd41:GFPhigh cells in $Shp2^{wt}$, $Shp2^{D61G/wt}$ and $Shp2^{D61G/D61G}$ zebrafish embryos at 5dpf were counted and percentage of embryos with either 0-50, 50-75 or 75-100 cd41:GFPhigh cells was plotted. (k) WISH of 5dpf $Shp2^{wt}$ and $Shp2^{D61G/wt}$ embryos using *ß-globin* specific probe. Scale bar,150µm. (l) Quantification of *ß-globin* expression in $Shp2^{wt}$, $Shp2^{D61G/wt}$ and $Shp2^{D61G/D61G}$ embryos scored as low, mid and high. (b,d,f,g,j,l) Measurements originate from at least three distinct experiments. Number on bars: number of embryos. (e,i) Error bars represent SEM. NS, not significant; *p < 0.05, ANOVA complemented by Tukey HSD.

stimulation by Gcsfa and Gcsfb corresponds to the GM-CSF stimulation in human [27]. Compared to their wt siblings, colonies developed from the whole kidney marrow (WKM) cells from Shp2^{D61G} zebrafish exposed to *Gcsfa* and *Gcsfb* were larger in size and number, demonstrating an enhanced GM colony forming ability (figure 2 h,i). Additionally, Shp2^{D61G} mutant embryos displayed a mild decrease in number of thrombocyte, marked by CD41-GFP^{high} in the *Tg(cd41:GFP/ kdrl:mCherry-CAAX)* transgenic line, and number of *β-globin*

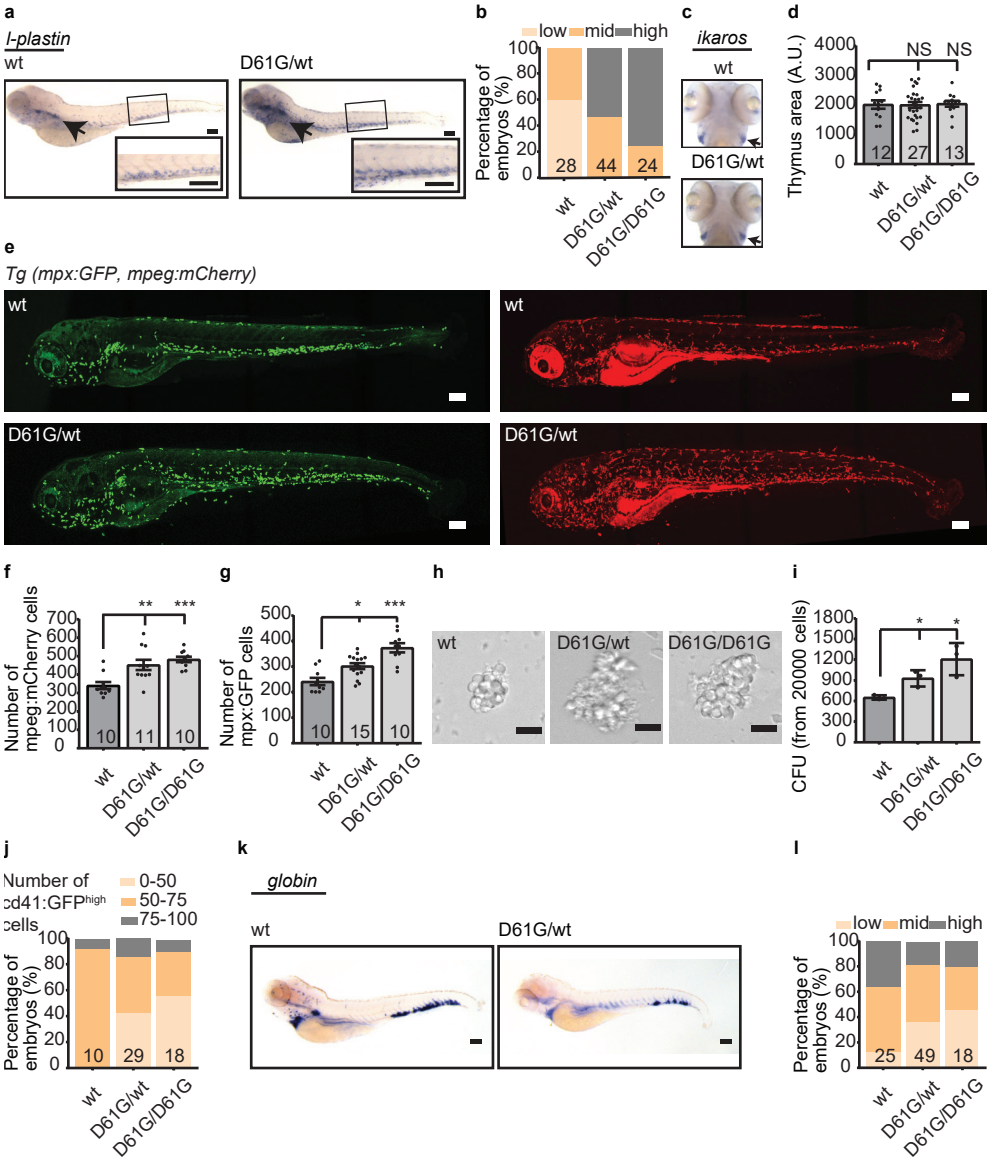

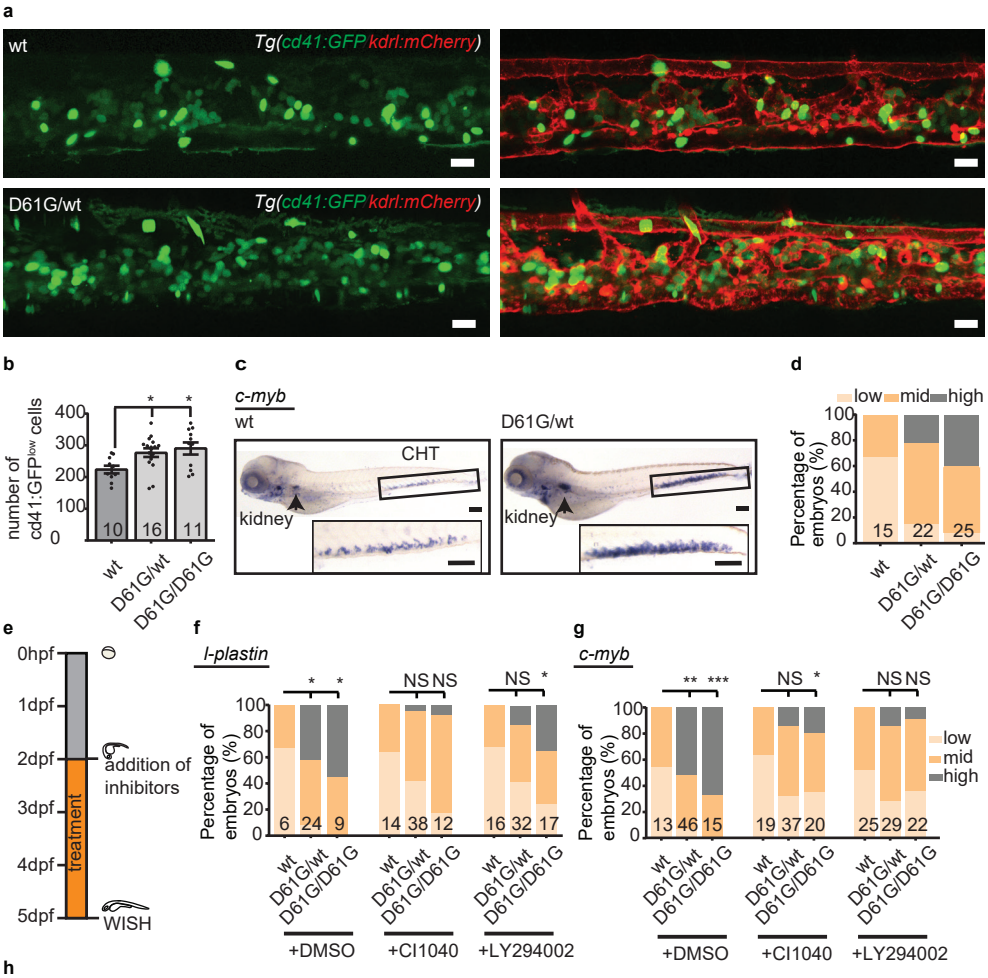

Figure 3. Shp2^{D61G} induces JMML-like phenotype that originates in HSPCs, depends on MAPK and PI3K pathway and is transplantable into secondary recipient. (a) Representative images of the CHT region of Shp2^{wt} and Shp2^{D61G} zebrafish embryos in the *Tg(cd41:GFP/ kdrl:mCherry-CAAX)* background at 5dpf. cd41:GFP^{low} cells mark HSPCs and cd41:GFP^{high} cells thrombocytes. Scale bar, 20µm. (b) The low intensity cd41:GFP positive cells in the CHT region were counted. Error bars represent standard error of the mean (SEM). *p < 0.05, ANOVA complemented by Tukey HSD. (c) WISH of 5dpf Shp2^{wt} and Shp2$^{D61G/wt}$ embryos using *c-myb* specific probe. Head kidney (arrow) and CHT (box) are indicated; zoom-in in insert. Scale bars, 150µm. (d) Quantification of *c-myb* WISH. *C-myb* expression in Shp2^{wt}, Shp2$^{D61G/wt}$ and Shp2$^{D61G/D61G}$ embryos was scored as low, mid and high. (e)

positive erythrocytes (figure 2 j-k). The observed defects on all different blood lineages examined here were stronger in the homozygous Shp2$^{D61G/D61G}$ than heterozygous Shp2$^{D61G/wt}$ embryos. Our findings suggest that the Shp2^{D61G} mutant zebrafish embryos develop multilineage hematopoietic defects reminiscent of NS/JMML like MPD and NS/JMML observed in NS patients, all in a Shp2-D61G dose dependent manner.

NS/JMML-like phenotype has its origin in defective HSPCs and is dependent on both MAPK and AKT signaling

NS/JMML-like MPD and NS/JMML are considered to have their origin in defective HSCs. Correspondingly, an increased number of HSPCs marked by CD41-GFP^{low} was observed in the CHT region of Shp2^{D61G} zebrafish embryos in the *Tg(cd41:GFP/ kdrl:mCherry-CAAX)* transgenic line (figure 3 a,b). This was further supported by the increased *c-myb* signal both in the CHT region and the head kidney of the mutant embryos (figure 3 c,d). Shp2^{D61G} mutation seems to affect both proliferation and apoptosis of HSPCs, evident by an increase in CD41-GFP cells positive for phosphohistone H3 (pHis3), a marker for late G2 and M phase and a decrease in Acridine orange positive cells in the CHT region, marking apoptotic cells (figure S3).

To determine whether the observed blood defects were driven by the Shp2-mediated RAS-MAPK and PI3K signaling pathways, *c-myb* and *l-plastin* markers were investigated by WISH in embryos treated continuously between 2 and 5dpf with either MEK inhibitor CI1040 or PI3K inhibitor LY294002 (figure 3e). MEK inhibitor led to strong inhibition of expansion of both HSPCs and myeloid lineage in mutant embryos (figure 3 f,g), indicating an essential role of the RAS-MAPK pathway in the observed defects. The PI3K pathway appeared to affect Shp2-D61G driven expansion of HSPCs strongly (figure 3g), whereas its role in expansion of the myeloid lineage in mutant embryos was less prominent (figure 3f).

Finally, we tested whether the observed myeloid expansion was reconstituted upon transplantation of the WKM cells harvested from Shp2$^{D61G/wt}$ animals in the *Tg(mpx:GFP/ mpeg:mCherry)* background into the optically clear recipient *prkdc*$^{-/-}$ immunodeficient zebrafish [28]. Animals injected with mutant WKM cells (3/5) accumulated GFP- and mCherry- positive cells near the site of injection starting at 14 days and increasing until 28 days. By contrast, animals injected with WKM cells from control sibling animals with wt Shp2a (5/5) lacked any GFP- and mCherry- positive cells (figure 3h).

These data indicate that the JMML-like blood defect developed in the Shp2^{D61G} zebrafish has its origin in malignant HSPCs, is dependent on both MAPK and AKT signaling pathways and is transplantable into a secondary recipient.

Schematic overview of the treatments with MEK inhibitor CI1040 and PI3K inhibitor LY294002. Embryos were continuously treated from 48hpf until 5dpf, when WISH was performed and expression of the (f) *l-plastin* and (g) *c-myb* marker was scored as low, mid and high. NS, not significant; *p < 0.05, **p<0.01, ***p<0.001, Chi-squared test. (h) WKM cells harvested from Shp2^{wt} and Shp2^{D61G} zebrafish in the *Tg(mpx:GFP/ mpeg:mCherry)* background were injected into the peritoneum of adult *prkdc*$^{-/-}$ zebrafish. Recipients were monitored by fluorescence imaging. (b,d,f,g) Measurements originate from at least three distinct experiments. Number on bars: number of embryos.

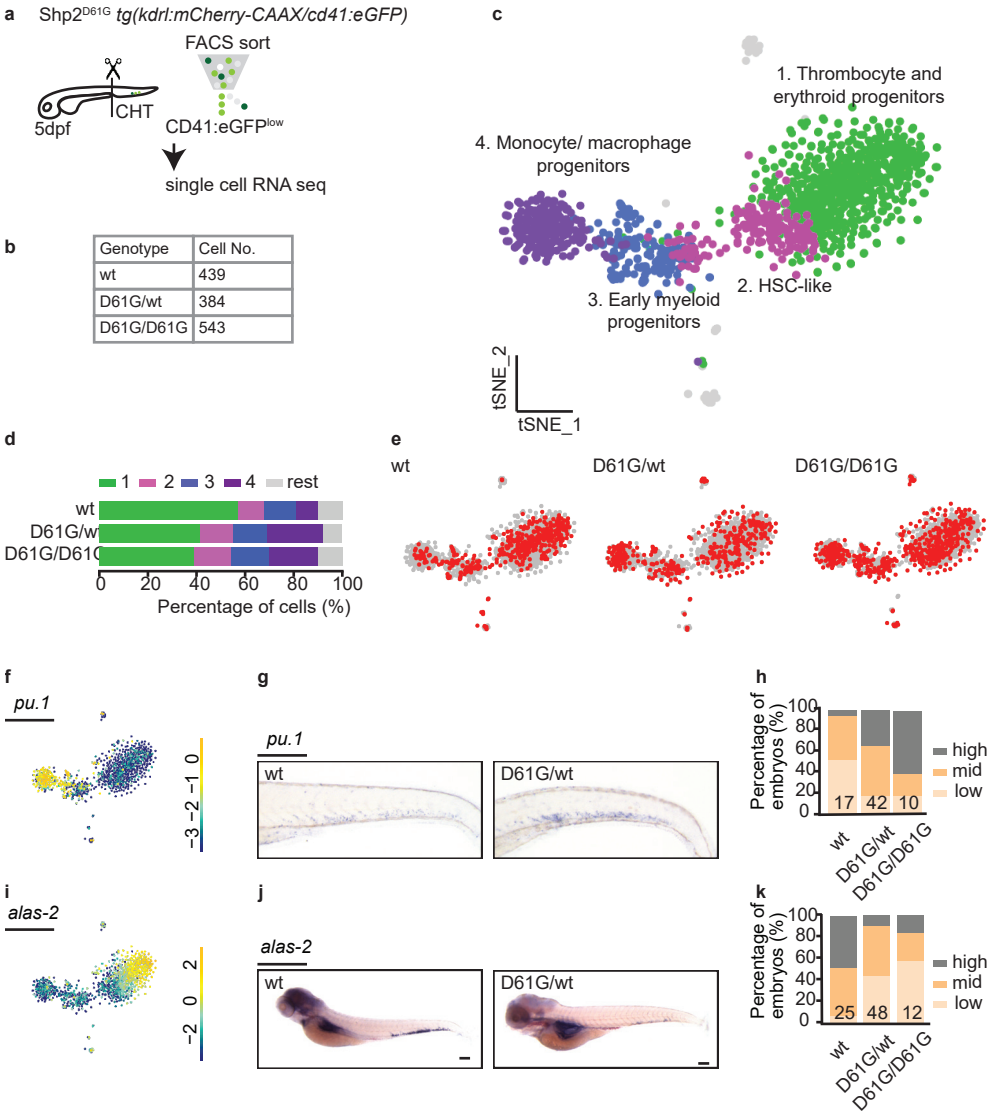

Figure 4: Transformation of Shp2^{D61G} HSPCs studied by single cell RNA sequencing. (a) Schematic representation of the experimental procedure. At 5dpf, CHTs from Shp2^{wt}, Shp2$^{D61G/wt}$ and Shp2$^{D61G/D61G}$ embryos in the *Tg(cd41:GFP/ kdrl:mCherry-CAAX)* background were isolated. Cells were dissociated and separated by FACS, based on cd41:GFP^{low} expression, prior to single cell RNA sequencing, as described in the Methods section. (b) Number of cells of distinct genotypes used in single cell RNA sequencing analysis. (c) tSNE maps generated using the cells of all three (Shp2^{wt}, Shp2$^{D61G/wt}$ and Shp2$^{D61G/D61G}$) genotypes. Single cells from 4 major clusters are marked in violet, blue, pink and green and their identities based on marker gene expression are indicated. Minor clusters are marked in grey. (d) Barplots showing the percentage of cells of Shp2^{wt}, Shp2$^{D61G/wt}$ and Shp2$^{D61G/D61G}$ genotype in distinct clusters. (e) Cells of distinct genotypes Shp2^{wt}, Shp2$^{D61G/wt}$ and Shp2$^{D61G/D61G}$ are visualized in tSNE maps

Myeloid bias is established during the early differentiation of Shp2D61G HSPCs

In an effort to better understand the pathogenesis mechanisms in the Shp2^{D61G} mutant HSPCs, single cell RNA sequencing was performed on CD41-GFP^{low} cells derived from 5dpf Shp2^{wt}, Shp2$^{D61G/wt}$ and Shp2$^{D61G/D61G}$ zebrafish embryos in the *Tg(cd41:GFP/ kdrl:mCherry-CAAX)* transgenic background (figure 4 a,b). To group cells based on their transcriptional program, unsupervised clustering was performed using the RaceID3 package[29], clusters were visualized by t-distributed stochastic neighbor embedding (t-SNE) and 4 major clusters were further analyzed (figure 4c). Based on the differentially expressed genes and GO term analysis, cells from Cluster 1 were determined to be thrombocyte and erythroid progenitors, Cluster 2 HSC-like HSPCs, Cluster 3 early myeloid progenitors and Cluster 4 monocyte/macrophage progenitors (figure 4c, figure S4 a, table S1). A small subset of cells in Cluster 4 represented more differentiated neutrophils (figure S4 b).

HSPCs of either Shp2^{wt} or mutant Shp2$^{D61G/wt}$ and Shp2$^{D61G/D61G}$ genotypes were present in all 4 major HSPCs compartments, indicating that distinct HSPCs phenotypes were maintained on a gene transcription level. However, the distribution of cells in clusters differed among genotypes. An overrepresentation of mutant Shp2$^{D61G/wt}$ and Shp2$^{D61G/D61G}$ cells was observed in the HSC-like HSPCs cluster and monocytes/macrophages progenitors cluster, whereas these were underrepresented in the thrombocyte and erythroid progenitors cluster (figure 4 d,e). To validate this observation, we investigated the expression of *pu.1* and *alas2* markers in Shp2^{D61G} embryos of different genotypes by WISH. In the single cell RNA sequencing dataset, expression of *pu.1* and *alas2* was upregulated in the myeloid progenitors and erythroid progenitors, respectively (figure 4 f,i). An increased number of *pu.1* positive cells was detected by WISH in 5dpf old Shp2^{D61G} embryos compared to their Shp2^{wt} siblings (figure 4 g,h), whereas the number of *alas2* positive cells in Shp2^{D61G} mutants was decreased (figure 4 j,k). Taken together, single cell RNA sequencing suggests that defects during early HSPCs differentiation initiate the multilineage NS/JMML-like phenotype observed in Shp2^{D61G} embryos.

Excessive proinflammatory response contributes to the pathogenesis of the NS/JMML-like phenotype

We further analyzed the cluster of monocyte/macrophage progenitors, in which we observed an overrepresentation of mutant Shp2^{D61G} cells (figure 5a). Functional annotation of the differentially expressed genes and the GO-term enrichment analysis revealed presence of genes involved in inflammation (figure 5a, table S1). Among the top 10 differentially expressed genes was the known JMML-associated inflammatory cytokine *il1b* [30,31]. Also other proinflammatory genes were highly expressed, such as *gcsfa, gcsfb, irg1, tnfaip3, nfkbiaa, ccl35.2* and *ccl34b.1* (figure 5 a,b, table S1). Interestingly, expression of inflammation-related genes, such as *gcsfa, gcsfb, il1b, irg1* and *nfkbiaa*, was constrained

in red. (f) tSNE maps showing log2-transformed read-counts of *pu.1*. (g) Representative images of the WISH staining for *pu.1* expression in 5dpf Shp2^{wt} and Shp2^{D61G} zebrafish embryos. Scale bar,100µm. (h) Expression of the *pu.1* marker scored as low, mid and high. (i) tSNE maps showing log2-transformed read-counts of *alas-2*. (j) Representative images of the WISH staining for *alas-2* expression in the tail region of 5dpf Shp2^{wt} and Shp2^{D61G} zebrafish embryos. Scale bar, 100µm. (k) Expression of the *alas-2* marker scored as low, mid and high. (h,k) Number on bars: number of embryos.

to the cells of mutant Shp2^{D61G} genotype in the monocyte/macrophage progenitors cluster, while a monocyte marker *timp2a* was equally expressed by cells of distinct genotypes (figure 5b).

The high expression of IL-1β was validated in mutant embryos in vivo, in which IL-1β -eGFP positive cells were present in the CHT region of Shp2^{D61G} embryos in the T*g(il1b:eGFP/mpeg:mCherry)* transgenic background (figure 5c). The IL-1β -eGFP positive cells overlapped partially with the branched cells that contained a high mpeg:mCherry signal, indicating macrophages, while the remaining IL-1β -eGFP positive cells were round in shape and contained little or no mpeg-mCherry signal.

Finally, we asked whether the excessive inflammatory response has a role in the pathogenesis of the observed phenotype. We exposed embryos to the anti-inflammatory corticosteroid dexamethasone continuously between 2 and 5dpf. A robust effect of the dexamethasone treatment on both expansion of myeloid lineage and HSPCs was observed, as determined by WISH for the *c-myb* and *l-plastin* markers (figure 5 d,e). These results show that the expanded monocyte/macrophage progenitors exhibited a pro-inflammatory phenotype and uncovered a profound role for inflammation in pathogenesis of NS/JMML. Strikingly, these monocyte/macrophage progenitors seem to have an essential role during initiation of the NS/JMML-like phenotype, in that an anti-inflammatory agent rescued the expansion of the myeloid lineage and HSPCs, revealing a new angle for combating (NS)/JMML.

Discussion

Here, we focused on the hematological phenotype observed in Shp2^{D61G} zebrafish embryos. In line with the characteristics typical for NS/JMML-like MPD and NS/JMML in human patients [12], Shp2^{D61G} embryos displayed expansion of the myeloid lineage, increased sensitivity to GM-CSF, mild anemia and thrombocytopenia (figure 2). Furthermore, the observed blood defect was transplantable to secondary recipients and had its origin in the defective HSPCs compartment. A similar phenotype was observed in NS *Ptpn11*^{D61G} mouse model, which develops NS/JMML-like MPD. However, these defects were observed in mice of 5 months old and they were never studied at the earlier, embryonic stages, which may be more relevant for disease initiation, since NS/JMML-like MPD and NS/JMML in patients appears at the very early age, often immediately after birth[31–33]. To uncover novel pathogenesis mechanisms during early HSPCs differentiation, we investigated the transcriptomes of these cells. The HSPCs compartment is heterogeneous, consisting of multipotent stem cells and progenitors of distinct blood lineages. Since in the Shp2^{D61G} mutants multiple blood lineages are affected simultaneously, single cell RNA sequencing was performed in order to separate subpopulations of HSPCs and uncover subtle gene expression differences, which would not be possible by bulk sequencing. A single cell RNA sequencing dataset of the GFP-CD41^{low} cells, corresponding to HSPCs, was generated both for Shp2^{D61G} mutants and their wt siblings. The identities of HSPCs subpopulations matched the ones previously described [34], and they were all recognized in both Shp2^{D61G} mutant and

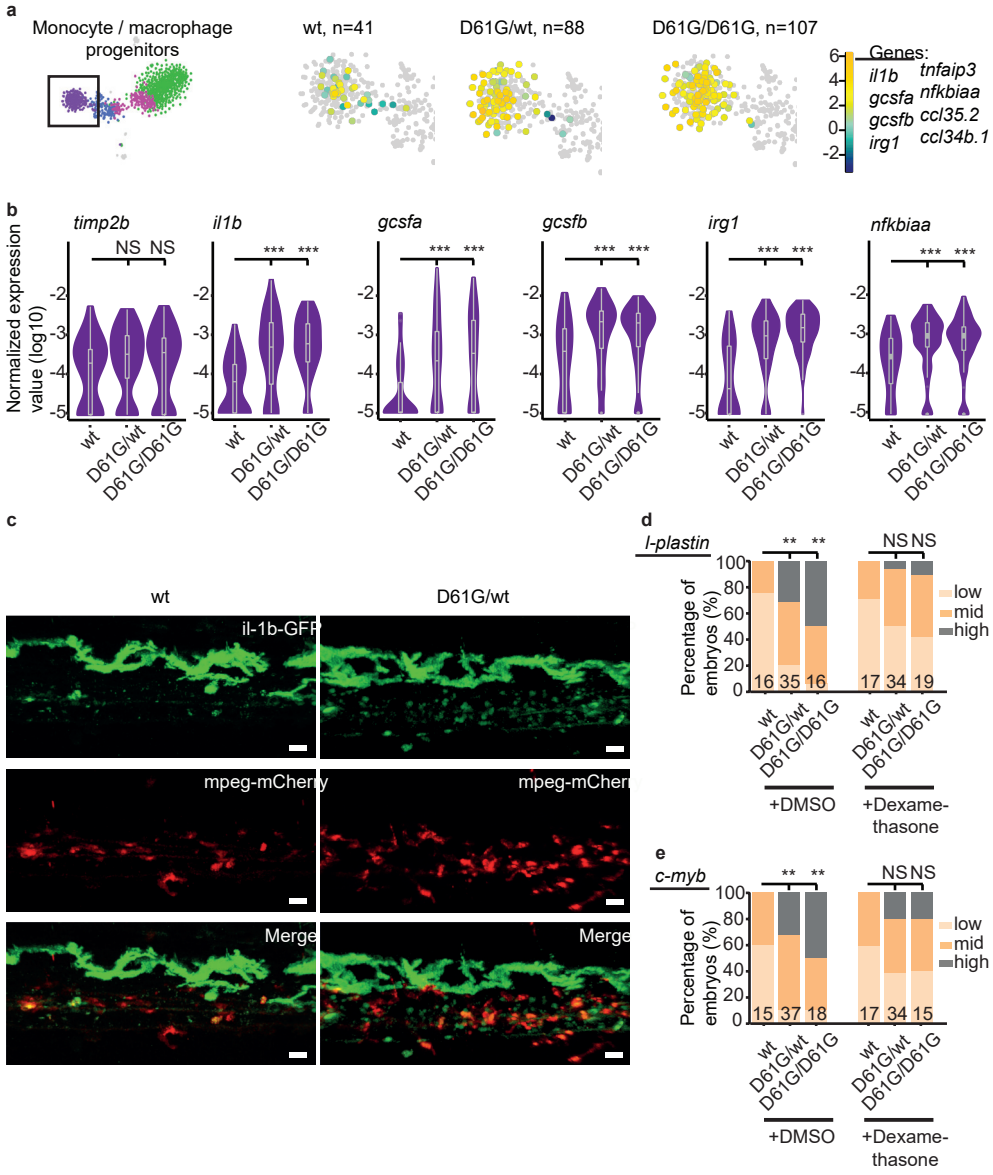

Figure 5: Inflammatory response in monocyte/ macrophage progenitors in Shp2^{D61G} embryos. (a) The monocyte/ macrophage progenitors cluster (boxed on the tSNE map on left) was analyzed in detail. log2-transformed sum of read-counts of selected inflammation-related genes from the top 50 differentially expressed genes in the cells of the monocyte/macrophage progenitors cluster, with genotype and number of cells (n) indicated above. (b) Violin plots show the expression of specific genes in monocyte/macrophage progenitors of Shp2^{wt}, Shp2$^{D61G/wt}$ and Shp2$^{D61G/D61G}$ genotypes. NS, not significant, ***p < 0.001, t-test. (c) *In vivo* imaging of the CHT region of Shp2^{wt} and Shp2$^{D61G/wt}$ zebrafish embryos in the *Tg(il1b:eGFP/ mpeg:mCherry)* background at 5dpf. Representative images are shown. Scale bar is 20µm.Embryos were continuously treated from 48hpf until 5dpf with Dexamethasone, when WISH was performed and expression of the (d) *l-plastin* and (e) *c-myb* marker was scored as low, mid and high. Measurements originate from at least three distinct experiments. Number on bars: number of embryos. NS, not significant; *p < 0.05, **p<0.01, Chi-squared test.

wt genotype. Remarkably, we observed an enrichment of mutant HSPCs in the monocyte/macrophage progenitor cluster and their depletion in thrombocyte and erythroid progenitor cluster, corresponding to phenotypes observed for the more differentiated blood lineages. The generated dataset represents a valuable resource for future studies on mechanisms involved in initiation of NS/JMML and NS/JMML-like MPD.

Our exploration of the differentially expressed genes in the cells of monocyte/macrophage progenitor cluster uncovered upregulation of pro-inflammatory genes specifically in the cells derived from Shp2^{D61G} mutants (figure 5). A proinflammatory status, with high levels of cytokines, such as IL-1β, TNF-α, GM-CFS, has been previously assigned to JMML in human patients and mouse models, and shown to be generated by myeloid cells[30,31,35–37]. The inflammatory response may be initiated in a cell autonomous way or in response to signals from the microenvironment. Dong *et al*. suggested that IL-1β is secreted by differentiated monocytes which get recruited upon the Chemokine (C-C motif) ligand 3 (CCL3) secretion by the cells of bone marrow microenvironment containing activating SHP2 mutations[31]. However, the levels of CCL3 in the bone marrow of four NS patients varied. Our findings indicate that the proinflammatory status of the monocyte/macrophage lineage is initiated early during their differentiation. Hence, proinflammatory reprograming of the monocyte/macrophage lineage might be endogenously driven at least in part, and detailed mechanisms remain to be elucidated in the future. The role of inflammation as one of the drivers in myeloid leukemogenesis is emerging [38,39]. For instance, IL-1β is known to induce proliferation of HSCs and their differentiation into the myeloid lineage [31,40]. Here we demonstrate that dampening inflammation using the glucocorticoid dexamethasone, partially rescued the observed blood phenotype in Shp2^{D61G}, suggesting that the inflammatory response evoked in the cells of myeloid/macrophage lineage is important driver of the NS/JMML-like blood defect and may be a potential drug target for (NS)/JMML and (NS)/JMML-like MPD. In addition to the effect of anti-inflammatory treatment (figure 5), we demonstrated that targeting MAPK and PI3K pathway also led to partial reversal of the blood phenotype in Shp2^{D61G} zebrafish embryos (figure 3 e-g), further emphasizing previously assigned role of these pathways in transformation of HSCs upon Shp2 activation [41] and their therapeutic potential. Treatment of JMML and JMML-like MPD remains challenging, with no existing drug therapies. Our results emphasize the potential of the NS zebrafish model as a powerful tool for future in vivo drug screens.

To our knowledge, the Shp2^{D61G} mutant zebrafish we developed is the first NS zebrafish model carrying a Shp2a-D61G mutation at its endogenous locus generated by CRISPR/Cas9- based knock-in technology. Strikingly, phenotypes developed by the Shp2^{D61G} zebrafish corroborate closely with the phenotypes displayed by human NS patients and the existing NS mouse models (figure 1). Our model presents an exciting novel tool for depicting pathogenesis mechanisms of NS with its complex traits and for finding novel therapies for this as yet poorly treatable condition.

Embryonic lethality is only partial in the Shp2^{D61G} homozygous zebrafish, while in the NS Shp2^{D61G} homozygous mice it is fully penetrant, due to severe heart valvoseptal defects [33]. Valvoseptal defects are also the most common cardiac defects in NS patients carrying a Shp2 mutation [42]. Shp2^{D61G} zebrafish displayed mild and severe heart edemas and changes in the heart rate, ejection fraction and cardiac output, while the striking heart

malformations were not present (figure 1, figure S1). However, to obtain a better insight, a thorough assessment of the heart structure, focusing on valvoseptal components would be required in the future. The observed difference in penetrance of embryonic lethality might also be due to underlying genetic modifiers [43]. Finally, the genetic background of mice was shown to significantly affect embryonic lethality in distinct NS mouse models [44,45] and might also be important in Shp2^{D61G} zebrafish. In conclusion, we identified a profound role of proinflammatory phenotype initiated during early priming of monocyte/macrophage progenitor cells in NS/JMML and suggest treatment with anti-inflammatory agents as a possible therapeutic strategy for this poorly treatable condition.

Methods

Zebrafish husbandry

All procedures involving experimental animals were approved by the animal experiments committee of the Royal Netherlands Academy of Arts and Sciences (KNAW), Dierexperimenten commissie protocol HI18-0702, and performed under the local guidelines in compliance with national and European law. The following zebrafish lines were used in the study: Tübingen longfin (TL, wild type), *Tg(cd41:GFP/kdrl:mCherry-CAAX)* [46,47], *Tg(mpx:GFP/ mpeg:mCherry)*[48,49], *TgBAC(il1b:eGFP)sh445* [50], *ptpn11b*$^{-/-}$ [19], *prkdc*$^{-/-}$ [28] and the novel Shp2^{D61G} zebrafish line. Raising and maintenance of zebrafish was performed according to [51,52]. When required, pigmentation of embryos was blocked by adding phenylthiourea (PTU) (Sigma Aldrich, St. Louis, MO, USA, Ref: P7629) at a concentration of 0.003% (v/v) to the E3 medium at 24hpf.

Generation of the Shp2^{D61G} zebrafish line

The Shp2^{D61G} zebrafish line was generated using the previously described CRISPR/Cas9-based knock-in approach [25]. The sgRNA targeting exon 3 of the *ptpn11a* gene (5'-GGAGACTATTACGACCTGTA-3') was designed using the CHOP-CHOP database (http://chopchop.cbu.uib.no/), further processed according to the previously published guidelines [53] and finally transcribed using the Ambion MEGAscript T7 kit (TermoFisher Scientific, Waltham, MA, USA, Ref: AMB13345). The sgRNA, constant oligonucleotide and template oligonucleotide were all generated by Integrated DNA Technologies (IDT, Coralville, IA, USA) as standard desalted oligos and template oligonucleotide was further purified using the QIAquick Nucleotide Removal Kit (Qiagen, Hilden, Germany, Ref: 28304). The oligonucleotide used for the homology repair is 59 nucleotides long and besides the D61G mutation, contains three additional silent mutations in proximity of the PAM site. The sequence of template oligonucleotide is 5'-GAGTGGCAAACTTCTCTCCACCATATAA ATCGTAATAGCCTCCTGTGTTTTGAATCTTA-3'. Tübingen longfin wt zebrafish embryos at the one-cell-stage were injected directly in the cell with 1 nl of the injection mixture containing 18.75 ng/ml of sgRNA, 37.5 ng/ml of template oligonucleotide and 3.6 mg/ml of Cas9 protein in 300 mM KCl. Cas9 protein was a gift from the Niels Geijsen laboratory at the Hubrecht Institute. The injected embryos were grown into the adulthood. F0 generation zebrafish were outcrossed with the wt zebrafish. DNA extracted from the 12 distinct 1dpf old F1 generation embryos was screened for the correct insertion of the template oligonucleotide. Screening was done by Sanger sequencing (Macrogen Europe B.V., Amsterdam, The Netherland) of the 225 bp long PCR product encompassing the genomic regions of the CRISPR target sites, which was generated using the forward 5'-TCATCTCCTCACTAGGCGAAAT-3' and reverse primer 5'- TATGTATGTGCTCACCTCTCGG-3'. The efficiency of the knock-in was 1.8% (1 founder zebrafish in 54 screened primary injected zebrafish). F1 generation was then established from the F0 founder. F1 generation adults were finclipped and sequenced for the presence of the mutation. All experiments were performed in zebrafish embryos and adults from the F3 and F4 generation. For most

of the experiments, embryos were derived from an incross of Shp2$^{D61G/wt}$ animals. After the experimental procedure, embryos were lysed and genotyped by sequencing as described above. Western blotting was performed as previously described [54] using the Shp2 (Santa Cruz Biotechnology, Dallas, TX, USA, Ref: SC-280) and β-tubulin (Merck Millipore, Burlington, MA, USA Ref: CP06) antibodies.

Phenotyping of the NS traits

Body axis lengths were measured from the tip of the head to the end of the trunk in the bright-field images of laterally positioned embryos, larva and adults, which were anesthetized in 0.1% MS-222. Alcian blue (Sigma Aldrich, Ref: A5268) staining was performed as previously described [22], on PTU-treated 4dpf old embryos, which were anesthetized in 0.1% MS-222 and fixed in 4% PFA overnight. Embryos were positioned on their back in 70% glycerol in PBS and imaged with Leica M165 FC stereomicroscope. Analysis was performed in ImageJ. In vivo high-speed brightfield imaging of the embryonic hearts from PTU-treated embryos at 5dpf, which were anesthetized in 0.1% MS-222 and embedded in 0.3% UltraPure agarose (Thermo Fisher Scientific) prepared in E3 medium containing 16 mg/ml MS-222. Measurements were performed at 28°C using a Leica DM IRBE inverted light microscope (Leica Microsystems) with a Hamamatsu C9300-221 high-speed CCD camera (Hamamatsu Photonics, Hamamatsu, Japan). Imaging was conducted at 150 frames per seconds (fps) using Hokawo 2.1 imaging software (Hamamatsu Photonics) for a period of 10 seconds (approximately 30 cardiac cycles). Heart rate measurements and contractility parameters were analysed using ImageJ. Volumes were analysed using ImageJ by drawing an ellipse on top of the ventricle at end-diastole and end-systole. Averages of three measurements per heart were determined. End diastolic and end systolic volume (EDV/ESV) were calculated by: (4/3)*(π)*(major axis/2)*((minor axis/2)^2). Stroke volume (SV) by: EDV-ESV. Ejection fraction (EF) by: (SV/EDV)*100. Cardiac output (CO) by: SV*Heart rate.

Whole mount in situ hybridization

PTU-treated embryos were anesthetized in 0.1% MS-222 (Sigma Aldrich, Ref: A5040) and fixed in 4% PFA for at least 12h at 4°C. WISH was performed as described in [55]. Probes specific for *myl7, vhmc* and *ahmc* were described in [19]. Probes specific for *c-myb*, *l-plastin, pu.1, gata1, ikaros, b-globin* and *alas-2* were described in [56,57]. Subsequently, embryos were mounted in 70% glycerol in PBS and imaged with Leica M165 FC stereomicroscope (Leica Microsystems, Wetzlar, Germany). Images were processed in ImageJ (U. S. National Institutes of Health, Bethesda, MD, USA). Abundance of the probe signal was scored as low, mild or high.

Inhibitors treatment

PTU-treated embryos were incubated with either 0.15μM of CI1040 (Sigma Aldrich, Ref: PZ0181), 4μM LY294002 (Sigma Aldrich, Ref: L9908) or 10μM of Dexamethasone (Sigma Aldrich, Ref: D4902) continuously from 24hpf until 5dpf. At 5dpf embryos were fixed and half of the embryos was processed for WISH using probe specific for *c-myb* and the other

half using probe specific for *l-plastin*. Images were processed in ImageJ. Abundance of the probe signal was scored as low, mild or high.

Confocal microscopy

All confocal imaging was performed on a Leica SP8 confocal microscope (Leica Microsystems). Embryos were mounted in 0.3% agarose. Live embryos were anesthetized in MS-222. Whole embryos were imaged using a 10X objective and z-stack step size of 3µm, while the CHT area with 20X objective and z-stack step size of 1µm. The number of CD41-GFP^{low} cells was determined by imaging the CHT of the living 5dpf old embryos of the Shp2^{wt}, Shp2$^{D61G/wt}$ and Shp2$^{D61G/D61G}$ siblings in the *Tg(cd41:GFP/ kdrl:mCherry-CAAX)* transgenic background, while the number of CD41-GFP^{high} cells was determined by imaging whole embryos, which were fixed for 2h in 4% PFA prior to imaging. To determine the number of mpx-GFP and mpeg-mCherry cells, whole live 5dpf old embryos of the Shp^{2wt}, Shp2$^{D61G/wt}$ and Shp2$^{D61G/D61G}$ line in the *Tg(mpx:GFP/ mpeg:mCherry)* transgenic background were imaged. Imaris V9.3.1 (Bitplane, Zurich, Switzerland) was used to reconstruct 3D images and count individual GFP and/or mCherry positive cells.

Phosphorylated Histone 3 (pHis3) staining

PTU-treated 5dpf old Shp2^{D61G} embryos in the *Tg(cd41:GFP/ kdrl:mCherry-CAAX)* transgenic background were fixed in 2% PFA overnight and stained as described in [58]. Primary pHis3 antibody (1:500 in blocking buffer, Abcam, Cambridge, UK, Ref: ab5176) and secondary GFP antibody (1:200 in blocking buffer, Aves Labs Inc. Tigard, OR, USA, GFP-1010) were used. Embryos were mounted in 0.3% agarose, their CHT was imaged using the SP8 confocal microscope and 3D images were subsequently reconstructed using Imaris.

Acridine orange staining

PTU-treated embryos at 5dpf were incubated in 5µg/ml of Acridine orange (Sigma Aldrich, Ref: A6014) in E3 medium, for 20 minutes at room temperature. They were then washed 5 times for 5 minutes in E3 medium, anesthetized in MS-222 and mounted in 0.3% agarose. Whole embryos were imaged with SP8 confocal microscope and 3D images were reconstructed using Imaris.

Isolation of CD41-GFP^{low} cell population and single-cell RNA sequencing

From 24hpf onwards embryos were grown in PTU-containing medium. The CHTs of approximately 50 Shp2^{wt}, Shpt$^{D61G/wt}$ and Shp2$^{D61G/D61G}$ embryos in T*g(cd41:GFP/ kdrl:mCherry-CAAX)* transgenic background at 5dpf were dissected and collected in Leibovitz-medium (TermoFisher Scientific, Gibco, Ref: 11415049). After washing with PBS0 the CHTs were dissociated with TryplE (TermoFisher Scientific, Gibco, Ref: 12605036) for 45 minutes at 32°C. The resulting cell suspension was washed with PBS0, resuspended in PBS0 supplemented with 2mM EDTA, 2% FCS and 0.5µg/ml DAPI (Sigma Aldrich, Ref: D9542) and passed through a 40µm Falcon cell strainer. DAPI staining was used to exclude dead cells [59]. Cells with CD41-GFP^{low} positive signal were subjected to fluorescence-activated cell sorting (FACS) with an influx cytometer (BD Biosciences, San Jose, CA,

USA). Single-cell RNA sequencing was performed according to an adapted version of the SORT-seq [60] with adapted primers described in [61]. In short, single cells were FACS sorted, as described above, on 384-well plates containing 384 primers and Mineral oil (Sigma Aldrich). After sorting, plates were snap-frozen on dry ice and stored at -80°C. For amplification cells were heat-lysed at 65°C followed by cDNA synthesis using the CEL-seq2 [62] and robotic liquid handling platforms. After the second strand cDNA synthesis, the barcoded material was pooled into libraries of 384 cells and amplified using in vitro transcription. Following amplification, the rest of the CEL-seq2 protocol was followed for preparation of the amplified cDNA library, using TruSeq small RNA primers (Illumina, San Diego, CA, USA). The DNA library was paired-end sequenced on an Illumina Nextseq™ 500 (Illumina), high output, with a 1x75 bp Illumina kit (R1:26 cycles, index read: 6 cycles, R2:60 cycles).

Data analysis of single-cell RNA sequencing

During sequencing, Read1 was assigned 26 base pairs and was used for identification of the Ilumina library barcode, cell barcode and unique molecular identifier. Read2 was assigned 60 base pairs and used to map to the reference transcriptome of Zv9 Danio rerio. Data was demultiplexed as described in [63]. Single cell transcriptomics analysis was done using the RaceID3 algorithm [29], following an adapted version of the RaceID manual (https://cran.r-project.org/web/packages/RaceID/vignettes/RaceID.html) using R-3.5.2. In total 768 cells per genotype were sequenced for the datasets. After removing cells with less than 1000 UMIs and only keeping genes that were detected with al least 3 UMIs in 1 cell, 439 wt, 384 D61G/wt and 543 D61G/D61G cells were left for further analysis. Batch effects observed for plates which were prepared on different days was removed using the scran function. 4 major clusters and 5 minor clusters were identified. The minor clusters contained 130 cells in total and were excluded from further analysis for statistical reasons. Differential gene expression analysis was done as described in [60] with an adapted version of the DESseq2 [64]. GO term enrichment analysis for differentially expressed genes of each major cluster was performed using the DAVID Bioinformatics Resources 6.8 (https://david.ncifcrf.gov/).

Colony forming assay

Whole kidney marrows (WKMs) of the three adult Shp2^{wt}, Shp2$^{D61G/wt}$ and Shp2$^{D61G/D61G}$ siblings in the *Tg(mpx:GFP/ mpeg:mCherry)* transgenic background were dissected and collected in PBS supplemented with 5% FBS. The tissue was mechanically dissociated and filtered through a 70 µm and 40 µm Falcon cell strainer. Cell pellet was resuspended in PBS supplemented with 5% FBS. 1.6 ml of solution containing 20 000 cells in media, which was prepared as described in [27], and 100 ng/ml of granulocyte colony stimulating factor a and b (Gscfa and Gcsfb, gift from the Petr Bartunek lab, Institute of Molecular Genetics, Academy of Sciences of the Czech Republic v.v.i. Prague) was plated per well of a 12 well plate in a duplicate. Cells were grown in humidified incubators at 32°C, 5% CO2. After 2 days colonies were imaged using the EVOS microscope (TermoFisher Scientific), examined for the presence of GFP and mCherry fluorescence, and enumerated.

Transplantation experiments

Zebrafish kidney marrow transplantation were performed as previously described [28,65]. In short, tissues were isolated from donor Shp2$^{D61G/wt}$ or wild type animals in the *Tg(mpx:GFP/mpeg:mCherry)* background following Tricaine (Western Chemical, Brussels, Belgium) overdose. Excised tissues from dissected fish are placed into 500 µl of 0.9x PBS + 5% FBS on a 10-cm Petri dish. Single-cell suspensions were obtained by maceration with a razor blade, followed by manual pipetting to disassociate cell clumps. Cells were filtered through a 40-µm Falcon cell strainer, centrifuged at 1,000 g for 10 min, and resuspended to the 2 x 107 cells/ml. 5-µl suspension containing 105 kidney marrow cells were injected into the peritoneal cavity of each recipient fish using a 26s Hamilton 80366 syringe. Cellular engraftment was assessed at 0, 7, 14, 28 dpt by epifluorescence microscopy.

Statistical analysis

Data was plotted in GraphPad Prism 7.05 (GraphPad Software Inc., San Diego, CA, USA), except for the violin plots of gene expression, which were plotted in R using ggplot2 [66]. Statistical difference analysis was performed using the one-way ANOVA supplemented by Tukey's HSD test in GraphPad Prism 7.05, except for the gene expression differences in single cell RNA sequencing data, where T-test was performed in Rstudio 1.1.463 (Rstudio, Boston, MA, USA), and the treatment WISH experiments, where Chi-squared test was performed in GraphPad Prism 7.05. Significant difference was considered when $p<0.05$ (*p<0.05, **p<0.01, ***p<0.001, NS=non significant).

Acknowledgements

We thank the laboratory of Niels Geijsen (Hubrecht Institute) for providing us with Cas9 protein, Petr Bartunek and Olga Machanova (Institute of Molecular Genetics, Academy of Sciences of the Czech Republic v.v.i. Prague) and Geert Wiegertjes (University Wageningen) for cytokines and carp serum, Stefan van der Elst for assistance with FACS sorting, Hubrecht Institute animal caretakers for animal support and Single Cell Discoveries and Chloé Baron for support with single cell RNA sequencing. This work was supported by E-Rare grant NSEuroNet (JdH), NIH grants R01CA211734 (D.M.L) and R24OD016761 (D.M.L), the MGH Research Scholar Award (D.M.L.) and Alex Lemonade Stand Foundation (C.Y.).

Conflict of of interest disclosure

The authors declare no competing interests.

Authorship

MS: Conceptualization, Methodology, Formal analysis, Investigation, Data Curation, Writing - Original Draft, Visualization

SBF: Investigation, Formal analysis, Data Curation, Methodology, Writing - Review & Editing

CY, QY: Investigation- performed transplantation experiments, Data Curation, Formal analysis, Methodology, Writing - Review & Editing

SMK: Investigation- provided assistance with heart function analysis, Methodology, Resources, Writing - Review & Editing

JB: Conceptualization, Supervision, Writing - Review & Editing

DML: Conceptualization, Supervision, Writing - Review & Editing

JDH: Conceptualization, Supervision, Funding acquisition, Project administration, Writing - Original Draft

References

1. Sanchez-Vega, F. *et al.* Oncogenic Signaling Pathways in The Cancer Genome Atlas. *Cell* **173**, 321-3e10 (2018).
2. Rauen, K. A. The RASopathies. *Annu. Rev. Genomics Hum. Genet.* **14**, 355–369 (2013).
3. Tajan, M., Paccoud, R., Branka, S., Edouard, T. & Yart, A. The RASopathy Family: Consequences of Germline Activation of the RAS/MAPK Pathway. *Endocr. Rev.* **39**, 676–700 (2018).
4. Roberts, A. E., Allanson, J. E., Tartaglia, M. & Gelb, B. D. Noonan syndrome. *Lancet* **381**, 333–342 (2013).
5. Gelb, B. D. & Tartaglia, M. Noonan syndrome and related disorders: dysregulated RAS-mitogen activated protein kinase signal transduction. *Hum. Mol. Genet.* **15**, R220–R226 (2006).
6. Tajan, M., de Rocca Serra, A., Valet, P., Edouard, T. & Yart, A. SHP2 sails from physiology to pathology. *Eur. J. Med. Genet.* **58**, 509–525 (2015).
7. Tartaglia, M. *et al.* Mutations in PTPN11, encoding the protein tyrosine phosphatase SHP-2, cause Noonan syndrome. *Nat. Genet.* **29**, 465–468 (2001).
8. Tajan, M., de Rocca Serra, A., Valet, P., Edouard, T. & Yart, A. SHP2 sails from physiology to pathology. *Eur. J. Med. Genet.* **58**, 509–525 (2015).
9. Tartaglia, M. *et al.* PTPN11 Mutations in Noonan Syndrome: Molecular Spectrum, Genotype-Phenotype Correlation, and Phenotypic Heterogeneity. *Am. J. Hum. Genet.* **70**, 1555–1563 (2002).
10. Matozaki, T., Murata, Y., Saito, Y., Okazawa, H. & Ohnishi, H. Protein tyrosine phosphatase SHP-2: A proto-oncogene product that promotes Ras activation. *Cancer Sci.* **100**, 1786–1793 (2009).
11. Niemeyer, C. M. & Flotho, C. Juvenile myelomonocytic leukemia: who's the driver at the wheel? *Blood* **133**, 1060–1070 (2019).
12. Strullu, M. *et al.* Juvenile myelomonocytic leukaemia and Noonan syndrome. *J. Med. Genet.* **51**, 689–697 (2014).
13. Kratz, C. P. The mutational spectrum of PTPN11 in juvenile myelomonocytic leukemia and Noonan syndrome/myeloproliferative disease. *Blood* **106**, 2183–2185 (2005).
14. Chang, T. Y., Dvorak, C. C. & Loh, M. L. Bedside to bench in juvenile myelomonocytic leukemia: insights into leukemogenesis from a rare pediatric leukemia. *Blood* **124**, 2487–2497 (2014).
15. Emanuel, P., Bates, L., Castleberry, R., Gualtieri, R. & Zuckerman, K. Selective hypersensitivity to granulocyte-macrophage colony-stimulating factor by juvenile chronic myeloid leukemia hematopoietic progenitors. *Blood* **77**, 925–929 (1991).
16. Locatelli, F. & Niemeyer, C. M. How I treat juvenile myelomonocytic leukemia. *Blood* **125**, 1083–1090 (2015).
17. Jindal, G. A., Goyal, Y., Burdine, R. D., Rauen, K. A. & Shvartsman, S. Y. RASopathies: unraveling mechanisms with animal models. *Dis. Model. Mech.* **8**, 1167–1167 (2015).
18. Patterson, V. L. & Burdine, R. D. Swimming toward solutions: Using fish and frogs as models for understanding <scp>RASopathies</scp>. *Birth Defects Res.* **112**, 749–765 (2020).
19. Bonetti, M. *et al.* Distinct and overlapping functions of ptpn11 genes in zebrafish development. *PLoS One* **9**, (2014).
20. Jopling, C., van Geemen, D. & den Hertog, J. Shp2 Knockdown and Noonan/LEOPARD Mutant Shp2–Induced Gastrulation Defects. *PLoS Genet.* **3**, e225 (2007).
21. Niihori, T. *et al.* Germline-Activating RRAS2 Mutations Cause Noonan Syndrome. *Am. J. Hum. Genet.* **104**, 1233–1240 (2019).
22. Paardekooper Overman, J. *et al.* PZR Coordinates Shp2 Noonan and LEOPARD Syndrome Signaling in Zebrafish and Mice. *Mol. Cell. Biol.* **34**, 2874–2889 (2014).
23. Runtuwene, V. *et al.* Noonan syndrome gain-of-function mutations in NRAS cause zebrafish gastrulation defects. *Dis. Model. Mech.* **4**, 393–399 (2011).
24. Liu, K., Petree, C., Requena, T., Varshney, P. & Varshney, G. K. Expanding the CRISPR Toolbox in Zebrafish for Studying Development and Disease. *Front. Cell Dev. Biol.* **7**, 1–15 (2019).
25. Tessadori, F. *et al.* Effective CRISPR/Cas9-based nucleotide editing in zebrafish to model human genetic cardiovascular disorders. *Dis. Model. Mech.* **11**, dmm035469 (2018).
26. Tessadori, F. *et al.* Identification and Functional Characterization of Cardiac Pacemaker Cells in Zebrafish. *PLoS One* **7**, e47644 (2012).
27. Svoboda, O. *et al.* Ex vivo tools for the clonal analysis of zebrafish hematopoiesis. *Nat. Protoc.* **11**, 1007–1020 (2016).
28. Moore, J. C. *et al.* Single-cell imaging of normal and malignant cell engraftment into optically clear prkdc-null SCID zebrafish. *J. Exp. Med.* **213**, 2575–2589 (2016).
29. Herman, J. S., Sagar & Grün, D. FateID infers cell fate bias in multipotent progenitors from single-cell RNA-seq data. *Nat. Methods* **15**, 379–386 (2018).
30. Bagby, G. C., Dinarello, C. A., Neerhout, R. C., Ridgway, D. & McCall, E. Interleukin 1-dependent paracrine granulopoiesis in chronic granulocytic leukemia of the juvenile type. *J. Clin. Invest.* **82**, 1430–1436 (1988).
31. Dong, L. *et al.* Leukaemogenic effects of Ptpn11 activating mutations in the stem cell microenvironment. *Nature* **539**, 304–308 (2016).

32. Araki, T. *et al.* Mouse model of Noonan syndrome reveals cell type– and gene dosage–dependent effects of Ptpn11 mutation. *Nat. Med.* **10**, 849–857 (2004).
33. Xu, D. *et al.* A germline gain-of-function mutation in Ptpn11 (Shp-2) phosphatase induces myeloproliferative disease by aberrant activation of hematopoietic stem cells. *Blood* **116**, 3611–3621 (2010).
34. Athanasiadis, E. I. *et al.* Single-cell RNA-sequencing uncovers transcriptional states and fate decisions in haematopoiesis. *Nat. Commun.* **8**, (2017).
35. Freedman, M. H. *et al.* Central role of tumour necrosis factor, GM-CSF, and interleukin 1 in the pathogenesis of juvenile chronic myelogenous leukaemia. *Br. J. Haematol.* **80**, 40–48 (1992).
36. Hamarsheh, S. *et al.* Oncogenic KrasG12D causes myeloproliferation via NLRP3 inflammasome activation. *Nat. Commun.* **11**, 1659 (2020).
37. Zhao, W., Wang, L. & Yu, Y. Gene module analysis of juvenile myelomonocytic leukemia and screening of anticancer drugs. *Oncol. Rep.* **40**, 3155–3170 (2018).
38. Arranz, L., Arriero, M. del M. & Villatoro, A. Interleukin-1β as emerging therapeutic target in hematological malignancies and potentially in their complications. *Blood Rev.* **31**, 306–317 (2017).
39. Craver, B., El Alaoui, K., Scherber, R. & Fleischman, A. The Critical Role of Inflammation in the Pathogenesis and Progression of Myeloid Malignancies. *Cancers (Basel).* **10**, 104 (2018).
40. Pietras, E. M. *et al.* Chronic interleukin-1 exposure drives haematopoietic stem cells towards precocious myeloid differentiation at the expense of self-renewal. *Nat. Cell Biol.* **18**, 607–618 (2016).
41. Pandey, R., Saxena, M. & Kapur, R. Role of SHP2 in hematopoiesis and leukemogenesis. *Curr. Opin. Hematol.* 1 (2017) doi:1097/MOH.0000000000000003
42. Karnik, R. & Geiger, M. Cardiac Manifestations of Noonan Syndrome. *Pediatr. Endocrinol. Rev.* **16**, 471–476 (2019).
43. Riordan, J. D. & Nadeau, J. H. From Peas to Disease: Modifier Genes, Network Resilience, and the Genetics of Health. *Am. J. Hum. Genet.* **101**, 177–191 (2017).
44. Araki, T. *et al.* Noonan syndrome cardiac defects are caused by PTPN11 acting in endocardium to enhance endocardial-mesenchymal transformation. *Proc. Natl. Acad. Sci.* **106**, 4736–4741 (2009).
45. Hernández-Porras, I., Jiménez-Catalán, B., Schuhmacher, A. J. & Guerra, C. The impact of the genetic background in the Noonan syndrome phenotype induced by K-Ras V14I. *Rare Dis.* **3**, e1045169 (2015).
46. Hogan, B. M. *et al.* ccbe1 is required for embryonic lymphangiogenesis and venous sprouting. *Nat. Genet.* **41**, 396–398 (2009).
47. Lin, H. F. *et al.* Analysis of thrombocyte development in CD41-GFP transgenic zebrafish. *Blood* **106**, 3803–3810 (2005).
48. Ellett, F., Pase, L., Hayman, J. W., Andrianopoulos, A. & Lieschke, G. J. mpeg1 promoter transgenes direct macrophage-lineage expression in zebrafish. *Blood* **117**, e49–e56 (2011).
49. Renshaw, S. A. *et al.* A transgenic zebrafish model of neutrophilic inflammation. *Blood* **108**, 3976–3978 (2006).
50. Ogryzko, N. V. *et al.* Hif-1α–Induced Expression of Il-1β Protects against Mycobacterial Infection in Zebrafish. *J. Immunol.* **202**, 494–502 (2019).
51. Aleström, P. *et al.* Zebrafish: Housing and husbandry recommendations. *Lab. Anim.* **0**, 1–12 (2019).
52. Westerfield, M. The zebrafish book. A guide for the laboratory use of zebrafish (Danio rerio). 4th ed. *Univ. Oregon Press. Eugene* (2000).
53. Gagnon, J. A. *et al.* Efficient Mutagenesis by Cas9 Protein-Mediated Oligonucleotide Insertion and Large-Scale Assessment of Single-Guide RNAs. *PLoS One* **9**, e98186 (2014).
54. Hale, A. J. & den Hertog, J. Shp2–Mitogen-Activated Protein Kinase Signaling Drives Proliferation during Zebrafish Embryo Caudal Fin Fold Regeneration. *Mol. Cell. Biol.* **38**, 1–15 (2017).
55. Thisse, C. & Thisse, B. High-resolution in situ hybridization to whole-mount zebrafish embryos. *Nat. Protoc.* **3**, 59–69 (2008).
56. Choorapoikayil, S., Kers, R., Herbomel, P., Kissa, K. & Den Hertog, J. Pivotal role of Pten in the balance between proliferation and differentiation of hematopoietic stem cells in zebrafish. *Blood* **123**, 184–190 (2014).
57. Hu, B. *et al.* Zebrafish eaf1 suppresses foxo3b expression to modulate transcriptional activity of gata1 and spi1 in primitive hematopoiesis. *Dev. Biol.* **388**, 81–93 (2014).
58. Choorapoikayil, S., Kuiper, R. V., De Bruin, A. & Den Hertog, J. Haploinsufficiency of the genes encoding the tumor suppressor Pten predisposes zebrafish to hemangiosarcoma. *DMM Dis. Model. Mech.* **5**, 241–247 (2012).
59. Blokzijl-Franke, S. *et al.* Phosphatidylinositol-3 kinase signaling controls survival and stemness of hematopoietic stem and progenitor cells. *Oncogene* **40**, 2741–2755 (2021).
60. Muraro, M. J. *et al.* A Single-Cell Transcriptome Atlas of the Human Pancreas. *Cell Syst.* **3**, 385–394 (2016).
61. Van Den Brink, S. C. *et al.* Single-cell sequencing reveals dissociation-induced gene expression in tissue subpopulations. *Nat. Methods* **14**, 935–936 (2017).
62. Hashimshony, T. *et al.* CEL-Seq2: sensitive highly-multiplexed single-cell RNA-Seq. *Genome Biol.* **17**, 77 (2016).
63. Grün, D., Kester, L. & van Oudenaarden, A. Validation of noise models for single-cell transcriptomics. *Nat. Methods* **11**, 637–640 (2014).

64. Love, M. I., Huber, W. & Anders, S. Moderated estimation of fold change and dispersion for RNA-seq data with DESeq *Genome Biol.* **15**, 1–21 (2014).
65. Tang, Q. *et al.* Optimized cell transplantation using adult rag2 mutant zebrafish. *Nat. Methods* **11**, 821–824 (2014).
66. Wickham, H. ggplot2: Elegant Graphics for Data Analysis. *Springer Int. Publ.* 2009 (2009).

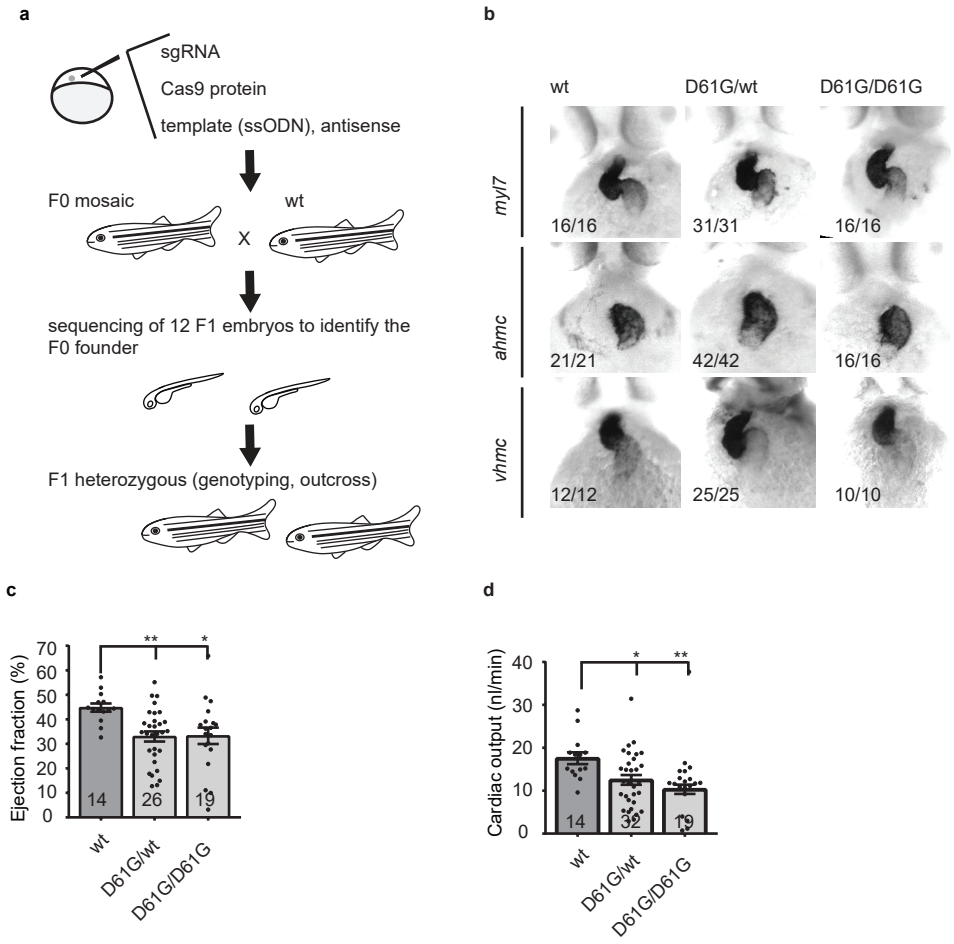

Figure S1. Heart function, but not heart morphology, is defective in Shp2^{D61G} zebrafish embryos. (a) Schematic representation of the procedure used to establish the Shp2^{D61G} mutant line, as described in the Materials and Methods section. (b) Representative images of the WISH staining for *myl7*, *ahmc* and *vhmc* expression in the hearts of 3dpf old Shp2^{wt}, Shp2$^{D61G/wt}$ and Shp2$^{D61G/D61G}$ zebrafish embryos. Numbers in the pictures indicate the number of embryos with the phenotype represented in the image. (c) Ejection fraction and (d) cardiac output determined from the high speed videos of the heart of 5dpf old Shp2^{wt}, Shp2$^{D61G/wt}$ and Shp2$^{D61G/D61G}$ zebrafish embryos. Measurements originate from at least three distinct experiments. Numbers on the bars depict the number of embryos. Error bars represent standard error of the mean (SEM). *p < 0.05; **p < 0.01, ***p < 0.001, NS, non significant, ANOVA complemented by Tukey HSD.

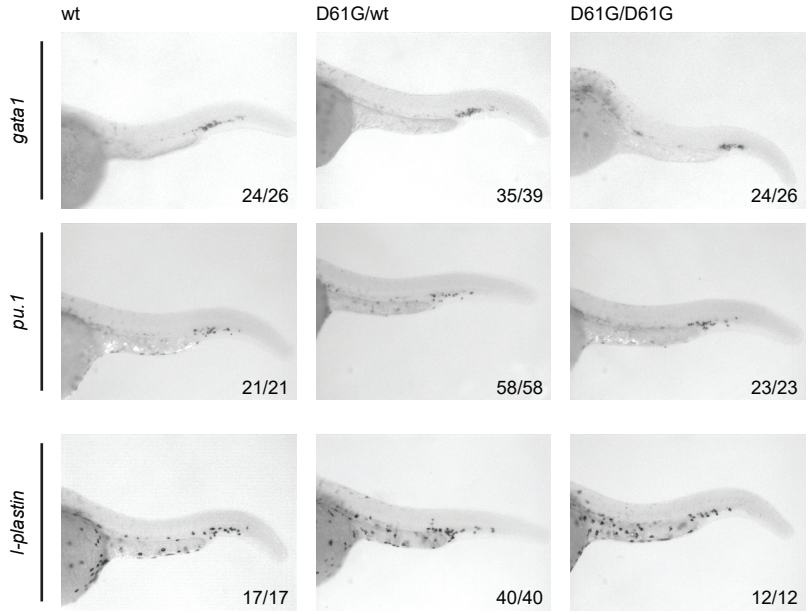

Figure S2. Shp2^{D61G} zebrafish display normal primitive hematopoiesis. Representative images of the WISH staining for *gata1*, *pu.1* and *l-plastin* expression in the tail region of 48hpf old Shp2^{wt}, Shp2$^{D61G/wt}$ and Shp2$^{D61G/D61G}$ zebrafish embryos. Scale bar is 250µm. Numbers in the pictures indicate the number of embryos with the phenotype represented in the image.

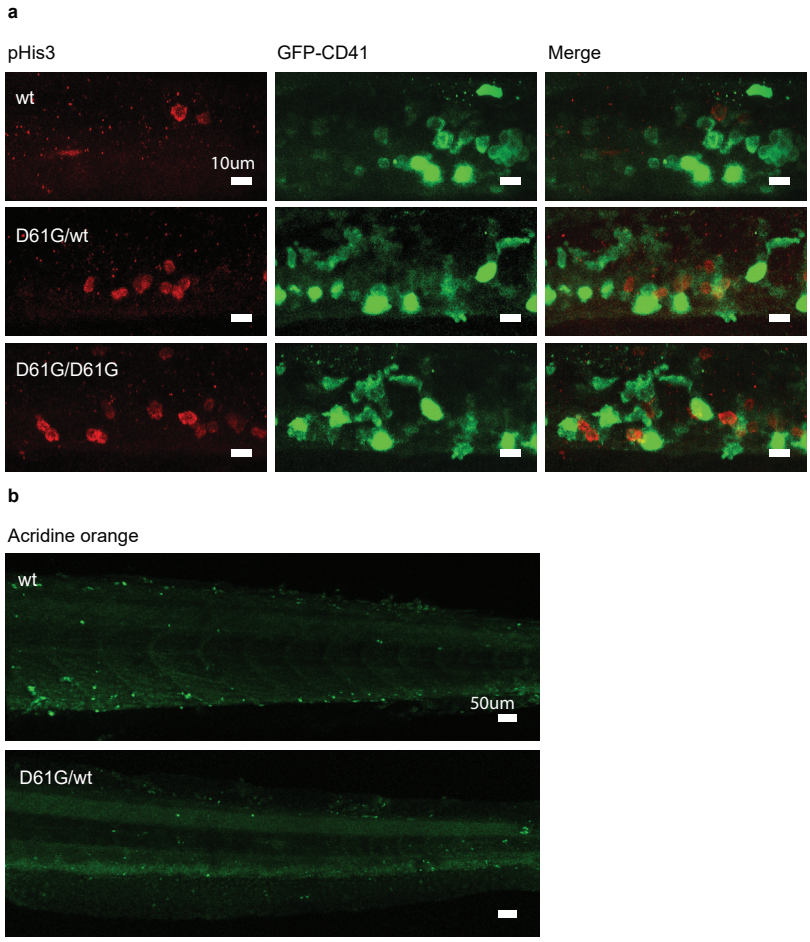

Figure S3. Enhanced proliferation and reduced apoptosis in the CHT of Shp2^{D61G} zebrafish embryos. (a) Cell proliferation was assessed in the CHT region of 5 dpf old Shp2^{wt}, Shp2$^{D61G/wt}$ and Shp2$^{D61G/D61G}$ embryos in the *Tg(cd41:GFP)* background by immunohistochemistry using antibodies specific for pHis3 and GFP. Cells positive for both GFP and pHis3 are indicated with white arrows in the Merge panel. Scale bar is 10µm. (b) Representative images of the Acridine orange staining of the CHT region of the 5dpf old Shp2^{wt} and Shp2$^{D61G/wt}$ embryos. Scale bar is 50µm.

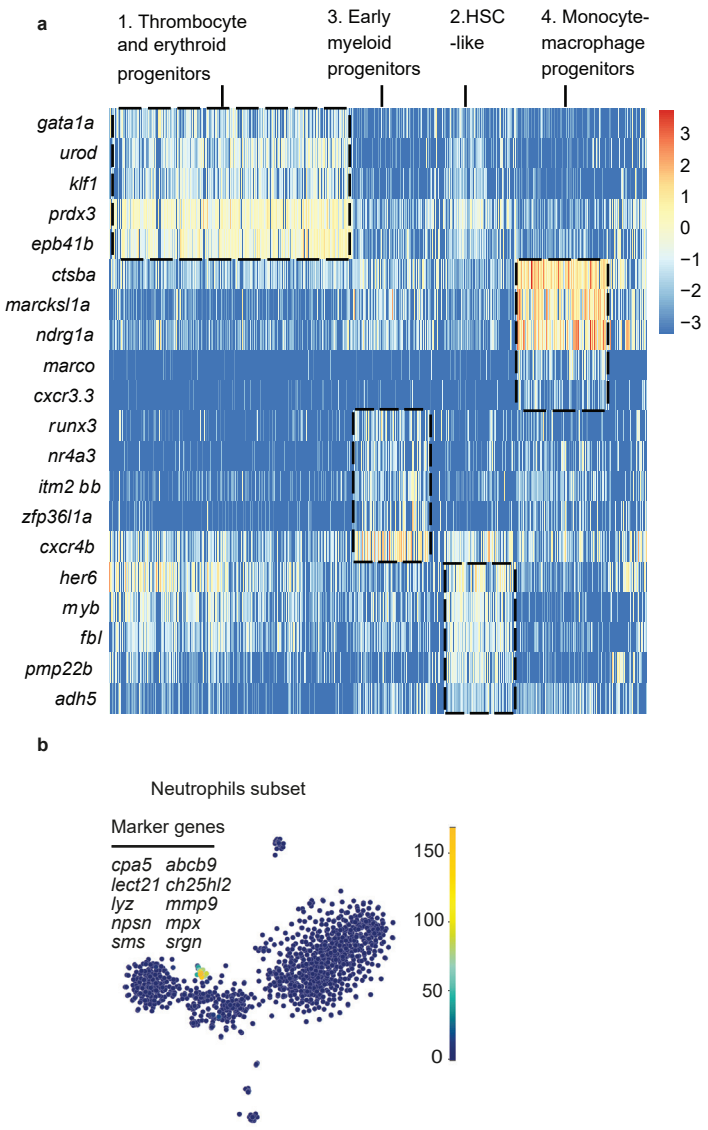

Figure S4. Identities of different HSPCs subpopulations based on expression of representative genes. (a) Heat map showing scaled expression [log TPM (transcripts per million) values] of representative genes (y-axis) in all cells (x-axis). Cells belonging to distinct clusters are squared with a dashed line and cluster identity is indicated on the top of the heat map. Cells from cluster 2 express typical hematopoietic stem cell markers, such as *c-myb* and *her6* (*HES1* analogue in human). Cluster 1 is characterized by expression of genes characteristic for thrombocyte and erythroid differentiation, such as *gata1a* and *klf1*. Cells from cluster 3 express early myeloid progenitor markers, such as *runx3* and *cxcr4b*. Cells from cluster 4 expresse genes typical for both monocyte and macrophages, such as *marco* and *ctsba*. (b) tSNE maps showing the sum of total read-counts of selected neutrophil specific genes.

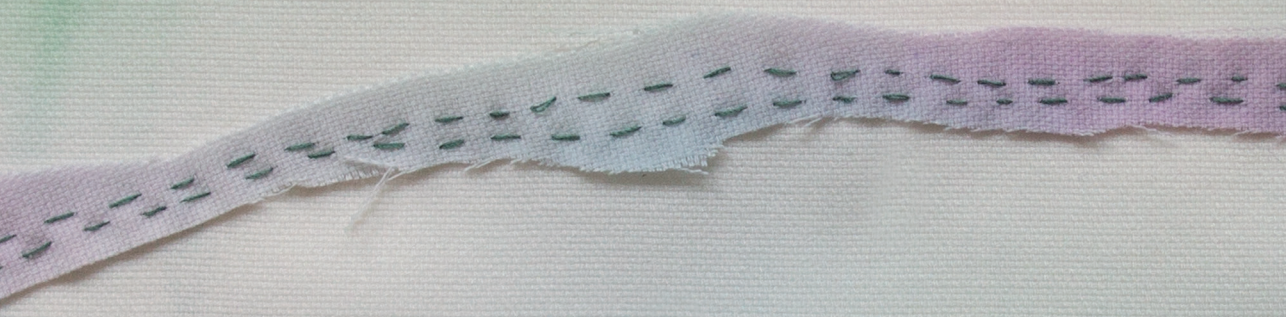

Chapter 4

Shp2b is Required for Normal Ontogeny of Hematopoietic Stem and Progenitor Cells

Blokzijl-Franke S, van Zanten L and den Hertog J

Abstract

Hematopoiectic Stem and Progenitor cells (HSPCs) are multipotent cells giving rise to all blood lineages during life. In zebrafish, HSPCs emerge from the ventral wall of the dorsal aorta (VDA) in an endothelial hematopoietic transition (EHT). *PTPN11* encodes an essential protein tyrosine phosphatase (PTP), that is required for normal development. We investigated the role of *ptpn11a* and *ptpn11b* in hematopoiesis in zebrafish. Through *in vivo* live imaging, we discovered that *ptpn11b* mutant embryos showed disintegrating cells upon emergence from the VDA, an effect that is rescued after micro-injection with *ptpn11b. Ptpn11a* mutants do not show this phenotype. The surviving HSPCs in *ptpn11b* mutant embryos colonized the CHT normally, albeit in lower numbers, and committed to all blood lineages. We conclude that *ptpn11b* is essential during the definitive wave of hematopoiesis, but that knock-out of *ptpn11b* does not lead to adult zebrafish with developmental defects.

Introduction

Stem cells are a particular type of cells that maintain self-renewal capacity and may differentiate into multiple cell types at the same time. HSPCs are multi-potent cells giving rise to all blood lineages during life [1–3]. All vertebrates undergo two waves of hematopoiesis: the primitive wave in which primitive erythrocytes and myeloid cells are produced and the definitive wave in which HSPCs are generated that will later found the adult hematopoietic organs [2,4]. At the start of the definitive wave, HSPCs emerge from the floor of the dorsal aorta (VDA) in a process called endothelial hematopoietic transition [5–7]. During EHT cells bend from the VDA after which they detach and then transiently colonize the fetal liver in mammals [8] or the caudal hematopoietic tissue (CHT) in zebrafish [9]. In the CHT HSPCs expand and differentiate into all blood lineages and supply the developing embryo with mature blood cells. Next, HSPCs migrate to colonize the thymus and bone marrow in mammals [8] or the thymus and whole kidney marrow in fish [9] to produce adult blood cells of all lineages.

HSPCs are tightly regulated in terms of dormancy, self-renewal and differentiation by environmental cues, such as cytokines and growth factors. Dysregulation of these cues can result in blood disorders, including hematologic malignancies. SHP2, encoded by *PTPN11*, is a ubiquitously expressed protein tyrosine phosphatase (PTP) with two Src homology 2 (SH2) domains that are essential for normal development [10–12]. SHP2 is a positive effector of extracellular regulated kinase (ERK)/MAPK signaling, downstream of most receptor tyrosine kinases (RTKs) [11,12]. SHP2 is also involved in other signaling pathways, such as the Jak-STAT pathway [12] and the PI3K-AKT pathway [11]. Alterations in the catalytic activity of SHP2 due to missense mutations in *PTPN11* have been implicated in pathogenesis of Noonan syndrome (NS), NS with Multiple Lentigenes (NS-ML, formerly known as LEOPARD syndrome) and juvenile myelomonocytic leukemia (JMML) [13,14]. SHP2 also plays an important role during hematopoiesis [15–19]. Mouse models with conditional deletion of *Ptpn11*, encoding SHP2, show a depleted functional HSPCs pool and fail to reconstitute recipients because of defects in homing, self-renewal and survival [20,21]. Given the pathways in which *Ptpn11* plays a role, deregulation of SHP2 has broad consequences for hematopoiesis.

Zebrafish are an excellent model to further investigate the role of *ptpn11* in hematopoiesis *in vivo* as development occurs externally and embryos are transparent [22]. The zebrafish genome encodes two *ptpn11* genes: *ptpn11a* and *ptpn11b*, encoding Shp2a and Shp2b, respectively [23]. Both Shp2a and Shp2b are highly homologous to human SHP2 and harbor catalytic activity, but they differ in their expression during early embryonic development, with *ptpn11a* being constantly expressed up until 5 dpf and *ptpn11b* becoming upregulated over this time [24]. *Ptpn11a*$^{-/-}$ mutant embryos as well as *ptpn11a*$^{-/-}$ *ptpn11b*$^{-/-}$ double mutant embryos are embryonically lethal from 5-6 dpf onwards, whereas *ptpn11b*$^{-/-}$ embryos do not show developmental defects, grow up to adulthood and are viable and fertile [24]. We imaged the emergence of HSPCs from the VDA *in vivo* in *ptpn11* mutant embryos, which showed surprising defects. Furthermore, we performed *in situ* hybridization to analyze expression patterns during the definitive wave of hematopoiesis.

Our results indicate that lack of Shp2b resulted in less HSPCs during the definitive wave, but that this effect did not influence the ability to engage in all blood lineages.

Results

Ptpn11b knock-out results in disintegrating HSPCs during EHT

In zebrafish, endothelial cells from the ventral wall of the dorsal aorta (VDA) transform into HSPCs in a process called endothelial hematopoietic transition (EHT) [7]. Next, HSPCs join the blood flow in the underlying posterior cardinal vein (PCV) to transiently seed the caudal hematopoietic tissue (CHT) [5,7,9] and afterwards reside in the adult hematopoietic organs, the thymus and head kidney. We imaged EHT events in the aorta gonad mesonephros (AGM) by time-lapse confocal imaging of an area spanning five adjacent intersegmental vessels in *ptpn11a* and *ptpn11b* mutant embryos in the *tg(kdrl:eGFP)* background from 35 to 48 hpf (figure 1 a-l). The floor of the aorta in *ptpn11a* and *ptpn11b* mutant embryos displayed the characteristic contraction then bending of cells towards the subaortic space [7], indicating that the initiation of EHT was normal in these mutant embryos. In *ptpn11a*$^{-/-}$*ptpn11b*$^{+/+}$ and *ptpn11a*$^{-/-}$*ptp11b*$^{+/-}$ embryos EHT progressed normally and we did not observe any abortive EHT events (n=3 and n=5, table s1). However, the majority of *ptpnb11b*$^{-/-}$ mutant embryos (78%) showed EHT events that were abortive, in that they failed to detach and disintegrated (n=50) (figure 1 i-l, table 1). In contrast, in *ptpn11b*$^{+/+}$ (n=21) or *ptpn11b*$^{+/-}$ (n=18) mutant embryos in total only 4 disintegrating HSPCs were observed (figure 1a-h, table 1, Fisher's exact test with multiple testing correction $p<0.001$). To verify that the observed effects were caused by the lack of functional *ptpn11b*, we microinjected synthetic *ptpn11b* mRNA in *ptpn11b*$^{-/-}$ mutant embryos at the one-cell stage and monitored EHT events in the AGM by time-lapse confocal imaging. 47% of the imaged embryos showed no abortive events (figure 1n, Fisher's Exact test, $p<0.05$). Hence, *ptpn11b*$^{-/-}$ mutant embryos show disintegrating HSPCs during EHT which are rescued upon

	Number of embryos showing normal emerging HSPCs	Number of embryos showing disintegrating HSPCs
Ptpn11b$^{+/+}$	18	3
Ptpn11b$^{+/-}$	17	1
Ptpn11b$^{-/-}$	11	39
Ptpn11b$^{-/-}$ injected with 120 pg *ptpn11b* mRNA	9	10

Table 1. The number of embryos showing disintegrating HSPCs after EHT in the AGM was determined in all *ptpn11b* genotypes by confocal time lapse imaging. A Chi square test and Fisher's exact test was used for statistical analysis (*** $p<0.001$, * $p<0.05$)

microinjection of *ptpn11b* mRNA. This suggests that *ptpn11b,* but not *ptpn11a*, is required for normal emergence of HPSCs during EHT.

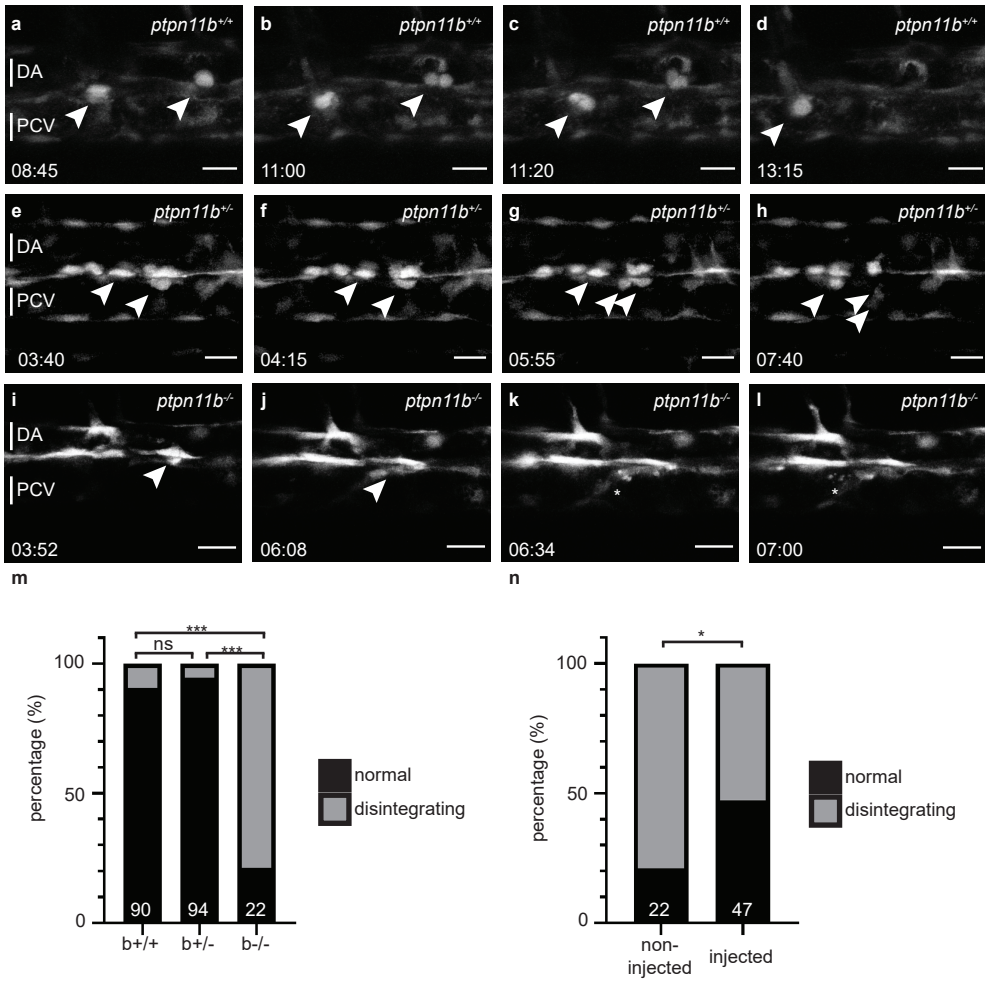

Figure 1. HSPCs disintegrate upon emergence from the VDA in *ptpn11b*$^{-/-}$ embryos. (a-l) Four-dimensional imaging of *tg(kdrl:eGFP) ptpn11b*$^{+/+}$, *ptpn11b*$^{+/-}$ or *ptpn11b*$^{-/-}$ mutant zebrafish embryos between 35 hpf and 48 hpf. Arrowheads: HSPCs undergoing EHT; asterisk: disintegrating HSPCs. Confocal image z-stacks (2µm step size, with 20x objective and 1.5 zoom; anterior to the left; maximum projections of a representative embryo; time in hh:mm. Scale bar: 20µm; DA: dorsal aorta; PCV: posterior cardinal vein). (m) The percentages of embryos that show normal EHT and disintegrating EHT events. Percentages of normal EHT events are displayed. Original observations are shown in table 1. Fisher's exact tests were performed on table 1 (*** p<0.001). (n) The percentage of embryos that show normal EHT and disintegrating EHT events after microintjection at the one-cell stage with synthetic *ptpn11b* mRNA (120pg). Percentages of normal EHT events are displayed. Original observations are shown in table 2. Fisher's Exact test was used for statistical analysis on table 2. * p<0.05.

*The number of HSPCs that colonize the CHT is reduced in **ptpn11b**$^{-/-}$ mutant embryos*

Following EHT, HSPCs transiently colonize the CHT [9]. We quantified the number of HSPCs that seeded the CHT at 48 hpf, *i.e.* by the peak of HSPC emergence from the VDA, using *tg(cd41:eGFP)* embryos, which express low GFP (GFP^{low}) in HSPCs [25,26]. Consistent with our earlier imaging where 78% of the *ptpnb11b*$^{-/-}$ embryos showed disintegrating HSPCs,

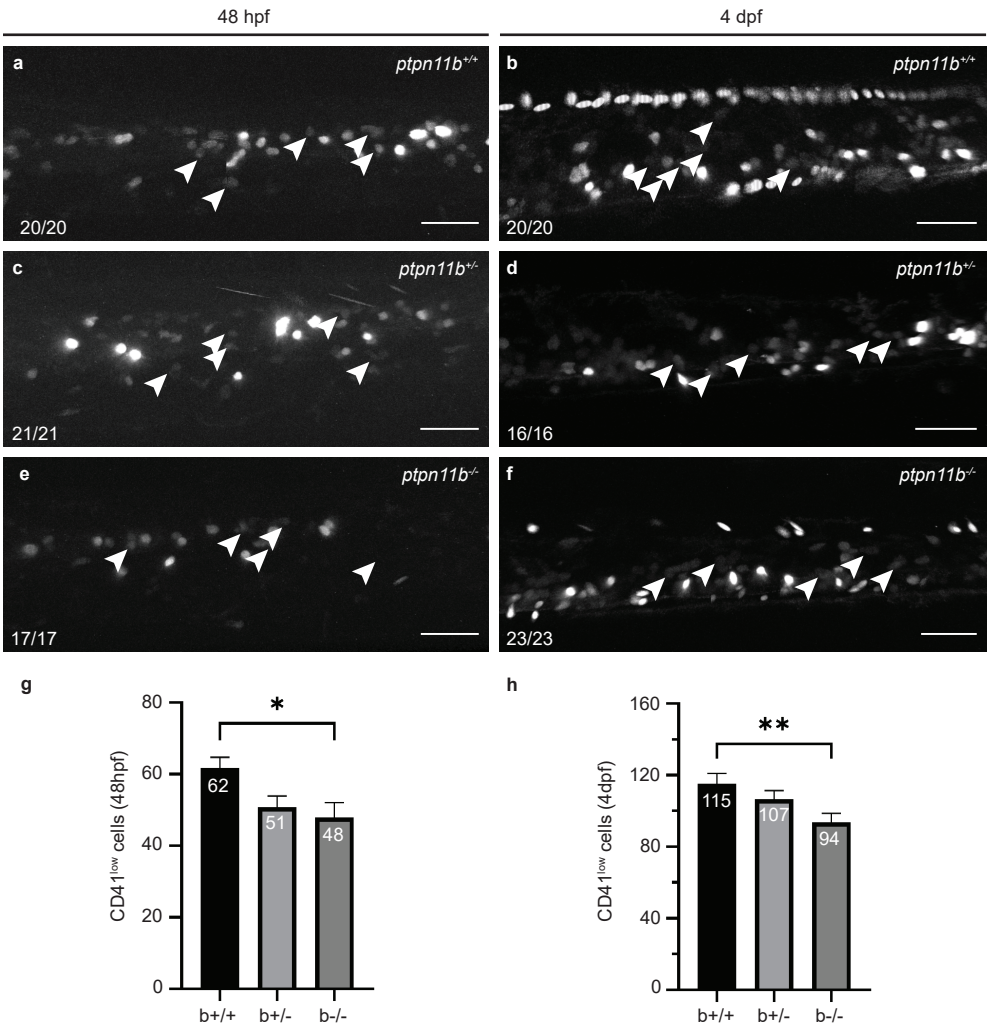

Figure 2. Reduced numbers of HSPCs in *ptpn11b*$^{-/-}$ embryos. (a, f) The number of GFP^{low} HSPCs at 48 hpf (a, c, e) or 4 dpf (b, d, f) in the CHT of *tg(cd41:eGFP) ptpn11b*$^{+/+}$, *ptpn11b*$^{+/-}$ and *ptpnb*$^{-/-}$ is expressed as average number of cells (g,h). Selected GFP^{low} HSPCs are indicated by arrowheads (a-f). GFPhigh cells are thrombocytes circulating swiftly through the vasculature. Anterior to the left; Images were taken with a 40x objective and 2µm z-stepsize. Scale bar = 50µm. Representative embryos are shown and the number of embryos that showed this pattern/ total number of embryos is indicated. Error bars indicate standard error of the mean (SEM). Shapiro Wilk test for normal distribution and One-Way ANOVA were used for statistical analysis; *p<0.05, **p<0.01.

23% less GFP^{low} HPSCs were detected in the CHT of *ptpn11b*$^{-/-}$ mutant embryos at 48 hpf compared to *ptpn11b*$^{+/+}$ mutant embryos (figure 2), which was statistically signficicant (One-way ANOVA, p<0.05). *Ptpn11b*$^{+/-}$ mutant embryos showed no statistically significant difference compared to *ptpnb*$^{+/+}$ mutant embryos, even though numbers of cd41^{low} cells appear to be decreasing. After seeding, HSPCs start to proliferate in the CHT before migrating to their final destination, the adult hematopoietic organs, the thymus and whole kidney marrow. This reduction of HSPCs in the CHT at 48 hpf persisted through 4 dpf in *ptpnb11b*$^{-/-}$ mutant embryos (figure 2n). These data suggest that the effect of disintegrating HSPCs around EHT persists during seeding of the CHT and later on during proliferation and maturation of HSPCs in the CHT.

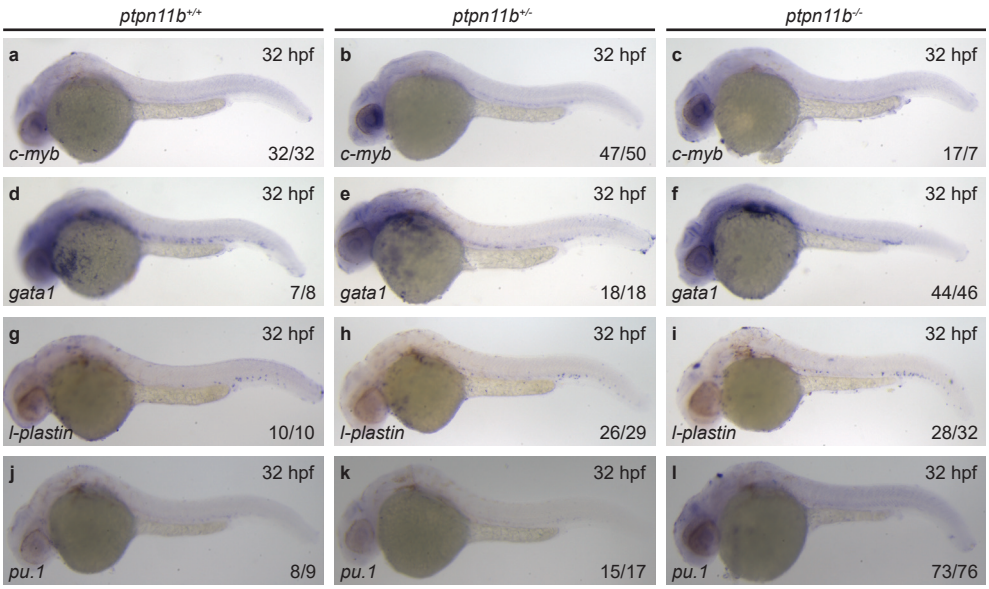

Figure 3. HSPCs of *ptpn11b*$^{-/-}$ embryos at 48hpf engage in all blood lineages and show no differences compared to their siblings. (a-l) *ptpn11b*$^{+/+}$, *ptpn11b*$^{+/-}$ and *ptpn11b*$^{-/-}$ embryos were fixed at 32 hpf. Markers for primitive blood lineages were assessed by whole mount *in situ* hybridization. *C-myb* (HSPCs, a-c), *gata1* (primitive erythroid lineage, d-f), *l-plastin* and *pu.1* (primitive myeloid lineage, g-l). Representative embryos are shown, with anterior to the left. The number of embryos that showed a particular pattern/total number of embryos is indicated in the bottom right corner of each panel.

The onset of the definitive wave is independent of ptpn11b

The onset of the definitive wave starts at 32 hours post fertilization (hpf) with the specification of the endothelial cells that will become HSPCs in the floor of the dorsal aorta (DA) in the AGM region, a conserved process between mammals and zebrafish [5–7]. The hemogenic endothelium of the DA and its HSPCs progeny is marked by *c-myb* [9,27]. We found that *c-myb* is not differently expressed in *ptpn11b*$^{-/-}$ mutant embryos compared to their siblings at the onset of the definitive wave (figure 3 a-c). Lineage markers for primitive erythroid (figure 3 d-f) and myeloid (figure 3 g-l) fate also did not show

differences in expression levels between *ptpn11b*$^{-/-}$ embryos and their siblings at 32hpf. These data suggest that *ptpn11b* does not affect the onset of the definitive wave.

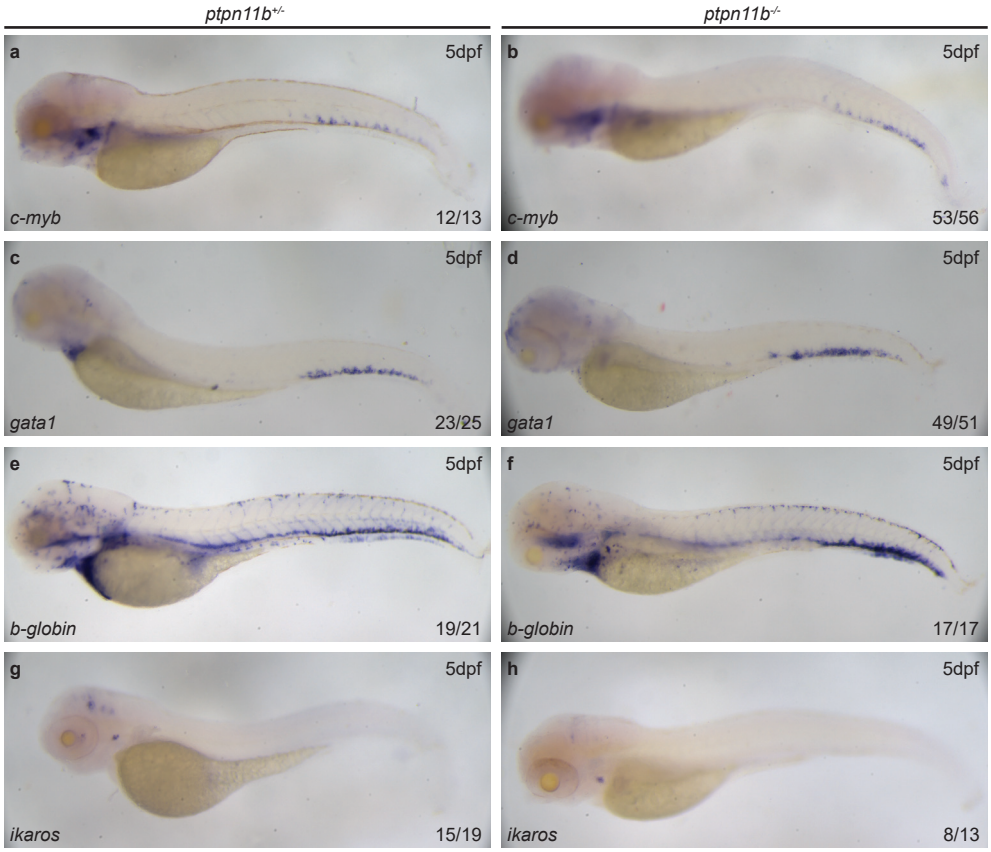

Figure 4. HSPCs of *ptpn11b*$^{-/-}$ embryos at 5 dpf engage in all blood lineages and show no differences compared to their siblings. *Ptpn11b*$^{+/-}$ and *ptpn11b*$^{-/-}$ mutant embryos were fixed at 5 dpf. Markers for definitive bloodlineages were assessed by whole mount *in situ* hybridization. *C-myb* (HSPCs, a, b), *gata1* and *b-globin* (erythroid lineage, c-f) and *ikaros* (lymphocyte lineage, g-h). Representative embryos are shown, with anterior to the left. The number of embryos that showed a particular pattern/total number of embryos is indicated in the bottom right corner of each panel.

Ptpn11b is not essential for HSPCs to engage in all blood lineages

To investigate the consequences of lack of Shp2b function for the various definitive blood lineages originating from HSPCs we performed *in situ* hybridization with a panel of blood progenitor markers. First, we determined expression of *c-myb* (HSPCs) at 5 dpf. We detected expression in the CHT, indicating that homing of HSPCs was not dependent on *ptpn11b*. We did not see any differences in expression levels between *ptpn11b* mutant embryos and their siblings (figure 4 a, b). To assess the erythroid lineages *gata1* and

b-globin markers were evaluated, together with *ikaros* to evaluate the lymphoid lineage. The erythroid lineage showed no differences in expression between *ptpn11b*$^{-/-}$ mutant embryos when compared to *ptpn11b*$^{+/-}$ (figure 4 c-f). *Ptpn11b* mutant embryos also did not show altered expression levels of the lympoid marker *ikaros*, when compared to their siblings (figure 4 g, h). These results show that lack of *ptpn11b* signaling did not block specification of particular blood lineages.

Discussion

We used zebrafish mutant embryos lacking functional Shp2 to investigate how loss of Shp2 affects early stages of hematopoiesis. Zebrafish have two *ptpn11* genes, which both encode functional Shp2 proteins. *Ptpn11a* is an essential gene, in that *ptpn11a* knock-out embryos are embryonic lethal at 5-6 dpf. In contrast, *ptpn11b* knock-outs do not show obvious developmental defects and grow up to adulthood. Surprisingly, knock-out of *ptpn11a* did not affect the ontogeny of HSPCs, but knock-out of *ptpn11b* did. Characterization of zebrafish *ptpn11b*$^{-/-}$ mutant embryos led to the unexpected finding that 78% of *ptpn11b*$^{-/-}$ mutant embryos show disintegrating HSPCs upon emergence from the VDA during EHT at the onset of the definitve wave (figure 1). The difference between *ptpn11a* and *ptpn11b* in early stages of hematopoiesis remains to be determined. Perhaps there is a subtle difference in function of Shp2a and Shp2b. Alternatively, the difference in expression pattern of *ptpn11a* and *ptpn11b* [24] may be responsible for the difference in consequences of knock-out of *ptpn11a* and *ptpn11b*. *Ptpn11a* is abundantly expressed at all developmental stages, whereas *ptpn11b* expression levels are low early on, and increase to the same level as *ptpn11a* at 5 dpf.

Apoptosis of zebrafish HSPCs has been reported before. *Grechetto* mutants harbor an inactivating mutation in the *cleavage and polyadenylation specificity factor 1 (cpsf1)* gene and display defects in maintenance of HSPCs later in development. Appropriate numbers of HSPCs are specified initially, but their numbers are decreasing in the CHT due to apoptosis [28]. The defects in definitive hematopoiesis in *grechetto* mutants occur later than in *ptpn11b*$^{-/-}$ mutants, and are likely caused by different mechanisms. *Runx1* expression is required in the endothelial cell to achieve EHT [29]. Consistently, Runx1 knockdown in zebrafish embryos results in abortive EHT events, in that endothelial cells contract and initiate EHT, but then disintegrate [7]. As very few HSPCs escape this fate and the CHT is not seeded [7], as opposed to in the *ptpn11b*$^{-/-}$ mutant embryo, it is likely that the mechanisms underlying these EHT defects are distinct. Recently we have shown that *ptena*$^{-/-}$*ptenb*$^{-/-}$ mutant embryos show disintegrating HSPCs after emergence from the VDA, which is caused by hyperactivation of the PI3K-pathway [30]. The involvement of the PI3K pathway is complex, because inhibition of PI3K in wild type zebrafish embryos also results in disintegration of part of the HSPCs upon emergence from the VDA. It has been shown that SHP2 is required for PI3K activation upon EGF binding/activation [31,32] and other receptor tyrosine kinases [33–35]. It has also been reported that Shp2 acts upstream of Akt/PKB signaling [36,37]. However, in *Ptpn11a*$^{-/-}$ and *ptpn11b*$^{-/-}$ zebrafish mutants Akt-activation was not affected [24]. Therefore, it is likely that the mechanism underlying the EHT defects in

ptena$^{-/-}$*ptenb*$^{-/-}$ mutants is distinct from the defects in *ptpn11b*$^{-/-}$ embryos.

After emerging from the VDA, the surviving HSPCs enter circulation and seed the CHT. Approximately 20% less HSPCs colonized the CHT at 48 hpf and the number of HSPCs in the CHT at 4 dpf was also approximately 20% less in *ptpn11b*$^{-/-}$ mutant embryos, compared to *ptpn11b*$^{+/+}$ embryos (figure 2). We observed a trend that *ptpn11b*$^{+/-}$ mutant embryos had fewer HSPCs in the CHT than *ptpn11b* wild type embryos, but more than *ptpn11b*$^{-/-}$ mutant embryos. These differences were not signficant and it remains to be determined definitively whether there is a *ptpn11b* dose-dependent effect in the number of HSPCS in the CHT.

Surviving HSPCs from *ptpn11b*$^{-/-}$ mutants engage in all blood lineages and expression levels of markers are similar between mutants and their siblings (figure 3 and 4). This is in contrast with studies in other species. In an *in vitro* hematopoietic differentiation assay, homozygous *Shp2* mutant embryonic stem (ES) cells exhibited severely decreased differentiation capacity to erythroid and myeloid progenitors [38]. This *in vitro* result was supported by *in vivo* chimeric animal analyses, in which neither erythroid nor myeloid progenitor cells of *Shp2* mutant origin were detected in the fetal liver or bone marrow of chimeric animals that were derived from mutant ES cells and wild-type embryos [39]. Moreover, development of lymphoid lineages was blocked in *Shp2*$^{-/-}$ chimeric mice [40]. An explanation for this discrepancy may be that zebrafish have 2 *ptpn11* genes, *ptpn11a* and *ptpn11b*, that are differentially expressed as discussed above. It is interesting to note that previously it was thought that *ptpn11b* did not play a role during early embryonic development due to its low expression [24]. Here, we show that *ptpn11b*$^{-/-}$ mutants do show developmental defects early on in the definitive wave of hematopoiesis, but overcome these defects at the end of the definitive wave.

In conclusion, we characterized mutant zebrafish embryos lacking functional Shp2 during the definitive wave of hematopoiesis. We found that *ptpn11b*, but not *ptpn11a*, is required for normal emergence of HSPCs from the VDA. Despite that *ptpn11b*$^{-/-}$ mutants have fewer numbers of HSPCs, they do not seem to be affected by this and are fertile and viable.

Methods

Ethics statement

All animal experiments described in this manuscript were approved by the local animal experiments committee (Hubrecht Institute: Koninklijke Nederlandse Academie van Wetenschappen-Dierexperimenten commissie) and performed according to local guidelines and policies in compliance with national and European law.

Zebrafish husbandry

Ptpn11a$^{-/-}$, *ptpn11b*$^{-/-}$ [24],*Tg(kdrl:eGFP)*[41] and *Tg(cd41:eGFP)*[25] were maintained according to FELASA guidelines, crossed, raised and staged as described[42–44]. *Ptpn11* mutant fish (embryos) were genotyped by sequencing[24]. From 24hpf onwards, all embryos were grown in phenylthiourea (PTU)-containing medium at a concentration of 0.003% (v/v) to block pigmentation.

Constructs, mRNA synthesis and microinjections

Ptpn11 was cloned previously [45]. P*tpn11b* was cloned in the vector pCS2+ using Gibson Assembly and linearized with NotI. To synthesize 5'capped sense mRNA, the mMessage mMachine SP6 kit (Ambion) was used. mRNA injections were performed at the one-cell stage using a total of 120 pg of mRNA.

Confocal, fluorescence and time-lapse imaging

Fluorescence images of transgenic embryos were acquired using Leica SP8 using a 40x objective and 2µm z-stack stepsize and time-lapse-imaging using Leica SPE, SPE Live and SP5 with a 20x objective and 2µm z-stack stepsize as described [7,30]. The number of CD41-GFP^{low} cells was determined by imaging the CHT of living 48hpf or 4dpf *ptpnb*$^{+/+}$, *ptpnb*$^{+/-}$ or *ptpnb*$^{-/-}$ old embryos in the *tg(CD41:eGFP)* background. Imaris (Bitplane) was used to reconstruct 3D images and count individual GFP^{low} cells. For all live imaging, embryos were anesthetized with tricaine[42], mounted on a glass cover dish with 0.7% low melting agarose and covered with standard E3 medium.

In situ hybridization

Whole mount *in situ* hybridization was performed according to standard protocol [46] and images were taken using a Leica M165 FC stereomicroscope. Probes specific for *c-myb*, *l-plastin, pu.1*, *gata1*, *ikaros* and *b-globin* were described in [47,48].

Statistical analysis

Data was plotted in Graphpad Prism 9.01. Statistical difference analysis was performed using Fisher's Exact test with multiple testing correction (FDR) (figure 1) and Shapiro-Wilk

test to test for Gaussian distribution and One-Way ANOVA supplemented by Tukey's HSD test (figure2). Significant difference was considered when $p<0.05$ ($p<0.05$= *, $p<0.01$ = **, $p<0.001$= ***).

Acknowledgements

Authors would like to thank Mark Reijnen and animal care takers for excellent management fo the fish facility. Microscopy was done in the Hubrecht Imaging Centre.

Authorship

S.B.F. and J.d.H. designed experiments. S.B.F. and L.v.Z. performed the experiments and analysed the data. S.B.F. and J.d.H. wrote the manuscript. J.d.H. supervised the work.

References

1. Kondo, M. *et al.* Biology of Hematopoietic stem cells and progenitors: implication for clinical application. *Annu. Rev. Immunol.* **21**, 759–806 (2003).
2. Orkin, S. H. & Zon, L. I. Hematopoiesis: An Evolving Paradigm for Stem Cell Biology. *Cell* **132**, 631–644 (2008).
3. Stachura, D. L. *et al.* Clonal analysis of hematopoietic progenitor cells in the zebrafish. *Blood* **118**, 1274–1282 (2011).
4. Galloway, J. L., Wingert, R. A., Thisse, C., Thisse, B. & Zon, L. I. Loss of Gata1 but not Gata2 converts erythropoiesis to myelopoiesis in zebrafish embryos. *Dev. Cell* **8**, 109–116 (2005).
5. Bertrand, J. Y. *et al.* Haematopoietic stem cells derive directly from aortic endothelium during development. *Nature* **464**, 108–111 (2010).
6. Boisset, J. C. *et al.* In vivo imaging of haematopoietic cells emerging from the mouse aortic endothelium. *Nature* **464**, 116–120 (2010).
7. Kissa, K. & Herbomel, P. Blood stem cells emerge from aortic endothelium by a novel type of cell transition. *Nature* **464**, 112–115 (2010).
8. Godin, I. & Cumano, A. The hare and the tortoise: An embryonic haematopoietic race. *Nat. Rev. Immunol.* **2**, 593–604 (2002).
9. Murayama, E. *et al.* Tracing Hematopoietic Precursor Migration to Successive Hematopoietic Organs during Zebrafish Development. *Immunity* **25**, 963–975 (2006).
10. Dance, M., Montagner, A., Salles, J. P., Yart, A. & Raynal, P. The molecular functions of Shp2 in the Ras/Mitogen-activated protein kinase (ERK1/2) pathway. *Cell. Signal.* **20**, 453–459 (2008).
11. Feng, G. S. Shp-2 tyrosine phosphatase: Signaling one cell or many. *Exp. Cell Res.* **253**, 47–54 (1999).
12. Neel, B. G., Gu, H. & Pao, L. The 'Shp'ing news: SH2 domain-containing tyrosine phosphatases in cell signaling. *Trends Biochem. Sci.* **28**, 284–293 (2003).
13. Liu, X. & Qu, C.-K. Protein Tyrosine Phosphatase SHP-2 (PTPN11) in Hematopoiesis and Leukemogenesis . *J. Signal Transduct.* **2011**, 1–8 (2011).
14. Nabinger, S. C. & Chan, R. J. Shp2 function in hematopoietic stem cell biology and leukemogenesis. *Curr. Opin. Hematol.* **19**, 273–279 (2012).
15. Schubbert, S. *et al.* Functional analysis of leukemia-associated PTPN11 mutations in primary hematopoietic cells. *Blood* **106**, 311–317 (2005).
16. Mohi, M. G. *et al.* Prognostic, therapeutic, and mechanistic implications of a mouse model of leukemia evoked by Shp2 (PTPN11) mutations. *Cancer Cell* **7**, 179–191 (2005).
17. Chan, R. J. *et al.* Human somatic PTPN11 mutations induce hematopoietic-cell hypersensitivity to granulocyte-macrophage colony-stimulating factor. *Blood* **105**, 3737–3742 (2005).
18. Chan, R. J., Johnson, S. A., Li, Y., Yoder, M. C. & Feng, G. A definitive role of Shp-2 tyrosine phosphatase in mediating embryonic stem cell differentiation and hematopoiesis. *Blood* **102**, 2074–2080 (2003).
19. Chan, R. J. & Feng, G. S. PTPN11 is the first identified proto-oncogene that encodes a tyrosine phosphatase. *Blood* **109**, 862–867 (2007).
20. Zhu, H. H. *et al.* Kit-Shp2-Kit signaling acts to maintain a functional hematopoietic stem and progenitor cell pool. *Blood* **117**, 5350–5361 (2011).
21. Chan, G. *et al.* Essential role for Ptpn11 in survival of hematopoietic stem and progenitor cells. *Blood* **117**, 4253–4261 (2011).
22. Lieschke, G. J. & Currie, P. D. Animal models of human disease: zebrafish swim into view. *Nat. Rev. Genet.* **8**, 353–367 (2007).
23. van Eekelen, M., Overvoorde, J., van Rooijen, C. & den Hertog, J. Identification and expression of the family of classical protein-tyrosine phosphatases in zebrafish. *PLoS One* **5**, 1–16 (2010).
24. Bonetti, M. *et al.* Distinct and overlapping functions of ptpn11 genes in zebrafish development. *PLoS One* **9**, (2014).
25. Lin, H. F. *et al.* Analysis of thrombocyte development in CD41-GFP transgenic zebrafish. *Blood* **106**, 3803–3810 (2005).
26. Bertrand, J. Y. *et al.* Characterization of purified intraembryonic hematopoietic stem cells as a tool to define their site of origin. *Proc. Natl. Acad. Sci. U. S. A.* **102**, 134–139 (2005).
27. Gering, M. & Patient, R. Hedgehog signaling is required for adult blood stem cell formation in zebrafish embryos. *Dev. Cell* **8**, 389–400 (2005).
28. Bolli, N. *et al.* Cpsf1 is required for definitive HSC survival in zebrafish. *Blood* **117**, 3996–4007 (2011).
29. Chen, M. J., Yokomizo, T., Zeigler, B. M., Dzierzak, E. & Speck, N. A. Runx1 is required for the endothelial to haematopoietic cell transition but not thereafter. *Nature* **457**, 887–891 (2009).
30. Blokzijl-Franke, S. *et al.* Phosphatidylinositol-3 kinase signaling controls survival and stemness of hematopoietic stem and progenitor cells. *Oncogene* **40**, 2741–2755 (2021).
31. Zhang, S. Q. *et al.* Receptor-Specific Regulation of Phosphatidylinositol 3'-Kinase Activation by the Protein Tyrosine Phosphatase Shp *Mol. Cell. Biol.* **22**, 4062–4072 (2002).
32. Wang, L. *et al.* A ERK/RSK-mediated negative feedback loop regulates M-CSF-evoked PI3K/AKT activation in

macrophages. *FASEB J.* **32**, 875–887 (2018).
33. Schaeper, U. *et al.* Distinct requirements for Gab1 in Met and EGF receptor signaling in vivo. *Proc. Natl. Acad. Sci. U. S. A.* **104**, 15376–15381 (2007).
34. Agazie, Y. M. & Hayman, M. J. Molecular Mechanism for a Role of SHP2 in Epidermal Growth Factor Receptor Signaling. *Mol. Cell. Biol.* **23**, 7875–7886 (2003).
35. Wu, C. J. *et al.* The tyrosine phosphatase SHP-2 is required for mediating phosphatidylinositol 3-Kinase/Akt activation by growth factors. *Oncogene* **20**, 6018–6025 (2001).
36. Edouard, T. *et al.* Functional Effects of PTPN11 (SHP2) Mutations Causing LEOPARD Syndrome on Epidermal Growth Factor-Induced Phosphoinositide 3-Kinase/AKT/Glycogen Synthase Kinase 3β Signaling. *Mol. Cell. Biol.* **30**, 2498–2507 (2010).
37. Kontaridis, M. I., Swanson, K. D., David, F. S., Barford, D. & Neel, B. G. PTPN11 (Shp2) mutations in LEOPARD syndrome have dominant negative, not activating, effects. *J. Biol. Chem.* **281**, 6785–6792 (2006).
38. Qu, C. K. *et al.* A deletion mutation in the SH2-N domain of Shp-2 severely suppresses hematopoietic cell development. *Mol. Cell. Biol.* **17**, 5499–5507 (1997).
39. Qu, C.-K. *et al.* Biased Suppression of Hematopoiesis and Multiple Developmental Defects in Chimeric Mice Containing Shp-2 Mutant Cells. *Mol. Cell. Biol.* **18**, 6075–6082 (1998).
40. Qu, C.-K., Nguyen, S., Chen, J. & Feng, G.-S. Requirement of Shp-2 tyrosine phosphatase in lymphoid and hematopoietic cell development. *Blood* **97**, 911–914 (2001).
41. Jin, S.-W., Beis, D., Mitchell, T., Chen, J.-N. & Stainier, D. Y. R. Cellular and molecular analyses of vascular tube and lumen formation in zebrafish. *Development* **132**, 5199–209 (2005).
42. Westerfield, M. The zebrafish book. A guide for the laboratory use of zebrafish (Danio rerio). 4th ed. *Univ. Oregon Press. Eugene* (2000).
43. Kimmel, C. B., Ballard, W. W., Kimmel, S. R., Ullmann, B. & Schilling, T. F. Stages of embryonic development of the zebrafish. *Dev Dyn* **203**, 253–310 (1995).
44. Aleström, P. *et al.* Zebrafish: Housing and husbandry recommendations. *Lab. Anim.* **0**, 1–12 (2019).
45. Jopling, C., van Geemen, D. & den Hertog, J. Shp2 Knockdown and Noonan/LEOPARD Mutant Shp2–Induced Gastrulation Defects. *PLoS Genet.* **3**, e225 (2007).
46. Thisse, C. & Thisse, B. High-resolution in situ hybridization to whole-mount zebrafish embryos. *Nat. Protoc.* **3**, 59–69 (2008).
47. Choorapoikayil, S., Kers, R., Herbomel, P., Kissa, K. & Den Hertog, J. Pivotal role of Pten in the balance between proliferation and differentiation of hematopoietic stem cells in zebrafish. *Blood* **123**, 184–190 (2014).
48. Hu, B. *et al.* Zebrafish eaf1 suppresses foxo3b expression to modulate transcriptional activity of gata1 and spi1 in primitive hematopoiesis. *Dev. Biol.* **388**, 81–93 (2014).

table S1. The number of embryos showing disintegrating HSPCs after EHT in the AGM was determined in all ptpn11b genotypes by confocal time lapse imaging.

ptpn11	a+/+b+/+	a+/-b+/+	a-/-b+/+	a+/+b+/-	a+/-b+/-	a-/-b+/-	a+/+b-/-	a+/-b-/-	a-/-b-/-
total	6	12	3	4	9	5	18	22	10
normal EHT	6	9	3	3	9	5	4	5	2
disintegrating EHT event	0	3	0	1	0	0	14	17	8

Chapter 5

Loss of *kdrl* Marks the Shift From Embryonic to Adult HSPCs

Blokzijl-Franke S, Solman S and den Hertog J

Abstract

Hematopoietic stem/progenitor cells (HSPCs) are multipotent cells giving rise to all blood cells during life. Hematopoiesis occurs in two waves in all vertebrates during embryonic development. During the second wave, HSPCs are generated that produce all blood lineages during the rest of the organism's life. Using a combination of an endothelial expression marker (kdrl) and a HSPC marker (cd41) in zebrafish embryos, we isolated a subpopulation of cd41^{low} HSPCs, which expressed kdrl. Using scRNA sequencing, we found that this subpopulation has a distinct differentiation fate compared to cd41^{low} HSPCs. Live imaging of both kdrl/cd41^{low} and cd41^{low} HSPCs showed that both HSPCs existed at the same time in the caudal hematopoietic tissue (CHT) in zebrafish. In an *in vitro* colony forming unit (CFU) assay, we observed that particularly the embryonic kdrl/cd41^{low} HSPCs formed colonies. Surprisingly, kdrl/cd41^{low} cells were also observed in adult whole kidney marrow (WKM). In adults, predominantly cd41^{low} cells lacking kdrl expression formed colonies. We conclude that the loss of kdrl marks a shift in potential of cd41^{low} HSPCs from embryos to adults.

Introduction

Hematopoietic stem/progenitor cells (HPSCs) are at the base of the hematopoietic system. They have the essential function of long-term maintenance and production of all mature blood cell lineages during the lifespan of an organism. During development they have the unique capacity for self-renewal and differentiation into multiple cell types at the same time [1,2]. In all vertebrates, two waves of hematopoiesis occur during embryonic development. First, a primitive wave, independent of HSPCs[3], in which primitive erythrocytes and myeloid cells are produced. The main function for the primitive wave is production of red blood cells that facilitate oxygenation, which is required because the embryo is growing quickly. This is followed by a definitive wave in which HSPCs are generated. Cells differentiate into separate blood lineages and colonize the adult hematopoietic organs. These processes take place in all vertebrates in a similar manner, although small differences have been observed between species.

In zebrafish, HSPCs emerge from the ventral wall of the dorsal aorta (VDA), then migrate to the caudal hematopoietic tissue (CHT) where they mature and then migrate to the thymus and whole kidney marrow (WKM). The definitive wave starts in zebrafish around 32 hours post fertilization (hpf) with the emergence of HSPCs from a subpopulation of endothelial cells in the VDA [4,5]. After emerging from the VDA, HSPCs migrate to the CHT[6], where they expand and mature over the course of approximately two days, resulting in an increase in HSPC numbers[7]. At around 4 dpf, HSPCs begin to seed the WKM, where they remain, self-renew, and differentiate to produce blood for the rest of the lifespan of the zebrafish [8].

Our understanding of early hematopoiesis in the zebrafish is mainly derived from *in vivo* live imaging. Unique properties of the zebrafish model organism facilitated pioneering imaging experiments due to the optical transparency during embryonic development. A variety of transgenic zebrafish lines have been generated, which mark specific cell populations through use of tissue-specific promoters driving expression of fluorescent proteins. HSPCs can be followed using transgenic lines expressing a fluorescent protein under HSPC-specific promotors, such as *c-myb*, *cd41* and *runx1* [9–12]. When combined with endothelial transgenic markers, such as *kdrl*, HSPCs can be imaged when they start to emerge from the VDA [4,5,13]. The past years we have gained an increasing understanding of how HSPCs are established and how they produce blood for a lifetime, but we are still far away from a complete understanding of how HSPCs are formed, how they are maintained and how they manage to produce blood of all lineages for the rest of the lifetime of the organism.

Here, we used single cell RNA sequencing to investigate RNA expression in cd41^{low} HSPCs and a kdrl-positive subpopulation during embryonic development. Furthermore, we used live imaging to investigate the fate of this subpopulation and an *in vitro* functional assay to show a shift in potential of cd41^{low} HSPCs between embryonic development and adulthood.

Results

Flow cytometry reveals the existence of both kdrl/cd41^{low} and cd41^{low} cells in the CHT of 5dpf old embryos.

The transgenic *tg(cd41:eGFP)* line is widely used to visualize developing HSPCs in the zebrafish embryo [5,14,15], as these embryos express low levels of GFP (cd41^{low}) in HSPCs [9,16]. These low levels of GFP are easily distinguished from the high levels of GFP (cd41^{high}) in thrombocytes in this transgenic line [9]. Often *tg(cd41:eGFP)* embryos are combined with an endothelial line *tg(kdrl:mCherry-CAAX)* to visualize nascent HSPCs derived from hemogenic endothelium. Intuitively, kdrl-positive cells are the origin of HSPCs, as the kdrl marker is carried over from the endothelial cells where they derived from. Cells from CHTs of 5 dpf old *tg(kdrl:mCherry-CAAX/cd41:eGFP)* embryos were subjected to FACS sorting, selecting for expression of both markers. We observed that there was not only a population of cd41^{low} HSCPs, as expected, but also a population of kdrl/cd41^{low} HSPCs (figure1). Cd41^{low} HSPCs were more abundant than kdrl/cd41^{low} HSPCs. Note that gating of the FACS was chosen such that cd41^{high} cells were not selected at all (figure 1).

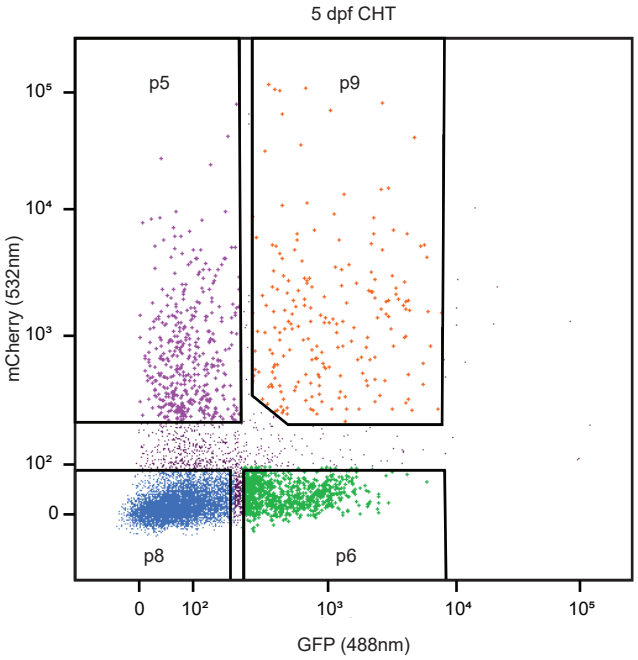

Figure 1. Flow cytometry reveals the existence of both kdrl/cd41^{low} and cd41^{low} in the CHTs of 5 dpf old *tg(kdrl:mCherry-CAAX/cd41:eGFP)* **embryos.** CHTs of wildtype embryos (5dpf, ~500) were sorted for kdrl/cd41^{low} expression, dissected, pooled, dissociated and submitted to FACS sorting. Final FACS gating for sorting after selecting only single, viable cells. P8= negative cells, p6=cd41^{low} cells, p5=kdrl cells, p9=kdrl/cd41^{low} cells.

scRNA seq reveals distinct differentiation fates of kdrl/cd41^{low} and cd41^{low} cells in the CHT of 5 dpf old embryos.

To investigate transcriptomic differences between kdrl/cd41^{low} and cd41^{low} HSPC populations, we sorted kdrl+/cd41^{low} and cd41^{low} cells from the CHTs of 5 dpf old embryos from the double transgenic *tg(kdrl:mCherry-CAAX/cd41:eGFP)* background. The CHTs of ~500 embryos were isolated by dissection at 5 dpf and then pooled. The cells were then dissociated and sorted for kdrl+/cd41^{low} or only cd41^{low} expression using FACS, after which the SORT-Seq protocol was performed [17]. Of the 747 cells in total, 527 cells remained after filtering. RaceID3 was used for differential gene expression analysis and clustering of the cells [18] (figure 2). The resulting t-SNE map highlighted particular cell types, in line with recent scRNA-seq studies of hematopoietic organs of zebrafish [19–25], which expressed validated hematopoietic lineage markers (table S1). Kdrl/cd41^{low} cells had an uneven distribution over cluster 1 and 2. In cluster 1, kdrl/cd41^{low} cells were overrepresented compared to cd41^{low} cells, whereas they were underrepresented in cluster 2. Cd41^{low} cells had the opposite uneven distribution (Fisher's exact test, $p<0.001$). Cells from cluster 3 were evenly distributed between kdrl/cd41^{low} and cd41^{low} cells ($p=0.11$) (figure 2 b,c). Cells in cluster 1 expressed myeloid progenitor-related genes, such as *runx3, pu.1* (also known as *spi1b*) and *cebpb* [26] (figure 2 d). Cluster 2 is characterized by cells expressing genes related to thrombocyte/erythrocyte progenitors (TEP) (*gata1a, klf1*[19,26]) (figure 2 f). Cells in cluster 3 express genes indicative of HSPCs, including *c-myb, pmp22b* and *her6,* consistent with expression in mammalian HSCs and zebrafish HSPCs [19,21,22,27] (figure 2 e). All markers that were used to identify clusters are listed in table S1 [28], the distribution of expression of selected markers is depicted in t-SNE maps or using violin plots (figure 2d-i) and upregulated genes per cluster (in descending order, with fold change >1 and $p<0.01$) is listed in table S2. These data indicate that kdrl/cd41^{low} cells might have the tendency to differentiate slightly more towards common myeloid progenitors, whereas cd41^{low} cells might have a more thrombocyte/erythrocyte progenitor cell fate. Despite the apparent difference in cell fates between kdrl/cd41^{low} cells and cd41^{low} cells, the HSPC cluster did not show a significant difference based on these two markers, suggesting that both cell types have similar capacities to produce HSPCs.

Imaging of Kdrl/cd41^{low} and cd41^{low} cells in the CHT

To verify the FACS results that the CHT contains both kdrl/cd41^{low} and cd41^{low} HSPC populations, the CHTs of 48 hpf and 5 dpf old wild type zebrafish embryos in the *tg(kdrl:mCherry-CAAX/cd41:eGFP)* background were imaged. At both timepoints kdrl/cd41^{low} and cd41^{low} positive cells were present in the CHT (figure 3 a,b). Our scRNA-seq data indicated that the cell fates of kdrl/cd41^{low} and cd41^{low} cells were distinct. Kdrl/cd41^{low} positive HSPCs were more myeloid progenitor oriented and cd41^{low} positive HSPCs more thrombocyte/erythrocyte progenitor oriented. Next, we used the double transgenic *tg(gata:dsRED/kdrl:eGFP)* line, marking erythrocytes (*gata*) and endothelial cells (*kdrl*). The more myeloid fate of kdrl/cd41^{low} cells would suggest that in *tg(gata:dsRED/kdrl:eGFP)* embryos we would not expect any double positive cells. As expected, we observed no gata/kdrl positive cells in the CHT of 5 dpf old embryos (figure 3 c). In double transgenic *tg(gata:dsRED/cd41:eGFP)* embryos, we expected gata/cd41^{low} positive cells, because cd41^{low} positive cells had a more thrombocyte/erythrocyte progenitor fate. Indeed, we

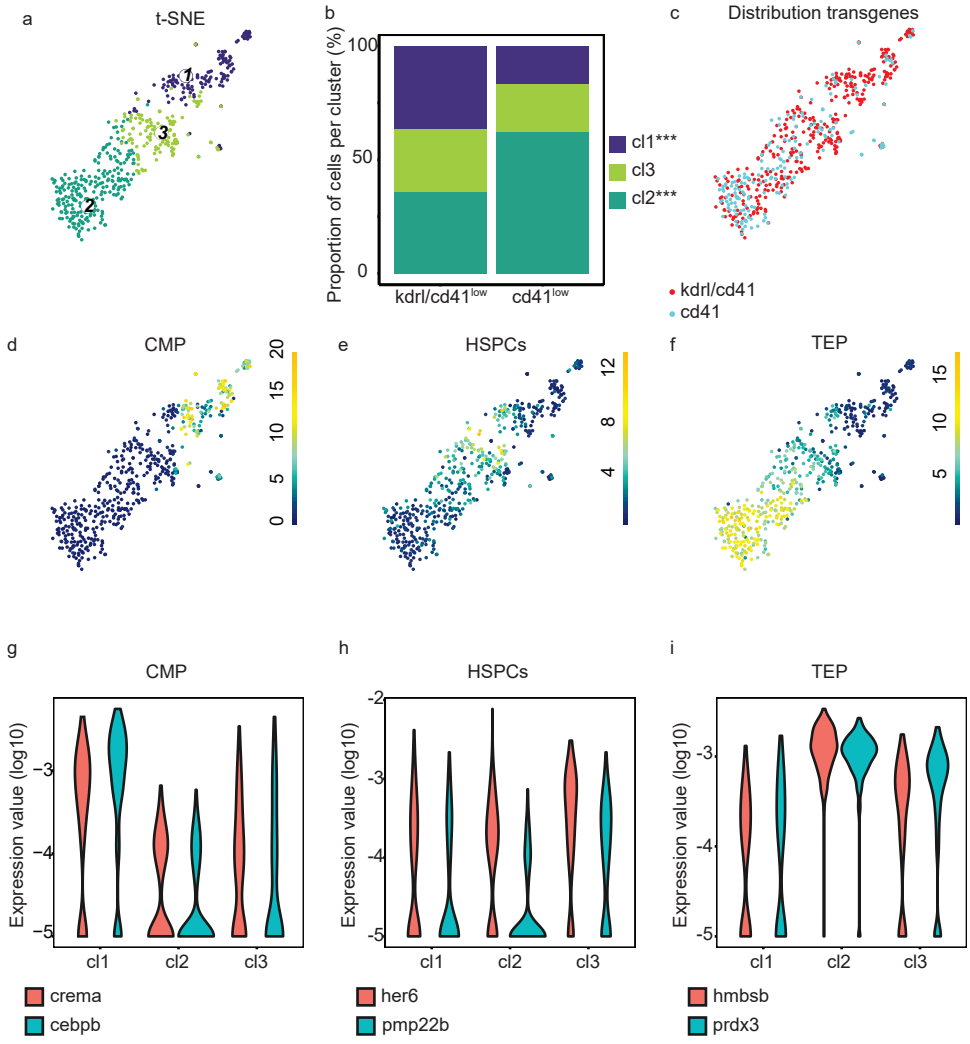

Figure 2. scRNA seq reveals CMP and TEP fates, respectively in kdrl/cd41^{low} and cd41^{low} HSPCs. CHTs of wildtype embryos (5dpf, ~500) were dissected, pooled, dissociated, FACS sorted and submitted to SORT-seq. (a) Visualization of k-medoid clustering and cell-to-cell distances using t-SNEs. Each dot represents a single cell. Colors and numbers indicate cluster and correspond to colors in b. In total 527 cells are shown. (b) The percentage of kdrl/cd41^{low} or cd41^{low} cells from the different clusters. Fisher's exact test with multiple testing correction (Fdr) were used for statistical analysis ***p<0.001. (c) t-SNE map highlighting the distribution of kdrl/cd41^{low} or cd41^{low} cells. (d-f) t-SNEs maps highlighting the expression of marker genes for each of the different cell types found. Transcript counts are given in a linear scale. (g-i) Normalized expression of signature genes for cluster identities using violin plots. Normalized expression value is plotted on a log10 scale. Common myeloid progenitors (CMP), hematopoietic stem/progenitor cell (HSPCs), Thrombocyte/erythrocyte progenitors (TEP).

found gata/cd41^{low} positive cells in the CHT of 5 dpf old embryos (figure 3 d). This further strengthens the finding that two populations of HSPCs might be distinguished based on the kdrl and cd41 markers, with one being oriented towards the myeloid progenitor fate, whilst the other is more oriented towards a thrombocyte/erythrocyte progenitor fate.

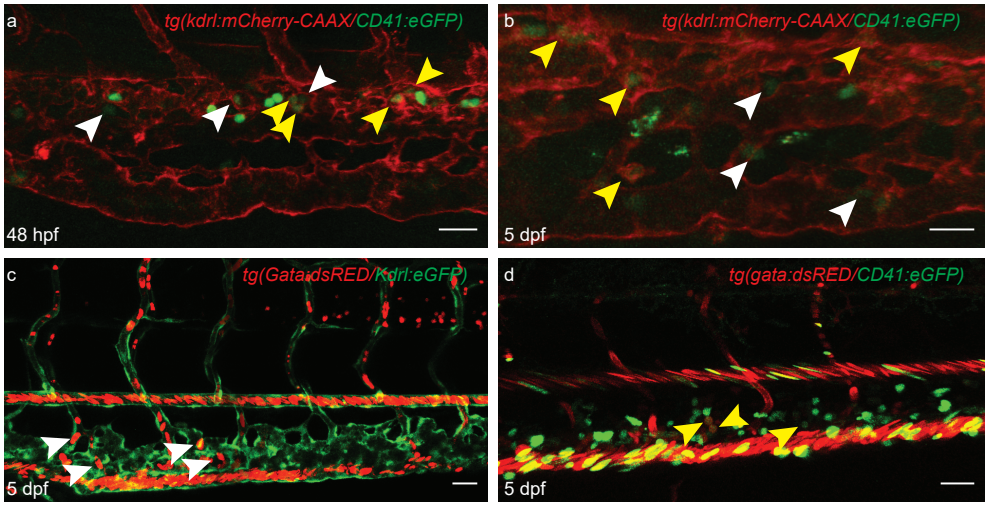

Figure 3. Live imaging of embryos with various transgenic backgrounds. (a,b) CHTs of *tg(kdrl:mCherry-CAAX/cd41:eGFP)* 48 hpf (a) or 5 dpf (b) old embryos. The vasculature is highlighted in red (mCherry) and GFP^{low} HSPCs are highlighted in green. (c) CHTs of *tg(gata:dsRED/Kdrl:eGFP)* of 5 dpf old embryos. Vasculature is highlighted in green (GFP) and blood cells are highlighted in red (dsRED). (d) CHTs of *tg(gata:dsRED/CD41:eGFP)*. Blood cells are highlighted in red (dsRED) and GFP^{low} HSPCs are highlighted in green. Yellow arrowheads indicate double positive cells, white arrowheads indicate single positive cells. Scale bar is 30 µm.

5

In vitro kdrl/cd41^{low} cells, but not cd41^{low} cells from 5dpf old CHTs differentiated into different lineages

To further investigate functional differences between kdrl/cd41^{low} and cd41^{low} HSPCs, we used an *in vitro* clonal differentiation assay, the colony forming unit assay (CFU-assay). Cells from the CHT of 5 dpf old embryos in the *tg(kdrl:mCherry-CAAX/cd41:eGFP)* background were first selected for expression of the two markers, then dissected, dissociated and sorted for kdrl/cd41^{low}, cd41^{low}, kdrl-positive and negative expression (figure 1). Cells were then plated in a semi-solid medium and cultured for several days in the presence of growth factors specific for either an erythroid or myeloid lineage [29]. We noticed that kdrl/cd41^{low} HPSCs from the CHTs of 5 dpf old embryos gave rise to significantly more colonies in both the erythroid lineage as well as the myeloid lineage compared to kdrl-positive, cd41^{low} and negative cells ($p<0.05$) (figure 4 a-d). Moreover, cd41^{low} cells gave rise to significantly more colonies compared to negative cells in both conditions ($p<0.05$) (figure 4 c, d). However only when differentiated to a myeloid fate the number of colonies from cd41^{low} cells was significantly different from kdrl-positive cells ($p<0.01$) (figure 4 d). In both conditions, kdrl-positive cells gave rise to a similar number of colonies as negative cells (p=ns) (figure 4 c,

d). All comparisons are listed in table S3. These data suggest that at 5 dpf kdrl/cd41^{low} cells are the main population of cells with the ability to give rise to colonies. Cd41^{low} cells do have the ability to give rise to some colonies, but to a significantly lesser extent than the kdrl/cd41^{low} double positive cells.

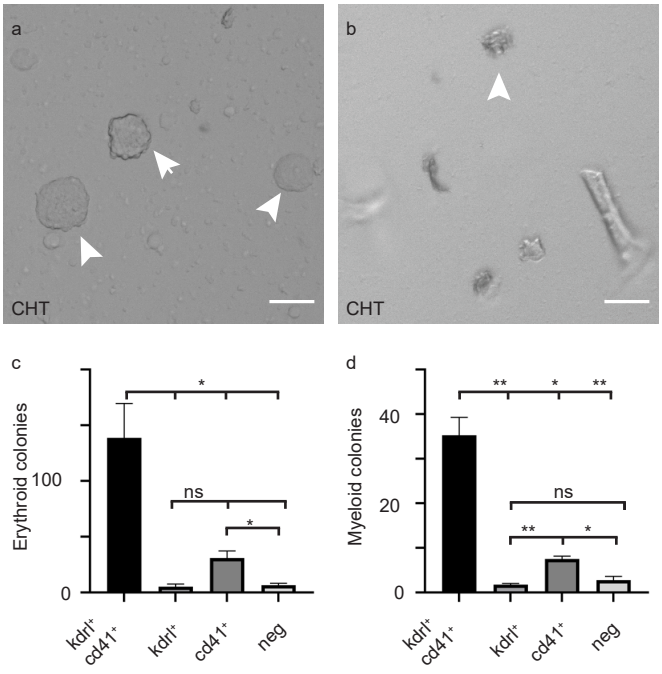

Figure 4. kdrl/cd41^{low} cells are the main HSPCs population with the ability to differentiate into different lineages at 5 dpf. (a,b) Representative images of colonies grown in methylcellulose for 2 or 5 days in the presence of Epo for an erythroid lineage (a), or Gcsfa and Gcsfb for myeloid lineages (b). Colonies developed from kdrl/cd41^{low} or cd41^{low} cells from the CHT at 5dpf from embryos in the *tg(kdrl:mCherry-CAAX/cd41:eGFP)* background. (c,d) Quantification of colony numbers from 2 different experiments from kdrl/cd41^{low} or cd41^{low} cells from CHTs of 5dpf old embryos. Scale bar is 50µm. White arrowheads indicate colonies. Error bars represent standard error of the mean (SEM). Ns non-significant, *p<0.05, **p<0.01, ***p<0.001, one-way ANOVA complemented by Tukey HSD test. For all comparisons see table S1.

Kdrl/cd41^{low} and cd41^{low} HSPCs exist in adult WKM, with cd41^{low} HSPCs having the ability to differentiate into different lineages

Next, we wondered whether kdrl was still a marker for adult HSPCs and whether kdrl and cd41 together mark HSPCs in the adult WKM. To investigate this, we used FACS to isolate kdrl/cd41^{low} and cd41^{low} cells from adult whole kidney marrow (WKM), the site of adult hematopoiesis [8] from *tg(kdrl:mCherry-CAAX/cd41:eGFP)* fish. Double positive kdrl/cd41^{low} cells were indeed isolated, indicating that in the adult blood producing organ, these cells persist, although in much fewer numbers than cd41^{low} HSPCs (figure 5 a). To investigate

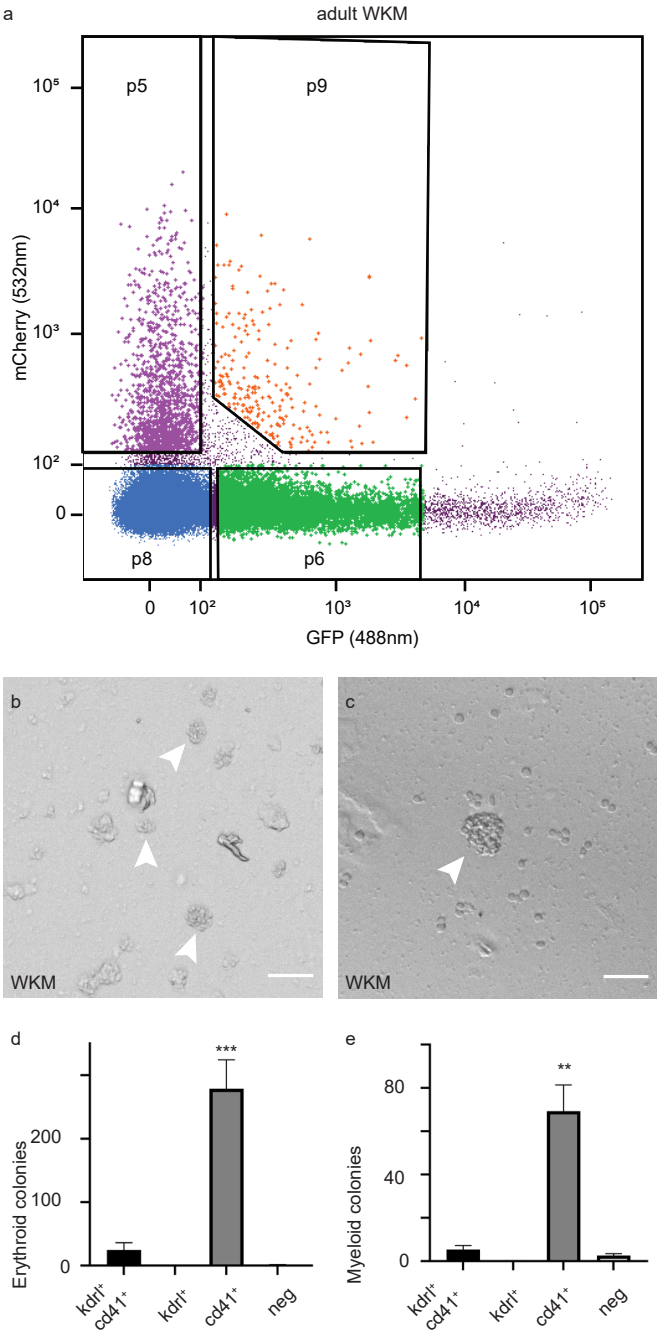

Figure 5. Cd41^{low} cells are the main population of HSPCs from adult WKM with the ability to differentiate into distinct lineages. (a) Flow cytometry of *tg(kdrl:mCherry-CAAX/ cd41:eGFP)* adult WKM zebrafish reveals the existence of both kdrl/cd41^{low} and cd41^{low} cells. Adult WKMs were dissected and submitted to FACS sorting. Final FACS gating for sorting after selecting only single, viable cells. P8= negative cells, p6=cd41^{low} cells, p5=kdrl cells, p9=kdrl/ cd41^{low} cells. (b,c) Representative images of colonies grown in methylcellulose for 2 or 5 days in the presence of Epo for erythroid lineage (b), or Gcsfa and Gcsfb for myeloid lineages (c). Colonies developed from kdrl/cd41^{low} or cd41^{low} cells from the WKM from adult zebrafish in the *tg(Kdrl:mCherry-CAAX/ cd41:eGFP)* background.(d,e) Quantification of colony numbers from 3 different experiments from kdrl/cd41^{low} or cd41^{low} cells from WKM tissue from adult zebrafish. Scale bar is 50µm. White arrowheads indicate colonies. Error bars represent standard error of the mean (SEM). Ns non-significant, *p<0.05, **p<0.01, ***p<0.001, one-way ANOVA complemented by Tukey HSD test. For all comparisons see table S1.

whether the kdrl/cd41^{low} and cd41^{low} cells were functional HSPCs, we performed CFU-assays in a similar manner as described above for 5 dpf embryos, but used adult WKM tissue as source of HSPCs. Surprisingly, only cd41^{low} cells gave rise to significant colony formation of both the erythroid and myeloid lineages (figure 5 b-d).

Double positive kdrl/cd41^{low} cells, single positive kdrl cells and negative cells did not lead to significant colony formation (figure 5 b-d). All comparisons are listed in table S3. These results indicate that in adult zebrafish, cd41^{low} cells represent the only population that has the capacity to give rise to colonies. This suggests that a shift takes place from the embryonic phase to the adult phase. First, double positive kdrl/cd41^{low} HSPCs form the main population of HSPCs that are able to differentiate into different lineages, and later, during adulthood, single positive cd41^{low} HSPCs take on this role.

Discussion

We used zebrafish in a *tg(kdrl:mCherry-CAAX/cd41:eGFP)* background to isolate cd41^{low} HSPCs from the CHTs of 5 dpf old embryos. Surprisingly, we also found kdrl/cd41^{low} HSPCs in the CHT of 5 dpf old embryos (figure 1). This is interesting, as only cd41^{low} is normally used to mark HSPCs at this stage [6,14,30]. Using scRNA sequencing we characterized transcriptional differences between kdrl/cd41^{low} and cd41^{low} HSPCs in 5 dpf old embryos. Kdrl/cd41^{low} and cd41^{low} HSPCs did not show distinct differences at their most stem cell like state, but, unexpectedly, showed distinct differentiation capabilities in our scRNA sequence dataset. It seems that kdrl/cd41^{low} HSPCs have a more myeloid progenitor fate, whereas cd41^{low} HSPCs have a more thrombocyte/erythrocyte progenitor fate (figure 2). Functional analyses using CFU assays indicated that kdrl/cd41^{low} cells and to a much lesser extent cd41^{low} cells give rise to colonies. Surprisingly, colonies formed to a similar extent under conditions that favor myeloid cells as that favor erythroid cells, despite the apparent difference in cell fate observed by scRNAseq (cf. figure 2 and 4). The discrepancy with our scRNA sequencing data might be due to the sensitivity of the *in vitro* assay, in that the results of the scRNA sequencing data might be too subtle to pick up. Another explanation is that the potential to differentiate in either direction is present in kdrl/cd41^{low} cells and exogenous factors in the CFU assay drive colony formation under both conditions. *In vivo,* lower concentrations of these factors or other factors may be involved in determining the fate of HSPCs [7,31,32].

In adults, we also observed both kdrl/cd41^{low} and cd41^{low} cells, albeit the proportion of kdrl/cd41^{low} was greatly reduced. The CFU assay using adult kdrl/cd41^{low} and cd41^{low} cells showed that predominantly the cd41^{low} cells formed colonies. Again, colonies formed under conditions that favor either myeloid or erythroid cells (figure 5). It has been shown before in adult hematopoietic tissue that cd41 is not only expressed in HSPCs (cd41^{low}) and thrombocytes (cd41^{high}), but also in erythroid and myeloid lineages, in both zebrafish and mice [9,15,33,34]. This might explain why cd41^{low} cells gave rise to multiple lineages. Our results suggest that kdrl/cd41^{low} cells represent colony forming stem cells in embryos, whereas cd41^{low} cells that do not express kdrl have this capacity in adults.

As cd41 is expressed in both myeloid and erythroid lineages, it is possible that we captured these cells and that another mechanism is responsible for the different lineages we find in our scRNA sequencing data. It has been shown in mice that the fate of common myeloid-erythroid progenitors to become either megakaryocyte/erythroid progenitors or myeloid progenitors is dependent on relative levels of GATA1 and PU.1 (reviewed in [35]). Overexpression of GATA1 leads to reprogramming of myeloid cells into erythroid and megakaryocytic differentiation [36], and overexpression of PU.1 represses erythropoiesis and promotes myeloid differentiation in erythroid lineages [37]. In zebrafish, loss of gata1 transforms primitive blood precursors into myeloid cells at the expense of erythrocytes [38], indicating a similar mechanism as in the previously described studies. Another study in mice suggests that within the HSC population (Lin-,Sca1+,cKit+, LSK), CD41 marks the earliest common myeloid progenitors, as opposed to the orginal common myeloid progenitor which resides outside of the LSK fraction, and inititiates the priming of both GATA1 and PU.1 transcription factors in early hematopoiesis [15]. It would be interesting to perform a differential gene expression comparison by scRNA seq between cd41^{low} cells and kdrl/cd41^{low} cells from adult WKM, which would allow us to compare the levels of *gata1* and *pu.1* and many other genes in our dataset.

Recently, scRNA sequencing has been widely used to study the process of HSPCs differentiation, using various transgenic zebrafish lines. Athanasiadis *et al.* used 8 different transgenic lines to capture the whole differentiation continuum in adult WKM tissue, which resulted in a differentiation lineage tree, based on transcriptional changes. Even though global transcriptional changes before and after the branching point are continuous, the probability of HSPCs transitioning to either erythroid, monocytic, neutrophilic or thromboid state is determined only by a subset of highly relevant genes [19]. Xue *et al.* showed that the lineage-restricted process that HSPCs undergo in the adult WKM also takes place in the CHT, based on subclustering of HSPCs into different lineage fates [25]. These results are consistent with our results, where we observed subtle differentiation states within the HSPCs population. We suggest that HSPCs that already tend towards a more myeloid fate might be distinguished by the *kdrl* marker in addition to cd41^{low} expression.

In the context of cd41^{low} HSPCs with and without kdrl, it would be interesting to speculate about long-term HSPCs and short-term HSPCs. Long term-HSCs are quiescent, whereas short-term HSCs proliferate more [1]. The kdrl/cd41^{low} HSPCs may represent the short-term HSPCs, as these HSPCs proliferate quickly in the CHT during embryonic development, after which they migrate to the adult hematopoietic organs. During adulthood, only the long-term cd41^{low} HSPCs survive and are responsible for the production of blood for the rest of the lifespan of the zebrafish. Future work should focus on analysis of cell proliferation of cd41^{low} and kdrl/cd41^{low} cells in adult WKM to verify the proliferative state of these two groups of cells. In addition, scRNA seq of cd41^{low} and kdrl/cd41^{low} cells from adult WKM may provide insight into differences of these two groups of cells and into differences with embryonic HSPCs. Investigating the regulatory mechanism underlying the two different cd41^{low} populations at different stages will further expand our knowledge about HSPCs and may provide insight into short- and long-term HSPCs. Eventually, these insights may contribute to development of efficient stem cell-based therapies [39,40].

Methods

Ethics statement

All animal experiments described in this manuscript were approved by the local animal experiments committee (Hubrecht Institute: Koninklijke Nederlandse Academie van Wetenschappen-Dierexperimenten commissie) and performed according to local guidelines and policies in compliance with national and European law.

Zebrafish husbandry

Tg(kdrl:eGFP)[41]*, tg(cd41:eGFP)*[9] and *gata1:dsRED*[8] were maintained according to FELASA guidelines, outcrossed, raised and staged as described [42–44]. When needed embryos were grown in phenylthiourea (PTU)-containing medium (0.003%, v/v) to block pigmentation.

Confocal microscopy

All confocal imaging was performed on a Leica SP8 confocal microscope (Leica Microsystems). Embryos were mounted in 0.7% low-melting agarose. Live embryos were anesthetized in MS-222. CHTs at 5dpf were imaged using a 40x objective and z-stack step size of 2 µm. AGMs at 36 hpf were imaged using a 20x objective and z-stack step size of 2µm. Imaris (Bitplane) was used to reconstruct 3D images.

Flow cytometry

Whole kidney marrows (WKMs) from adult zebrafish in the *tg(kdrl:mCherry-CAAX/cd41:eGFP)* background were dissected and collected in PBS supplemented with 5% FBS. The tissue was mechanically dissociated and filtered through a 70µm and 40µm filter. Cell pellet was resuspended in PBS supplemented with 5% FBS and 0.5µg/ml (DAPI) 4′6-diamidino-2-phenylindole. Cells with $kdrl^{+}$, $cd41^{low}$, $kdrl^{+}/cd41^{low}$ signal and negative cells were subjected to FACS using a BD FACS AriaII and BD FACS Fusion.

Embryos (5 dpf) in the *tg(kdrl:mCherry-CAAX/cd41:eGFP)* background were first sorted for expression of both kdrl and cd41 expression, then CHTs were dissected and collected in Leibovitz-medium (L15). After washing with PBS0, CHTs were deyolked with calcium-free Ringer's solution (116mM NaCl, 2.9mM KCl and 5 mM HEPES) and cells were dissiociated with TrypLE (Gibco) for 45 minutes at 32°C. The resulting cell suspension was washed with PBS0 and resuspended in PBS0 supplemented with 5% FBS and 0.5µg/ml DAPI and passed through a 40µm filter. DAPI staining was used to exclude dead cells. Cells with $kdrl^{+}/cd41^{low}$ and $kdrl^{-}/cd41^{low}$ signal were subjected to FACS using a BD FACS AriaII and BD FACS Fusion [28].

Colony Forming Unit assay

Cells from either WKM or 5dpf CHT were isolated by flow cytometry as described above. 900µl of solution containing 1000 cells in media, which was prepared as described [29], and 100 ng/ml granulocyte colony stimulation factor a and b (gcsfa, gcsfb) or erythropoietin (epo) (gift from the Petr Bartunek lab, Institute of Molecular Genetics, Academy of Sciences of the Czech Republic v.v.i Prague) was plated per well of a 24 well plate in duplicate. Cells were grown in humidified incubators at 32°C, 5% CO2. Colonies were imaged and enumerated using EVOS microscope (Thermo Fisher Scientific after 2 or 5 days for myeloid or erythoid lineages, respectively.

scRNA-seq with SORT-seq

Single cell RNA sequencing was performed by Single Cell Discoveries BV (Utrecht, The Netherlands), according to an adapted version of the SORT-seq protocol [17], with adapted primers described in [45]. In short, single cells were FACS sorted as described above, in 384-well plates containing 384 primers and Mineral oil (Sigma). After sorting, plates were snap-frozen on dry ice and stored at -80°C. For amplification cells were heat-lysed at 65°C followed by cDNA synthesis using the CEL-seq2 protocol[46] and robotic liquid handling platforms. After second strand cDNA synthesis, the barcoded material was pooled into libraries of 384 cells and amplified using IVT. Following amplification, the rest of the CEL-seq2 protocol was followed for preparation of the amplified cDNA library, using TruSeq small RNA primers (Illumina). The DNA library was paired-end sequenced on an Illumina NextseqTM 500, high output, with a 1x75bp Illumina kit (R1:26 cycles, index read 6 cycles, R2:60 cycles).

Data analysis of scRNA-seq

During sequencing, Read1 was assigned 26 base pairs and was used for identification of the Illumina library barcode, cell barcode and unique molecular identifier (UMI). Read2 was assigned 60 base pairs and used to map to the reference transcriptome of Zv9 *Danio rerio.* Data was demultiplexed as described in [47]. Single cell transcriptomics analysis was done using the RaceID3 algorithm, following an adapted version of the RaceID manual (https://cran.r-project.org/web/packages/RaceID/vignettes/RaceID.html) using R. In total 747 cells were sequenced for the datasets. After removing cells with less than 1500 UMIs and only keeping genes that were detected with at least 5 UMIs in 5 cells, 527 cells were left for further analysis. The number of initial clusters was set at 3 after careful consideration [28]. Differential gene expression analysis was done as described in [17] with an adapted version of the Deseq [48].

Data sharing

For original data, please contact j.denhertog@hubrecht.eu.

scRNA data are available at GEO under accession number GSE173100

Acknowledgments

Authors would like to thank Mark Reijnen and animal care takers for excellent management of the fish facility. Microscopy was done in the Hubrecht Imaging Centre. The authors are grateful to Petr Bartunek and his lab members for reagents for the Colony Forming Units assays.

Authorship

S.B.F. and M.S. designed experiments. S.B.F. performed experiments and analysed the data. S.B.F. and J.d.H. wrote the manuscript. J.d.H. supervised the work.

References

1. Orkin, S. H. & Zon, L. I. Hematopoiesis: An Evolving Paradigm for Stem Cell Biology. *Cell* **132**, 631–644 (2008).
2. Kondo, M. *et al.* Biology of Hematopoietic stem cells and progenitors: implication for clinical application. *Annu. Rev. Immunol.* **21**, 759–806 (2003).
3. Bertrand, J. Y. *et al.* Definitive hematopoiesis initiates through a committed erythromyeloid progenitor in the zebrafish embryo. *Development* **134**, 4147–4156 (2007).
4. Kissa, K. & Herbomel, P. Blood stem cells emerge from aortic endothelium by a novel type of cell transition. *Nature* **464**, 112–115 (2010).
5. Bertrand, J. Y. *et al.* Haematopoietic stem cells derive directly from aortic endothelium during development. *Nature* **464**, 108–111 (2010).
6. Murayama, E. *et al.* Tracing Hematopoietic Precursor Migration to Successive Hematopoietic Organs during Zebrafish Development. *Immunity* **25**, 963–975 (2006).
7. Xue, Y. *et al.* The Vascular Niche Regulates Hematopoietic Stem and Progenitor Cell Lodgment and Expansion via klf6a-ccl25b. *Dev. Cell* **42**, 349-3e4 (2017).
8. Traver, D. *et al.* Transplantation and in vivo imaging of multilineage engraftment in zebrafish bloodless mutants. *Nat. Immunol.* **4**, 1238–1246 (2003).
9. Lin, H. F. *et al.* Analysis of thrombocyte development in CD41-GFP transgenic zebrafish. *Blood* **106**, 3803–3810 (2005).
10. North, T. E. *et al.* Prostaglandin E2 regulates vertebrate haematopoietic stem cell homeostasis. *Nature* **447**, 1007–1011 (2007).
11. Anderson, H. *et al.* Hematopoietic stem cells develop in the absence of endothelial cadherin 5 expression. *Blood* **126**, 2811–2820 (2015).
12. Bee, T. *et al.* The mouse Runx1 +23 hematopoietic stem cell enhancer confers hematopoietic specificity to both Runx1 promoters. *Blood* **113**, 5121–5214 (2009).
13. Kissa, K. *et al.* Live imaging of emerging hematopoietic stem cells and early thymus colonization. *Blood* **111**, 1147–56 (2008).
14. Ma, D., Zhang, J., Lin, H. F., Italiano, J. & Handin, R. I. The identification and characterization of zebrafish hematopoietic stem cells. *Blood* **118**, 289–297 (2011).
15. Miyawaki, K. *et al.* CD41 Marks the Initial Myelo-Erythroid Lineage Specification in Adult Mouse Hematopoiesis: Redefinition of Murine Common Myeloid Progenitor. *Stem Cells* **33**, 976–987 (2015).
16. Bertrand, J. Y. *et al.* Characterization of purified intraembryonic hematopoietic stem cells as a tool to define their site of origin. *Proc. Natl. Acad. Sci. U. S. A.* **102**, 134–139 (2005).
17. Muraro, M. J. *et al.* A Single-Cell Transcriptome Atlas of the Human Pancreas. *Cell Syst.* **3**, 385–394 (2016).
18. Herman, J. S., Sagar & Grün, D. FateID infers cell fate bias in multipotent progenitors from single-cell RNA-seq data. *Nat. Methods* **15**, 379–386 (2018).
19. Athanasiadis, E. I. *et al.* Single-cell RNA-sequencing uncovers transcriptional states and fate decisions in haematopoiesis. *Nat. Commun.* **8**, (2017).
20. Baron, C. S. *et al.* Single-cell transcriptomics reveal the dynamic of haematopoietic stem cell production in the aorta. *Nat. Commun.* **9**, (2018).
21. Buenrostro, J. D. *et al.* Integrated Single-Cell Analysis Maps the Continuous Regulatory Landscape of Human Hematopoietic Differentiation. *Cell* **173**, 1535-15e16 (2018).
22. Kowalczyk, M. S. *et al.* Single-cell RNA-seq reveals changes in cell cycle and differentiation programs upon aging of hematopoietic stem cells. *Genome Res.* **25**, 1860–1872 (2015).
23. Lai, S. *et al.* Comparative transcriptomic analysis of hematopoietic system between human and mouse by Microwell-seq. *Cell Discov.* **4**, (2018).
24. Nestorowa, S. *et al.* A Single Cell Resolution Map of Mouse Haematopoietic Stem and Progenitor Cell Differentiation Running title: Single Cell Map of HSPC Differentiation. *Blood* **128**, 20–32 (2016).
25. Xue, Y. *et al.* A 3D Atlas of Hematopoietic Stem and Progenitor Cell Expansion by Multi-dimensional RNA-Seq Analysis. *Cell Rep.* **27**, 1567-15e5 (2019).
26. Davidson, A. J. & Zon, L. I. The 'definitive' (and 'primitive') guide to zebrafish hematopoiesis. *Oncogene* **23**, 7233–7246 (2004).
27. Baron, C. S. *et al.* Cell Type Purification by Single-Cell Transcriptome-Trained Sorting. *Cell* **179**, 527-5e19 (2019).
28. Blokzijl-Franke, S. *et al.* Phosphatidylinositol-3 kinase signaling controls survival and stemness of hematopoietic stem and progenitor cells. *Oncogene* **40**, 2741–2755 (2021).
29. Svoboda, O. *et al.* Ex vivo tools for the clonal analysis of zebrafish hematopoiesis. *Nat. Protoc.* **11**, 1007–1020 (2016).
30. Tamplin, O. J. *et al.* Hematopoietic stem cell arrival triggers dynamic remodeling of the perivascular niche. *Cell* **160**, 241–252 (2015).
31. Cabezas-Wallscheid, N. & Trumpp, A. Potency finds its niches. *Science (80-.).* **351**, 126–127 (2016).
32. Wattrus, S. J. & Zon, L. I. Stem cell safe harbor: the hematopoietic stem cell niche in zebrafish. *Blood Adv.* **2**,

3063–3069 (2018).
33. Sanada, C. *et al.* Adult human megakaryocyte-erythroid progenitors are in the CD34+CD38mid fraction. *Blood* **128**, 923–933 (2016).
34. Kobayashi, I. *et al.* Enrichment of hematopoietic stem/progenitor cells in the zebrafish kidney. *Sci. Rep.* **9**, 1–11 (2019).
35. Graf, T. Differentiation plasticity of hematopoietic cells. *Blood* **99**, 3089–3101 (2002).
36. Iwasaki, H. *et al.* GATA-1 converts lymphoid and myelomonocytic progenitors into the megakaryocyte/erythrocyte lineages. *Immunity* **19**, 451–462 (2003).
37. Yamada, T. *et al.* Lineage switch induced by overexpression of Ets family transcription factor PU.1 in murine erythroleukemia cells. *Blood* **97**, 2300–2307 (2001).
38. Galloway, J. L., Wingert, R. A., Thisse, C., Thisse, B. & Zon, L. I. Loss of Gata1 but not Gata2 converts erythropoiesis to myelopoiesis in zebrafish embryos. *Dev. Cell* **8**, 109–116 (2005).
39. Challen, G. A., Boles, N., Lin, K. K. Y. & Goodell, M. A. Mouse hematopoietic stem cell identification and analysis. *Cytom. Part A* **75**, 14–24 (2009).
40. Lin, H. T., Otsu, M. & Nakauchi, H. Stem cell therapy: An exercise in patience and prudence. *Philos. Trans. R. Soc. B Biol. Sci.* **368**, 4–6 (2013).
41. Jin, S.-W., Beis, D., Mitchell, T., Chen, J.-N. & Stainier, D. Y. R. Cellular and molecular analyses of vascular tube and lumen formation in zebrafish. *Development* **132**, 5199–209 (2005).
42. Aleström, P. *et al.* Zebrafish: Housing and husbandry recommendations. *Lab. Anim.* **0**, 1–12 (2019).
43. Kimmel, C. B., Ballard, W. W., Kimmel, S. R., Ullmann, B. & Schilling, T. F. Stages of embryonic development of the zebrafish. *Dev Dyn* **203**, 253–310 (1995).
44. Westerfield, M. The zebrafish book. A guide for the laboratory use of zebrafish (Danio rerio). 4th ed. *Univ. Oregon Press. Eugene* (2000).
45. Van Den Brink, S. C. *et al.* Single-cell sequencing reveals dissociation-induced gene expression in tissue subpopulations. *Nat. Methods* **14**, 935–936 (2017).
46. Hashimshony, T. *et al.* CEL-Seq2: sensitive highly-multiplexed single-cell RNA-Seq. *Genome Biol.* **17**, 77 (2016).
47. Grün, D., Kester, L. & van Oudenaarden, A. Validation of noise models for single-cell transcriptomics. *Nat. Methods* **11**, 637–640 (2014).
48. Love, M. I., Huber, W. & Anders, S. Moderated estimation of fold change and dispersion for RNA-seq data with DESeq *Genome Biol.* **15**, 1–21 (2014).

table S1. Marker genes

Cluster/Cell type	**Gene**	**ENSDARG**
Thrombocyte/erythrocyte progenitors	*hmbsb*	ENSDARG00000055991
	prdx3	ENSDARG00000032102
	urod	ENSDARG00000006818
	uros	ENSDARG00000027491
	tubb1	ENSDARG00000053066
	klf1	ENSDARG00000017400
	gata1a	ENSDARG00000013477
	epb41b	ENSDARG00000029019
Erythrocyte progenitors	*alas2*	ENSDARG00000038643
	cahz	ENSDARG00000011166
	hbbe2	ENSDARG00000045143
	hbae3	ENSDARG00000079305
	rhag	ENSDARG00000019253
	epor	ENSDARG00000090834
HSPCs	*myb*	ENSDARG00000053666
	her6	ENSDARG00000006514
	ahcy	ENSDARG00000005191
	pmp22b	ENSDARG00000060457
	ncl	ENSDARG00000002710
	adh5	ENSDARG00000080010
	hmga1a	ENSDARG00000028335
	fbl	ENSDARG00000053912
	mycb	ENSDARG00000007241
	dkc1	ENSDARG00000016484
	pes	ENSDARG00000018902
	meis1b	ENSDARG00000012078
	tal1 (scl)(Davidson & Zon 2004)	ENSDARG00000019930
	gata2b	ENSDARG00000009094
HSPCs	*gfi1aa*	ENSDARG00000020746
	adgrg1	ENSDARG00000027222_

Cluster/Cell type	Gene	ENSDARG
Myeloid progenitor	*crema*	ENSDARG00000023217
	itm2bb	ENSDARG00000041505
	runx3	ENSDARG00000052826
	cebpb	ENSDARG00000042725
	cxcr4b	ENSDARG00000041959
	zfp36l1a	ENSDARG00000016154
	coro1a	ENSDARG00000054610
	nr4a3	ENSDARG00000055854
	pu.1 (spi1b)	ENSDARG00000000767
Neutrophil progenitor	*cpa5*	ENSDARG00000021339
	lect2l	ENSDARG00000033227
	npsn	ENSDARG00000010423
	sms	ENSDARG00000008155
	abcb9	ENSDARG00000056200
	ch25hl2	ENSDARG00000038728
	mpx	ENSDARG00000019521
	lyz	ENSDARG00000057789
	srgn	ENSDARG00000077069
	mmp9	ENSDARG00000042816
Monocyte progenitor	*marco*	ENSDARG00000059294
	ctss2.2	ENSDARG00000013771
	mfap4	ENSDARG00000090783
	marckls1a	ENSDARG00000039034
	ctsba	ENSDARG00000055120
	cxcr3.3	ENSDARG00000070669
	timp2b	ENSDARG00000075261
	lgmn	ENSDARG00000039150
	ndrg1a	ENSDARG00000032849
EHT markers	*edn2*	ENSDARG00000017255
	efna1b	ENSDARG00000018787
	cdh5	ENSDARG00000075549
	krt18	ENSDARG00000018404
	krt8	ENSDARG00000058358

Cluster/Cell type	Gene	ENSDARG
EHT markers	*dab2*	ENSDARG00000031761
	serpinh1b	ENSDARG00000019949
	anxa2a	ENSDARG00000003216
	ctsla	ENSDARG00000007836
	hapln1b	ENSDARG00000068516
	clic2	ENSDARG00000010625
	cd81a	ENSDARG00000036080
	tie1	ENSDARG00000004105

table S2. Upregulated genes 5 dpf old embryos

1	2	3
ENSDARG00000057789_lyz	ENSDARG00000087390_hbbe1.3	ENSDARG00000082180
ENSDARG00000010423_npsn	ENSDARG00000089124_hbae1.3	ENSDARG00000058337
ENSDARG00000019521_mpx	ENSDARG00000079305_hbae3	ENSDARG00000014329_npm1a
ENSDARG00000042816_mmp9	ENSDARG00000011166_cahz	ENSDARG00000080337_ AC024175.4
ENSDARG00000075664_si:ch1073-429i10.1	ENSDARG00000038643_alas2	ENSDARG00000084962
ENSDARG00000012395_mmp13a	ENSDARG00000089475_hbae1	ENSDARG00000096145
ENSDARG00000077069_srgn	ENSDARG00000045143_hbbe2	ENSDARG00000060457_pmp22b
ENSDARG00000023188_lcp1	ENSDARG00000077504_si:ch211-103n10.5	ENSDARG00000041895_cad
ENSDARG00000044129_ FP015823.1	ENSDARG00000089963_hbbe1.1	ENSDARG00000043317_kita
ENSDARG00000077777_tmsb4x	ENSDARG00000088330_ AL935210.1	ENSDARG00000070212
ENSDARG00000021339_cpa5	ENSDARG00000055991_hmbsb	ENSDARG00000006514_her6
ENSDARG00000033227_lect2l	ENSDARG00000006818_urod	ENSDARG00000012820_nop56
ENSDARG00000054610_coro1a	ENSDARG00000042310	ENSDARG00000082753_ AC024175.17
ENSDARG00000006029_lta4h	ENSDARG00000012881_slc4a1a	ENSDARG00000016484_dkc1
ENSDARG00000027063_arpc1b	ENSDARG00000045144_hbz	ENSDARG00000053666_myb
ENSDARG00000026829_cotl1	ENSDARG00000026655_tspo	ENSDARG00000028323
ENSDARG00000091038	ENSDARG00000096667_si:dkey-25o16.2	ENSDARG00000062138_ranbp10
ENSDARG00000042725_cebpb	ENSDARG00000053066_tubb1	ENSDARG00000022410_rrp12
ENSDARG00000004034_arhgdig	ENSDARG00000090689_hbbe1.2	ENSDARG00000077264_wdr43
ENSDARG00000079736	ENSDARG00000029019_epb41b	ENSDARG00000030789_ddx18
ENSDARG00000095351_ CU914776.2	ENSDARG00000008840_hmbsa	ENSDARG00000031756_mef2aa
ENSDARG00000041959_cxcr4b	ENSDARG00000030490_sptb	ENSDARG00000055868_rsl1d1
ENSDARG00000035326_nccrp1	ENSDARG00000057206_nmt1b	ENSDARG00000002710_ncl
ENSDARG00000070398	ENSDARG00000023713_aqp1a.1	ENSDARG00000041088
ENSDARG00000008155_sms	ENSDARG00000034852_nt5c2l1	ENSDARG00000043126_blf
ENSDARG00000093124_scpp8	ENSDARG00000006260_tuba8l4	ENSDARG00000036549_agpat3
ENSDARG00000058348_scinlb	ENSDARG00000045142_hbae5	ENSDARG00000030441_ppa1b
ENSDARG00000014348_stk17b	ENSDARG00000020890_tmod4	ENSDARG00000053912_fbl

1	2	3
ENSDARG00000041524	ENSDARG00000025200	ENSDARG00000073850_hdac7b
ENSDARG00000031153	ENSDARG00000017400_klf1	ENSDARG00000040503_sb:cb81
ENSDARG00000095556_ CR318588.4	ENSDARG00000044212_ CR735126.1	ENSDARG00000007241_mycb
ENSDARG00000063295_myh9a	ENSDARG00000027491_uros	ENSDARG00000087504
ENSDARG00000086337_si:dkey-102g19.3	ENSDARG00000018461_zgc:56095	ENSDARG00000045776_cnbpa
ENSDARG00000068784_VSIR	ENSDARG00000013110_dmtn	ENSDARG00000018902_pes
ENSDARG00000086869	ENSDARG00000008678_snx3	ENSDARG00000043304_nop2
ENSDARG00000071437_ptprc	ENSDARG00000052815	ENSDARG00000005191_ahcy
ENSDARG00000088091_pfn1	ENSDARG00000054929_ zgc:110540	ENSDARG00000033440_metap1
ENSDARG00000090730_ zgc:158446	ENSDARG00000002790_ap2m1a	ENSDARG00000039887_c1qbp
ENSDARG00000025147_cd63	ENSDARG00000025350_prdx2	ENSDARG00000076526_gar1
ENSDARG00000056600_papss2b	ENSDARG00000009315_clgn	ENSDARG00000016548_eif5b
ENSDARG00000038458	ENSDARG00000032102_prdx3	ENSDARG00000070670_crip2
ENSDARG00000017653_rgs13	ENSDARG00000088554	ENSDARG00000070228_cdk6
ENSDARG00000055186_ccr9a	ENSDARG00000015551_fth1a	ENSDARG00000017568
ENSDARG00000039884	ENSDARG00000004926	ENSDARG00000014123
ENSDARG00000058593_sri	ENSDARG00000010792_cdc25b	ENSDARG00000056186_eif5a2
ENSDARG00000037870_actb2	ENSDARG00000023330_anp32b	ENSDARG00000060065_ubap2b
ENSDARG00000032868_pde4ba	ENSDARG00000008333_znfl2a	ENSDARG00000052480_pdcd11
ENSDARG00000089706_ANPEP	ENSDARG00000054447_slc29a1b	ENSDARG00000014587_slc38a5b
ENSDARG00000002021_pygb	ENSDARG00000042894_tyms	ENSDARG00000014591_ilf2
ENSDARG00000075989_arpc2	ENSDARG00000038792_klf17	ENSDARG00000023290_fabp3
ENSDARG00000041505_itm2bb	ENSDARG00000068822_purba	ENSDARG00000056160_hspd1
ENSDARG00000039007_eno3	ENSDARG00000035423	ENSDARG00000010246_prmt1
ENSDARG00000007769_sult5a1	ENSDARG00000003462_fech	ENSDARG00000056167_hspe1
ENSDARG00000026350_wasb	ENSDARG00000071697_zgc:66433	ENSDARG00000078691_gigyf1
ENSDARG00000010556_ CABZ01030094.1	ENSDARG00000093572_lamc3	ENSDARG00000039578_pa2g4a
ENSDARG00000038010_rac2	ENSDARG00000058725_rfesd	ENSDARG00000010194_eif4bb
ENSDARG00000020929_fam49ba	ENSDARG00000038097_pigq	ENSDARG00000096403_ CT027638.1
ENSDARG00000038728_ch25hl2	ENSDARG00000019507_mcm5	ENSDARG00000006200_eif4g1a
ENSDARG00000023217_crema	ENSDARG00000040163_prim1	ENSDARG00000044220
ENSDARG00000042876_abracl	ENSDARG00000068820_h2afva	ENSDARG00000035751_ipo7

1	2	3
ENSDARG00000068233_CD53	ENSDARG00000014013_lbr	ENSDARG00000076532_si:ch211-222l21.1
ENSDARG00000076562	ENSDARG00000020944_ezra	ENSDARG00000070657_pa2g4b
ENSDARG00000056200_abcb9	ENSDARG00000075180_tmem14ca	ENSDARG00000021702_pdcd4a
ENSDARG00000018283_cyba	ENSDARG00000058226_ak3	ENSDARG00000011125_snrpb
ENSDARG00000074656_ctss2.1	ENSDARG00000055498_si:ch1073-184j22.1	ENSDARG00000008109
ENSDARG00000033735_ncf1	ENSDARG00000020442_snx5	ENSDARG00000016173_cct3
ENSDARG00000058225_arpc4l	ENSDARG00000087554_cdk1	ENSDARG00000019253_rhag
ENSDARG00000000767_spi1b	ENSDARG00000074581_add2	ENSDARG00000070083_atp5b
ENSDARG00000043257_ckbb	ENSDARG00000024295_slc11a2	ENSDARG00000052856_khdrbs1a
ENSDARG00000059110	ENSDARG00000043493_cltca	ENSDARG00000013351_cirbpb
ENSDARG00000058647_hck	ENSDARG00000043665_glrx5	ENSDARG00000028335_hmga1a
ENSDARG00000071491_nrros	ENSDARG00000014017_rrm1	ENSDARG00000009447_atp5g3b
ENSDARG00000016939_itgb2	ENSDARG00000017864	ENSDARG00000010149_atp5a1
ENSDARG00000058858	ENSDARG00000077620_cdca7a	ENSDARG00000029150_hsp90ab1
ENSDARG00000012987_gpia	ENSDARG00000045618_clta	ENSDARG00000059654_eif3ba
ENSDARG00000035652_sat1a.1	ENSDARG00000022934	ENSDARG00000015862_rpl5b
ENSDARG00000015343_pgd	ENSDARG00000085091	ENSDARG00000030602_rps19
ENSDARG00000057882_arpc3	ENSDARG00000043250_ppm1ab	ENSDARG00000011201_rplp2l
ENSDARG00000078547_si:ch211-264f5.2	ENSDARG00000058471_plk1	ENSDARG00000011405_rps9
ENSDARG00000035018_thy1	ENSDARG00000042533_gstm.1	ENSDARG00000056119_eef1g
ENSDARG00000062049_hmha1b	ENSDARG00000057432	ENSDARG00000039641
ENSDARG00000055276_rel	ENSDARG00000086112_si:ch211-266i6.3	
ENSDARG00000036074_cebpa	ENSDARG00000059473_kank4	
ENSDARG00000075748_NCKAP1L	ENSDARG00000020504_h3f3b.1	
ENSDARG00000002131_celf2	ENSDARG00000093182_eif2ak1	
ENSDARG00000034427_hn1l	ENSDARG00000040485_dfna5b	
ENSDARG00000088283_si:ch73-248e21.5	ENSDARG00000077383_anxa11a	
ENSDARG00000078092_limd2	ENSDARG00000076590_atad2	
ENSDARG00000052656_si:ch211-193e13.5	ENSDARG00000043137_cdca8	
ENSDARG00000021113_ptmaa	ENSDARG00000038066_kpna2	
ENSDARG00000017298	ENSDARG00000002659_mapre1b	
ENSDARG00000007682_ppdpfa	ENSDARG00000005454_tacc3	

1	2	3
ENSDARG00000024314_herpud1	ENSDARG00000061591_abcb10	
ENSDARG00000053836_si:ch211-284o19.8	ENSDARG00000013477_gata1a	
ENSDARG00000037746_actb1	ENSDARG00000001558_kifc1	
ENSDARG00000056615_cybb	ENSDARG00000054155_pcna	
ENSDARG00000087188_nfil3-6	ENSDARG00000071863_itgb1a	
ENSDARG00000055713_fmnl1a	ENSDARG00000020114_slc20a1a	
ENSDARG00000078619_pnp5a	ENSDARG00000002194_rhd	
ENSDARG00000075261_timp2b	ENSDARG00000063345	

table S3. All comparisons used in the Colony Forming Unit assay.

Tukey's multiple comparisons test	5dpf erythroid	5dpf myeloid	WKM erythroid	WKM myeloid
kdrl/cd41 vs kdrl	*	**	ns	ns
kdrl/cd41 vs cd41	*	*	****	**
kdrl/cd41 vs neg	*	**	ns	ns
kdrl vs cd41	ns	**	****	**
kdrl vs neg	ns	ns	ns	ns
cd41 vs neg	*	*	****	**

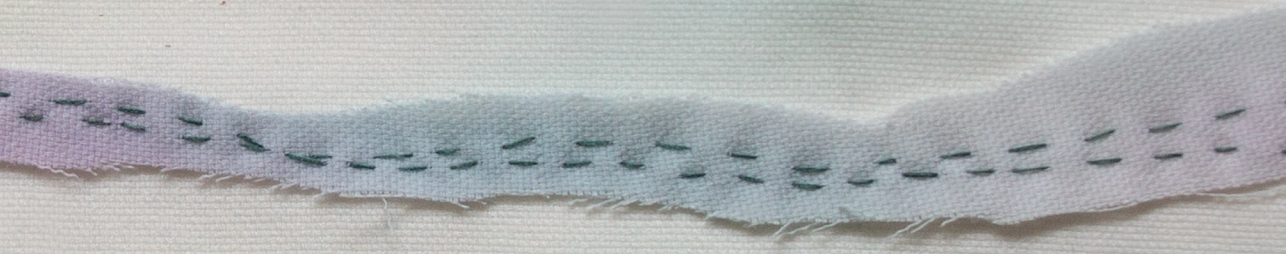

Chapter 6

Summarizing Discussion

The molecular program regulating hematopoiesis is a highly conserved process in vertebrates, even though sites of hematopoiesis differ between fish and mammals, which makes new findings in zebrafish applicable to mammalian hematopoiesis [1]. Zebrafish (*Danio rerio)* have a number of unique advantages, such as external fertilization, transparency during embryonic development and large numbers of eggs produced by a single adult zebrafish pair. The combination of translucent embryos and the feasibility of genetic modifications, including the generation of transgenic (reporter) lines as well as knock-outs and knock-ins of genes make it possible to visualize *in vivo* early hematopoietic processes ranging from following the birth of hematopoietic stem/progenitor cells (HSPCs) to following the migratory route to the different hematopoietic organs. In the last century, HSPCs have been the intense focus of research and we gained numerous insights into hematopoiesis during embryonic development. The work described in this thesis contributes to the understanding of zebrafish hematopoiesis by identifying two protein tyrosine phosphatases (PTPs) that are necessary for normal hematopoiesis: phosphatase and tensin homologue ten (Pten) and Src homology domain 2 containing phosphatase (Shp2). In addition, we identified a marker that marks the shift from embryonic to adult hematopoietic stem/progenitor cells (HSPCs) in zebrafish. Below we describe our major findings, highlighting the roles of Pten and Shp2 in hematopoiesis.

The tumour suppressor PTEN is required for zebrafish hematopoiesis (chapter 2)

The tumor suppressor Phosphatase and Tensin homologue Ten (PTEN) is a PTP that counteracts phosphatidylinositol-3-kinase (PI3K) and acts upstream in the PI3K/Akt pathway [2]. In **chapter 2**, we demonstrated for the first time that loss of Pten results in aberrant hematopoiesis in zebrafish. During the endothelial-hematopoietic transition (EHT) in the aorta-gonad-mesonephros (AGM) when HSPCs emerge, embryos lacking Pten showed apoptotic HSPCs and 50% less HSPCs than their siblings. Restoring Pten expression or inhibiting PI3K activity during this stage rescued the emergence of HSPCs in embryos lacking Pten expression. Surprisingly, inhibition of PI3K activity in wild type embryos induced a similar phenotype as observed in embryos lacking Pten. This suggests that a moderate level of PI3K activity is required during the emergence of HSPCs. Both too high and too low activity is detrimental for emerging HSPCs.

Loss of Pten is known to lead to increased Akt signalling and increased proliferation in tumour cells [3,4]. There is an inversed correlation between proliferation and differentiation [5]. Embryos lacking Pten expression show increased proliferation of HSPCs [6] and subsequently, arrested differentiation of the different blood lineages, supporting this notion.

Using single cell RNA sequencing, we observed two HSPCs clusters at the onset of definitive hematopoiesis, one having more stem cell-like characteristics and the other having more progenitor-like characteristics. Upon PI3K-inhibition, predominantly the HSPCs cluster exhibiting the more stem cell-like properties was lost. It would be very interesting to explore if a similar phenotype is observed in embryos lacking Pten

expression. Currently this is not feasible, as mutant embryos cannot be distinguished from their siblings at this stage. At the end of definitive hematopoiesis, PI3K inhibition arrested differentiation, increasing HSPCs fate, in contrast to loss of Pten expression, which showed an increased differentiation at the expense of HSPCs fate. Together, this suggests the requirement of balanced PI3K activity to regulate the stemness of HSPCs at the end of definitive hematopoiesis.

Overall, our results suggest that PI3K signalling controls the survival and stemness of HSPCs. Future research should include an in-depth validation of the genes we found to distinguish between the two HSPCs populations we observed at the onset of definitive hematopoiesis. These genes should be validated by whole mount *in situ* hybridization, quantative PCR and eventually by creating genetic knock-out zebrafish embryos or transgenic zebrafish lines. Furthermore, research should investigate long-term and short-term HSCs regarding the surviving HSPCs in embryos lacking Pten expression. Long-term HSCs are quiescent, whereas short-term HSCs show increased proliferation [7]. As a first step, *in vitro* differentiation assays, such as colony-forming-unit assays (as described in **Chapter 3** and **Chapter 4**), might give additional information about self-renewal and differentiation properties of the surviving HSPCs. Moreover, it would be interesting, but very challenging, to perform transplantation experiments to see if the surviving HSPCs in either embryos lacking Pten expression or embryos with inhibited PI3K signalling have the ability to fully reconstitute hematopoiesis in lethally irradiated zebrafish [8]. Transplantation experiments are the gold standard for identifying long-term HSCs based on their ability to self-renew and differentiate into all blood lineages in a recipient host. However, there are a few challenges. First, enrichment of long-term HSCs is difficult, as there are few antibodies to zebrafish cell surface proteins that reliably mark HSCs. The use of transgenic lines that mark HSCs would be the logical step, but the genes used for these lines (for example *c-myb*, *runx1* or *cd41*) often express fluorescent proteins not only in HSCs but also in more progenitor-like cells, making it difficult to enrich for HSCs [9]. Second, the immune system fends off all foreign cells, creating a potential barrier for transplanted HSPCs. For successfull transplantation assays the major histocompatibility genes (MHC) should be compatible between host and donor, something that is exceedingly difficult to obtain, due to lack of true inbred zebrafish strains [10,11]. Thirdly, zebrafish have multiple MHCI and MHCII loci on different chromosomes, in contrast to mammals, resulting in unreliable predictions after genotyping if host and donor are compatible [12].

Generating a novel zebrafish mutant of a common Noonan Syndrome associated mutation Shp2-D61G (chapter 3)

Src homology domain 2 (Shp2) mutations are frequently found in patients with Noonan Syndrome (NS) and Noonan Syndrome with multiple lentigines (NS-ML) [13–15]. Asp61 is one of the most commonly mutated residues in NS patients [15,16]. Hematological defects are observed in NS patients. Juvenile myelomonocytic leukemia (JMML)-like myeloproliferative

diseases, which can progress into the aggressive and often fatal JMML form (NS/JMML) [17,18] are observed in a proportion of NS children. In **chapter 3**, we generated a mutant zebrafish line carrying a Shp2a-D61G (Asp to Gly) mutation that displayed several characteristic traits of NS and NS-ML patients. We focused on the hematological phenotype, as we observed an expansion of the myeloid lineage, an increased sensitivity to myeloid differentiation factors, mild anemia and thrombocytopenia (low platelet count). The expansion of the myeloid lineage was both observed using scRNA sequencing and in *in vitro* differentiation assays and these myeloproliferative defects resemble hallmarks of JMML in human patients. We observed an upregulation of pro-inflammatory genes in the myeloid lineage early during differentiation, suggesting that the inflammatory response might be involved in the onset of JMML. High levels of cytokines, produced by myeloid cells, have been reported in JMML patients and mouse models [19–23]. The hematological phenotype of Shp2^{D61G} mutant zebrafish embryos was partially rescued by inhibition of inflammation. This is especially interesting, because to date, there are no drug therapies for NS/JMML.

Overall, our results show that we were able to generate a novel zebrafish model that displays several characteristics of NS and NS-ML patients and NS mouse models, and notably the hematological phenotype. Our model is particularly interesting as hematological defects in NS patients often appear at a very young age and zebrafish are ideally suited as a tool to study defects during embryonic development [21,24,25]. Further research should focus on the therapeutic potential of dampening the inflammatory response by different drugs. This could be tested with an *in vivo* drugs screen in zebrafish embryos for instance with a panel of inflammation inhibitors. Furthermore, research into heart defects in NS and NS-ML patients should be performed, as these are quite common [26]. The zebrafish mutant we generated did not show similar heart malformations as in NS patients, but these mutant fish did display heart oedemas and changes in heart rate and cardiac output. It would be interesting to see if our zebrafish mutant is a good tool to investigate the heart defects in NS patients, especially as nowadays there are exciting new techniques available in zebrafish to study *in vivo* cardiac electrophysiology [27], facilitating identification of mild defects in heart function.

The role of Shp2b during zebrafish hematopoiesis (chapter 4)

Shp2, encoded by Ptpn11, is not only important in NS and NS-ML, but is also essential during development and is involved in several signalling pathways, such as the (ERK)/MAPK signalling pathway, the Jak-STAT pathway and the PI3K pathway [28–30]. Moreover, Shp2 has been found to be involved in hematopoiesis, with mouse models lacking conditional Ptpn11, showing a depleted HSC pool and defects in homing, self-renewal and survival of HSCs [31–34]. Zebrafish harbor two *ptpn11* genes, *ptpn11a* and *ptpn11b*, both encoding functional Shp2 proteins, Shp2a and Shp2b. In **chapter 4**, we investigated the role of Shp2a and Shp2b in zebrafish embryos during hematopoiesis. Surprisingly, we found that lack of Shp2a did not affect the ontogeny of HSPCs, but that lack of Shp2b did. The majority

of zebrafish embryos lacking Shp2b showed disintegrating HSPCs upon emergence from the AGM during EHT at the onset of definitive hematopoiesis. This is interesting, as it was shown earlier that *ptpn11a* is abundantly expressed during all developmental stages, whereas *ptpn11b* has a very low expression early on that increases to the same levels as *ptpn11a* at 5 dpf [35]. The effect of abortive events during the onset of definitive hematopoiesis is still seen at later stages, in that fewer HSPCs were observed to seed the next transient hematopoietic organ. However, the surviving HSPCs did engage in all blood lineages and we observed no differences at later stages between embryos lacking Ptpn11b expression and their siblings. This is in contrast with several studies performed in mice, where the lack of Shp2 leads to decreased differentiation towards erythroid, lymphoid and myeloid cell fates [36–38].

Together, our results suggest that *ptpn11b* is required for normal emergence of HSPCs at the onset of definitive hematopoiesis and that *ptpn11b* mutants overcome these defects at the end of definitive hematopoiesis. It would be interesting to investigate if lack of ptpn11b expression shows earlier defects in hematopoiesis, for instance during the primitive wave.

Further research should focus on the interaction between Pten and Ptpn11 in hematopoiesis in zebrafish during development. We show that both Pten (**chapter 2**) and ptpn11 (**chapter 4**) are essential for normal hematopoiesis. In adult mice it has been shown that Pten and Shp2 have opposite effects on myelopoiesis and leukemogenesis. Selective loss of Pten in mice results in a long-term decline of HSCs and development of myeloproliferative disorders, indicating a preventive role of Pten for these disorders [39,40]. Whereas loss of Shp2 leads to suppressed HSPCs self-renewal and differentiation [31,32,41], dominant-activating mutations of Shp2 lead to increased risks of developing myeloproliferative disorders [15,18] (see also **chapter 3**). When Shp2 is deleted in mice that already lack Pten in hematopoietic cells, the effect of loss of Pten is negated and the phenotype is rescued [42]. However, these mice suffer from lethal anemia, indicating that Pten and Shp2 cooperate in erythropoiesis [42]. It would be very interesting to study in more depth how these pathways interact with each other in zebrafish.

Loss of *kdrl* marks the shift from embryonic to adult HSPCs in zebrafish (chapter 5)

It is possible to visualize HSPCs in the zebrafish embryo using fish in different transgenic backgrounds. HSPCs are marked by several genes, such as *c-myb, cd41,* and *runx1* [43–46] and when combined with an endothelial marker, for example *kdrl*, HSPCs can be followed when they start to emerge from the AGM at the onset of the definitive wave [47,48]. In **chapter 5** we demonstrated for the first time that loss of the endothelial marker *kdrl* marks the shift of embryonic HSPCs to adult HSPCs. In 5 dpf old zebrafish embryos expressing fluorescent markers for cd41 (HSPCs) and kdrl (endothelial) we observed both kdrl/cd41^{low} and cd41^{low} HSPCs. Surprisingly, scRNA sequencing revealed transcriptional differences between kdrl/cd41^{low} and cd41^{low} HSPCs, not in their most stem cell-like state, but in their differentiation

capabilities. Kdrl/cd41^{low} HSPCs appeared to have a more myeloid progenitor fate, whereas cd41^{low} HSPCs had a more thrombocyte/erythrocyte progenitor fate. Functional *in vitro* assays indicated that kdrl/cd41^{low} HSPCs were mainly able to form colonies and differentiate into different blood cell fates. In adult zebrafish with the same transgenic background, we also observed both kdrl/cd41^{low} and cd41^{low} HSPCs. Unexpectedly, cd41^{low} HSPCs were now the only HSPCs that were able to differentiate into different blood cell fates. Cd41 is not only expressed in HSPCs, but also in erythroid and myeloid lineages, which might explain the differentiation into different lineages [45,49].

Overall, our results suggest that in both embryos and adult zebrafish a subpopulation of HSPCs exist, that in addition to expression of cd41, also express kdrl. In embryos, kdrl/cd41^{low} HSPCs are able to differentiate into several lineages *in vitro*, whereas in adults only cd41^{low} HSPCs, that do not express kdrl, have this ability. Hence, loss of kdrl expression marks the shift from embryonic to adult HSPCs. Future research should focus on the relation of long-term and short-term HSPCs in combination with these markers. Kdrl/cd41^{low} cells possibly represent short-term HSPCs, as these cells proliferate quickly in the CHT during embryonic development, whereafter they migrate to the adult hematopoietic organs. During adulthood, long-term cd41^{low} HSPCs are responsible for replenishing the HSPCs pool and producing all different blood cells. Analysing cell proliferation properties of kdrl/cd41^{low} and cd41^{low} HSPCs in adult WKM using scRNA sequencing might give us insights into transcriptional differences between these two groups of cells and into differences compared to embryonic HSPCs. It would be interesting to investigate if the HSPCs also show distinct differentiation capabilities and if these are comparable with embryonic HSPCs. Moreover, future work should focus on young adolescent zebrafish, to validate the results we have observed in embryonic and adult HSPCs and to see if there is a gradual shift from embryonic HSPCs to adult HSPCs or that there is a more abrupt shift.

Concluding remarks

To conclude, we show that zebrafish embryos lacking functional Pten or Shp2 show disrupted hematopoiesis during development, attributed to perturbed PI3K and MAPK signalling, respectively (**Chapters 2,3 and 4**). We show that a fine balance of PI3K signalling is required for normal hematopoiesis and that the level of PI3K influences the level of stemness of HSPCs (**chapter 2**). Lack of *ptpn11b* expression leads to disrupted emergence of HSPCs, but surprisingly these defects were overcome at a later stage and led to viable and fertile zebrafish (**chapter 4**). We generated a novel zebrafish model carrying a common NS-patient associated mutation and demonstrated that this model recapitulates major NS traits in human patients and is a good model to study this disorder (**chapter 3**). Lastly, we show that loss of an endothelial marker marks the transition from embryonic to adult HSPCs (**chapter 5**). All together, we show that the zebrafish is a versatile model organism which is powerful in modelling human disease and in unravelling more fundamental research questions.

References

1. Davidson, A. J. & Zon, L. I. The 'definitive' (and 'primitive') guide to zebrafish hematopoiesis. *Oncogene* **23**, 7233–7246 (2004).
2. Song, M. S., Salmena, L. & Pandolfi, P. P. The functions and regulation of the PTEN tumour suppressor. *Nat. Rev. Mol. Cell Biol.* **13**, 283–296 (2012).
3. Alva, J. A., Lee, G. E., Escobar, E. E. & Pyle, A. D. Phosphatase and tensin homolog regulates the pluripotent state and lineage fate choice in human embryonic stem cells. *Stem Cells* **29**, 1952–1962 (2011).
4. Alimonti, A. *et al.* Subtle variations in Pten dose determine cancer susceptibility. *Nat. Genet.* **42**, 454–458 (2010).
5. Reya, T., Morrison, S. J., Clarke, M. F. & Weissman, I. L. Stem cells, cancer, and cancer stem cells. *Nature* **414**, 105–111 (2001).
6. Choorapoikayil, S., Kers, R., Herbomel, P., Kissa, K. & Den Hertog, J. Pivotal role of Pten in the balance between proliferation and differentiation of hematopoietic stem cells in zebrafish. *Blood* **123**, 184–190 (2014).
7. Orkin, S. H. & Zon, L. I. Hematopoiesis: An Evolving Paradigm for Stem Cell Biology. *Cell* **132**, 631–644 (2008).
8. Traver, D. *et al.* Transplantation and in vivo imaging of multilineage engraftment in zebrafish bloodless mutants. *Nat. Immunol.* **4**, 1238–1246 (2003).
9. Gansner, J. M., Dang, M., Ammerman, M. & Zon, L. I. *Transplantation in zebrafish*. *Methods in Cell Biology* vol. 138 (Elsevier Ltd, 2017).
10. Monson, C. A. & Sadler, K. C. Inbreeding Depression and Outbreeding Depression Are Evident in Wild-Type Zebrafish Lines. *Zebrafish* **7**, 189–197 (2010).
11. Shinya, M. & Sakai, N. Generation of Highly Homogeneous Strains of Zebrafish Through Full Sib-Pair Mating. *G3 Genes|Genomes|Genetics* **1**, 377–386 (2011).
12. Sültmann, H., Mayer, W. E., Figueroa, F., O□Huigin, C. & Klein, J. Organization of Mhc Class II B genes in the Zebrafish (Brachydanio rerio). *Genomics* **23**, 1–14 (1994).
13. Gelb, B. D. & Tartaglia, M. Noonan syndrome and related disorders: dysregulated RAS-mitogen activated protein kinase signal transduction. *Hum. Mol. Genet.* **15**, R220–R226 (2006).
14. Tajan, M., de Rocca Serra, A., Valet, P., Edouard, T. & Yart, A. SHP2 sails from physiology to pathology. *Eur. J. Med. Genet.* **58**, 509–525 (2015).
15. Tartaglia, M. *et al.* Mutations in PTPN11, encoding the protein tyrosine phosphatase SHP-2, cause Noonan syndrome. *Nat. Genet.* **29**, 465–468 (2001).
16. Matozaki, T., Murata, Y., Saito, Y., Okazawa, H. & Ohnishi, H. Protein tyrosine phosphatase SHP-2: A proto-oncogene product that promotes Ras activation. *Cancer Sci.* **100**, 1786–1793 (2009).
17. Niemeyer, C. M. & Flotho, C. Juvenile myelomonocytic leukemia: who's the driver at the wheel? *Blood* **133**, 1060–1070 (2019).
18. Strullu, M. *et al.* Juvenile myelomonocytic leukaemia and Noonan syndrome. *J. Med. Genet.* **51**, 689–697 (2014).
19. Bagby, G. C., Dinarello, C. A., Neerhout, R. C., Ridgway, D. & McCall, E. Interleukin 1-dependent paracrine granulopoiesis in chronic granulocytic leukemia of the juvenile type. *J. Clin. Invest.* **82**, 1430–1436 (1988).
20. Freedman, M. H. *et al.* Central role of tumour necrosis factor, GM-CSF, and interleukin 1 in the pathogenesis of juvenile chronic myelogenous leukaemia. *Br. J. Haematol.* **80**, 40–48 (1992).
21. Dong, L. *et al.* Leukaemogenic effects of Ptpn11 activating mutations in the stem cell microenvironment. *Nature* **539**, 304–308 (2016).
22. Zhao, W., Wang, L. & Yu, Y. Gene module analysis of juvenile myelomonocytic leukemia and screening of anticancer drugs. *Oncol. Rep.* **40**, 3155–3170 (2018).
23. Hamarsheh, S. *et al.* Oncogenic KrasG12D causes myeloproliferation via NLRP3 inflammasome activation. *Nat. Commun.* **11**, 1659 (2020).
24. Araki, T. *et al.* Mouse model of Noonan syndrome reveals cell type– and gene dosage–dependent effects of Ptpn11 mutation. *Nat. Med.* **10**, 849–857 (2004).
25. Xu, D. *et al.* A germline gain-of-function mutation in Ptpn11 (Shp-2) phosphatase induces myeloproliferative disease by aberrant activation of hematopoietic stem cells. *Blood* **116**, 3611–3621 (2010).
26. Karnik, R. & Geiger, M. Cardiac Manifestations of Noonan Syndrome. *Pediatr. Endocrinol. Rev.* **16**, 471–476 (2019).
27. van Opbergen, C. J. M. *et al.* Optogenetic sensors in the zebrafish heart: a novel in vivo electrophysiological tool to study cardiac arrhythmogenesis. *Theranostics* **8**, 4750–4764 (2018).
28. Dance, M., Montagner, A., Salles, J. P., Yart, A. & Raynal, P. The molecular functions of Shp2 in the Ras/Mitogen-activated protein kinase (ERK1/2) pathway. *Cell. Signal.* **20**, 453–459 (2008).
29. Feng, G. S. Shp-2 tyrosine phosphatase: Signaling one cell or many. *Exp. Cell Res.* **253**, 47–54 (1999).
30. Neel, B. G., Gu, H. & Pao, L. The 'Shp'ing news: SH2 domain-containing tyrosine phosphatases in cell signaling. *Trends Biochem. Sci.* **28**, 284–293 (2003).

31. Chan, G. *et al.* Essential role for Ptpn11 in survival of hematopoietic stem and progenitor cells. *Blood* **117**, 4253–4261 (2011).
32. Zhu, H. H. *et al.* Kit-Shp2-Kit signaling acts to maintain a functional hematopoietic stem and progenitor cell pool. *Blood* **117**, 5350–5361 (2011).
33. Mohi, M. G. *et al.* Prognostic, therapeutic, and mechanistic implications of a mouse model of leukemia evoked by Shp2 (PTPN11) mutations. *Cancer Cell* **7**, 179–191 (2005).
34. Schubbert, S. *et al.* Functional analysis of leukemia-associated PTPN11 mutations in primary hematopoietic cells. *Blood* **106**, 311–317 (2005).
35. Bonetti, M. *et al.* Distinct and overlapping functions of ptpn11 genes in zebrafish development. *PLoS One* **9**, (2014).
36. Qu, C. K. *et al.* A deletion mutation in the SH2-N domain of Shp-2 severely suppresses hematopoietic cell development. *Mol. Cell. Biol.* **17**, 5499–5507 (1997).
37. Qu, C.-K. *et al.* Biased Suppression of Hematopoiesis and Multiple Developmental Defects in Chimeric Mice Containing Shp-2 Mutant Cells. *Mol. Cell. Biol.* **18**, 6075–6082 (1998).
38. Qu, C.-K., Nguyen, S., Chen, J. & Feng, G.-S. Requirement of Shp-2 tyrosine phosphatase in lymphoid and hematopoietic cell development. *Blood* **97**, 911–914 (2001).
39. Zhang, J. *et al.* PTEN maintains haematopoietic stem cells and acts in lineage choice and leukaemia prevention. *Nature* **441**, 518–522 (2006).
40. Yilmaz, Ö. H. *et al.* Pten dependence distinguishes haematopoietic stem cells from leukaemia-initiating cells. *Nature* **441**, 475–482 (2006).
41. Zhu, H. H. & Feng, G. S. The dynamic interplay between a PTK (Kit) and a PTP (Shp2): In hematopoietic stem and progenitor cells. *Cell Cycle* **10**, 2241–2242 (2011).
42. Zhu, H. H. *et al.* Shp2 and Pten have antagonistic roles in myeloproliferation but cooperate to promote erythropoiesis in mammals. *Proc. Natl. Acad. Sci. U. S. A.* **112**, 13342–7 (2015).
43. Anderson, H. *et al.* Hematopoietic stem cells develop in the absence of endothelial cadherin 5 expression. *Blood* **126**, 2811–2820 (2015).
44. Bee, T. *et al.* The mouse Runx1 +23 hematopoietic stem cell enhancer confers hematopoietic specificity to both Runx1 promoters. *Blood* **113**, 5121–5214 (2009).
45. Lin, H. F. *et al.* Analysis of thrombocyte development in CD41-GFP transgenic zebrafish. *Blood* **106**, 3803–3810 (2005).
46. North, T. E. *et al.* Prostaglandin E2 regulates vertebrate haematopoietic stem cell homeostasis. *Nature* **447**, 1007–1011 (2007).
47. Bertrand, J. Y. *et al.* Haematopoietic stem cells derive directly from aortic endothelium during development. *Nature* **464**, 108–111 (2010).
48. Kissa, K. & Herbomel, P. Blood stem cells emerge from aortic endothelium by a novel type of cell transition. *Nature* **464**, 112–115 (2010).
49. Kobayashi, I. *et al.* Enrichment of hematopoietic stem/progenitor cells in the zebrafish kidney. *Sci. Rep.* **9**, 1–11 (2019).

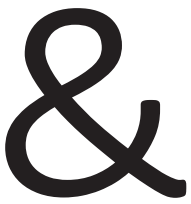

Addendum

Nederlandse samenvatting

Hematopoiese

Zonder bloed kan ons lichaam niet functioneren. Bloed voorziet het lichaam van zuurstof en voedingsstoffen, het verwijdert afvalstoffen, vervoert hormonen en speelt een grote rol in het immuunsysteem. Bloed bestaat uit een mix van cellen die deze functies uitvoeren (figuur 1). Rode bloedcellen verzorgen het transport van zuurstof, witte bloedcellen maken deel uit van de immuunrespons, bloedplaatjes zorgen ervoor dat het bloed kan stollen als er schade aan een bloedvat optreedt. Voor het grootste deel bestaat bloed uit plasma (ongeveer 55%), wat bestaat uit water waarin eiwitten, mineralen, vetten, suikers,

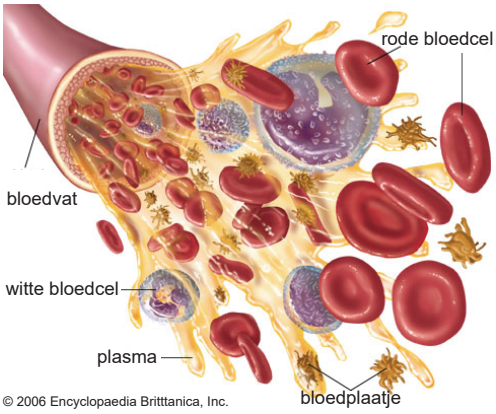

Figuur 1. De verschillende componenten waaruit bloed bestaat. Rode bloedcellen, witte bloedcellen, bloedplaatjes en plasma vormen de vier hoofdbestanddelen van bloed.

antilichamen en hormonen zijn opgelost. De hoofdfunctie van plasma is het transport van bloedcellen en deze componenten door het lichaam.

Bloedcellen hebben een beperkte levensduur. Rode bloedcellen leven ongeveer 3 maanden, bloedplaatjes 10 dagen en witte bloedcellen 2 dagen. Er is dus een constante aanvoer nodig van nieuwe bloedcellen. Hematopoiese is het proces waarbij alle cellulaire componenten waaruit bloed bestaat worden geproduceerd. De cel die voornamelijk verantwoordelijk is voor de productie van bloedcellen is de hematopoietische stamcel (HSC). Stamcellen zijn cellen die instaat zijn om te kunnen delen in een stamcel en in een meer gedifferentieerde cel.

Een HSC kan dus delen en een nieuwe HSC vormen, en tegelijkertijd een (voorloper van een) meer gespecialiseerde cel vormen, bijvoorbeeld een rode of witte bloedcel. In volwassen zoogdieren bevinden HSCs zich in het beenmerg, van waaruit alle bloedcellen worden geproduceerd. Dit is echter niet de locatie waar HSCs gevormd worden. Tijdens

de embryonale ontwikkeling en latere ontwikkeling verandert de locatie waar HSCs zich bevinden. HSCs komen voort uit speciale cellen uit het endotheel van de aorta tijdens de embryonale ontwikkeling, zogenaamde hemogene endotheelcellen. Deze endotheelcellen van de aorta ondergaan een transformatie in een serie stappen wat uiteindelijk leidt tot de vorming van HSCs (figuur 2). De hemogene endotheelcellen nemen een ronde vorm aan, waar ze eerst een meer ovale vorm hadden en dan start de expressie van genen die karakteristiek zijn voor HSCs. Vanuit de aorta migreren de HSCs dan naar de volgende, tijdelijke locatie, de lever en milt. Daar vermeerderen en rijpen de HSCs verder, waarna de uiteindelijke locatie wordt bereikt, het beenmerg.

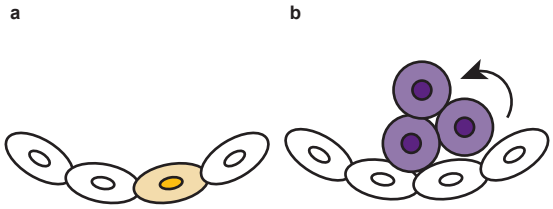

Figuur 2. De transitie van een endotheelcel naar een hematopoietische stamcel in muis. De wand van de aorta. (a) In geel een hemogene endotheelcel die op het punt staat de transformatie naar een HSC te ondergaan. (b) de endotheelcel heeft een ronde vorm aangenomen en start met de expressie van genen karakteristiek voor HSCs (paars).

Onderzoek naar hematopoiese

Onderzoek naar hematopoiese wordt gedaan in meerdere model organismes, waaronder de kip, de muis en de zebravis. Mensen en muizen hebben een zeer vergelijkbare embryonale ontwikkeling, waarbij de vorming van organen ook grote overeenkomsten vertoont. Dit is een van de redenen dat muizen vaak gebruikt worden als model organisme. Een groot nadeel van het gebruik van muizen tijdens de embryonale ontwikkeling is dat bij muizen, net als mensen, de embryo's intern ontwikkelen. Dit maakt het observeren en manipuleren van processen tijdens de ontwikkeling erg lastig. De embryonale ontwikkeling van zebravissen is goed te vergelijken met de ontwikkeling van mensen en muizen, maar zebravissen hebben niet de nadelen die muizen wel hebben. Zebravissen worden daarom steeds vaker als model organisme gebruikt voor embryonaal onderzoek (figuur 3a). Het grootste voordeel van de zebravis is dat de embryonale ontwikkeling buiten het lichaam van de vis plaats vindt en dat embryo's de eerste vijf dagen transparant zijn. Dit maakt het observeren en manipuleren van processen tijdens de embryonale ontwikkeling eenvoudiger dan in model organismes met een interne ontwikkeling. Daar komt bij dat de embryonale ontwikkeling in zebravissen erg snel gaat, binnen 24 uur na de bevruchting lijkt het embryo al op een vis, beweegt het en klopt het hartje (figuur 3 b-f).

Fysiologisch lijken zebravissen erg op zoogdieren. Zo hebben zebravissen een hart, lever, nieren en hematologisch systeem, met vergelijkbare functies als bij mensen. Er zijn echter wel verschillen, zo ook tijdens hematopoiese. Het eerste verschil is dat we

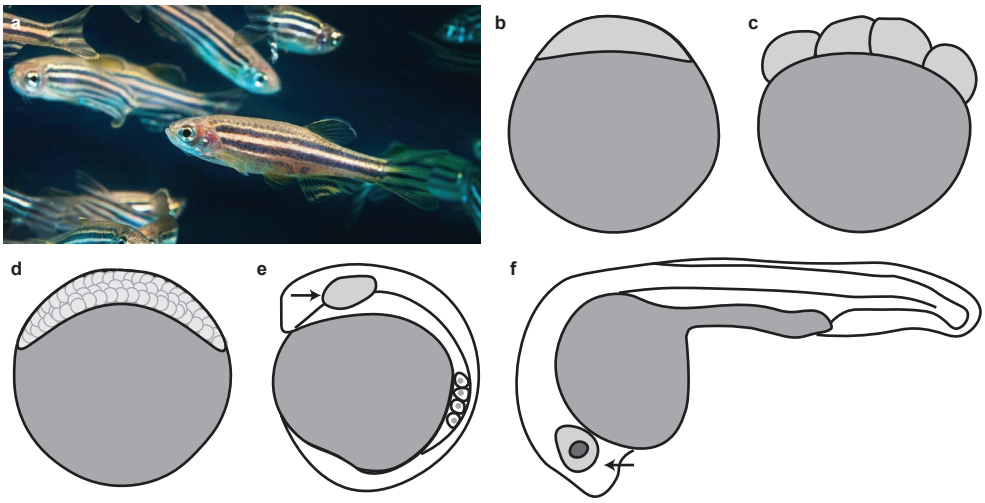

Figuur 3. De zebravis. (a) volwassen zebravissen. (b) bevruchte zygote, 1-cel stadium, enkele minuten na bevruchting. (c) 8-cel stadium, 75 minuten na bevruchting. (d) dome-stadium, 4 uur na bevruchting. (e) 4-somieten stadium, 11 uur na bevruchting. Het oog wordt nu zichtbaar (pijl). (f) 24 uur na bevruchting. Links de kop en rechts de staart. De pijl wijst het oog aan.

in zebravissen de pure HSCs niet kunnen onderscheiden van HSCs die al iets meer zijn gedifferentieerd naar een specifiek type bloedcel. We noemen deze mix van cellen daarom hematopoietische stam/progenitor cellen (HSPCs). HSPCs komen voort uit de aorta, in eenzelfde soort proces als beschreven voor zoogdieren. Maar waarin HSPCs in zoogdieren in kleine clusters verschijnen, die nog aan de wand van de aorta vastgehecht zijn, verschilt dit proces in zebravissen. In zebravissen ondergaan hemogene endotheelcellen ook een serie van transformaties wat leidt tot een HSPC. Het proces begint met een hemogene endotheelcel die weg buigt van de aorta (figuur 4 a) en daarna een ronde vorm aanneemt (figuur 4b) en van de wand van de aorta afsplitst (figuur 4c). Op dit moment is de transformatie compleet en is de expressie van genen die karakteristiek zijn voor HSPCs begonnen. HSPCs betreden nu de bloedsomloop in de ader liggend onder de aorta. In zebravissen is dit proces goed 'live' te volgen met behulp van confocale microscopie (**hoofdstuk 2, figuur 1**). Nadat de HSPCs de bloedcirculatie hebben betreden lokaliseren ze naar de 'caudal hematopoietic tissue' (CHT) in de staart. Dit is te vergelijken met de lever in zoogdieren. In de CHT vermeerderen de HSPCs zich en rijpen ze verder voordat ze zich naar de uiteindelijke hematopoietische organen in de zebravis verplaatsen: de nieren en de thymus.

Inhoud van dit proefschrift

In **hoofdstuk 1** beschrijf ik uitgebreid de achtergrondinformatie om de komende vier hoofdstukken goed te kunnen plaatsen. Het gaat dieper in op de moleculaire signalering mechanismen die tijdens hematopoiese plaatsvinden en wat de consequenties zijn als deze mechanismen verstoord zijn.

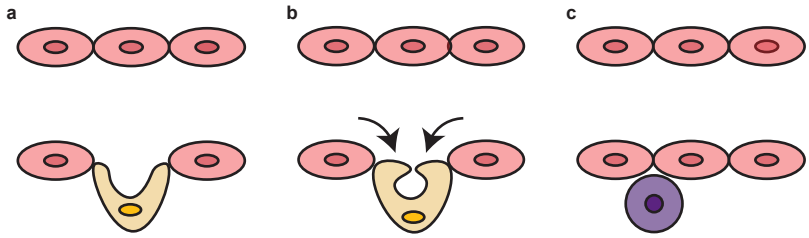

Figuur 4. De transitie van een endotheelcel naar een hematopoietische stam/progenitor cel in zebravissen. Afgebeeld is de aorta. (a) een hemogene endotheelcel (in geel) start met de transitie naar een HSC, waarbij de cel doorbuigt. (b) Vervolgens buigt de cel naar binnentoe en is zo in staat om van de wand van de aorta af te splitsen. (c) De endotheelcel is nu volledig getransformeerd tot HSPC en betreedt de bloedsomloop in de daaronder liggende ader.

In **hoofdstuk 2** beschrijven we het effect van PI3K signalering op hematopoiese in zebravissen. PI3K signalering is een belangrijk cel signaleringsmechanisme dat de cellulaire respons op externe factoren reguleert, onder andere cel proliferatie (figuur 5). Cel proliferatie is een proces dat sterk gereguleerd moet worden, daar ongecontroleerde cel proliferatie kan leiden tot kanker. Onder normale omstandigheden wordt de PI3K signalering gereguleerd door Pten, dat de respons van PI3K remt, en uiteindelijk de cellulaire respons. In **hoofdstuk 2** beschrijven we voor de eerste keer dat een deel van de HSPCs die voortkomen uit de aorta desintegreerden in zebravissen die geen functioneel Pten hadden. Als we de Pten functie herstelden of als we PI3K signalering remden, dan observeerden we normale hematopoiese in deze embryo's. Tot onze verrassing zagen wij, wanneer we in normale embryo's PI3K signalering remden, een soortgelijk beeld als in embryo's die geen functioneel Pten bezaten. Dit suggereert dat de hoeveelheid PI3K activiteit belangrijk is voor het ontstaan van HSPCs. Te veel PI3K signalering leidt tot de dood van HSPCs, maar te weinig PI3K signalering ook. Een gematigde hoeveelheid lijkt noodzakelijk voor normale hematopoiese. Om beter te begrijpen waardoor de ene helft van de HSPCs overleefde bij een te hoog of te laag niveau van PI3K signalering hebben we gebruik gemaakt van single cell RNA sequencing. Dit stelde ons in staat om van één cel heel nauwkeurig vast te stellen welke genen actief zijn, en zo subtiele verschillen tussen cellen te vinden. In de periode dat HSPCs uit de aorta voortkomen, observeerden we twee subtiel verschillende soorten HSPCs: HSPCs die meer stamcel-achtige kenmerken vertoonden en HSPCs die al iets meer gedifferentieerd leken te zijn. Wanneer PI3K signalering geremd wordt, verloren we de HSPCs met de meest stamcel-achtige kenmerken. Later tijdens de hematopoiese konden we deze twee HSPCs soorten niet meer van elkaar onderscheiden, maar zagen we dat remming van PI3K signalering leidde tot meer HSPCs en verminderde differentiatie tot de verschillende bloedcellen. Overactivatie van PI3K signalering leidde juist tot vermindering van HSPCs en toegenomen differentiatie tot de verschillende bloedcellen. Al met al laten we in dit hoofdstuk zien dat PI3K signalering de overleving en stamcelgehalte van HSPCs reguleert.

In **hoofdstuk 3** hebben we de zebravis gebruikt om een specifieke patiënt mutatie die

vaak voorkomt in Noonan Syndroom (NS) beter te begrijpen. Noonan Syndroom is een ontwikkelingsstoornis die ongeveer 1:1500 mensen treft en kenmerken zijn een korte lichaamslengte, hart defecten en uitgesproken gelaatstrekken, zoals wijd uiteenstaande ogen, laaggeplaatste oren en een korte brede hals. Andere kenmerken zijn dat een deel van de kinderen met deze aandoening een zeer zeldzame vorm van leukemie ontwikkelt (juveniele myelomonocytaire leukemie, JMML), met een mogelijk erg agressief en fataal verloop. Mutaties in het eiwit SHP2 veroorzaken vaak NS, waarbij SHP2-D61G een van de meest voorkomende mutaties is. Deze mutatie hebben we via CRISPR/Cas9 in het genoom van de zebravis aangebracht, zodat we de hematologische defecten konden bestuderen tijdens de embryonale ontwikkeling om zo tot een beter begrip te komen van het ontstaan van JMML in deze patiënten. De zebravissen die deze mutatie droegen ontwikkelden dezelfde kenmerken als NS-patiënten, zoals een kortere lichaamslengte, wijd uiteenstaande ogen en hematologische defecten die kenmerkend zijn voor JMML. We ontdekten dat de ontstekingsrespons mogelijk betrokken is bij de aanvang van JMML, en dat wanneer onstekingsremmers werden toegediend aan zebravissen met de Shp2a-D61G mutatie de hematologische defecten minder ernstig waren. Dit is interessant, want tot nu toe zijn er geen medicijnen voor JMML in NS-patiënten. Al met al laten we in dit hoofdstuk zien dat de zebravis geschikt is om menselijke ziektes te modelleren en dat het bestuderen tijdens de embryonale ontwikkeling daarvan goed mogelijk is.

In **hoofdstuk 4** richten we ons verder op de rol van Shp2 tijdens hematopoiese in zebravissen. Afgezien van de rol die Shp2 in Noonan Syndroom speelt, is het ook betrokken bij embryonale ontwikkeling, verschillende signaleringsmechanismes, waaronder het PI3K signaleringsmechanisme en is het betrokken bij hematopoiese. Door een duplicatie van een groot deel van het genoom bevatten zebravissen twee varianten van Shp2, Shp2a en Shp2b, die beide functioneel zijn. Om de rol van Shp2a en Shp2b te bestuderen tijdens hematopoiese in de embryonale ontwikkeling hebben we gebruik gemaakt van 'live' microscopie en *in situ* hybridisatie, een techniek om genexpressie mee te bestuderen. We ontdekten dat zebravissen die geen functioneel Shp2a bezaten geen defecten vertoonden tijdens hematopoiese, maar dat embryo's zonder functionerend Shp2b wel defecten lieten zien. Deze embryo's vertoonden HSPCs die in stukken uit een spatten wanneer de HSPCs uit de aorta voortkwamen. Op latere tijdstippen tijdens de embryonale ontwikkeling was dit effect nog steeds zichtbaar, in de vorm van een lager aantal HSPCs in het tijdelijke hematopoietische orgaan in de staart, de CHT. De overlevende HSPCs waren wel in staat om te differentiëren naar alle typen bloedcellen en aan het eind van de embryonale ontwikkeling en in volwassen vissen zagen we geen hematologische defecten meer. Dit laat zien dat Shp2b nodig is tijdens het proces waarin HSPCs worden gevormd, maar dat embryo's zonder Shp2b deze defecten later overwinnen.

De zebravis is uitermate geschikt om te gebruiken in 'live' microscopie doordat embryo's transparant zijn tijdens de embryonale ontwikkeling. Door middel van transgene lijnen kunnen we specifieke cellen, weefsels of structuren markeren met een gekleurd fluorescent label, bijvoorbeeld groen of rood. Zo kunnen we bijvoorbeeld het vaatstelsel labelen met de kleur groen, terwijl we tegelijkertijd al het bloed rood labelen. Op deze manieren zijn er tientallen combinaties te maken. Om de allereerste HSPCs te vinden wanneer deze uit de aorta komen, wordt vaak een transgene lijn gebruikt waarbij de endotheelcellen rood gelabeld zijn (deze marker heet 'kdrl') en de HSPCs groen gelabeld

zijn (deze marker heet ‘cd41’). Aan het eind van de embryonale ontwikkeling gebruiken we vaak alleen de transgene lijn waarbij de HSPCs groen zijn gelabeld. In **hoofdstuk 5** ontdekten we dat aan het eind van de embryonale ontwikkeling er een subpopulatie van HSPCs lijkt te bestaan, die niet alleen *cd41* tot expressie brengen, maar ook *kdrl*. Single cell RNA sequencing liet zien dat deze populaties verschilden in de genen die ze tot expressie brachten. Beide populaties toonden expressie van HSPCs-kenmerken, maar kdrl/cd41 HSCs leken meer gedifferentieerd te zijn naar myeloïde cellen, terwijl cd41 HSPCs meer neigden naar thrombocyt/erythrocyt cellen. Om dit te verifiëren hebben we gebruik gemaakt van een *in vitro* differentiatie analyse, waarbij cellen in medium geplaatst worden met de desbetreffende differentiatie factoren voor een bepaald type bloedcel. Aan het einde van de embryonale ontwikkeling waren alleen kdrl/cd41 HSPCs in staat om te differentiëren naar beide type bloedcellen, terwijl cd41 HSPCs hier niet toe in staat waren. In volwassen zebravissen was dit juist omgekeerd, hier waren alleen cd41 HSPCs, zonder *kdrl* expressie, in staat om te differentiëren naar de verschillende type bloedcellen. Al met al, lijkt het verlies van *kdrl* expressie de overgang van embryonale HSPCs naar volwassen HSPCs te markeren.

Als laatste plaats ik in **hoofdstuk 6** onze bevindingen van de vorige hoofdstukken in een grotere context aan de hand van recente vakliteratuur en ik bespreek de implicaties voor verder onderzoek.

English summary

This thesis describes the use of zebrafish, *Danio rerio*, to unravel the complexity of hematopoiesis in the developing embryo with an emphasis on the role of two phosphatases.

In **chapter 1**, we provide a background for the following four chapters, with a general introduction to hematopoiesis during embryonic development and the similarities between hematopoiesis between zebrafish and mice. Furthermore, we highlight the role of two phosphatases, *Pten* and *Ptpn11*, during embryonic development and more specifically during hematopoiesis. Last, we give a short overview of the role of *PTEN* and *PTPN11* in human health and disease.

Chapter 2 focuses on the role of Pten during hematopoiesis. To analyse the role of Pten we used embryos lacking Pten expression with various transgenic markers to visualize hematopoiesis. Embryos lacking Pten expression display, among other things, increased PI3K activity. We found that embryos lacking Ptenshowed less hematopoietic stem/progenitor cells (HSPCs) compared to their siblings, with a striking phenotype when HSPCs emerge in the aorta. When we compensated the lack of Pten expression by either restoring Pten expression or by inhibiting PI3K activity, we observed normal emergence of HSPCs and normal numbers of HSPCs. To our surprise, when we inhibited PI3K activity in wild type embryos, we observed a similar phenotype as in embryos lacking Pten expression. These results suggests that a moderate level of PI3K activity is required for emerging HSPCs.

When using single cell RNA sequencing, we observed two, subtly different, HSPCs clusters when HSPCs emerge from the aorta, one having more stem cell-like properties and the other having more progenitor-like characteristics. When PI3K activity was inhibited, we lost the more stem cell-like HSPCs. At the end of hematopoiesis during embryonic development, we observed that inhibiting PI3K activity led to increased HSPCs fate and arrested differentiation. In contrast to this, we observed increased differentiation and loss of HSPCs fate in embryos lacking Pten expression. Overall, this chapter shows that PI3K signalling controls the survival and stemness of HSPCs.

In **chapter 3** we used the zebrafish to model a specific patient mutation commonly observed in Noonan Syndrome (NS). We generated a mutant zebrafish line carrying a Shp2a-D61G mutation using the CRISPR/Cas9-technique. This mutant zebrafish displayed several characteristics of NS patients. Focusing on the hematological phenotype, these fish showed an expansion of the myeloid lineage, an increased sensitivity to myeloid differentiation factors, mild anemia and thrombocytopenia. Using both single cell RNA sequencing and an *in vitro* differentiation assay we observed this expansion of the myeloid lineage and we found that these defects resemble the hematological defects observed in human patients. Furthermore, we observed an upregulation of the pro-inflammatory genes in the myeloid lineage early during differentiation, indicating that the inflammatory response might be involved in the expansion of the myeloid lineage. The hematological phenotype of our mutant zebrafish line was partially rescued upon

inflammatory inhibition. Overall, we generated a novel zebrafish model that displays several characteristics of NS patients, which is particularly interesting as the hematological defects in human patients often appear at a very young age and zebrafish are ideally suited as a tool to study defects during embryonic development.

In **chapter 4** we focused on the role of Shp2a and Shp2b during zebrafish hematopoiesis. To this end, we performed live imaging and whole mount *in situ* hybridization on *ptpn11a* and *ptpn11b* mutant zebrafish embryos. Surprisingly, we found that lack of Shp2a did not affect the ontogeny of HSPCs, but that lack of Shp2b did. The majority of zebrafish embryos lacking Shp2b showed disintegrating HSPCs upon emergence from the aorta at the onset of definitive hematopoiesis. The effect of these abortive events is still seen at later stages during embryonic development, in that fewer HSPCs were observed to seed the next transient hematopoietic organ. However, the surviving HSPCs did engage in all blood lineages and we observed no differences at later stages between embryos lacking Ptpn11b expression and their siblings. Together, our results suggest that *ptpn11b* is required for normal emergence of HSPCs at the onset of the definitive wave of hematopoiesis and that *ptpn11b* mutants overcome these defects at the end of definitive hematopoiesis.

In **chapter 5** we unveil a subpopulation of HSPCs. These HSPCs do not only express the hematopoietic stem cell marker *cd41*^{low}, but also express the endothelial marker *kdrl*. Single cell RNA sequencing in zebrafish embryos revealed transcriptomic differences between HSPCs that express both kdrl/cd41^{low} and HSPCs that only express cd41^{low}. Kdrl/cd41^{low} HSPCs appear to have a more myeloid progenitor fate, whereas cd41^{low} HSPCs had a more thrombocyte/erythrocyte progenitor fate. When we used *in vitro* differentiation assays, we found that only kdrl/cd41^{low} HSPCs were able to differentiate into different blood cell fates. In adult zebrafish we observed both kdrl/cd41^{low} and cd41^{low} HSPCs as well, but found that only cd41^{low} HSPCs were able to differentiate into different blood cell fates. Overall, our results suggest that in both embryos and adult zebrafish a subpopulation of HSPCs exist. In embryos kdrl/cd41^{low} HSPCs are able to differentiate into several lineages *in vitro*, whereas in adults only cd41^{low} HSPCs, that do not express kdrl, have this ability. Hence, the loss of kdrl expression marks the shift from embryonic HSPCs to adult HSPCs.

Finally, **chapter 6** provides a summarizing discussion of the work presented in each previous chapter in the context of the latest publications in the field and the implications of our findings for future research.

Curriculum Vitae

Sasja Franke werd op 8 maart 1991 in Oldenzaal geboren. In 2010 behaalde zij haar gymnasium diploma aan het Twents Carmel College, locatie Lyceumstraat te Oldenzaal met het profiel Natuur en Techniek en Natuur en Gezondheid. In september van hetzelfde jaar begon zij met de opleiding Psychobiologie aan de Universiteit van Amsterdam. Na afronding van deze bachelor begon zij in 2013 aan de master Biomedical Sciences – Molecular Neuroscience van dezelfde universiteit. Als onderdeel van deze master heeft Sasja een onderzoeksstage van tien maanden gedaan in het Hubrecht Instituut in de groep van prof. dr. Jeroen den Hertog. Tijdens deze stage bestudeerde zij de rol van mono-ubiquitinatie van Pten tijdens de embryonale ontwikkeling. Vervolgens is zij voor een tweede onderzoeksstage voor 7 maanden naar het Verenigd Koninkrijk gegaan, waar zij in het MRC Laboratory for Cell Biology in Londen werkte in de groep van prof. dr. Antonella Riccio. Hier bestudeerde zij het effect van localizatie op 3'UTR shortening van mRNA in axonen. Na terugkomst is Sasja begonnen als PhD student bij het Hubrecht Instituut in Utrecht in de groep van prof. dr. Jeroen den Hertog, waar zij zich richtte op hematopoiese tijdens de embryonale ontwikkeling in zebravissen. De resultaten verkregen tijdens dit promotietraject staan beschreven in dit proefschrift.

List of publications

Published articles

Blokzijl-Franke S, Ponsioen B, Schulte-Merker S, Herbomel P, Kissa K, Choorapoikayil S and den Hertog J (2021). Phosphatidylinositol-3 kinase signaling controls survival and stemness of hematopoietic stem and progenitor cells. Oncogene 40(15):2741-55; doi: 10.1038/s41388-021-01733-5.

Andreassi C, Luisier R, Crerar H, Darsinou M, **Blokzijl-Franke S**, Lenn T, Luscombe N.M, Cuda G, Gaspari M, Saiardi A, Riccio A (2021). Cytoplasmic cleavage of IMPA1 3'UTR is necessary for maintaining axon integrity. Cell Reports 34(8):108778; doi: 10.1016/j.celrep.2021.108778.

Ciarlo C, Kaufman C.K, kinikoglu B, Michael J, Yang S, D'Amato C, **Blokzijl-Franke S**, den Hertog J, Schlaeger T.M, Zhou Y, Liao E, Zon L.I (2017). A chemical screen in zebrafish embryonic cells establishes that Akt activation is required for neural crest development. eLife 6; doi: https://doi.org/10.7554/eLife.29145.001

Stumpf M, **Blokzijl-Franke S**, den Hertog J. Fine-tuning of Pten localization and phosphatase activity is essential for zebrafish angiogenesis. PloS One 11(5); doi: 10.1371/journal.pone.0154771

Manuscripts submitted

Solman M, **Blokzijl-Franke S**, Yan C, Yang Q, Kamel S.M, Bakkers J, Langenau D.M, den Hertog J. Inflammatory response potentiates juvenile myelomonocytic leukemia in Shp2 mutant Noonan syndrome.

Dankwoord

Op een zonnige zomeravond is het moment dan ineens daar. Na bijna zes jaar is mijn promotie onderzoek dan echt afgerond, alleen de verdediging zelf staat nog op het programma. De afgelopen jaren zijn een groot avontuur geweest. Gelukkig heb ik dit avontuur niet alleen hoeven te beleven, anders ben ik bang dat ik al snel verdwaald zou zijn geweest en dan zou dit boekje er niet zijn geweest.

Allereerst wil ik **Jeroen** bedanken. Ik heb mijn eerste mailtje dat ik ooit aan je heb verstuurd nog gevonden, verzonden in oktober 2013 om te vragen of ik mijn masterstage in jouw lab kon uitvoeren. Ik had niet verwacht dat ik er vervolgens van december 2013 tot december 2020 zou rondlopen en mijn PhD bij je zou afronden. Dank voor het vertrouwen dat je altijd uitstraalde, voor de wetenschappelijke discussies en voor de ruimte die je me gaf om me persoonlijk te ontwikkelen. Tijdens de eerste lock-down in maart 2020 heb ik het enorm gewaardeerd dat je me de flexibiliteit gaf om te doen wat ik kon en niet te hameren op resultaten. We hebben heel wat meetings gehad waarin we niet alleen het project bespraken, maar ook of het thuiswerken te doen was met een dreumes in huis die de aandacht opeistte.

Verder wil ik mijn promoter **Jeroen Bakkers** bedanken. Dank voor je input tijdens onze meetings om mijn project in goede banen te leiden.

Lieve leden van het Jeroen den Hertog-lab. Het lab is de afgelopen jaren aanzienlijk gegroeid, en in dit geval was het zeker 'hoe meer zielen, hoe meer vreugd'. **John**, het gebeurt me echt niet vaak dat ik iemand tegen kom die nóg meer kan kletsen dan ik doe, maar in jou heb ik mijn meerdere gevonden. Dank voor al onze gesprekken, maar ook voor je enorme ervaring met kloneren en DNA isolatie en je bereidheid om deze te delen. **Jelmer**, ik snap werkelijk niet hoe je het doet, vroeg op de ochtend al zo ontzettend goedgemutst zijn. Dank voor alle jaren gezelligheid op ons kantoor en voor het accepteren dat ik tot 10.00 maar beter met rust gelaten kan worden en soms beter de hele dag. Ik ben ontzettend blij dat je op 7 september als mijn paranimf naast me staat tijdens de verdediging, met jouw positieve houding moet het goed komen. Ik hoop dat ik binnenkort je eigen boekje mag bewonderen! **Wouter**, onze eerste ontmoeting was op z'n zachts gezegd een ramp en dat was compleet mijn fout. Laten we het er maar op houden dat het zo'n dag was dat het beter zou zijn geweest als ik geen contact had gehad met mensen. Gelukkig is het later helemaal goed gekomen en bleken we erg goed te kunnen kletsen over van alles en nog wat. Dank voor alle goede gesprekken op kantoor, in het lab en op onze fietstochtjes naar huis. Ik bewonder je enthousiasme in de wetenschap enorm en denk dat je iets ontzettends gaafs van je project gaat maken. Ik kijk er naar uit dat je naast me staat op 7 september als mijn paranimf! **Petra**, we begonnen zo ongeveer gelijk en vonden elkaar al snel in onze organiseer-drang op het lab. Het 'oude-mannen-hok' werd steeds opgeruimder en bleef opgeruimd en zelfs John's bench moest er aan geloven. Gelukkig was jij 's ochtends ook niet altijd een held en dat maakte een kamer delen met retreats, masterclasses of de ochtend na de Christmas party een verademing. Allebei stil tegenover elkaar met een kop thee en allebei gelukkig. Ik wens je al het goeds toe samen met Sjoerd! **Maaike**, ik kan enorm bewonderen hoe strak, duidelijk en georganiseerd jij

kan werken. Ik klaagde altijd al over hoeveel genotypeer werk de Pten vissen met zich mee brachten, maar jij hebt me ruimschoots overtroffen met al je lijnen. Dank je wel voor je nuchterheid en directheid en het komt echt goed met je boekje! **Maja**, you didn't know anything about zebrafish when you started, but you caught on really quick. I'm happy we could incorporate the methylcellulose assay in the D61G manuscript (which will hopefully really soon turn into a paper). Thank you for our chats and discussions, they really helped finishing this thesis. **Ouyang**, thank you for all our chats. I'm super happy to hear you are almost defending yourself, well done! I wish you all the best in your life. **Daniëlle**, als PhD-student heb ik je maar heel kort meegemaakt, maar als student gelukkig wat langer. Ontzettend leuk dat je het JdH lab gaat versterken. Heel veel succes met je PhD, en echt, uiteindelijk komt het goed! **Lennart**, je was mijn enige student en zonder jou zou hoofdstuk 4 er niet geweest zijn. Samen ontdekten we dat Shp2b ook kan zorgen voor spectaculaire plaatjes tijdens de hematopoiese. Dank voor de leuke tijd die we gehad hebben!

Of all ex-members of the JdH-lab, I should start with **Miriam**. Miriam, after a very quiet student, you got me as a student. It was quite a shock, but I think we managed well. I would have never guessed that our lives would run parallel so much, with both of us doing our PhD on Pten and later, becoming moms within two days of eachother. Thank you teaching me the ins- and outs of zebrafish work and later for all our chats about pregnancy and baby-related stuff. I wish you, Enric and Elba all the best. **Suma**, we actually never were 'official' labmates in the JdH-lab, but as I took over your project, we interacted a lot. Thank you for teaching me how to mount those 36 hpf embryos and how to image them overnight. I admire how you kept enthousiastic about this project, even years later. We finally managed to finish the project with a nice publication and I'm lookin forward discussing my thesis with you when I defend. **Alex**, thank you for all your elaborate explanations, either in protocols or in real live. You taught me a lot, even after you left the Hubrecht. I wish you all the best! **Marieke**, je was relatief kort bij ons op het lab, maar je bracht wel een heleboel gezelligheid met je mee. Ik hoop dat je het heel erg naar je zin hebt op het AMC en dat je over een aantal jaar ook een boekje hebt.

Zonder onze buren en mede zebrafish mensen, het **Bakkers** lab was mijn tijd op het Hubrecht een stuk saaier geweest. **Melanie**, we hebben heel wat uurtjes afgekletst, en toen je nog lang haar had heb ik heel wat haarstijlen op je uitgeprobeerd. Ik denk niet dat ik ooit zo knuffelig wordt als jij, maar het is wat beter geworden. Ik ben ontzettend blij om je zo gelukkig te zien met je gezin en ik wens je al het goeds toe! **Sven,** onze kant was toch wel de 'lefty' side. Dank je wel voor alle gezelligheid, het kunnen klagen over de PhD, de pogingen om er bij ons een Japanse auto in te krijgen (helaas niet gelukt), hulp met R en het kunnen meepraten over gebroken nachten. Ik vond het maar niks dat je ons kantoorje verliet! Succes met de allerlaatste loodjes! **Sarah,** without you I wouldn't have survived the last months of PhD-life, especially in the weekends when almost nobody was around (except us two). Thank you for your infinite supply of energy boosters (aka candy, cake and chocolate) and the chats that went with it, it did help save the day. Good luck with the end of your PhD, you can do it! **Silja, Laurence, Dennis, Federico, Hessel, Phong** and **Sonja**, thank you all for your company in all fish-related spaces at the Hubrecht and for help and advice when I needed some. You really made being a fish-person awesome!

Ik wil de mensen van de fish facility heel erg graag bedanken voor al hun goede zorgen al die jaren. **Mark,** dank voor alle hulp als ik embryos moest opsturen naar de VS of binnen Europa en voor het begrip als ik weer eens iets te laat was met het doorzetten van mijn vislijnen. **Erma**, zonder jou zou ik het overzicht van de Pten lijnen helemaal zijn kwijtgeraakt. Dank je wel voor alle goede zorgen voor mijn baby-visjes! **Rob**, dank je wel voor al je tips om te zorgen dat mijn vissen 's ochtends wel wilden leggen en voor alle gezellige praatjes die we gemaakt hebben. **Bert**, **Luuk** en **Martijn,** dank je wel voor alle goede zorgen voor mijn vissen en voor het (bijna) nooit klagen als ik weer eens enorme hoeveelheden single boxes nodig had voor mijn genotyperingen. Zonder jullie allen was de fish facility lang niet zo gezellig geweest!

Gelukkig bestond het Hubrecht uit meer dan alleen 'Fish-people'. **Rianne,** dank je wel voor de gezelligheid tijdens celkweek, het maakte het daar een stuk minder eenzaam. **Wessel**, dank je wel voor de praatjes bij de koffiemachine (eigenlijk mijn kantoor, maar dat was bijna hetzelfde). Succes met het laatste deel van je PhD! **Zu,** the Hubrecht became a less bright place without our unicorn-girl. Thank you for all our nice chats, your support when I didn't see how my project could ever finish and for letting me play with your pink hair and different hairstyles. Maybe we live closer one day again! **Yuni**, you were secretly a member of the JdH lab for a little while. Thank you for our fun conversations! **Anna,** thank you for all your help with the mice-side of hematopoiesis. You taught me a lot about the field and we had big plans for the Pten mice. Sadly they didn't work out, but I enjoyed our time as lab-buddies. **Carla**, dank je wel voor het onderhouden van de Pten muislijn. Ik ben je eeuwig dankbaar dat ik niet de muis-faciliteit in hoefde! **Laurent** and **Bart,** thank you for all the help with either the mice side or the fish side of hematopoiesis and the discussions we had about it.

Ik kan er niet onderuit, mijn 'walk-of-shame' – mensen. Alle mensen die het aandurfden om me te helpen tijdens mijn R-tocht en geduldig al mijn vragen beantwoorden. Dank jullie wel. Zonder jullie was dit boekje er echt niet geweest en had ik nooit geleerd dat ik het stiekem best wel leuk vind om met R bezig te zijn. **Judith**, dank je wel voor alle hulp in het begin, wat was ik blij dat je ooit ook met HSCs had gewerkt en dat je me die eerste single cell experimenten op weg hebt kunnen helpen. **Marloes**, kleuren in expressie plotjes moeten er wel goed uit zien! Ik ben je ontzettend dankbaar dat je daar zoveel tijd in hebt gestoken en dat ik het zo van je mocht overnemen. Het ziet er nu toch wel heel strak uit! Dank je wel voor alle keren dat je me op weg hebt geholpen en voor alle gesprekken die daar uit voort vloeiden, tot verbazing van Jelmer. **Bas C**, je was een van de eersten die me hielp om echt te snappen wat ik aan het doen was, door duidelijk uit te leggen waarom code op een bepaalde manier geschreven moest worden. Ineens vielen een heleboel puzzelstukjes op hun plaats. Dank voor de uren die je me hebt geholpen en je geduldige uitleg. **Lennart, Mauro, Chloé**, **Maria** and all others who sacrificed precious hours to help me with R, thank you!

Dan de FACS faciliteit, **Stefan**, wat een eemalig experiment zou zijn groeide uit tot mijn regelmatige terugkeer voor het weer FACSen van zebrafish materiaal. Dank je wel voor het helpen met het opzetten van het experiment, zodat het enigszins te doen was en voor de leuke gesprekken die we hadden tijdens het FACSen. **Reinier**, toen ik later me meer ging focussen op het FACSen van volwassen zebrafish materiaal en het kweken hiervan heb

ik enorm kunnen profiteren van je enorme ervaring in de hematologie. Dank je wel voor alle hulp om de experimenten zo goed mogelijk voor elkaar te krijgen en voor de rust en kalmte die je op FACS dagen met je meebracht.

Ik zou nog vele malen langer kunnen doorgaan met het bedanken van alle mensen op het Hubrecht, maar dat zou een boekwerk op zichzelf kunnen zijn. Ik heb me altijd ontzettend thuis gevoeld op het Hubrecht en het was echt een ontzettend fijne plek om te werken, en dat komt voornamelijk door alle mensen die er werkten. **Lotte B, Caro, Tim,** en **Sven,** dank jullie wel een geweldig PV-jaar! **Bas M, Hester, Jenny, Maya, Sebastiaan, Josi, Juri, Jarjon, Roel, Maaike, Bram, Sanne, Stijn, Christa, Euclides, Jonas, Anko, Bastiaan, Pim, Alice, Wouter, Kim, Silke, Lotte van R, Angelica, Joep E, the IT-guys, the ladies from HR, reception**, **finance** and **the guys from technical services** and **domestic services,** thank you for all the fun times and making the Hubrecht such a special place!

Tijdens mijn PhD-traject kreeg ik de mogelijkheid om een 'teaching-sabbatical' te doen en ik heb hier ontzettend van genoten. **Marc,** dank voor je enthousiasme voor onderwijs en voor het vertrouwen dat ik dat wel kon. **Elianne, Myrthe, Bob, Laurens, Rianne, Charlotte, Sietske, Nilda, Jonas, Ron, Gisella, Krijn, Simone** en alle anderen van het BMW onderwijs team, dank jullie wel voor het warme bad waarin ik terecht kwam toen ik ineens bij Genoom als docent aan de slag ging. Ik heb heel erg veel van jullie geleerd en een heel erg leuke tijd gehad!

Lotte, ooit kende ik je alleen maar als de buurvrouw van Melanie, maar dat is op de een of andere manier veranderd in een hechte vriendschap. Ik mis het ontzettend dat we niet meer samen naar het werk fietsen, onze gezamelijke etentjes en onze klets momentjes. Gelukkig is Utrecht niet zo ver weg, maar toch. Je bent een ontzettend prachtig mens en ik mag me gelukkig prijzen dat ik je ken.

Marieke, we kennen elkaar ondertussen al een hele tijd. Als eerstejaars studenten Psychobiologie kwamen we in hetzelfde introductieweek-groepje en vanaf toen hebben we samen het studie-avontuur beleefd. Dank je wel voor alle leuke avonturen die we tijdens onze studietijd hebben beleefd, en ook nu nog gebeurt er van alles. Ik ben blij dat ik je heb leren kennen!

Jeske, ik weet niet anders dan dat we vriendinnen zijn, al heeft dat wel wat voeten in aarde gehad als ik onze moeders moet geloven. Dank je wel voor je vriendschap en eeuwige interesse in mijn studie projecten en later PhD project. Ik kan het enorm waarderen als we afspreken en heerlijk theeleuten of juist iets leuks ondernemen. Ik kan me niet voorstellen dat je geen vriendin van me zou zijn. Zorg goed voor jezelf!

Lieve **Blokzijl** familie, wat ben ik blij dat ik jullie als extra familie heb. **Herman** en **José,** ik had me geen lievere schoonouders kunnen wensen. Dank jullie wel dat jullie me altijd welkom hebben laten voelen en voor alle interesse in mijn project. **Jurjen** en **Inge, Hidde** en **Rutger** en **Nicole,** gratis en voor niets kreeg ik 3 knotsgekke, lieve zwagers en hun vriendinnen kado. Dank voor de gezelligheid en leuke gesprekken die we hebben! **Nicole**, we hadden net ontdekt dat die Blokzijl broers wel erg leuk waren en toen heb ik je denk ik al gevraagd of je ooit de omslag van mijn boekje zou willen ontwerpen. 10 jaar verder en eindelijk zijn we zo ver, dank je wel voor het prachtige ontwerp, ik vind het heel bijzonder

dat je het voor mij gemaakt hebt!

Lieve zusjes, **Loes** en **Jasmijn**, eindelijk is het af. Geen geklets meer over zebravissen, geen gezeur meer over de PhD. Maar maak je geen zorgen, ik verzin wel iets anders om over te mopperen. Ik ben ontzettend blij dat we nu zo dicht bij elkaar wonen en kan enorm genieten van het feit dat we zo even langs kunnen wippen bij elkaar. Jullie zijn de beste zusjes!

Jeffrey en **Mickel**, weer gratis en voor niets kreeg ik er twee hele toffe zwagers bij. Voor jullie geldt hetzelfde: ik vind het super dat we nu zo dichtbij wonen en jullie zoveel makkelijker kunnen bezoeken, ik had geen leukere zwagers kunnen wensen!

Lieve **pap** en **mam,** dank jullie voor alles. Het geeft heel veel vertrouwen dat ik altijd op jullie steun en liefde kan rekenen. Ik ben blij dat we nu weer dicht bij elkaar wonen!

Lars, je hebt ons leven aardig op de kop gezet en de PhD zeker niet altijd makkelijker gemaakt. Het maakte het leven wel heel bijzonder. Samen met jou op de fiets na het werk liedjes zingen over de dingen die we onderweg zagen relativeerde de PhD enorm. Net als die twee kleine armpjes om me heen als je even wilde knuffelen. Dank je wel dat je er bent, je bent een prachtig ventje!

Lieve, lieve **Maarten,** zonder jou was ik nooit zo ver gekomen. Dank je wel voor alle steun, bemoedigende woorden en voor het er gewoon zijn voor me. Op naar het volgende avontuur met ons gezinnetje. Ik houd van je!